



**Poly (styrene - co - maleic anhydride) and  
Polystyrene Grafted with Poly(ether amines):  
Synthesis, Characterization and Gas  
Separation Performance**

*Dissertation*

*zur Erlangung des akademischen Grades*

*Doktor der Naturwissenschaften*

*(Dr. rer. nat)*

*der Technischen Fakultät*

*der Christian-Albrechts-Universität zu Kiel*

***Diógenes Rojas***

***Kiel***

***2010***



**Poly (styrene - co - maleic anhydride) and  
Polystyrene Grafted with Poly(ether amines):  
Synthesis, Characterization and Gas  
Separation Performance**

*Dissertation*

*zur Erlangung des akademischen Grades*

*Doktor der Naturwissenschaften*

*(Dr. rer. nat)*

*der Technischen Fakultät*

*der Christian-Albrechts-Universität zu Kiel*

*Diógenes Rojas*

*Kiel*

*2010*

1. Gutachter Prof. Dr. Volker Abetz
  2. Gutachter Prof. Dr. Klaus Rätzke
- Datum der mündlichen Prüfung 15.11.2010

## ***Acknowledgement***

After a difficult but satisfactory challenge to complete my Ph.D. I would like to express my gratitude towards my supervisor Prof. Dr. Peter Simon. His kindness, suggestions, and observations have been an enormous contribution to my project; I hope to have a chance to continue in this productive exchange of ideas and experiences in the future. I am also thankful to Dr. Luis Antonio de Almeida Prado for the collaboration and fruitful discussion of ideas generating a better and qualified work.

Special thanks go to my co-workers at GKSS- Institute of Polymer Research (Helmholtz-Zentrum Geesthacht) for having been helpful and contributing to my work; namely, Susanne Novak, Maren Brinkmann, Karen-Marita Prause, Silvio Neumann, Carsten Scholles and Brigitte Lademann.

I also thank Dr. Wilfredo Yave and Dr. Carmen Nistor for the abundant information and discussion about the gas separation membrane.

Furthermore, I am grateful to Connie Kampmann to have been a great spiritual support during my journey to complete my Ph.D.

Finally, I would like to thank all of my family in Venezuela for understanding why I could not be near them during the last years.

*“Parao”*

“Sí; Pagué el precio que paga el que no vive arrodillao...”

Rubén Blades

## Table of Contents

<b>Table of Contents</b> .....	i
<b>List of Figures</b> .....	vii
<b>List of Tables</b> .....	xvi
<b>Chapter I Introduction</b> .....	1
1.1 CO <sub>2</sub> and CH <sub>4</sub> : Emissions and Management .....	2
• Polymer Membranes for Gas Separation .....	2
1.2 Motivation of the Thesis .....	3
1.3 Outline of the Work .....	3
1.4 Objectives .....	4
1.5 References .....	5
<b>Chapter II Theoretical Background</b> .....	7
2.1 Polystyrene and Poly(styrene-co-maleic anhydride): History, Properties and Applications .....	8
2.1.1 Polystyrene .....	8
2.1.2 Styrene-co-Maleic Anhydride.....	8
2.1.3 Properties of Polystyrene and Poly(styrene-co-maleic anhydride).....	9
2.2 Synthesis of PS, SMA and Polymer Structures .....	11
2.2.1 Synthesis of Polystyrene .....	11
2.2.2 Synthesis of Poly(styrene-co-maleic Anhydride).....	14
2.2.3 Polymeric Structure of the PS and SMA .....	17

2.3	Chemical Modification of PS and SMA: Grafting - Functionalization .....	18
2.3.1	Functionalization .....	18
2.3.2	Graft-Copolymers .....	19
2.4	Polyethylene Glycol: Structure and Characteristic.....	20
2.5	Poly(ether amines): Jeffamine (Mono-functional) Applications, Properties and Reactions .....	21
2.5.1	Reactions of Poly(ether amines) (Jeffamine).....	22
2.5.2	Direct Amidation.....	23
2.5.3	Properties and Applications of the Jeffamine.....	24
2.6	Graft-Copolymers via Sulfonation.....	25
	• Challenges of the Synthesis of Graft-Copolymer via Sulfonation.....	26
2.7	Membrane Based for Gas Separation. Theory Models.....	26
2.7.1	Solution-Diffusion Model .....	27
2.7.2	The Pore-Flow Model .....	27
2.8	Polymers Structures, Materials and Types of Membranes.....	33
2.9	Membranes Preparation and Classification by Morphology.....	36
	• Flow Configurations of Membrane Processes .....	37
2.10	Key Industrial Applications.....	40
	• Carbon Dioxide Separation.....	42
2.11	Permeability: Definition - Models, Polymer Structure and Permeation.....	43
2.11.1	Definition – Models .....	43
2.11.2	Relationship of Polymer Structure and Membrane Permeation.....	45
2.12	Robeson Models .....	51
2.13	References .....	54



<b>Chapter III Characterization and Instrumentation.....</b>	<b>60</b>
3.1 Thermal Analysis .....	60
3.1.1 Differential Scanning Calorimetry (DSC) .....	60
• DSC Measurements.....	62
3.1.2 Thermogravimetric Analysis (TGA).....	62
• TGA Measurements .....	63
3.2 Fourier Transform Infrared Spectroscopy (FT-IR).....	64
• FT-IR Measurements .....	65
3.3 Nuclear Magnetic Resonance Spectroscopy (NMR).....	65
• NMR Measurements.....	67
3.4 Gel Permeation Chromatography (GPC).....	67
• Gel Permeation Chromatography Measurements.....	71
3.5 Scanning Electron Microscopy (SEM).....	72
• Electron Microscopy Images.....	74
3.6 Elementary Analysis (EA) .....	74
• Elementary Analysis Measurements.....	75
3.7 References .....	77
<b>Chapter IV Grafting of Poly(styrene-co-maleic anhydride)</b>	
<b>via Maleic Anhydride with Poly(ether amines).....</b>	<b>79</b>
4.1 Experimental Part .....	80
4.1.1 Materials .....	80
4.1.2 Preparation of Graft-Copolymers .....	81
4.2 Results and Discussion.....	82

4.2.1	$^1\text{H-NMR}$ and $^{13}\text{C-NMR}$ Analysis .....	82
4.2.2	Gel Permeation Chromatography (GPC).....	87
4.3.3	Thermal Properties of the Graft-Copolymers.....	92
	4.3.3.1 <i>Differential Scanning Calorimetric (DSC)</i> .....	92
	4.3.3.2 <i>Variation of Glass Transition Temperature with the [PEG]</i> .....	97
	4.3.3.3 <i>Thermal Stability of the Graft-Copolymers (TGA)</i> .....	98
4.3	Conclusions .....	100
4.4	References .....	101
<b>Chapter V Grafting of Poly(styrene) and Poly(styrene-co-maleic anhydride)</b>		
	<b>via Sulfonation</b> .....	103
5.1.	Experimental Part .....	104
	5.1.1. Materials .....	104
	5.1.2. Graft-Copolymer Synthesis.....	104
	5.1.2.1 <i>Homogeneous Sulfonation of Polystyrene</i> .....	104
	5.1.2.2 <i>Amidation of the Sulfonated Polymer</i> .....	106
5.2	Results and Discussion .....	109
	5.2.1 Characterization: Evaluation of the Sulfonation.....	109
	5.2.1.1 <i>Sulfonation Degree by Elemental Analysis</i> .....	109
	5.2.1.2 <i>Gel Permeation Chromatography Analysis</i> .....	110
	5.2.1.3 <i>Thermal Analysis: DSC and TGA</i> .....	112
	• <i>Differential Scanning Calorimetric (DSC)</i> .....	112
	• <i>Thermogravimetric Analysis (TGA)</i> .....	114
	5.2.1.4 <i>FT-IR Spectroscopy</i> .....	116

5.2.2	Characterization of Graft-copolymer: SMA-SO <sub>3</sub> H-Jeffamine and PS-SO <sub>3</sub> H-Jeffamine.....	118
5.2.2.1	Analysis by <sup>1</sup> H-NMR .....	118
5.2.2.2	FT-IR Spectroscopy .....	122
5.2.2.3	Gel Permeation Chromatography.....	124
5.2.2.4	Thermal Analysis: DSC and TGA.....	125
	• Differential Scanning Calorimetric (DSC).....	125
	• Thermogravimetric Analysis (TGA).....	127
5.3	Conclusions .....	130
5.4	References .....	131

## **Chapter VI Membrane Properties of Series-ML,-MM and -MH and**

	<b>Series -GSMA and -GPSS.....</b>	<b>133</b>
6.1	Experimental Part .....	134
6.1.1	Preparation of the Membrane.....	134
6.1.2	Single Gas Measurements and Determination of Permeability.....	136
6.2	Results and Discussion .....	140
6.2.1	Characterization and Analysis of the Membranes	
	Series-ML, -MM, -MH by SEM .....	140
6.2.1.1	Membranes Based on Series-L Graft-Copolymer, -ML.....	140
6.2.1.2	Membranes Based on Series-M Graft-Copolymer, -MM.....	142
6.2.1.3	Membranes Based on Series-H Graft-Copolymer, -MH.....	144
6.2.2	Characterization and Analysis of the Membranes Series-GSMA and -GPSS by SEM.....	147

6.2.3	Membranes Properties of Series-ML, Series-MM and Series-MH .....	151
6.2.3.1	<i>Analysis of CO<sub>2</sub> Permeability and the CO<sub>2</sub>/N<sub>2</sub> Selectivity .....</i>	152
6.2.3.2	<i>Analysis of CH<sub>4</sub> Permeability and the CO<sub>2</sub>/CH<sub>4</sub> Selectivity ...</i>	160
6.2.3.3	<i>Comparison of Membranes Performance between Series-ML, -MM and -MH, Polyimides and others Polymers Reported .....</i>	162
6.2.5	Membranes Properties of Series-GSMA and Series-GPSS .....	170
6.2.5.1	<i>Membranes Properties Dependency with the PEG Content .....</i>	171
6.2.5.2	<i>Membranes Properties Dependency with Tg .....</i>	173
6.3	Conclusions .....	176
6.4	References .....	178
<b>Chapter VII Summary .....</b>		<b>181</b>
7.1	Summary .....	181
7.2	Zusammenfassung .....	184
<b>Chapter VIII Appendix .....</b>		<b>189</b>

## List of Figures

<b>Figure 1.1:</b> Schematic overview of the components of the global climate system that is relevant to climate changes, their processes and interactions, and some elements that may change, reproduced from IPCC-Technical paper II.....	1
<b>Figure 1.2:</b> Radiative forcing, relative to 1750, of all the long-lived greenhouse gases. The NOAA Annual Greenhouse Gas Index (AGGI), which is indexed to 1 for the year 1990, is shown on the right axis .....	2
<b>Figure 2.1:</b> Structure of Polystyrene, Polystyrene-co-maleic anhydride .....	9
<b>Figure 2.2:</b> Synthesis of polystyrene via anionic polymerization .....	14
<b>Figure 2.3:</b> Copolymerization diagram for the system styrene / maleic anhydride ( $r_1 \approx 0.0095$ , $r_2 \approx 0$ ).....	15
<b>Figure 2.4:</b> Polymer Structures .....	17
<b>Figure 2.5:</b> Functionality and structure. (a) Functionality via esterification or amidation, (b) Functionality via ester exchange.....	18
<b>Figure 2.6:</b> Six basic modes of linking two or more polymers are identified .....	20
<b>Figure 2.7:</b> Structures and characteristic of poly(ether amines) (Jeffamine mono-amine) .....	22
<b>Figure 2.8:</b> Direct Amidation .....	24

<b>Figure 2.9:</b> Molecular transport through membranes can be described by a flow through permanent pores or by the solution-diffusion mechanism .....	29
<b>Figure 2.10:</b> Schematic representation of the nominal pore size and best Theoretical model for the principal membrane separation processes .....	33
<b>Figure 2.11:</b> Some polymer applicable in membrane preparation .....	35
<b>Figure 2.12:</b> Chemical structure of polyimides .....	36
<b>Figure 2.13:</b> Membrane classifications according to the morphology.....	36
<b>Figure 2.14:</b> Composite membranes: support PAN and a graft-copolymer in the top Micrographs taken in polymer research institute-GKSS, thanks to Marion Adelhord.....	38
<b>Figure 2.15:</b> Flow configurations of membrane processes: cross-flow and dead-end filtrations .....	40
<b>Figure 2.16:</b> Flow scheme of one-stage and two-stage membrane separation plants to remove carbon dioxide from natural gas.....	42
<b>Figure 2.17:</b> Diffusion coefficient as a function of molar volume for a variety of permeants in natural rubber and in poly(vinyl chloride), a glassy polymer .....	46
<b>Figure 2.18:</b> Gas sorption coefficient as a function of molar volume for natural rubber membranes.....	47

<b>Figure 2.19:</b> Permeability as a function of molar volume for a rubbery and a glassy polymer.....	49
<b>Figure 2.20:</b> Principle idea of a copolymer suitable for CO <sub>2</sub> separation.....	51
<b>Figure 2.21:</b> Upper bound Relationships for CO <sub>2</sub> /CH <sub>4</sub> Separation (Carbon dioxide - methane selectivity vs oxygen permeability).....	52
<b>Figure 3.1:</b> Schematic DSC Apparatus; heaters, samples and references Pan and the regulate heat flow from computer .....	61
<b>Figure 3.2:</b> Layout of FTIR system .....	64
<b>Figure 3.3:</b> Schematic diagram of NMR spectrometer.....	65
<b>Figure 3.4:</b> The two different volumen available in the GPC column.....	68
<b>Figure 3.5:</b> Idealized dependency of the molecular weight and elution volume $V_e$ .....	69
<b>Figure 3.6:</b> A typical elugrams of the some graft-copolymers prepared in this thesis .....	71
<b>Figure 3.7:</b> Layout of the instrumentation of SEM.....	74
<b>Figure 3.8:</b> Basic scheme of Elementary Analysis equipmemnt.....	76
<b>Figure 4.1:</b> Structure of $\alpha$ -amino- $\omega$ -methoxy polyether (Jeffamine <sup>®</sup> ).....	81
<b>Figure 4.2:</b> Scheme and strategy of the amidation reaction.....	81

<b>Figure 4.3:</b> $^1\text{H}$ -NMR spectrum of the polymer H-1 in acetone- $\text{d}_6$ , structure and assignment of the spectrum .....	83
<b>Figure 4.4:</b> $^{13}\text{C}$ -NMR spectrum of the polymer H-1 in $\text{CDCl}_3$ , structure and assignments .....	85
<b>Figure 4.5:</b> Elugrams of the graft-copolymer (graft) and content of residual Jeffamine (RJ).....	87
<b>Figure 4.6:</b> Scheme to remove the residual Jeffamine (RJ), e.g. solvent in (ethanol) and solvent out ( <i>iso</i> -propanol) .....	89
<b>Figure 4.7:</b> DSC heating thermograms of: (a) L-2, M-2 and H-2, (b) L-3, M-3 and H-3 and (c) L-5, M-4 and H-4, $\Delta T = T_{\text{final}} - T_{\text{initial}}$ of the glass transition process .....	96
<b>Figure 4.8:</b> Dependency of the graft copolymers' glass transition temperature $T_g$ on the PEG content.....	97
<b>Figure 5.1:</b> Reaction scheme of homogeneous sulfonation: (A) acetylsulfate generation (sulfonating agent) (B) and (B) sulfonation of PS.....	106
<b>Figure 5.2:</b> Reaction of grafting of sulfonated polystyrene with poly(ether amide).....	107
<b>Figure 5.3:</b> DSC for (a) SMA- $\text{SO}_3\text{H}$ and (b) PS- $\text{SO}_3\text{H}$ samples.....	113
<b>Figure 5.4:</b> TGA of (a) SMA(7%) and (b) PS after sulfonation between 25 - 320°C .....	115-116



<b>Figure 5.5:</b> Infrared spectrum of (a) SMA (7%) after sulfonation and (b) PS after sulfonation.....	117
<b>Figure 5.6:</b> <sup>1</sup> H-NMR spectra in CDCl <sub>3</sub> of graft-copolymer of PS-SO <sub>3</sub> H grafted with Jeffamine (XTJ 506) and structural assignment.....	118-119
<b>Figure 5.7:</b> <sup>1</sup> H-NMR spectra in CDCl <sub>3</sub> of graft-copolymer of SMA-SO <sub>3</sub> H with Jeffamine XTJ 506 and, identification of the structure.....	121
<b>Figure 5.8:</b> FTIR spectrum: (a) SMA-SO <sub>3</sub> H(35)-Jeffamine and (b) PS-SO <sub>3</sub> H(23)-Jeffamine.....	123
<b>Figure 5.9:</b> DSC thermograms for (a) GSMAS and (b) GPSS series.....	126
<b>Figure 5.10:</b> TGA Analysis of (a) GSMAS and (b) GPSS copolymers.....	127
<b>Figure 5.11</b> Crosslinking reaction of PS-SO <sub>3</sub> H(x).....	129
<b>Figure 6.1:</b> Principle idea of a copolymer suitable for CO <sub>2</sub> separation using graft-copolymer.....	134
<b>Figure 6.2:</b> Flow - Scheme of composite membrane preparation .....	135
<b>Figure 6.3:</b> Dip-coating equipment, coating stage.....	136
<b>Figure 6.4:</b> Assemble of a Membrane test cell.....	136
<b>Figure 6.5:</b> Pressure increase test unit (a): (1) gas inlet, (2) chamber for liquid samples, (3) feed pressure volume, (4) membrane test cell, (5) permeate volume, (6) vacuum pump, and (PTPI) pressure sensor.....	138

<b>Figure 6.6:</b> Principle time run of a pressure increase measurement.....	139
<b>Figure 6.7:</b> A picture of the pressure increase test unit.....	139
<b>Figure 6.8:</b> SEM images (cross-section) of the membranes based on L-1 .....	140
<b>Figure 6.9:</b> SEM images (cross-section) of the membranes based on L-2 .....	141
<b>Figure 6.10:</b> SEM images (cross-section) of the membranes based on L-3 .....	141
<b>Figure 6.11:</b> SEM images (cross-section) of the membranes based on L-4 .....	141
<b>Figure 6.12:</b> SEM images (cross-section) of the membranes based on L-5 .....	142
<b>Figure 6.13:</b> SEM images (cross-section) of the membranes based on M-1 .....	143
<b>Figure 6.14:</b> SEM images (cross-section) of the membranes based on M-2 .....	143
<b>Figure 6.15:</b> SEM images (cross-section) of the membranes based on M-3 .....	143
<b>Figure 6.16:</b> SEM images (cross-section) of the membranes based on M-4 .....	144
<b>Figure 6.17:</b> SEM images (cross-section) of the membranes based on H-1 .....	144
<b>Figure 6.18:</b> SEM images (cross-section) of the membranes based on H-2 .....	144
<b>Figure 6.19:</b> SEM images (cross-section) of the membranes based on H-3 .....	145
<b>Figure 6.20:</b> SEM images (cross-section) of the membranes based on H-4 .....	145
<b>Figure 6.21:</b> Tentative scheme of interaction between the PAN support layer and graft-copolymers of L-, M- and H-type.....	146

<b>Figure 6.22:</b> SEM images (cross-section) of the membranes based on GSMAS-1 (E).....	148
<b>Figure 6.23:</b> SEM images (cross-section) of the membranes based on GSMAS-2 (F).....	148
<b>Figure 6.24:</b> SEM images (cross-section) of the membranes based on GSMAS-3 (G).....	148
<b>Figure 6.25:</b> SEM images (cross-section) of the membranes based on GPSS-1 (C) .....	149
<b>Figure 6.26:</b> SEM images (cross-section) of the membranes based on GPSS-2 (D) .....	149
<b>Figure 6.27:</b> SEM images (cross-section) of the membranes based on GPSS-3 (H) .....	149
<b>Figure 6.28:</b> possible dipole-dipole interactions between PAN: (a) GSMAS and (b) GPSS .....	150
<b>Figure 6.29:</b> Variation of the CO <sub>2</sub> permeability in dependency of the PEG content .....	153
<b>Figure 6.30:</b> Variation of $\alpha$ CO <sub>2</sub> / N <sub>2</sub> in dependency of the PEG content.....	154
<b>Figure 6.31:</b> Variation of the CO <sub>2</sub> -permeability with the glass transition temperature for the graft copolymer based membranes.....	157
<b>Figure 6.32:</b> Schematic of the fractional free volume model characterizing the effect of copolymer composition, temperature, and CO <sub>2</sub> fugacity of the feed gas.....	158

<b>Figure 6.33:</b> Variation of selectivity ( $\text{CO}_2 / \text{N}_2$ ) with the glass transition temperature for the graft copolymer, series-MH, -MM and -MH, based membranes .....	159
<b>Figure 6.34:</b> Variation of the $\text{CH}_4$ permeability in dependency of the PEG content for the graft copolymer based.....	161
<b>Figure 6.35:</b> $\text{CO}_2 / \text{CH}_4$ selectivity of in dependency of the PEG content for the graft copolymer based membranes .....	162
<b>Figure 6.36:</b> Structures types of: (a) polyimides (b) 6FDA moiety (c) graft-copolymer .....	163
<b>Figure 6.37:</b> Experimental permeability of gases into polyimides and other polymers, relationship between log selectivity ( $\text{CO}_2/\text{N}_2$ ) and log permeability ( $\text{CO}_2$ ) and the theoretical upper bound limit defined by Freeman´s theory. (*) MH´s,(▲)PMDA, (◇)6FDA, (Δ)BPDA, (●)BTDA, (+) PC and (△) PIM1 und PIM7.....	166
<b>Figure 6.38:</b> Double logarithmic plot of the dependency of the $\text{CO}_2/\text{CH}_4$ selectivity in dependency of the $\text{CO}_2$ –permeability. The theoretical upper bound limits are calculated according to Freeman´s and Robeson´s theory, respectively. MH´s (*), PMDA (○), 6FDA (◆), BPDA (△), BTDA (+), PC-PIM1 PIM7 (×) .....	168
<b>Figure 6.39:</b> Effect of PEG content on $\text{CO}_2$ permeability at 35°C for membranes based on GPSS and GSMAS series.....	172
<b>Figure 6.40:</b> Effect of PEG content on the $\text{CO}_2/\text{N}_2$ selectivity at 35°C for membranes based on GPSS and GSMAS series.....	173

<b>Figure 6.41:</b> Effect of the glass transition temperature ( $T_g$ ) on $\text{CO}_2$ permeability at 35°C for the GPSS and GSMAS series... ..	174
<b>Figure 6.42:</b> Effect of the glass transition temperature ( $T_g$ ) on the $\text{CO}_2/\text{N}_2$ selectivity at 35°C for the GPSS and GSMAS series .....	175
<b>Figure 8.1:</b> Idealized structure of sulfonated poly(styrene-co-maleic anhydride).....	193

## List of Tables

<b>Table 2.1:</b>	Overview of the properties of polystyrene and poly(styrene-co-maleic anhydride).....	10
<b>Table 2.2:</b>	Poly(ether amine) properties.....	25
<b>Table 2.3:</b>	Current gas separation industry players .....	41
<b>Table 2.4:</b>	Permeabilities in Barrer [ $10^{-10}\text{cm}^3(\text{STP})\cdot\text{cm}/\text{cm}^2\cdot\text{s}\cdot\text{cmHg}$ ] measured with pure gases, at the temperatures given.....	50
<b>Table 2.5:</b>	Permeability and permselectivity data for polymers of interest for membrane separation, Barrer [ $10^{-10}\text{cm}^3(\text{STP})\cdot\text{cm}/\text{cm}^2\cdot\text{s}\cdot\text{cmHg}$ ]	53
<b>Table 4.1:</b>	Experimental data of the reaction .....	82
<b>Table 4.2:</b>	Weight percentages of PEG, PS and PPG in the graft-copolymer as determined by $^1\text{H-NMR}$ .....	86
<b>Table 4.3:</b>	Apparent number average molar mass ( $M_n$ ) and polydispersity (D), the degree of grafting (DG) and number of chain ( $N_c$ ), as determined by GPC for the graft copolymers and SMA(7) .....	90
<b>Table 4.4:</b>	Glass transition temperatures, $T_g$ , heat capacity $\Delta c_p$ and variation of the $T_g$ with respect to the parent poly(styrene-co-maleic anhydride) in dependency of the PEG content .....	93
<b>Table 4.5:</b>	Results of the thermo gravimetric analysis for the graft-copolymers.....	99

<b>Table 5.1:</b>	Experimental data of the sulfonation of SMA and PS .....	108
<b>Table 5.2:</b>	Elemental Analysis (EA) of the sulfonated polymers .....	109
<b>Table 5.3:</b>	Gel permeation chromatography results .....	111
<b>Table 5.4:</b>	DSC results in SMA-SO <sub>3</sub> H and PS-SO <sub>3</sub> H.....	114
<b>Table 5.5:</b>	Content of PEG, PS and PPG in the grafted copolymers.....	122
<b>Table 5.6:</b>	Molar masses ( <i>M<sub>n</sub></i> ) and polydispersity (D) grafted copolymers .....	124
<b>Table 6.1:</b>	Properties of different types of PAN.....	135
<b>Table 6.2:</b>	Thickness of the membranes based on series-ML, -MM and -MH.....	147
<b>Table 6.3:</b>	Thickness of the membrane based on (series-GSMAS and series-GPSS).....	151
<b>Table 6.4:</b>	Flow, permeability of CO <sub>2</sub> and CH <sub>4</sub> at 35°C and 1 atm for the ML-, MM- and MH-type membranes.....	152
<b>Table 6.5:</b>	Permeability of gases for polyimides from literature and graft-copolymer (series-ML, -MM and -MH) prepared in this work .....	164 - 165
<b>Table 6.6:</b>	Transport properties and molecular parameters of penetrant gases.....	169
<b>Table 6.7:</b>	Flows, Permeability of CO <sub>2</sub> and CH <sub>4</sub> .....	170

<b>Table 6.8:</b>	CO <sub>2</sub> and CH <sub>4</sub> permeabilities as well as CO <sub>2</sub> /N <sub>2</sub> and CO <sub>2</sub> /CH <sub>4</sub> selectivities for membranes based on the GSMAS and GPSS polymers.....	171
-------------------	--	-----



## Chapter I Introduction

Anthropogenic climate change is rapidly becoming one of the major issues in environmental science. Global temperatures are expected to rise between 1.4 and 5.8°C by 2100 in the absence of climate change policies [1]. This increase in global temperatures is likely to cause a number of negative effects; including rising sea levels, changes in ecosystems, loss of biodiversity and reduction in crop yields [2], as illustrated by figure 1.1. These effects can be partially overcome by reductions in emissions of greenhouse gases. Reduction of greenhouse gas emissions can occur in a number of ways: such as enhanced energy efficiency, increased use of no-fossil fuel power sources, improved soil management and geological sequestration of carbon dioxide from significant greenhouse gas producing sources [3].

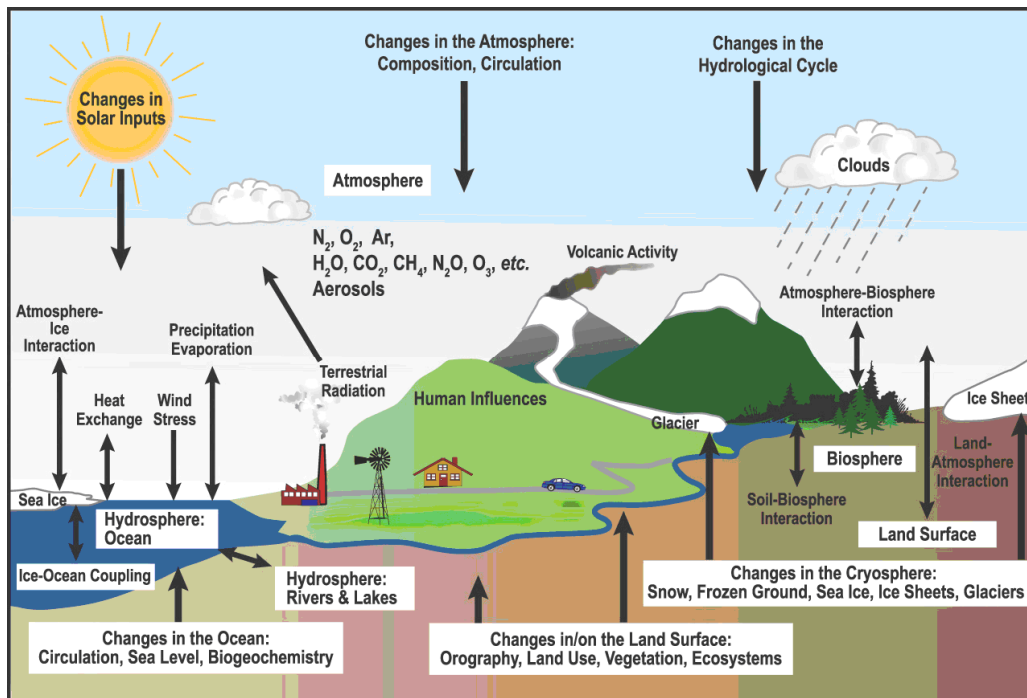


**Figure 1.1:** Schematic overview of the components of the global climate system that are relevant to climate changes, their processes and interactions, and some elements that may change, reproduced from IPCC-Technical paper II [4].

## 1.6 CO<sub>2</sub> and CH<sub>4</sub> : Emissions and Management

Figure 1.2 shows the Annual Greenhouse Gas Index (AGGI) [5], the index provides an easily understood and scientifically unambiguous point of comparison for tracking annual changes in levels of atmospheric greenhouse gases.

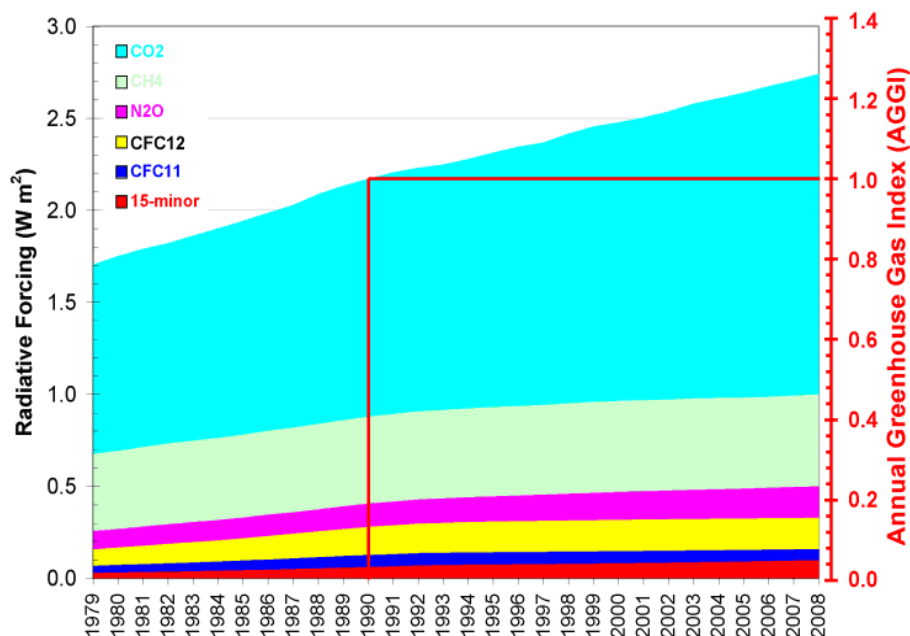


**Figure 1.2:** Radiative forcing, relative to 1750, of all the long-lived greenhouse gases. The NOAA Annual Greenhouse Gas Index (AGGI), which is indexed to 1 for the year 1990, is shown on the right axis [5].

### Polymer Membranes for Gas Separation

Membranes have been investigated for over 150 years [6,7], and since 1980 gas separation membranes have been used commercially [8]. Membranes are a low cost means of separating gases, when high purity gas streams are not vital, however the gas separation membranes are used in a number of industrial processes; such as the production of oxygen enriched air, separation of CO<sub>2</sub> and H<sub>2</sub>O from natural gas, purification of H<sub>2</sub>, and recovery of vapors from vent gases. A number of reviews examining gas separation membrane have been published [8-12]. Different strategies






towards the construction of more efficient membrane have suggested by Koros and Mahajan [13].

### **1.7 Motivation of the Thesis**

Since the 1990s it's evident that governments around the world are assuming and will assume in the 21<sup>st</sup> century specific climate policies to reduce greenhouse gas emissions (mitigation), hence the industrial sector must face new challenges to adapt itself to environmental regulations and to adjust all its industrial process to be more efficient and competitive. Hence, this thesis is presenting a study about the synthesis of new graft-copolymer materials which have currently been tested as gas separation membranes. These new materials can be used as an initial platform for an alternative technology in industrial processes to the management of gases as CO<sub>2</sub> and CH<sub>4</sub>.

### **1.3 Outline of the Work**

The thesis is presented throughout several chapters.

-  **Chapter I** General Introduction
-  **Chapter II** Exhibits a theoretical overview for this study.
-  **Chapter III** Description of characterization techniques.
-  **Chapter IV** Experimental part, analysis and discussion, grafting via maleic anhydride, Series-L,-M and -H
-  **Chapter V** Experimental part, analysis and discussion, grafting via sulfonation, GSMAS and GPSS.

- ✚ **Chapter VI** Performance of the membrane base on graft-copolymers in the separation of CO<sub>2</sub> and CH<sub>4</sub> as main gases and N<sub>2</sub> as reference gas
- ✚ **Chapter VII** is showing a summary of the thesis.

## 1.4 Objectives

### Graft-copolymer

- √ Synthesis of new graft-copolymers by a direct amidation of poly(styrene-co-maleic anhydride) using poly(ether amide)s as graft.
- √ Preparation of a second group of graft-copolymer by sulfonation of poly(styrene-co-maleic anhydride) and poly(styrene) and subsequent amidation reaction using poly(ether amide)s “jeffamine®”.
- √ Optimization of an experimental procedure to reach a maximum yield of the graft-copolymers and a minimum residual of the poly(ether amide).
- √ Identification and analysis of the structures of the graft-copolymers by <sup>1</sup>H-NMR, <sup>13</sup>C-NMR, GPC, FT-IR, etc and determination of the contents of residual poly(ethylene glycol).
- √ Study of the graft-copolymers' physical properties by thermal analysis (DSC and TGA).

### Gas Separation Membranes Performance

- √ Preparation of a series of composite membranes by casting technique using all the graft-copolymers synthesized on a PAN support.

- √ Analysis and identification of the graft-copolymers' morphology in the membranes by SEM.
- √ Determination of the membrane properties by a study of the permeability of CO<sub>2</sub> and CH<sub>4</sub> and the overall CO<sub>2</sub>/N<sub>2</sub> and CO<sub>2</sub>/CH<sub>4</sub> selectivity
- √ Study of the membrane properties and their dependency on the graft-copolymers' PEG content
- √ Determination of the model that identifies the permeability phenomenon in the membranes and their relation with the composition of the graft-copolymer.
- √ Identification of the membranes properties relation with thermal property of the graft-copolymer.
- √ Comparison of the CO<sub>2</sub> permeability, CO<sub>2</sub>/N<sub>2</sub> and CO<sub>2</sub>/CH<sub>4</sub> selectivities with data in the literature.

## 1.5 References

- [1] Houghton J. T., *Climate Change 2001: The Scientific Basis*, Cambridge University Press, Cambridge, 2001.
- [2] McCarthy J. J., Canziani O. F., Leary N. A., Dokken D. J., White K. S., *Climate Change 2001: Impacts, Adaptation, and Vulnerability*, Cambridge University Press, Cambridge, 2001.
- [3] Pacala S., Socolow R., *Science*, 305 (2004) 968.
- [4] Houghton J.T, Meira L. G., Griggs D. J. and Maskell K., *An Introduction to Simple Climate Models used in the IPCC Second Assessment Report*, Intergovernmental Panel on Climate Change © 1997, Geneva, Switzerland.

- 
- [5] Hofmann D.J., The NOAA Annual Greenhouse Gas Index, NOAA Earth System Research Laboratory, R/GMD, 325 Broadway Boulder, Colorado, USA, 2009, [www.esrl.noaa.gov/gmd/aggi/](http://www.esrl.noaa.gov/gmd/aggi/).
- [6] Graham T., *Journal of Membrane Science*, 100 (1995) 17.
- [7] Graham T., *Journal of Membrane Science*, 100 (1995) 9.
- [8] Baker R. W., *Industrial Engineering Chemistry Research*, 41 (2002) 1393.
- [9] Koros W. J., *Macromolecular Symposia*, 188 (2002) 13.
- [10] Mier G., Gas separation with polymer membranes, *Angewandte Chemie International Edition*, 37 (1998) 2960.
- [11] Stern S. A., *Journal of Membrane Science*, 94 (1994) 1.
- [12] Paul D. R., Yampol'skii, Y., *Polymer Gas Separation Membranes*, CRC Press, Boca Raton, U.S.A., 1994.
- [13] Koros, W. J. and Mahajan R., *Journal of Membrane Science*, 175, 2 (2000) 181.

## **Chapter II Theoretical Background**

---

In the beginning of the 20<sup>th</sup> century, after the existence of atoms and molecules in simple inorganic compounds was generally accepted, one came to realize that organic molecules are composed of linked atoms. At that time, man had been using natural polymers without knowing it, and had even synthesized numerous materials such as phenol resins (Bakelite), alkyd resins, polystyrene and poly (vinyl chloride). In 1920, Herman Staudinger was the first one to propose the polymer concept [1], in which thermoplastic materials are visualized as a mixture of long chain-molecules built from covalently connected monomer units that are. Polymers have high molecular weights, which gives them useful physical characteristics such as high viscosity, elasticity, and strength. Polymers are found everywhere [2]. Today, the existence of macromolecules is readily accepted in the scientific world, and polymer science is a vital branch of chemistry. A new polymer material could be an alternative to be applied in the field of gas separation membranes, because many industrially important membrane-based gas separation (GS) processes are based on asymmetric or composite membranes with ultra-thin skin polymer layers. This chapter is showing a resume of theoretical background of poly(styrene-co-maleic), poly(styrene), poly(ethylene glycol) and poly (ether amines) used as a base of the preparation of the new graft-copolymers and an overview of the field of gas separation membranes.

## **2.1 Polystyrene and Poly(styrene-co-maleic anhydride):**

### **History, Properties and Applications**

#### **2.1.1 Polystyrene**

Polystyrene has a long history of evolution behind it. In 1839, a German pharmacist named Eduard Simon discovered polystyrene [3]. Simon isolated a substance from natural resin, however, he did not know what he had discovered. It took another German, organic chemist, Staudinger, to realize that Simon's discovery comprised of long chains of styrene molecules, and was a plastic polymer. In 1922, Staudinger published his theories on polymers, stating that natural rubbers were made up of long repetitive chains of monomers that gave rubber its elasticity. He went on to write that the materials manufactured by the thermal processing of styrene were similar to rubber. In 1953, the Nobel Prize for Chemistry was awarded to Hermann Staudinger for his research. In 1930, the scientists at Badische Aniline & Soda-Fabrik (BASF) developed a way to manufacture polystyrene commercially. The Styrofoam is actually the most recognizable form and it was developed for Dow Chemical Co. in the U.S.

#### **2.1.2 Styrene-co-Maleic Anhydride**

The poly(styrene-co-maleic anhydride) (SMA) polymers are often used in blends or composites where interaction or reaction of the maleic anhydride provides desirable interfacial effects. The SMA is used in the automotive industry, primarily for interior parts. In general terms, there are two SMA types in the market, SMA(7) and SMA(14) with 7 and 14 weight percent of maleic anhydride units respectively. SMA® resins



from Sartomer Company are low molecular weight styrene/maleic anhydride copolymers. As there are most hydrophilic, SMA resins form high solids solutions in alkaline conditions and can be used to produce pigment dispersions, ink and overprint varnishes. Hydrophobic SMA resins are used as surface sizing compounds for paper and cross-linking agents for powder coatings and printed wiring boards. SMA resins are supplied commercially in solid form, either as powder or flake, or in liquid form, either as aqueous ammonium or sodium salt solutions.

### 2.1.3 Properties of Polystyrene and Poly(styrene-co-maleic anhydride)

Table N<sup>o</sup>1 shows a summary of the physical, chemical and thermal properties of the polystyrene and poly(styrene-co-maleic anhydride).

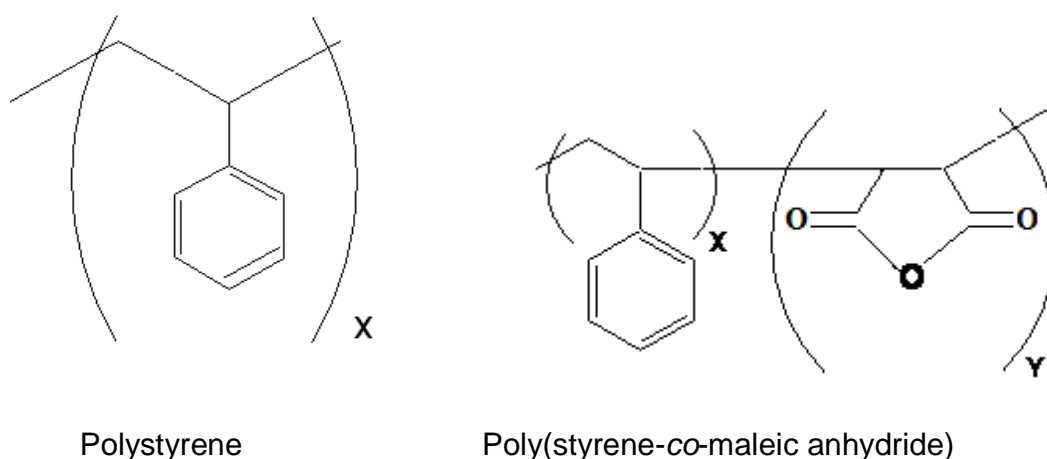


**Figure 2.1:** Structure of Polystyrene, Poly(styrene-co-maleic anhydride).

**Table 2.1:** Overview of the properties of polystyrene and poly(styrene-co-maleic anhydride) [4, 5].

Properties	Polystyrene	Poly(styrene-co-maleic anhydride)(7% wt MA)
<b>Molecular Formula</b>	C <sub>8</sub> H <sub>8</sub>	C <sub>8</sub> H <sub>8</sub> -C <sub>4</sub> H <sub>2</sub> O <sub>2</sub>
<b>(repeat unit)</b>		
<b>Fw (g/mol)</b>	104,15	S(104.15)
<b>(repeat unit )</b>		MA(78.01)
<b>ρ (g /cm<sup>3</sup>)<sup>25°C</sup> (Monomer)</b>	0.906	
<b>ρ (g /cm<sup>3</sup>)<sup>25°C</sup> (Polymer)</b>	1.047	1.08
<b>Tg (°C)</b>	100	124,4
<b>Tm (°C)</b>	200 - 250	230 - 270
<b>Tensile Strength (MPa)</b>	34	52
<b>Flexural Modulus (GPa)</b>	3	2. 3
<b>Elongation at Break (%)</b>	1.6	1.8
<b>Strain at Yield (%)</b>	1.4	2
<b>Max. Operating Temp. (°C)</b>	50	75
<b>Water Absorption (%)</b>	0.05	0.1
<b>Oxygen Index (%)</b>	18	19
<b>Appearance</b>	White powder or beads, or clear solid	Colorless, may be transparent
<b>Polymer Type</b>	Thermoplastic	Resins - Thermoplastic
<b>Characteristic</b>	Cheap, rigid, Brittle, good electrical properties, poor chemical resistance (organics)	Heat resistance. Similar price to ABS Limited chemical and UV resistance and is flammable

## **2.2 Synthesis of PS and SMA and Polymer Structures**

The polymerization reaction is the process of joining together small molecules by covalent bonds to produce high-molecular-weight polymers. Both natural and synthetic polymers are built from these simple units known as monomers, however, the range of properties that can be achieved depends on the strategy used to assemble these units. There are basically two approaches to polymer formation: chain growth and step growth polymerization. Chain growth polymerization involves combining monomers starting from a single reactive site and growing the polymer chain from that site. The reactive site can be a cation, an anion, or a radical. The type of chain growth polymerization selected depends on the monomers to be used and the requirements of the target polymer. Among the recent inventions in polymerization chemistry has been living polymerization which permits the growth of polymers with almost identical molecular weights and enables the creation of block copolymers or other polymers with well-controlled structures [6].

### **2.2.1 Synthesis of Polystyrene**

#### **Anionic Polymerization**

Synthesis of well-defined and copolymers with predetermined molecular weights, low polydispersities, precisely controlled end group functionalities and chain topologies is the ultimate target of preparative polymer chemistry [7]. In principle, such macromolecules can be made by living polymerization. Living polymerization was first defined by Szwarc [8] as a chain growth process without chain breaking reactions (transfer and termination). Such a polymerization provides end group control and

enables the synthesis of macromolecules with important architectures such as block copolymer by sequential monomer addition. Anionic polymerization is a living polymerization method which is considered as an important class of polymer-forming reactions. Although living polymers can be prepared through several mechanisms, anionic polymerization to date represents the most successful commercial application. Ionic polymerization, similar to radical polymerization, also has the mechanism of a chain reaction. The kinetics of ionic polymerization are, however, considerably different from that of radical polymerization:

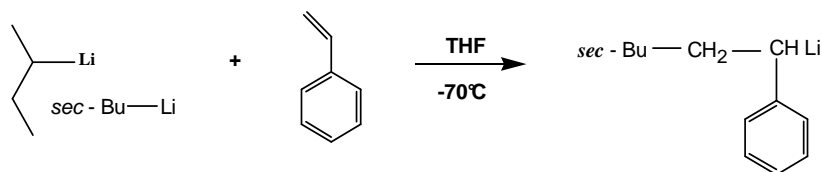
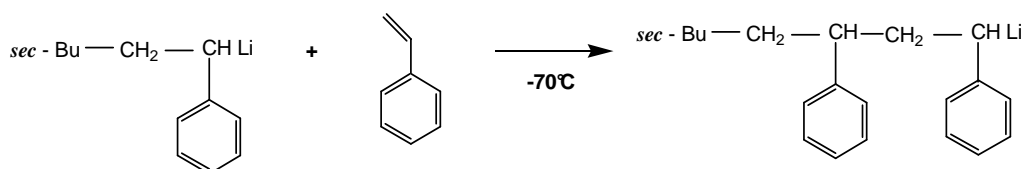
**The initiation reaction** of ionic polymerization needs only small activation energy. Therefore, the rate of polymerization depends only slightly on the temperature. Ionic polymerization occurs in many cases with explosive violence even at temperatures below 50°C (for example, the anionic polymerization of styrene at -75°C in tetrahydrofuran, or the cationic polymerization isobutylene at -100°C in liquid ethylene) [9,10].

**The propagation kinetics** for styrene polymerization with lithium as the counterion has been studied in both aromatic and aliphatic solvents. In the propagation step the rate is depended on the concentration of living polymer of this due to the association of the living polymer chains into dimers in hydrocarbon solvents. These dimers are not reactive for monomer addition and consequently a dissociation step to unassociated living chains is required [11].

**Termination.** With polymerization there is no compulsory chain termination through recombination, because the growing chains can not react with each other. Chain termination takes place only through impurities, or through the addition of certain compounds such as water, alcohols, acids, amines, or oxygen, and in general through compounds which can react with the polymerizing ions under the formation of neutral compounds or inactive ionic species.

In general terms, the rate of initiation is much faster than the rate of propagation; each initiator should start one polymer chain. If all these chains start at time zero and consume all the monomer during growth, a narrow molecular-weight distribution results. The number-average degree of polymerization is given by  $x_n = [M] / [I]$  where  $[M]$  is the initial monomer concentration and  $[I]$  is the initial initiator concentration both given in moles per unit volume.

When sec-butyl lithium is added to a monomer solution, the rate of both initiation and propagation depends on monomer concentration. If however, the initiator is "seeded" by adding some monomer and then added to the remaining monomer, only the propagation step is observed. Under these circumstances, the reaction is first order in monomer concentration [6]. See figure N 2.2.

**Initiation****Propagation****Termination**

**Figure 2.2:** Synthesis of polystyrene via anionic polymerization.

### 2.2.2 Synthesis of Poly(styrene-co-maleic anhydride)

If one polymerizes a mixture of different monomers, one usually obtains macromolecules whose structure contains all the monomers that are present in the reaction mixture. However, one should not expect that these monomers are present in the same ratio in the polymer molecules as in the monomer mixture. In an extreme case, one might even obtain on polymerizing a mixture of two monomers, M1 and M2, polymer molecules which consist exclusively of monomer M1 and other polymer which consist exclusively of monomer M2. In the case of SMA, fig. 2.3, the pairs  $M1, r_1$ , represents the styrene monomer, M1, and reaction rate of styrene ( $r_1$ ) and  $M2, r_2$ , and maleic anhydride monomer, M2, and reaction rate of maleic anhydride,  $r_2$ , one of the monomers does not polymerize by itself, or only very slowly (M2), and

then  $r_2$  becomes 0, maleic anhydride ( $r_2 = 0$ ). In such cases the polymerization stops as soon as the other monomer has been used up by azeotropic copolymerization. This is found to be the case with mixtures of styrene and maleic anhydride, remain as unconverted monomers. If more than 50 mol % styrene is present in the monomer mixture, then one obtains homopolymerization in addition to the M1-co-M2 copolymers. Figure 2.3, shows the copolymerization diagram for the system styrene ( $r_1$ ) / maleic anhydride ( $r_2$ ) ( $r_1 = 0.0095$  and  $r_2 \cong 0$ ), where  $r_1$  and  $r_2$  correspondent reaction rate in mol / liter / second of the each monomer during the polymerization process. In this case one finds a degenerate inflection

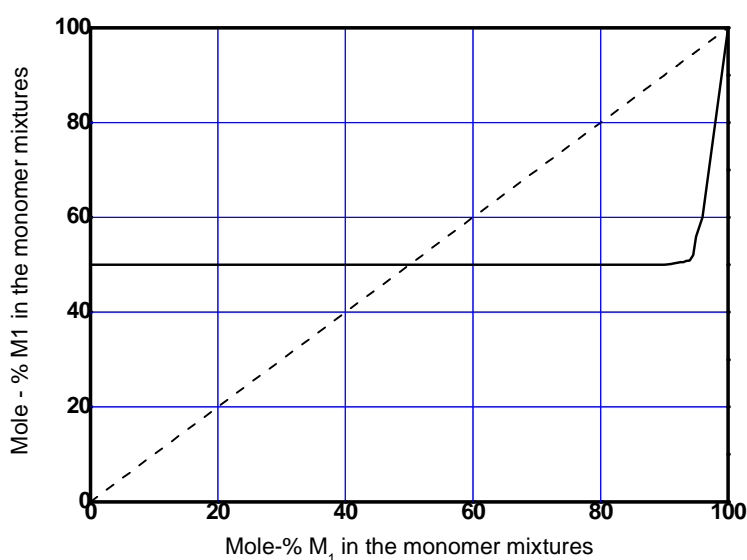


**Figure 2.3:**  
Copolymerization diagram for the system styrene / maleic anhydride ( $r_1 \approx 0.0095$ ,  $r_2 \approx 0$ ) [9].

curve where the inflection point is lengthened to an inflection tangent parallel to the x-axis. The curve shows that over a wide range one obtains copolymer with the same composition of styrene and maleic anhydride independent of the composition of the monomer mixture. This is the results of the strong alternating tendency of the system. If both parameters ( $r_1$ ,  $r_2$ ) are equal to 0, then one straight line parallel to the x-axis at

$d[M_1]$ -concentration = 50%. This is true for monomer pairs (Styrene and Maleic Anhydride) where each of the two monomers is unable to polymerize by itself. The chains of the copolymers resulting from such systems have a completely regularly alternating sequence of the structural units  $M_1$  and  $M_2$ , regardless of the composition of the monomer mixtures. Thus, while listed values of  $r_1 = 0$  and  $r_2 = 0$  for the preparation of copolymers with alternating structure depends entirely on the absolute magnitude of the corresponding reaction rate constants  $k_{12}$ , which represent, first the polymerization of styrene (1) and then maleic anhydride (2), and draw an analogy  $k_{21}$ , represent the polymerization of maleic anhydride (1) and then the styrene (2). It also happens that one of the monomers (for examples, maleic anhydride) is not polymerizable in the usual laboratory experiment, and that  $k_{11}$  is not exactly 0, but is very small [9].

In another side, the copolymerization of styrene with maleic anhydride creates a copolymer (SMA) which has a higher glass transition temperature than polystyrene and is chemically reactive with certain functional groups, especially with primary amines. SMA copolymers are available as base polymers in various styrene to maleic ratios (from 1:1 to 4:1 and beyond), and as partial monoesters. Altering the styrene to maleic anhydrides ratio changes the hydrophilic / hydrophobic balance of the polymer. As a representative of an alternating copolymer, poly(styrene-co-maleic anhydride) has been in focus to study the behavior of the copolymerization [11-13].



### 2.2.3 Polymeric Structure of the PS and SMA

Molecular architectures of polymers may be of a broad variety: a polymer can possess a linear or branched pattern, and at the same time be made up of identical monomer units (homopolymer) or a mixture of two or more monomers (copolymer, terpolymer, etc). Furthermore, the individual molecules may be covalently linked into a cross-linked macroscopic network. An important consequence is that branching interferes with the ordering of molecules, so that crystallinity decreases. Also, the melt flow properties and elastic behavior of polymers are greatly influenced by the degree of branching and the size of the branches. In the figure 2.4, different polymer architectures are shown [6].

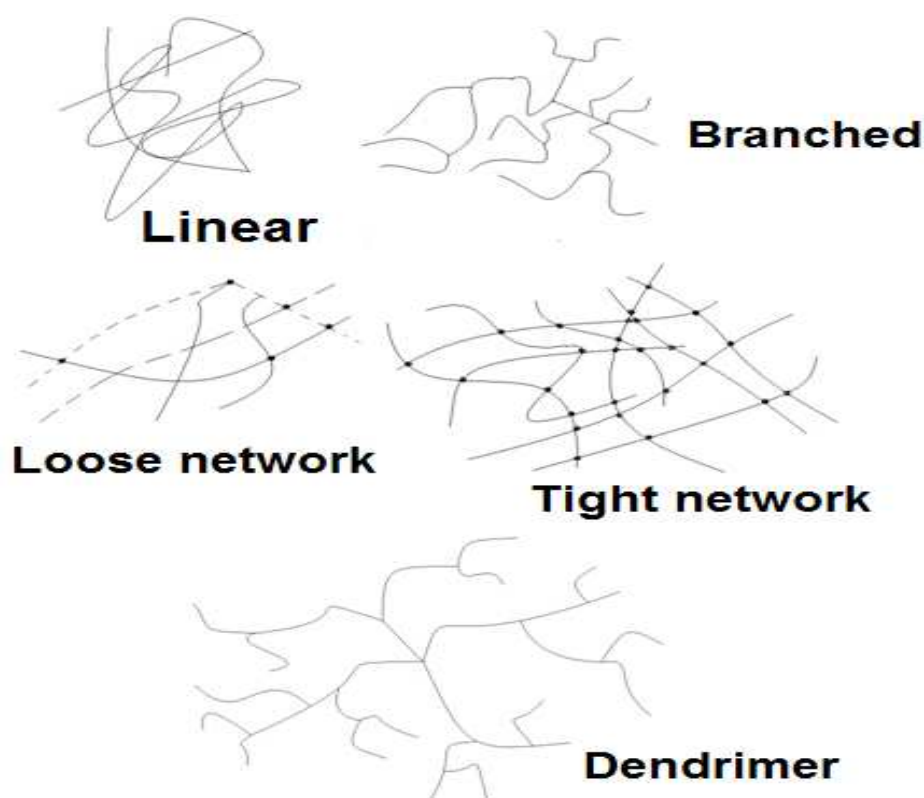


**Figure 2.4:** Polymer Structures.

## 2.3 Chemical Modification of PS and SMA: Grafting - Functionalization

### 2.3.1 Functionalization

A monomer can be converted to a polymer by any reaction that creates new bonds. Fundamental to any polymerization scheme is the number of bonds that a given monomer can form, examples are given in figure 2.5.

In principle, the synthesis of chain-like macromolecules always occurs through the reaction of bi-functional components with each other. This does not mean that the formation of macromolecules requires the monomers to have two preformed functional groups. Often the bi-functional character of the monomers arises only with the addition of an initiator, as for example, with vinyl compounds.

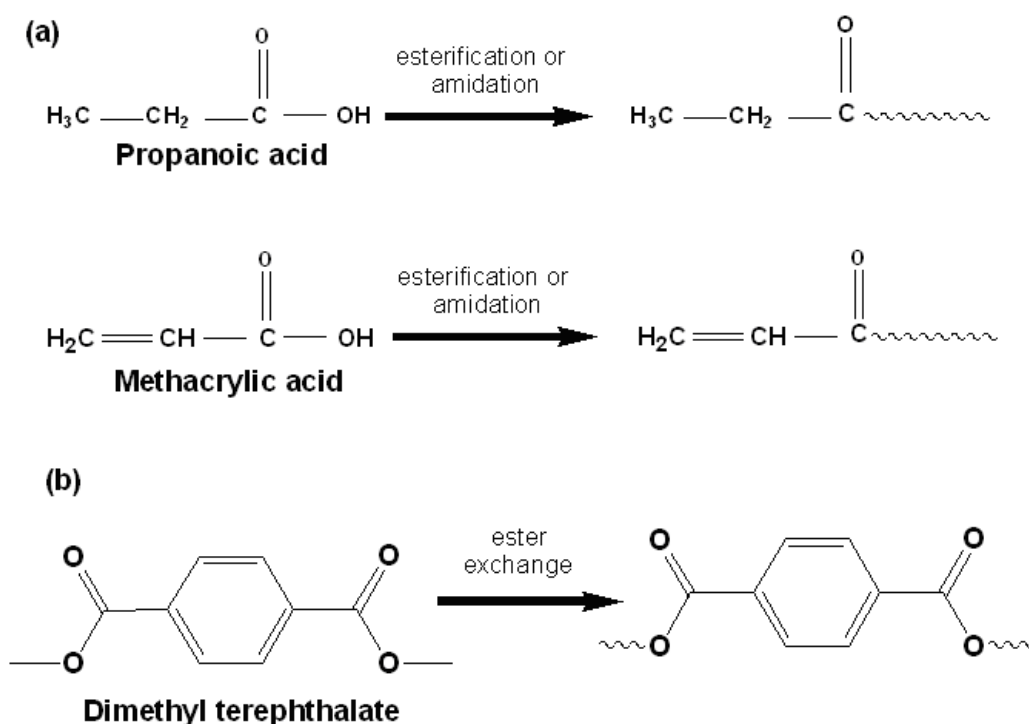


**Figure 2.5:** Functionality and structure. (a) Functionality via esterification or amidation, (b) Functionality via ester exchange [6].

### 2.3.2 Graft-Copolymers

A graft copolymer comprises a backbone species and a side chain species. The side chains “units” are different from those comprising the backbone chain. The name of a graft copolymers of A and B is written as



Although many of the block copolymers reported are actually highly blocked, some of the most important “graft copolymers” described in the literature have been shown to be only partly grafted, with much homopolymer being present. To some extent, then, the term *graft* copolymer may also mean, “polymer B synthesized in the immediate presence of polymer A”. Only by reading of the context can the two meanings be distinguished.

The “graft-copolymers” are soluble, at least in the ideal case. A conterminously grafted copolymer has polymer B grafted at both ends, or at various points along the structures to polymer A, and hence it is a network and not soluble (see structure (f) in figure 2.6). (a) A polymer blend, not chemically bonded together. (b): A graft copolymer (c): Block copolymer (d): A semi-interpenetrating polymer network constituted by an entangled combination of two polymers (e): An interpenetrating polymers network (f): A conterminously linked polymer, constituted by having the polymer II species linked, at both ends, onto polymer I.

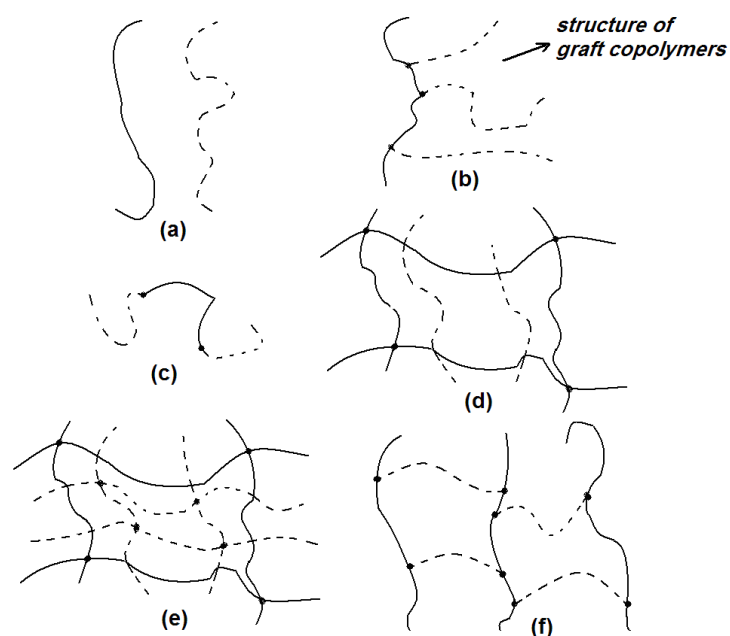
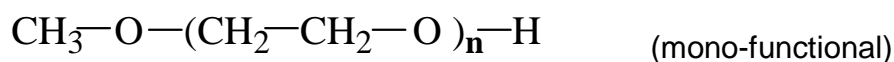


**Figure 2.6:** Six basic modes of linking two or more polymers are identified [6].

#### 2.4 Polyethylene Glycol: Structure and Characteristics

Poly(ethylene glycol) (PEG), also known as poly(ethylene oxide) (PEO) or polyoxyethylene (POE), is the most commercially important polyether. PEG, PEO or POE refers to an oligomer or polymer of ethylene oxide. The three names are chemically synonymous, but historically PEG has tended to refer to oligomers and polymers with a molecular mass below 20,000 g/mol, PEO refers to polymers with a molecular mass above 20,000 g/mol, and POE refers to a polymer of any molecular mass [14]. PEG and PEO are liquids or low-melting solids, depending on their molar masses. PEG's are prepared by polymerization of ethylene oxide and are commercially available over a wide range of molecular weights from 300 to 10,000,000 g/mol. While PEG and PEO with different molar masses find use in different applications and have different physical properties (e.g. viscosity) due to

chain length effects, their chemical properties are nearly identical. Different forms of PEG are also available dependent on the initiator used for the polymerization process. Their melting points vary depending on the molar mass of the polymer. PEG or PEO have the following structure:

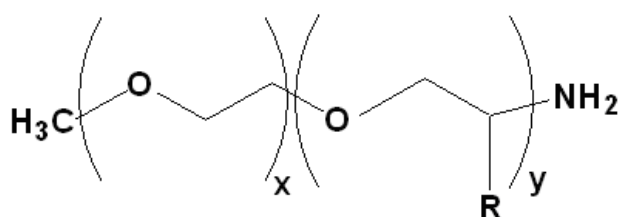


The numbers that are often included in the names of PEG's indicate their average molar masses, e.g. a PEG with  $n = 80$  would have an average molecular weight of approximately 3500 g/mol and would have been labeled PEG 3500. The block copolymers containing hydrophilic poly(ethylene oxide) (PEO) sequences together with hydrophobic segments have attracted considerable interest due to the remarkable properties of PEO chains [6,9].

## 2.5 Poly(ether amines): Jeffamine (Mono-functional) Applications,

### Properties and Reactions

A range of the polyetheramines is commercially available as "Jeffamine" (jeffamine®series). They contain a primary amino group attached to the end of a polyether chain. The polyether is normally based on either propylene oxide (PO), ethylene oxide (EO), or mixed PO/EO. Thus they are called "Polyetheramines". Historically, the Jeffamine polyetheramine family consisted of monoamines, diamines, and triamines based on this core structure, figure 2.7.



R = H for (EO), or CH<sub>3</sub> for (PO)

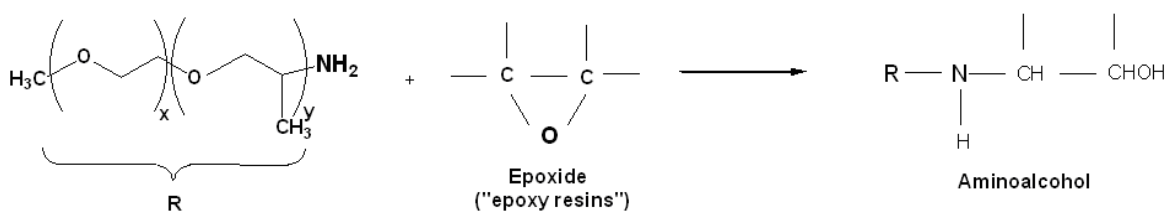
Polyetheramines	M (g/mol)	PEO / PPO Mol ratio	PEG (%)	Tm (°C)
XTJ 505	600	1/9	10	-40
XTJ 506	1000	19/3	86	29
M-2070	2000	31/10	76	17

**Figure 2.7:** Structures and characteristics of polyetheramines (Jeffamine mono-amine) [16]. Tm: melting temperature, M: molecular weight.

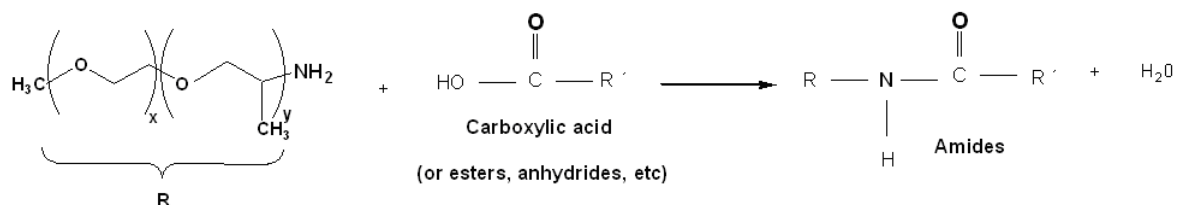
### 2.5.1 Reactions of Poly(ether amines) (Jeffamine)

The polyetheramines undergo reactions typical of primary amines. General reactions which have proved to be useful include:

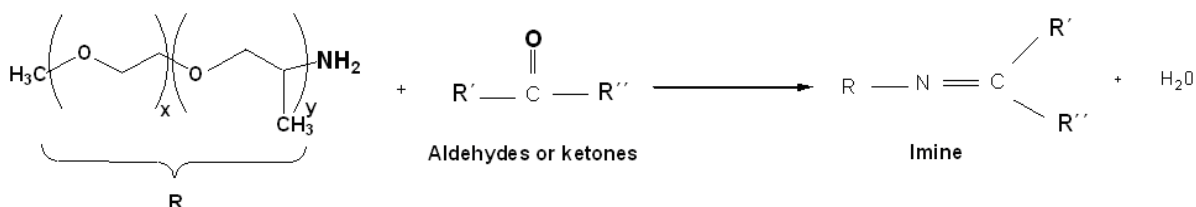
- (a) **Epoxy reactions** occur by the non-catalyzed addition of epoxides to Jeffamine. These alkoxyate react with each NH<sub>2</sub> functionality to produce aminoalcohols.



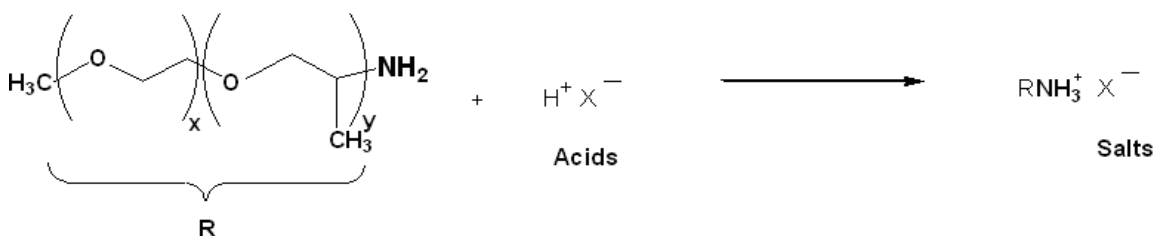
(b) **Amides** can be formed from Jeffamine by an acid-catalyzed reaction with carboxylic acids, lactams, anhydrides, or by ester-amide interchange reactions.



(c) **Imines** are formed by reacting Jeffamine amines with aldehydes or ketones, at elevated temperatures, while removing water.



(d) **Salts** of Jeffamine amines may be readily formed with a variety of organic and inorganic acids.



### 2.5.2 Direct amidation

In general, direct amidation is a reaction based on the attack of the amine on carboxyl acid or anhydride group. This reaction has the same rate as esterification, but in the amidation case the equilibrium is much favorable for product formation [17, 18], figure 2.8. One of the most reported examples is the direct amidation of carboxylic group with ammonia, however, only harsh chemical conditions (200°C, 7

bar pressure) have been described in an organic solvent at low temperature [19], more recently the amidation is used to improve single-walled carbon nanotube through of the direct amidation of terminal carboxylic group [20]. The amidation reaction on maleic anhydride, maleic acid and fumaric acid has been fully reported in the literature by Felthouse *et al* [18]. In this work a direct amidation on anhydride group content in poly(styrene-co-maleic anhydride) is used. In the chapter 4.1.2 the direct amidation conditions used in this work are described in detail.

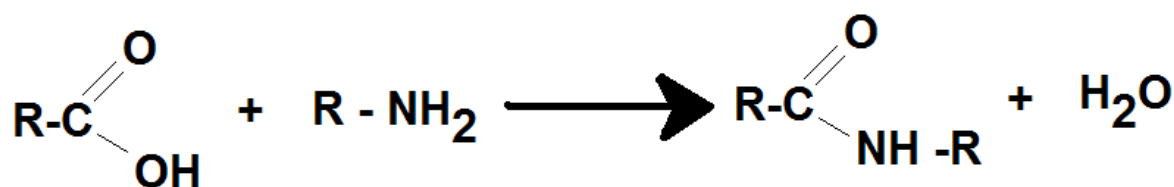


Figure N°2.8: Direct amidation

### 2.5.3 Properties and Applications of Jeffamine

The jeffamine polyetheramines undergo typical amine reactions, often imparting increased flexibility, toughness and low viscosity. The wide range of molecular weight, amine functionality, repeating unit type, and distribution can provide flexibility in the design of new compounds or mixtures see table 2.2.



**Table 2.2:** Poly(ether amine) properties [16]

Polyetheramines	$\rho^{25^\circ\text{C}}$ (g/mL)	mp (°C)	Primary Amine (% min)	Total Amine (% min)	H <sub>2</sub> O <sub>max</sub> (%)
<i>XTJ 505</i>	0.979	- 40	95	1.58 – 1.79	0.35
<i>XTJ 506</i>	1.066*	29	90	0.94	0.25
<i>M-2070</i>	1.072	17	95	0.45	0.25

(\*) measured at 38°C., mp = melting point,  $\rho^{25^\circ\text{C}}$  = density at 25°C.

## 2.6 Graft-Copolymers via Sulfonation

Graft copolymers, containing hydrophilic side chains, have been used in many industrial applications [21], for example, applications of graft or comb-like copolymers in the construction sector [22,23]. Academically, many papers were published on the subject of graft copolymers containing polyethylene glycol (PEG) and polyethylene glycol monomethyl ethers (mPEG) segments as a side chains [24-26]. One area of significant interest is the development of new methods for grafting PEG to backbone polymers [27-29]. Poly(styrene-co-maleic anhydride) sulfonate-polyetheramines should be a option as a new graft copolymer to be applied as a membrane in gas separation because the material is keeping the original mechanical properties of SMA and the sulfonate amine group is supplying the PEG-segment for the permeability of CO<sub>2</sub> into the membrane via gas solubility. Recently, there is considerable interest for the development of polyelectrolyte membrane as key component for fuel cells [30-32] but there is not sufficient information of graft copolymer for gas membrane separation. Various sulfonating methods of polystyrene have been proposed [33-35]. In this work

acetyl sulfate methods are used to obtain sulfonated polystyrene according to the literature [36-38].

- **Challenges of the Synthesis of Graft-Copolymer via Sulfonation.**

Generally, the sulfonation of high polymers as a method for the preparation of sulfonated ionomers displays the following basic problems: (i) a not random distribution of inserted  $\sim\text{SO}_3\text{H}$  groups along the PS chain; (ii) a possible chain-to-chain interaction that produces heterogeneity; (iii) the sulfonation proceeds with significant polymer degradation and (iv) the characterization of sulfonated polystyrene (PS –  $\text{SO}_3\text{H}$ ) could be complicated. The sulfonation of polystyrene with a relative low content of maleic anhydride should also be an interesting challenge during the development of this work, due to a competition between two possibilities: (a) the sulfonation of the benzenic ring or (b) the interaction of the  $\sim\text{SO}_3\text{H}$  group with the maleic anhydride group.

## **2.7 Membrane Based for Gas Separation. Theory models**

A membrane is an inter-phase that separates two phases and that may be acting as a selective material, regulating the transport of substances between those compartments. The most important property of the membrane is their ability to control the rate of the permeation of different gases. The two models used to describe the mechanism of permeation are illustrated in figure 2.9, the solution-diffusion and the pore-flow.

### **2.7.1 Solution-Diffusion Model**

In the solution-diffusion model the gas is assumed to dissolve in the membrane material and then to diffuse through the membrane with concentration gradients to the low pressure side, where the gas is desorbed. It is further assumed that sorption and desorption at the interfaces is fast compared to the diffusion rate through the polymer. The gas phase on the high and low pressure is in equilibrium with the polymer interface.

The gases are separated because of their different solubility coefficients in the membrane and the differences in the rates at which the materials diffuse through the membrane.

### **2.7.3 The Pore-Flow Model**

In this model, the gases are transported by pressure-driven convective flow through tiny pores. Separation occurs because one of the gases is excluded (filtered) from some of the pores in the membrane through which other gases move.

During the 1940s the pore-flow model was more accepted but after these years, the solution-diffusion model was used to explain transport of gases through dense non-porous polymer films. In the cases of reverse osmosis, the pore-flow model was hardly debated in the 1960s until 1970s [39-43]. Actually the solution- diffusion model is the most used to explain the transport mechanism phenomenon in membrane materials.

Diffusion, the basis of the solution-diffusion model, is the resulting of the series net molecules interaction which the matter it's transported from a region the higher concentration to other with lower concentration. Many researches believe that transportation is consequence of the constant random molecular motion because the frequently collision other considerate that in the case of large molecules they drive by collisions with solvent particles.

Diffusion is a time-dependent process, constituted by random motion of individual molecules causing statistical distribution of theses molecules, however after a period of time is difficult to have an explanation of the phenomenon due to that unclear individual molecule move. In general the diffusion is tied to notion of mass transfer, driven by a concentration gradient. A diffusion process example is shown when two adjacent systems with different gas concentration are separated by an interface, due to this difference in the number of molecules, a number of molecules will move from concentrated side to the less concentrated side across the interface. In 1855 Adolf Fick introduced the Fick's Law of diffusion, which governs the diffusion of a gas across a membrane [44]. In a diffusion process, the mass transfer velocity is proportional to the concentration gradient: inside the membrane, the flow of species (*i*) is given by Fick's law [45,46].

$$J_i = -D_i \frac{dc_i}{dx} \quad (2.1)$$

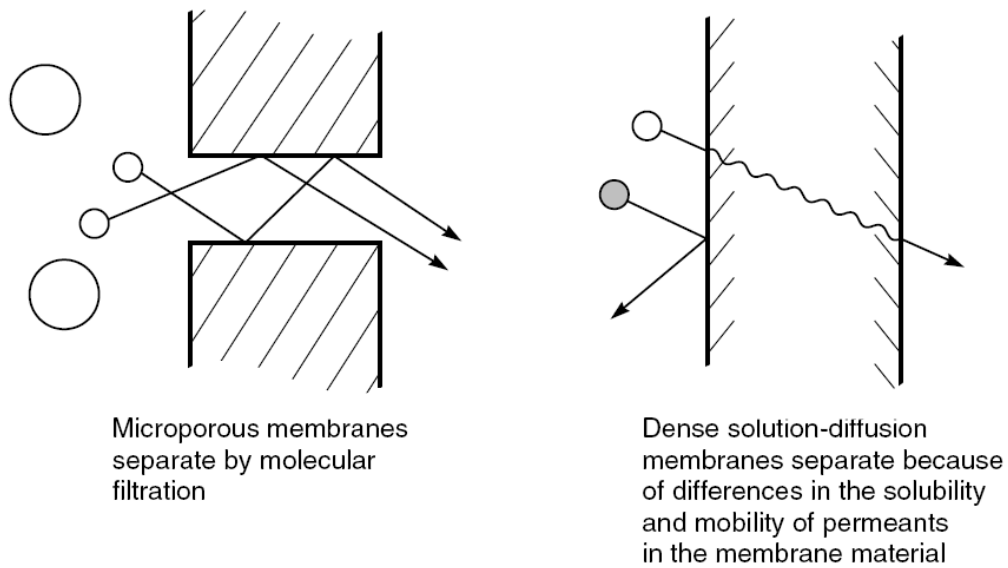


**Figure 2.9:** Molecular transport through membranes can be described by a flow through permanent pores or by the solution-diffusion mechanism reproduced from[45].

In equation (2.1)  $J_i$  is the rate of transfer of species  $i$  or flux ( $\text{g}/\text{cm}^2\cdot\text{s}$ ),  $dc_i/dx$  the concentration gradient of species  $i$  and,  $D_i$  is the diffusion coefficient ( $\text{cm}^2/\text{s}$ ); a measure of the mobility of the individual molecules. The minus sign shows that the direction of diffusion is down the concentration gradient. Assuming equilibrium at the interface for gases with low solubility in the membrane material, Henry's law, which relates concentrations,  $C_i$ , to partial pressure ( $p_i$ ) through the solubility coefficient  $S_i$ , can be used

$$C_i = p_i \times S_i \quad (2.2)$$

The partial pressure at the interface is assumed to be equal to that of the gas stream, neglecting the gas-film resistance. For a mixture of two species 1 and 2, substitution into equation (2.1) and integration yield.

$$J_1 = \frac{D_1 \times S_1}{l} (p_{f,i} - p_{p,i}) \quad (2.3)$$

where  $l$  is the membrane thickness,  $p_{f,i}$  and  $p_{p,i}$  are the partial pressures of gas 1 in the feed flow and in the permeate flow, respectively. The product  $D_1 \times S_1$  is the permeability and represents the ability of the species to cross the membrane. Gas separation by a membrane is a solution/dilution process: which gases dissolve in the membrane and diffuse through it at different rates, depends on their solubility in the material and the respective diffusivity. Hence the flowrate of  $i$  through a polymeric membrane,  $J_i$ , can be written as

$$J_i = Q_i (p_{f,i} - p_{p,i}) \quad (2.4)$$

Where  $Q_i$  is the membrane permeance for the gas  $i$  and  $p_{f,i}$  and  $p_{p,i}$  are the partial pressures of the gas  $i$  respectively, already defined in (2.3). Comparing equations (2.3) and (2.4) the membrane permeance is given by

$$Q_i = \frac{D_i \times S_i}{l} \quad (2.5)$$

Hence, permeance is the ratio between the product of the diffusion and the solubility in the membrane material for each individual gas  $i$ ,  $D_i$  and  $S_i$  respectively, and membrane thickness,  $l$ . Permeability is a function of pressure, temperature and gas mixture composition.

In the ideal case selectivity is defined as

$$\alpha = \frac{D_1 \times S_1}{D_2 \times S_2} \quad \text{or} \quad \alpha = \frac{P_1}{P_2} \quad (2.6)$$

Normally, the permeance increases with temperature, typically following the Arrhenius relationship between diffusion coefficient and temperature [47]. However, the solubility ( $S$ ) of gases generally decreases meanwhile the diffusion ( $D$ ) increases with increasing temperature. Hence,  $D$  and  $S$  follow in opposite directions.

Pressure-driven convective flow, the basis of the pore flow model, is most commonly used to describe flow in a capillary or porous medium [48]. The basis equation covering this type of transport is Darcy's law, which can be written as

$$J_i = K' C_i \frac{dp}{dx} \quad (2.7)$$

where  $dp/dx$  is the pressure gradient existing in the porous medium,  $C_i$  is the concentration of component  $i$  in the medium and  $K'$  is a coefficient reflecting the nature of the medium. Equation 2.7 can be integrated across the membrane to give Darcy's law in a different form

$$J_i = \frac{k (p_o - p_l)}{l} \quad (2.8)$$

where  $(p_o - p_l)$  represents the difference in pressure across the membrane,  $l$  is the membrane thickness,  $k$  is the Darcy's law coefficient, which represents the contribution of temperature, concentration, electromotive forces and can be reduced to chemical potential gradients.

In general, convective-pressure-driven membrane fluxes are high compared with those obtained by simple diffusion. The difference between the solution-diffusion and pore-flow mechanisms lies in the relative size and permanence of the pores. For membranes in which transport is best described by the solution-diffusion model and Fick's law, the free-volume elements in the membranes are tiny spaces between polymer chains caused by thermal motion of the polymer molecules (Note that the pores are not necessarily identical to the free volume. The dense membranes have no pores, but they still have a free volume). These volume elements appear and disappear on about the same timescale as the motions of the permeants traversing the membrane. On the other hand, for a membrane in which transport is best described by pore-flow model and Darcy's law, the pores are relatively large and fixed, do not fluctuate in position or volume on timescale of permeant motion, and are connected to one another. The larger the individual free volume elements (pores), the more likely they are to be present long enough to produce pore-flow characteristic in the membrane. As a rough rule of thumb, the transition between transient (solution-diffusion) and permanent (pore-flow) pore is in the 5 – 10 Å diameter range.



The average pore diameter in a membrane is difficult to measure directly and must often be inferred from the size of the molecules that permeate the membrane or by some other indirect technique. With this caveat in mind membranes can be organized into the three general groups shown in figure 2.10.

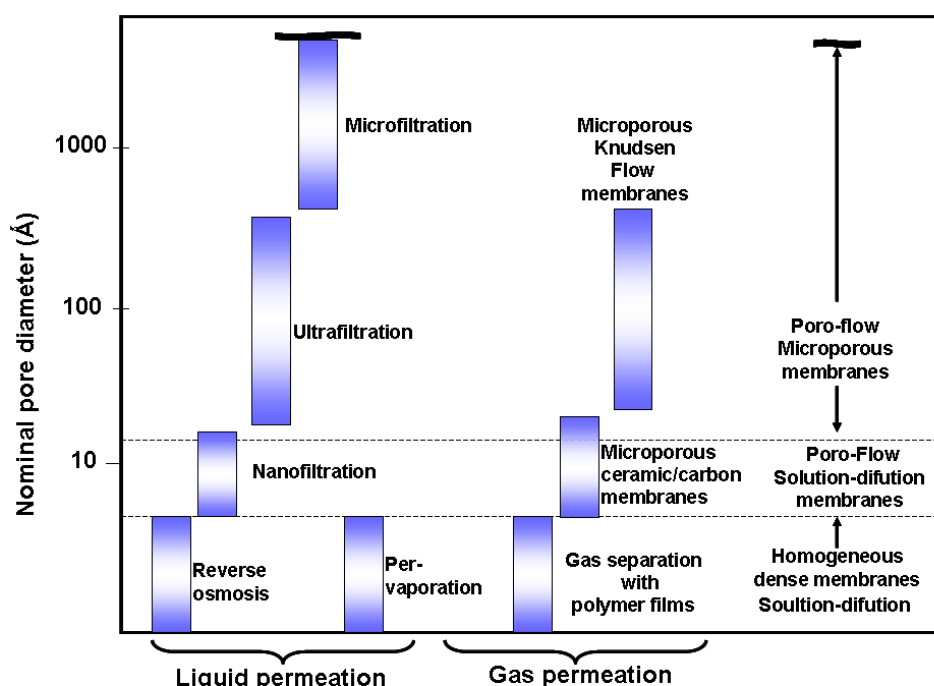


**Figure 2.10:** Schematic representation of the nominal pore size and best theoretical model for the principal membrane separation processes [45].

The solution-diffusion model applies to gas permeation in polymer films and it is associated with the phenomena of transport of gases down a pressure or concentration gradient. However, the process involves diffusion of molecules in a dense polymer. The pressure, temperature, and composition of the fluids on either side of the membrane determine the concentration of the diffusing species at the membrane surface in equilibrium with the fluid.

## **2.8 Polymers Structures, Materials and Types of Membranes**

A synthetic membrane can be fabricated from organic and/or inorganic materials including solids such as metals or ceramics, homogenous films (polymers), heterogeneous solids (polymer blends, mixed glasses), and liquids [49].

Inorganic materials such as aluminum oxides, silicon carbide, and zirconium oxide are base to produce ceramic membranes. They are very resistant to the action of aggressive media (acids, strong solvents) and stable chemically, thermally, mechanically, and biologically inert. Liquid membranes refer to a synthetic membrane made of non-rigid material and can be encountered in industry as: hollow-fiber containing liquid membranes, liquid membranes, emulsion liquid membranes, immobilized (supported), molten salts, and [49].

Polymeric membranes are very competitive in performance and economic aspects [49]. Some polymers are commercially available, but the choice of membrane polymer is not trivial. The polymer sometimes has to offer a low binding affinity for separated molecules (as in the case of biotechnology applications), and has to withstand the severe cleaning conditions. It must be compatible with chosen membrane fabrication technology. The polymer has to be a suitable membrane former in terms of its chains rigidity, chain interactions, stereo-regularity, and polarity of its functional groups. It can form amorphous and semi-crystalline structures, affecting the membrane performance characteristics. The polymer material has also to be synthesized at low prizes to comply with the low cost criteria of membrane separation process. Many membranes polymers are based on grafted, custom-modified, or produced as copolymer to improve their properties [50]. The most

common polymers in membrane synthesis are cellulose acetates, nitrates, among other cellulose esters (CA, CN, and CE), polysulfone (PSU), polyether sulfone (PESU), polyacrylonitrile (PAN), polyamide (PA), polyimide, polyethylene and polypropylene (PE and PP), polytetrafluoroethylene (PTFE), polyvinylidene fluoride (PVDF), polyvinylchloride (PVC), see figure 2.11.

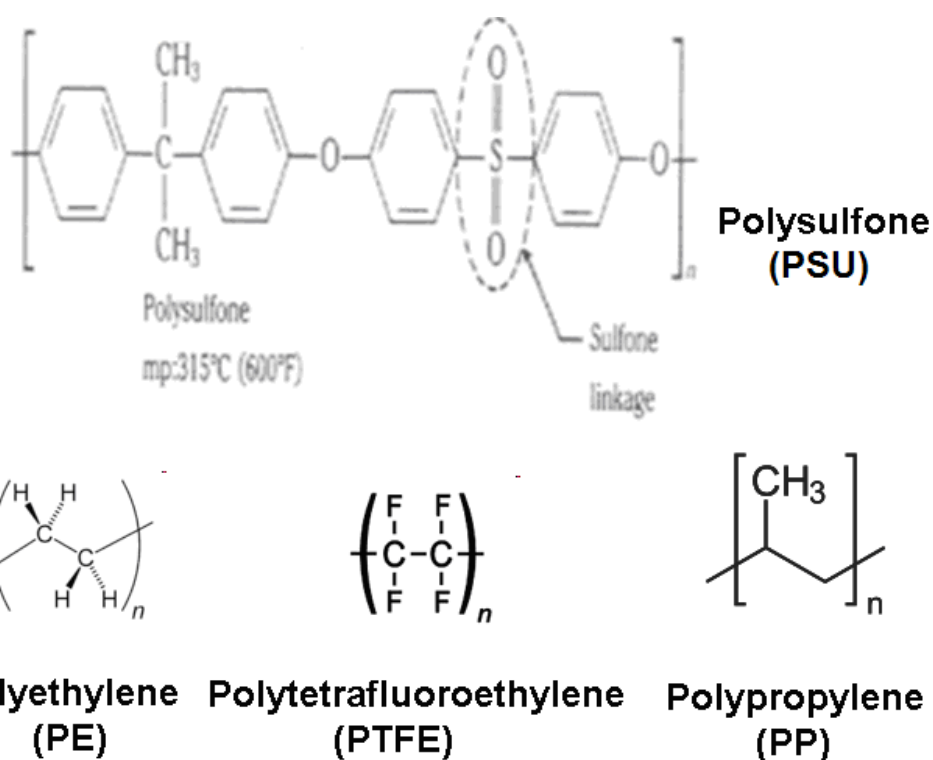


**Figure 2.11:** Some polymer applicable in membrane preparation.

Polyimides exhibit excellent gas separation performance and good physiochemical properties. Therefore, polyimide membranes have been extensively explored for their potential applications in natural gas purification. Molecular tailoring of polyimides is one approach that is utilized in the search for better membranes materials for  $\text{CO}_2 / \text{CH}_4$  separation. The molecular design of polyimides system whereby the chemical

constituents and configurations of the dianhydrides and/or diamines used for polyimide synthesis are varied in a systematic manner. The other category is the chemical fusion (copolymerization) of polyimides with polymers from other classes [51].

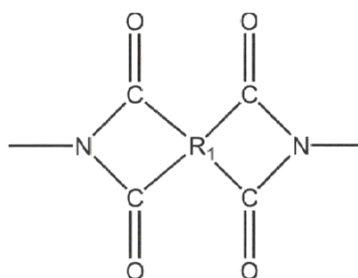


**Figure 2.12:** Chemical structure of polyimides

## 2.9 Membranes Preparation and Classification by Morphology

Different methods of polymer membrane preparation have been covered in several reviews and books [52-55]. Membranes can be classified, according to their morphology as shown in Figure 2.13.

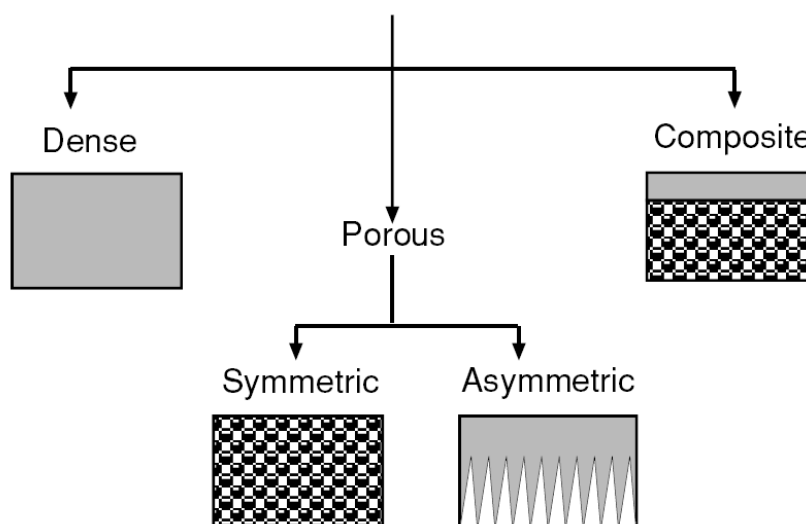


**Figure 2.13:** Membrane classification according to the morphology reproduced [53].

Synthetic membranes may be manufactured using organic and/or inorganic materials; they may be homogeneous or heterogeneous, symmetrical or asymmetrical, porous or dense, electrical neutral or charged; they may exhibit isotropic or anisotropic properties.

Dense and porous membranes are distinct from each other based on the size of separated molecules. Dense membranes are usually a thin layer of dense material utilized in the separation processes of small molecules (usually in gas or liquid phase). Dense membranes are widely used in industry for gas separations and reverse osmosis applications. Dense membranes can be synthesized as amorphous or heterogeneous structures. Polymeric dense membranes such as polytetrafluoroethylene and cellulose esters are usually fabricated by compression molding, solvent casting, and spraying of a polymer solution. The membrane structure of a dense membrane can be in a rubbery or a glassy state at a given temperature depending on its glass transition temperature, as discussed in chapter IV, V and VI, and also reported in the literature [56].

Porous membranes find application in the microfiltration, ultrafiltration, and dialysis applications. There is some controversy in a defining a “membrane pore”. The most commonly used theory assumes a cylindrical pore for simplicity. This model assumes that pores have the shape of parallel, nonintersecting cylindrical capillaries. The thicker porous membranes sometimes provide support for the thin dense membrane layers [57], forming the asymmetric membrane structures. The latter are usually produced by a lamination of dense and porous membranes.

Dense homogeneous polymer membranes are usually prepared (i) from solution by solvent evaporation (solution-casting) only or (ii) by extrusion of the molten polymer. However dense homogeneous membranes only have a practical meaning when made of highly permeable polymers such as silicone-based ones. Usually, the permeate flow across the membrane is quite low, since a minimal thickness is required to give the membrane mechanical stability. Most of the presently available membranes are porous or consist of a dense top layer on a porous structure also called composite membranes. The preparation of membrane structures with controlled pore size involves several techniques with relatively simple principles, but which are quite tricky.

An asymmetric structure characterizes most of the presently commercially available membranes, which are now produced from a wide variety of polymers, see figure 2.14.

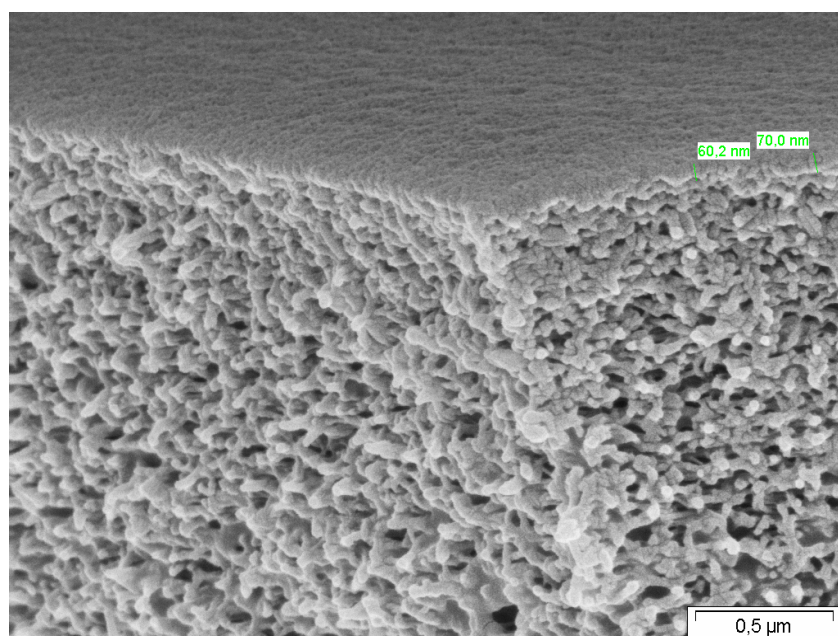


**Figure 2.14:** Composite membrane: support PAN and a graft-copolymer in the top, micrographs taken in polymer research institute-GKSS, thanks to Marion Adelbord.

There are two main flow configurations of membrane processes: cross-flow and dead-end filtrations. In cross-flow filtration the feed flow is tangential to the surface of membrane, the retentate is removed from the same side further downstream, whereas the permeate flow is tracked on the other side, see figure 2.15. In dead-end membranes are relatively easy to fabricate which reduces the cost of the separation process.

- **Flow Configurations of Membrane Processes**

**Cross-Flow Geometry**, is when the feed flow is tangential to the membrane, in consequence the retentate is removed from the same side further downstream and whereas the permeate flow is tracked on the other side. Only small part of the feed is used for permeate production, the largest part will leave the membrane. The cross-flow has a high energy cost. After all, the entire feed flow needs to be brought under pressure.

When **Dead-end Geometry** is used, all the feed enters perpendicular to the membrane surface and it is pressed through the membrane. In the case of mixed gases, for instance, part of feed will stay behind on the membrane while one of gas flows through. This depends on the material of the membrane. Consequentially, the gas will experience interaction to passing through the membrane. The dead-end membrane separation is usually a batch-type process, however, when feed pressure is continuous, this will result in a decreasing flux. After a certain amount of time the flux has decreased to such an extent, that the membrane will need cleaning. Dead-end is applied because the energy loss is less than cross-flow geometric. The

pressure that is need to press feed through a membrane is called “Trans Membrane Pressure (TMP)”

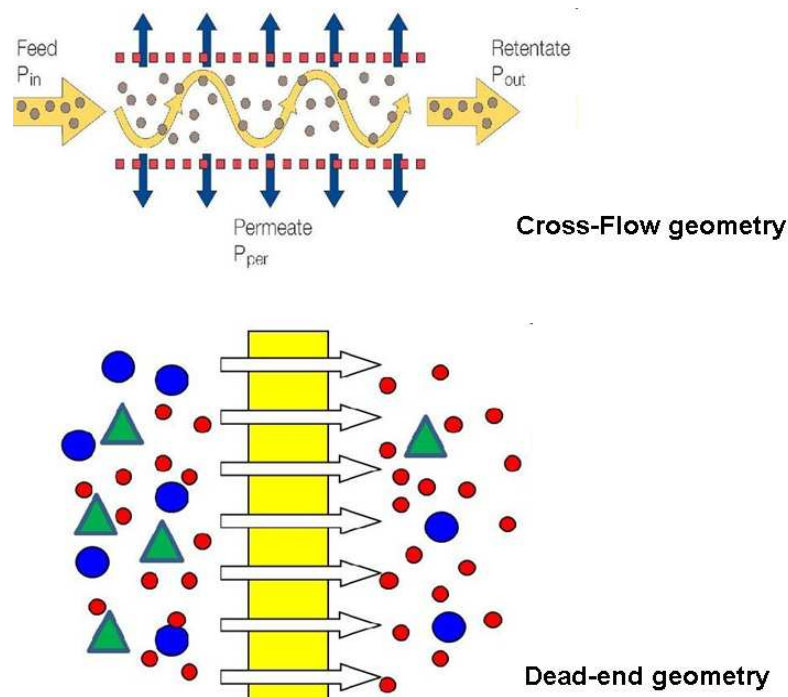


**Figure 2.15:** Flow configurations of membrane processes: cross-flow and dead-end filtrations

## 2.10 Key Industrial Applications

Membrane separation processes play a very important role in industrial separation processes. Membrane separation processes differ based on separation mechanisms and size of the separated particles. The widely used membrane processes include microfiltration, ultra-filtration, nano-filtration, reverse osmosis, electrolysis, dialysis, gas separation, vapour permeation, pervaporation, membrane distillation, and membrane contactors [56]. Dense membranes are utilized for gas separations (removal of  $\text{CO}_2$  from natural gas, separating  $\text{N}_2$  from air, organic vapour removal from air or nitrogen stream) and sometimes in membrane distillation.



Nowadays, gas permeation is a very well studied phenomenon, thus it is not surprising that membranes applications are present in different sizes scale. Membranes are used in laboratories (smaller sizes) and every day has more application in commercial analytical products and instruments [58]. At the beginning of the 1990s, was a common success for several companies the developed a made membranes materials for oxygen / nitrogen separation with selectivities of 7 to 8 and with a maximum of 28.000 standard cubic metres / day of 99 % nitrogen economically produce [52-54]. Other applications for separation of carbon dioxide from natural gas, organic vapours from air and nitrogen, and dehydration of air were developed. A list of the major companies involved in the membranes industry is show in the Table 2.3. In general, the trend for gas separation membranes is up, especially if some of the processes are developed to have control over CO<sub>2</sub> production [53,55].

**Table 2.3:** Current gas separation industry players

Company	Principal Markets (estimated annual sales)
<b>Permea (Air products)</b>	The large gas companies are mostly focused on N <sub>2</sub> / air (US\$ 75 million /yr) and H <sub>2</sub> separation (US\$ 25 million/ yr)
<b>Medal(Air Liquide)</b>	
<b>IMS (Praxair)</b>	
<b>Generon (MG Industries)</b>	
<b>Kvaemer</b>	Mostly natural gas separation (US\$ 20 million / yr)
<b>Separex (UOP)</b>	
<b>Cynara</b>	
<b>Whatman</b>	Vapor / gas separation, air dehydration, other (US \$ 25 million / yr)
<b>Ube</b>	
<b>GKSS Licensees</b>	

all the sales numbers have been estimated [53].

- **Carbon Dioxide Separation**

Grace (now Kraemer-GMS), Separex (UOP) and Cynara have installed a series of plants (more than 200) for carbon dioxide removal from natural gas and all these separation process was used membranes based on cellulose acetate membranes in hollow fiber and which have been used due to their higher selectivity. Figure 2.16 illustrate two schemes of typical carbon dioxide removal plants. Because the one-stage design has no moving parts, it is very competitive with other technologies especially if there is uses for the low-pressure permeate gas. Two-stage processes are more expensive because a large compressor is required to compress the permeate gas. However, the loss of methane with the fuel gas is much reduced [53].

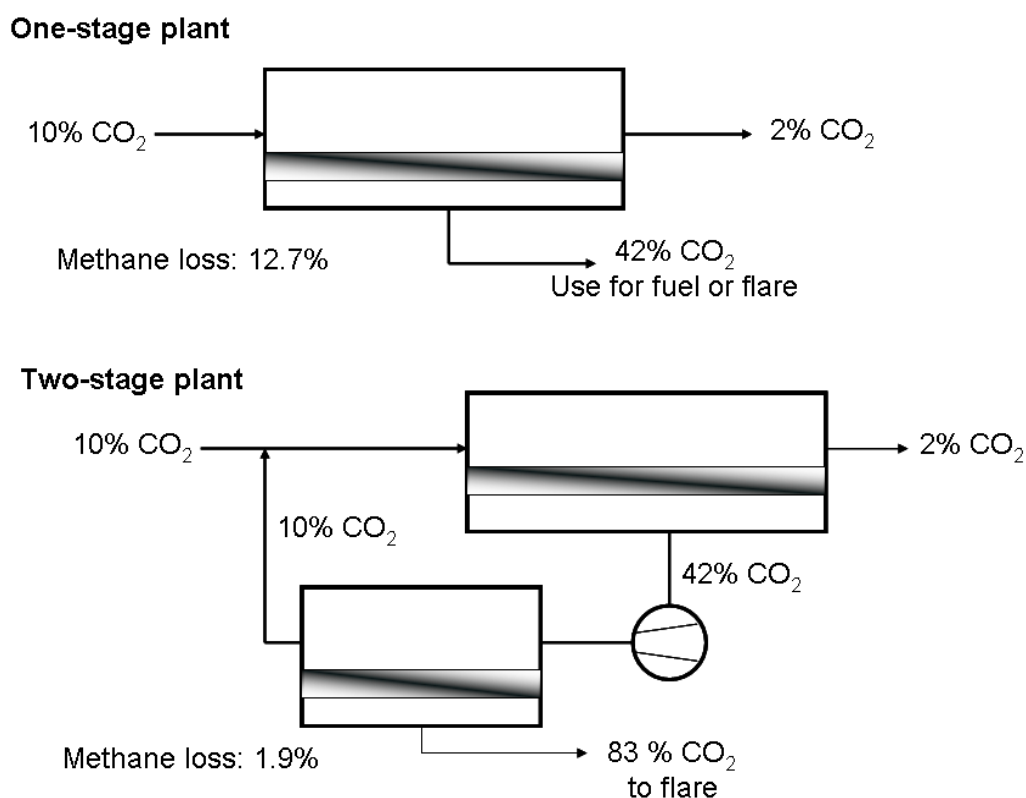


**Figure 2.16:** Flow scheme of one-stage and two-stage membrane separation plants to remove carbon dioxide from natural gas [53].

## 2.11 Permeability: Definition - Models, Polymer Structure and Permeation

### 2.11.1 Definition - Models

Some terms are required in the experimental characterization of gas transport properties of membranes; a more complete discussion can be found elsewhere [61,62]. As was mentioned in the section 2.7 of this chapter, generally, gas molecule is transported through a polymeric membrane by a solution – diffusion mechanism which can be represented by the relation expressed in the equation (2.3), page 28.

The relationship between permeability, diffusivity and solubility can be described by the following equation:

$$P = D \times S \quad (2.9)$$

where  $P$  is the permeability coefficient in  $(\text{cm}^3(\text{STP})\text{cm}/(\text{cm}^2\cdot\text{s}\cdot\text{Pa}))$ ; a measure of the flux of the membrane),  $D$  the diffusivity coefficient (in  $\text{cm}^2/\text{s}$ ; a measure of the mobility of the molecules within the membrane) and  $S$  is the solubility coefficient (in  $\text{cm}^3(\text{STP})/(\text{cm}^3\cdot\text{Pa})$ ; a measure of the solubility of gas molecules within the membrane). The common unit of  $P$  is in Barrer:

$$1 \text{ Barrer} = 10^{-10} \text{ cm}^3 (\text{STP}) \text{ cm} / (\text{cm}^2 \text{ s cmHg})$$

STP = Standard temperature and pressure

While  $P$  is a measure of polymer's permeability, a membranes permeance must also be determined. This is quantified using a term know as a gas permeation unit (GPU), commonly used to describe the gas transport of a membrane, as opposed to a membrane material. The GPU has a unit of  $10^{-6} \text{ cm}^3 (\text{STP}) \text{ cm}^{-2} \text{ s}^{-1} \text{ cmHg}^{-1}$ .

Experimentally,  $P$  is determined via the following relationship:

$$\frac{P}{l} = \frac{Q}{(A \times \Delta p)} \quad (2.10)$$

where  $l$  is the effective thickness of the membrane,  $Q$  the measure of the gas permeation rate through the membrane,  $A$  the surface area of the membrane and  $\Delta p$  is the pressure difference across the membrane. Another possibility to calculate the permeability is to measure the flux,  $J$ , and determined the thickness of the membrane,  $l$ , the relation can be written as

$$P = J \times l \quad (2.11)$$

The dual mode sorption provides another means of describing the sorption of gas molecules into a glassy membrane. The gas molecules are assumed to fit into two categories; molecules absorbed directly into the polymer matrix and molecules absorbed into micro-cavities within the polymer matrix. The concentration of molecules absorbed in the polymer matrix,  $c_D$ , and the concentration of molecules absorbed into micro-cavities,  $c_H$ , can be described by the following equations:

$$c_D = K_D \times p \quad (2.12)$$

$$c_H = \frac{c'_H \times b \times p}{(1 + b \times p)} \quad (2.13)$$

Where  $K_D$  is the Henry's Law coefficient,  $c'_H$  the hole saturation constant,  $p$  the pressure and  $b$  is the hole affinity constant. Hence, the total concentration of molecules,  $c$ , can be described as

$$c = c_D + c_H = (K_D \times p) + \left[ \frac{c'_H \times b \times p}{(1 + b \times p)} \right] \quad (2.14)$$

An experimental investigation of the dual-sorption model has been recently published by Wang, Cao and Chung [63].

### 2.11.2 Relationship of Polymer Structure and Membrane Permeation

Permeability can be expressed as the product  $D_i \times S_i$  of two terms. The diffusion coefficient,  $D_i$ , reflects the mobility of the individual gas molecules in the membrane material; the gas sorption coefficient,  $S_i$ , reflects the number of molecules dissolved in the membrane material. Thus, equation (2.9) can also be written as

$$\alpha_{ij} = \left[ \frac{D_i}{D_j} \right] \times \left[ \frac{S_i}{S_j} \right] \quad (2.15)$$

In this equation (2.15), the mobility selectivity is associate to the ratio of the diffusion coefficients of the two gases ( $i$  and  $j$ ),  $D_i / D_j$ , and reflect the sizes of the two molecules. The solubility selectivity is the ratio of the sorption coefficients of the two gases,  $S_i / S_j$ , and reflects the relative condensabilities of two gases. Large molecules interact with more segments of the polymer chain than do small molecules, therefore in all polymer materials the diffusion coefficient decreases with increasing molecular size. Consequently, the mobility selectivity is favorable to the passage of small molecules over larges ones. However, the mobility selectivity term is affected if the membrane material is above or below its glass transition temperature ( $T_g$ ). A membrane material below the  $T_g$  means the polymer chains are less able to move, in this cases the material is called a glassy polymer (tough and rigid). On the contrary, when the material is above the  $T_g$ , the polymer chains have more thermal energy to allow complexes movements (rotation, translation and so on) around the chain

backbone to become a rubber polymer (flexible) [55]. Figure 2.17 illustrates the relative mobility of gases by their diffusion coefficients for a rubber and glassy material.

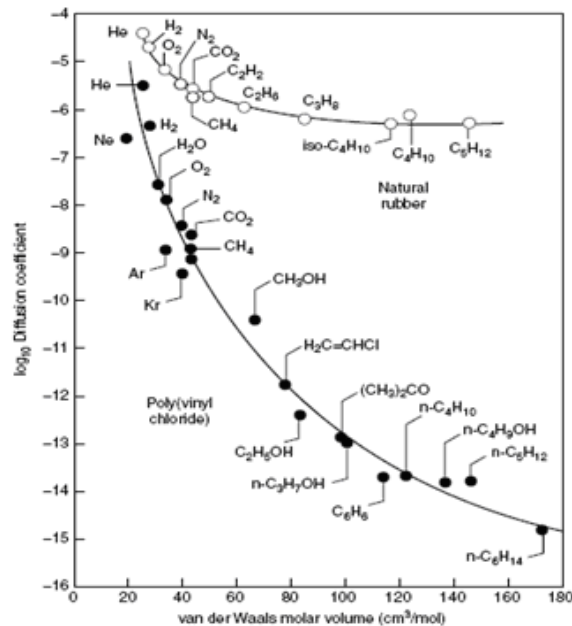


**Figure 2.17:** Diffusion coefficient as a function of molar volume for a variety of permeants in natural rubber and in poly(vinyl chloride), a glassy polymer (reproduced from [55]).

The diffusion coefficients decrease rapidly in glassy materials with increasing gas molecule size or kinetic diameter than diffusion coefficients in rubbers. For example, in the natural rubber the mobility of  $N_2$  is ten times higher than the mobility of  $n-C_5$ .

A second factor that affects the membrane selectivity is the sorption or solubility, in this cases the condensability of the gases into the material plays a very important role. The sorption coefficients increases with increasing condensability of the gases, and, as large molecules are usually more condensable than smaller ones, so the sorption coefficient increases with molecular diameter. Figure 2.18 exhibit the

dependence of gas sorption coefficient with molar volume. In this, for instant, hydrocarbons vapour, iso-C<sub>4</sub> or C<sub>5</sub>, show a higher sorption coefficient as O<sub>2</sub> and N<sub>2</sub>, hence, sorption selectivity favours larger, more condensable molecules. However, the difference between the sorption coefficients of gases in rubbery and glassy polymers is far less marked than the difference in the diffusion coefficients; hence it can be expected that in the glassy polymers the sorption coefficient decrease exponentially with the  $n$ , number of carbon of atoms of gases and the molecular diameter.

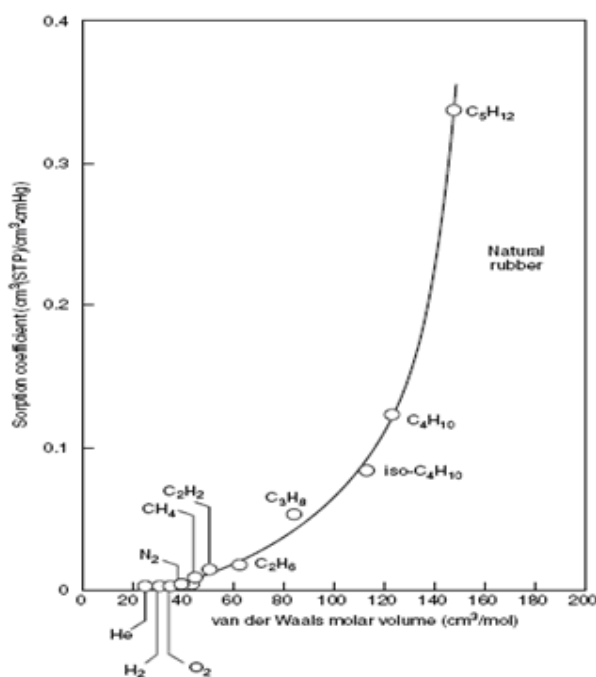


**Figure 2.18:** Gas sorption coefficient as a function of molar volume for natural rubber membranes reproduced from [55].

The figure 2.19 illustrates the difference between the mobility selectivity and the sorption selectivity term. In glassy polymer, permeability decline with increasing gas size, and small molecules permeate preferentially therefore the mobility term is dominant. For example, when is used to separate hydrocarbon vapour (C<sub>3</sub>H<sub>9</sub>) from

nitrogen ( $N_2$ ), glassy membrane (e.g. polyetherimide) preferentially permeate  $N_2$ . In rubbery polymers, for instance, when used to separate  $C_5H_{12}$  from  $N_2$ , rubbery membranes preferentially permeate the hydrocarbon vapour, because, permeability increases with increasing gas size, and larger molecules permeate preferentially, so the sorption selectivity is usually dominant.

The permeability of the gases in the membrane is a balance of two different effects. One is the diffusion (expressed by the diffusion coefficient,  $D_i$ ) which reflects the *mobility* of the individual gas molecules in the membrane material base and is mainly ruled by the gas molecular size (dominant term in glassy-like polymer. The second one is the sorption (expressed by the gas sorption coefficient, or solubility  $S_i$ ) which reflects the *number* of molecules dissolved in the membrane material base mainly ruled by the solubility of each gas in the membrane (dominant term in rubber-like polymer).

Robeson has summarized [64] the separation properties of polymer membranes in gas separation application, in the same direction Stern [61] has prepared a review of structure/property relations. The table 2.3 shows a compilation of these properties of some representative and widely used materials.



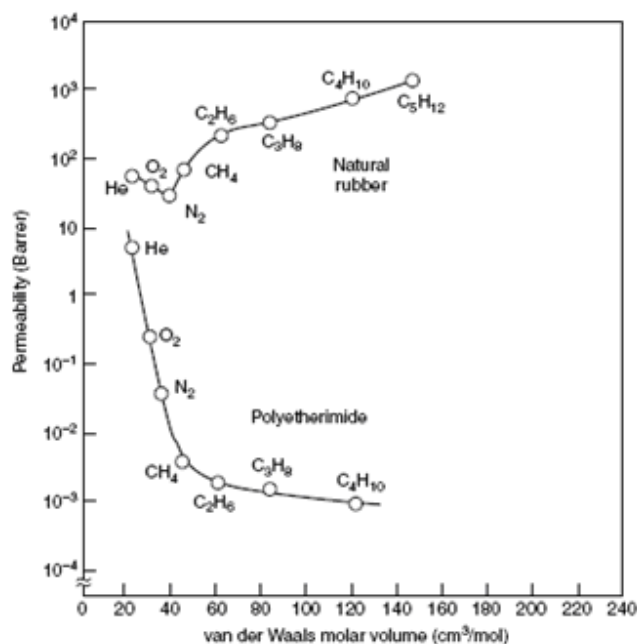


**Figure 2.19:** Permeability as a function of molar volume for a rubbery and a glassy polymer reproduced from [55].

The permeability with pure gas for several materials is listed in table 2.4. Normally the permeability can be determined using pure gases and the selectivity obtained from the ratio of pure gas permeabilities gives the ideal membrane selectivity, an intrinsic property of the membrane material. Nevertheless, a separation process of gas mixtures is more representative in practical conditions. If the gases in a mixture do not interact strongly with the membrane material, the pure gas intrinsic selectivity and the mixed gas selectivity will be equal. This is usually the case for mixtures of oxygen and nitrogen, for example, contrary to a CO<sub>2</sub>/CH<sub>4</sub> mixture, where the higher sorption of CO<sub>2</sub> affects the permeability of the other component. However, the pure gas selectivities are much more commonly reported in the literature than gas mixture data because they are easier to measure.

**Table 2.4:** Permeabilities in Barrer [ $10^{-10}\text{cm}^3(\text{STP})\cdot\text{cm}/\text{cm}^2\cdot\text{s}\cdot\text{cmHg}$ ] measured with pure gases, at the temperatures given, source of data [55].

Gas	Rubbers		Glasses		
	S. R. <sup>25°C</sup> ( $T_g = -129^\circ\text{C}$ )	N. R. <sup>30°C</sup> ( $T_g = -73^\circ\text{C}$ )	C. a. <sup>25°C</sup> ( $T_g = 124^\circ\text{C}$ )	P-Sulfone <sup>35°C</sup> ( $T_g = 186^\circ\text{C}$ )	P-imide <sup>60°C</sup> ( $T_g > 250^\circ\text{C}$ )
H <sub>2</sub>	550	41	24	14	50
He	300	31	33	13	40
O <sub>2</sub>	500	23	1.6	1.4	3
N <sub>2</sub>	250	9.4	0.33	0.25	0.6
CO <sub>2</sub>	2700	153	10	5.6	13
CH <sub>4</sub>	800	30	0.36	0.25	0.4
C <sub>2</sub> H <sub>6</sub>	2100	----	0.20	----	0.08
C <sub>3</sub> H <sub>8</sub>	3400	168	0.13	----	0.015
C <sub>4</sub> H <sub>10</sub>	7500	----	0.10	----	----

Silicone rubber (S.R.), Natural rubber (N.R.), Cellulose acetate (C.a.), P-Sulfone (polysulfone), Polyimide (P-imide)

Figure 2.20 shows the principle idea to apply of this work to improve the permeability of CO<sub>2</sub> with respect to other gases, using a combination of polystyrene in the main chain, glassy polymer, and rubbery polymer like with PEG-segments. The goal is to prepare and study a gas permeation membrane based on a graft-copolymer with a “good balance” between glassy and rubbery polymer but specifically with trend to have a different content of PEG-segments (rubbery polymer) and to improve the sorption and diffusion coefficients of CO<sub>2</sub> into the membrane and the same time to improve the mobility selective due to the chance with time of the rubbery polymer

configuration. Glassy polymer or hard segment is able to supply mobility to gases and offer mechanical properties to the graft-copolymer material.

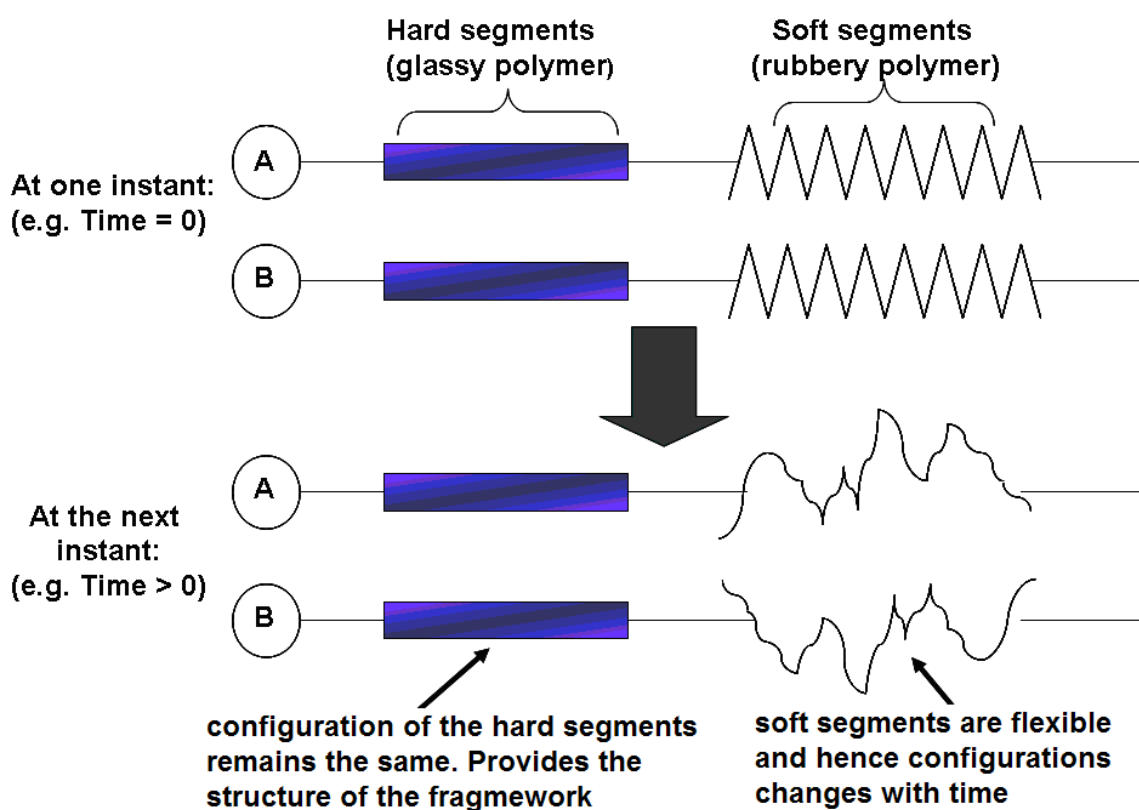


**Figure 2.20:** Principle idea of a copolymer suitable for CO<sub>2</sub> separation

## 2.12 Robeson Models

There appears to be a trade-off between selectivity and permeability, for example a highly selective membrane tends to have a low permeability. Robeson has suggested that the permeability - selectivity trade-off possesses an upper bound [60]

Figure 2.21 provides an example of this upper bound.

The upper bound can be described by the following equation:

$$\alpha_{A/B} = \frac{\beta_{A/B}}{(P_A)\lambda_{A/B}} \quad (2.16)$$

where  $\beta_{A/B}$  and  $\lambda_{A/B}$  are constants for each gas pair.

Subsequent to the publication of Robeson's paper [64], only a few examples of polymeric membranes have been published which exceed the upper bound. Koros and Mahajan have suggested that it may be possible to exceed the upper bound significantly by the use of "mixed-matrix membranes" [66]. These membranes consist of a polymeric membrane with a large volume of sub-micromolecular sieves.

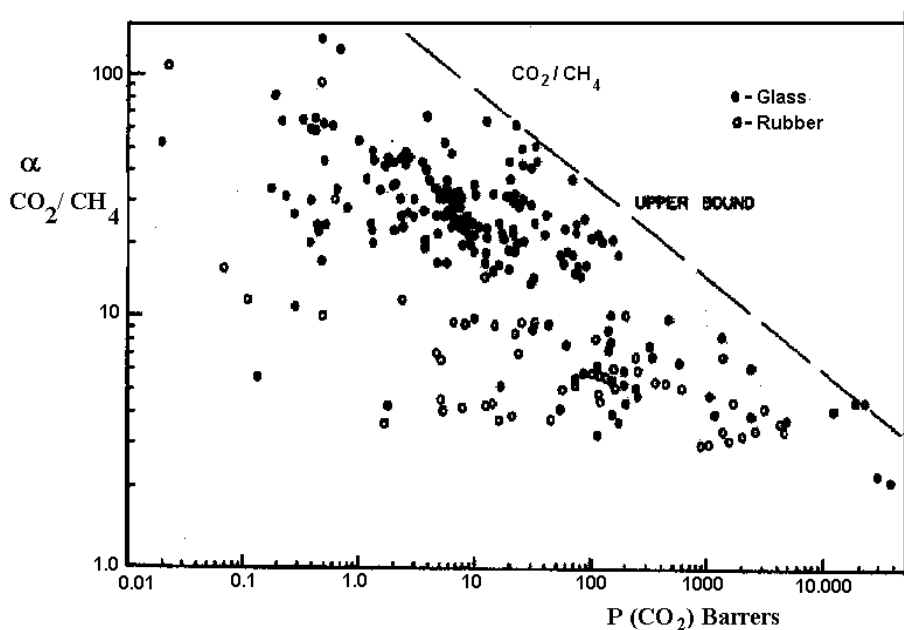


**Figure 2.21:** Upper bound relationship for CO<sub>2</sub>/CH<sub>4</sub> separation (Carbon dioxide - methane selectivity vs. CO<sub>2</sub> permeability) [64].

This approach could combine the processability of a membrane with the high performance characteristics of the molecular sieves. Examples of the polymers

proposed and/or utilized for gas separation are tabulated in Table 2.5 with their respective permeability and permselectivity values [67].

**Table 2.5:** Permeability and permselectivity data for polymers of interest for membrane separation, Barrer [ $10^{-10}\text{cm}^3(\text{STP})\cdot\text{cm}/\text{cm}^2\cdot\text{s}\cdot\text{cmHg}$ ], source of data [67].

Membranes	$P_{N_2}$ (Barrer)	$P_{CO_2}$ (Barrer)	$P_{CH_4}$ (Barrer)	$\alpha$ $CO_2/N_2$	$\alpha$ $CO_2/CH_4$
PTMSP <sup>(a)</sup>	6890	37000	18400	5.37	2.01
Poly(4-methyl-1-pentyne)	1330	10700	2900	8.05	1.98
Silicon Rubber	351	4550	1430	13.0	3.18
TMPA-6FDA (Polyimide) <sup>(b)</sup>	35.6	440	28.2	12.4	15.6
Poly(4-methyl-1-pentene)	6.7	84.6	14.9	0.14	5.68
PPO <sup>(c)</sup>	3.5	65.5	4.1	18.7	16.0
Tetrabromobisphenol	0.182	4.23	0.126	23.2	33.6
<b>A Polycarbonate</b>					
Polysulfone	0.20	4.9	0.21	24.5	23.3

<sup>a</sup>PTMSP = poly(trimethylsilylpropyne), <sup>b</sup>TMPA=2,3,5,6-tetramethyl phenylene diamine; 6-FDA= 5,5'-[1,1,1trifluoromethyl]ethylidene]bis-1,3 isobenzofurandione, <sup>c</sup> PPO = poly(2,6-dimethyl-1,4-phenylene oxide); temp. 25°C for PTMSP and poly(4-methyl-1-pentyne) other polymers at 35°C .

The polymers chosen for gas membranes separation are usually high  $T_g$ , amorphous polymers. Generally glassy polymers offer improved  $P / \alpha$  combinations desired for specific gas pair separation, hence is very important to measure the  $T_g$  for each new polymer and also the fractional free volume (FFV) associated.

The fractional free volume (FFV) is a measure of the theoretical volume of the polymer divided by the actual volume of the polymer. The fractional free volume is usually defined as [68],

$$FFV = \frac{(V - V_0)}{V} \quad (17)$$

Where  $V$  is the specific volume of the polymer at the temperature of interest, and  $V_0$  is the specific occupied volume at 0 K.  $V_0$  is estimated as 1.3 times the van der Waals volume of the polymer repeat unit, which is calculated using a group contribution method [69], in section 6.2.3.1, page 154.

### 2.13 References

- [1] Staudinger H., *Chemische Berichte* 53 (1920) 1073.
- [2] Herman M., *From Small Organic Molecules to Large: A Century of Progress, in Profiles, Pathways, and Dreams: Autobiographies of Eminent Chemists*, ed. Jeffrey Seeman (Washington, D. C.: American Chemical Society, 1993), p.9.
- [3] Simon E., *Justus Liebigs Annalen der Chemie* 31 (1839) 265.
- [4] Matweb "Material Property Data" [www.matweb.com/search/DataSheet](http://www.matweb.com/search/DataSheet)
- [5] Wilkinson A. N., Anthony J. R., *Polymer Processing and Structure Development*, Kluwer Publishers, Dordrecht -The Netherlands 1999.
- [6] Rodriguez Ferdinand, Cohen Claude, Ober Christopher, Lynden A. Archer *Principles of Polymer Systems* 5th. Edition, Taylor & Francis, New York – London, 1996.
- [7]. Flory, P. J. *Principles of Polymer Chemistry*. Ithaca, NY: Cornell University Press, 1953, pp. 106-132.

- [8] Szwarc M., *Nature*, 176 (1956) 1168.
- [9] Vollmert B., *Polymer Chemistry*, Springer-Verlag Inc. New York, 1973.
- [10] N. Hadjichristidis, H. Iatrou, S. Pispas, M. Pitsikalis, *Journal of Polymer Science: Part A: Polymer Chemistry*, 38 (2000) 3211.
- [11] Young, L. J. *Polymer Handbook*, 2<sup>nd</sup> ed.; Brandrup, J., Immergut, E. H. Eds.; Wiley-Interscience: New York, 1975.
- [12] Tsuchida E.; Tomono, T. *Makromolekulare Chemie* 141 (1971) 265.
- [13] Park E-U., Kim M-N., Lee I-M., Yoon J-S. *Journal of Polymer Science Part A: Polymer Chemistry*, 38 (2000) 2239.
- [14] Scientific Polymer Products Inc. 2006 Scientific Polymer Products Inc. All rights reserved. 6265 Dean Parkway, Ontario, NY 14519.
- [15] Xie H.-D. and Xie D., *Progress in Polymer Science* 24 (1999) 275.
- [16] Huntsman Corporation, *The Jeffamine® Polyoxyalkyleneamines Technical Bulletin*, Huntsman Corporation, Houston Texas, 2002.
- [17] Uglea V. C. and Negulescu I. I. *Synthesis and Characterization of Oligomers* CRC Press, Inc., Boca Ratón, U.S.A., 2000, pp. 72.
- [18] Felthouse T.R., Burnett J. C., Horrell B., Mummey M. J. and Kuo Y-J. *Technical Report*, Huntsman Petrochemical Corporation, Austin, U.S.A., 2001.
- [19] Litjens M., Straathof A., Jongejan J., Heijen J., *Tetrahedron*, 55 (1999) 12411.
- [20] Basiuk V., Basiuk E., Saniger-Blesa J-M., *Nano Letters*, 1 (2001) 657.
- [21] Qipeng, G., Tianru F., Tianlu C. and Zhiliu F. *Polymer Communication* 32 (1991) 22.

- [22] Liang D., Zhou S., Song L., Zaitsev V. and Chu B., *Macromolecules*, 32 (1999) 6362.
- [23] Riess G., Nervo J. and Rogez D., *Polymer Engineer Science* 17 (1977) 634.
- [24] Moreau, J., Lu, R. and Bury U.S patent No. 6.008.275.
- [25] Gramain, P. and Free, Y. *Macromolecule Chemistry* 188 (1987) 593.
- [26] Jannasch, P. and Wesslen, B. *Journal of Polymers Science Part A: Polymer Chemistry*, 31 (1993) 1519.
- [27] Gramain, P. and Frere, Y. *Polymer Communication* 27 (1986) 16.
- [28] Derand, H. and Wesslen, B. *Journal Polymer Science Part A: Polymer Chemistry* 33 (1995) 571.
- [29] Wesslen, B. and Wesslen, K.B. *Journal Polymer Science Part A: Polymer Chemistry* 27 (1989) 3915.
- [30] Saxena A., Tripathi B.P. and Shahi V. K., *Journal Physical Chemistry B*. 111 (2007) 12454.
- [31] Roeder J., Gomez D., Ponce M.L. and Nunez S: P. *Macromolecules Chemistry and Physics* 208 (2007) 467.
- [32] Fernyhough C.M., Young R.N., Ryan A. J. and Hutchings L.R. *Polymer* 47 (2006) 3455.
- [33] Kyozo-Kitano N., Fumishiro M., Toshimi T., U.S. patent No. 4.671.903
- [34] Kyozo-Kitano N., Fumishiro M., Toshimi T, Kokoku No. JP-B-51-37226
- [35] Kyozo-Kitano N., Fumishiro M., Toshimi T, Kokoku No. JP-B-51-37227
- [36] Martins C. R, Ruggeri G., De Paoli M-A., *Journal of the Brazilian Chemical Society* 4 (2003) 797.



- [37] Smitha B., Sridhar S., Khan A. A., *Journal of Membrane Science* 225 (2003) 63.
- [38] Makowski, H. S.; Lundberg, R.D.; Singhal, G. H.; *U.S. pat.* 3.870. 841.
- [39] Sourirajan S., *Reverse Osmosis*, Academic Press, New York (1970).
- [40] Yasuda H. and Peterlin A., *Journal of Applied Polymer Science* 17 (1973) 433.
- [41] Paul D.R., Ebra-Lima, O., *Journal of Applied Polymer Science* 14 (1970) 2201.
- [42] Paul D.R., Diffusive Transport in Swollen Polymer Membranes, in *Permeability of Plastic Films and Coatings*, H.B. Hopfenberg (ed.), Plenum Press, New York, (1974), pp. 35–48.
- [43] Paul D.R., *Separation Purification Methods* 5 (1976) 33.
- [44] Fick A., Über Diffusion, *Poggendorff's Annal. Physik Chem.* 94 (1855) 59.
- [45] Baker, R. W., *Membrane Technology and applications*, 2th. edition, published by McGraw-Hill, Jonh Wiley&Sons Ltd., West Sussex, England, 2004, chapter 2, pp.18.
- [46] Mulder, M., *Basic Principles of Membrane Technology*, Kluwer Academic Publishers, Dordrecht – The Netherlands, 1996, pp. 82, 340 – 365.
- [47] Alentiev, A.Y. and Yampolskii, Y.P. *Journal Membrane Science*, 165 (2000) 201.
- [48] Wijmans J.G., Baker, R. W. *Journal of Membrane Science* 107(1995)1.
- [49] Perry, R. H., Green D. H., *Perry's Chemical Engineer's Handbook*, 7<sup>th</sup> edition, McGraw-Hill, New York - USA, 1997.
- [50] Zeaman, Leos J., Zydney, Andrew L., *Microfiltration and Ultrafiltration, Principles and Applications*, New York, Marcel Dekker, Inc, 1996.

- [51] Xiao Y., Low B. T., Hosseini S.S., Chung T. S. and Paul D.R., *Progress in Polymer Science* 34 (2008) 561.
- [52] Mulder, M., *Basic Principles of Membrane Technology*, Kluwer Academic Publishers, Dordrecht - The Netherlands, 1991, pp. 54 – 69.
- [53] Nunez S.P., Peinemann K.-V., *Membrane Technology in The chemical Industry*. Edited by Wiley- VCH Verlag GmbH, electronic, 2001, Chapter 3, pp 8-11, chapter 7, pp. 268 – 277.
- [54] Koros, W.J., *Macromolecular Symposia*, 188 (2002) 13.
- [55] Baker R. W., *Membrane Technology and Applications*, Second Edition, John Wiley & Sons, Ltd, 2004, West Sussex, England, Chapter 3, pp 89 – 155, chapter 7, pp 298-299.
- [56] Pinnau, I., Freeman, B.D., *Membrane Formation and Modification*, ACS Symposium Series, ACS- publications, Washington DC, U.S.A, 1999.
- [57] Osada, Y., Nakagawa, T., *Membrane Science and Technology*, New York, Marcel Dekker Inc, 1992, chapter 2, pp.22-24.
- [58] Davis G., Lauks I. R., Pierce R. J., and Widrig C. A., “Method of measuring gas concentrations and microfabricated sensing device for practicing same” US Patent No. 5,514,253, Assigned to I-Stat Corporation, May 7, 1996.
- [59] Van Dijk C. P. and Fraley L. D., “Process for producing and utilizing an oxygen enriched gas”, US Patent No. 5,245,110, Assigned to Starchem, Inc., Sept. 14, 1993.

- [60] Van Dijk C. P., "Methanol production process using a high nitrogen content synthesis gas with a hydrogen recycle" US Patent No. 5,472,986, Assigned to Starchem, Inc., Dec. 5, 1995.
- [61] Mier G., *Angewandte Chemie International* Ed. 37 (1998) 2960.
- [62] Paul D.R., Yampol'skii Y.P. *Polymeric Gas Separation Membranes*, CRC Press, Boca Raton - U.S.A., 1994.
- [63] Wang R., Cao C., Chung, T.S., *Journal Membrane Science* 198 (2002) 259.
- [64] Robeson, L. M. *Journal Membrane Science* 62 (1991) 165.
- [65] Stern, S.A. *Journal Membrane Science* 94 (1994) 1.
- [66] Mahajan R., Koros W. J., *Polymer Engineering and Science*, 42 (2004) 1420.
- [67] Robeson L.M. *Current Opinion in Solid State & Materials Science*, 4 (1999) 549.
- [68] Lin H., Freeman B.D. Kalakkunnath S. Kalika D., *Journal of Membrane Science* 291 (2007) 131.
- [69] D. W. Van Krevelen, *Properties of Polymers: Their Correlation with Chemical Structure: Their Numerical Estimation and Prediction from Additive Group Contributions*, Elsevier, Amsterdam -The Netherlands, 1990.

## **Chapter III Characterization and Instrumentation**

---

This chapter is showing a description of the instruments and experimental techniques used through the thesis: e.g. thermal analysis (DSC, TGA), spectroscopy techniques ( $^1\text{H}$ - $^{13}\text{C}$ -NMR and FT-IR), GPC and SEM analysis.

### **3.2 Thermal Analysis**

Thermal Analysis includes all methods in which measurements are made of a physical property that changes as the temperature is varied. A number of the techniques can be also complemented by the addition of time or oscillatory variation to enhance the information that can be obtained from these measurements. The experiments can usually be divided into isothermal in which continuous measurements as a function of time and/or frequency are performed at a constant temperature and programmed temperature measurements where the temperature is varied in a well defined manner. These techniques include differential scanning calorimetry, DSC, and thermogravimetric analysis, TGA, [1].

#### **3.1.1 Differential Scanning Calorimetry (DSC)**

DSC is a technique in which the difference in energy inputs into a substance and a reference material is measured as a function of temperature whilst the substance and reference material are subjected to a controlled temperature program. Two modes, *power-compensation differential scanning calorimetry (power-compensation DSC)* and *heat-flux differential scanning calorimetry (heat-flux DSC)*, can be distinguished depending on the method of measurements used [2]. In this work is used the heat-flux

DSC technique for thermal analysis. The thermal measurement can be executed as follow; the sample is encapsulated in an aluminum pan and along with an empty reference, sits on a thermoelectric disk surrounded by a furnace. As the furnace temperature is changed, normally in a linear fashion, heat is transferred to the sample and reference through the thermoelectric disk. The differences in heat flow to the sample and reference are calculated from temperature differences which are determined by area thermocouples (using the thermal equivalent of Ohm's law). The equation for heat flow therefore is follows:

$$q = \Delta T / R \quad (3.1)$$

where  $q$  is the heat flow,  $\Delta T$  temperature difference between the sample and reference divided by resistance of the thermoelectric disk ( $R$ ).

The essential features of the DSC apparatus are show in Fig. 3.1. The sample is placed in sample pan, located in a block which can be heated (or cooled) at a programmed rate.

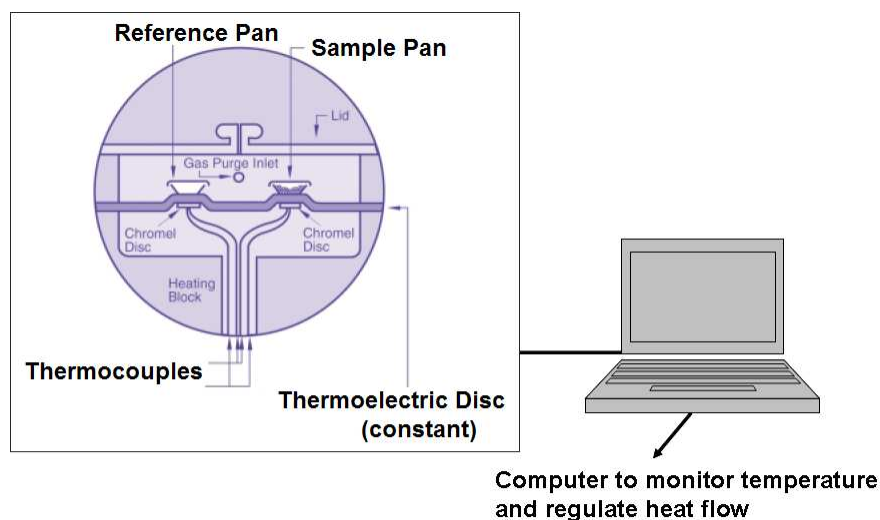


**Figure 3.1:** Schematic DSC Apparatus: heaters, samples and references pan and the regulate heat flow from computer [1,2].

- **DSC Measurements**

Differential scanning calorimetric (DSC) measurements were performed on a DSC 204 (Netzsch). The samples were dried in a vacuum oven at room temperature prior to the experiment. During the determination were used 10 mg of sample approximately. The heating-cooling-heating cycles were recorded in the temperature range from -150 to 250 °C at a scan rate of 10 K/min under nitrogen atmosphere which is also inert gas, high purity and less expense in comparison of argon, (55 ml/min and purity of 99.9999%). Temperature and the heat of transition were calibrated with an indium standard. In the 1<sup>st</sup> heating run all samples were annealed at the final temperature (250°C) for 0.5 min to remove the previous thermal history. The computer will plot the difference in heat output of the thermoelectric disk, so the result of DSC experiment is a curve of heat flux versus temperature. There are two different conventions: exothermic reaction in the sample shown with a positive pick or negative peak, depending on the kind of technology used in the experiment. This curve can be used to calculate the enthalpies of transitions. This is done by integrating the peak corresponding to a given transition.

### **3.1.2 Thermogravimetric Analysis (TGA)**

Thermogravimetric analysis is an analytical technique to measure the thermal stability of a material and its volatile components by monitoring the weight change that occurs as the specimen is heated. During the measurement the mass of the sample is recorded continuously while the temperature is increased at constant rate. The loss in weight of the sample is observed when volatile components are driven off as the temperature increases and at higher temperature the degradation of a polymer

occurs with the formation of volatile products. The weighing equipments in TGA should carry out the weighing of the samples in a controlled environment avoiding the effects of convection forces that arise in the heating chamber. If the atmosphere of measurement chamber influences the process of degradation then it should be controlled. Usually studies are carried out using argon or nitrogen as an inert atmosphere and oxygen as a reactive atmosphere. Significant differences can often be observed using two different techniques. The maximum temperature is selected so that the specimen weight is stable at the end of the experiment which implies that the degradation has taken place. The analysis of results relies on a high degree of precision in three measurements: weight, temperature, and temperature change. The ash content is the residual mass ( $M_{res}$ ) which remains after the complete degradation of the compound. In this work the degradation temperature and changes in weight analysis includes: temperature of the first degradation temperature, TID, temperature where a 10% mass loss has been detected,  $T_{d10}$ , and residual mass determined at the first degradation temperature,  $Res_{TID}$ . Thus degradation temperature distinguishes different samples and gives information about the stabilities of the different systems [3].

- **TGA Measurements**

Thermo gravimetric analysis (TGA) of the samples (15- 20 mg approximately) were carried out on TG 209 F1 Iris (Netzsch) with a heating rate 10 °C/min under argon flux 45 ml/min and purity of (99.9995% ) in an interval between 20°C – 600°C. Before measurement, all the samples were dried in an oven at 150°C for 60 min in N<sub>2</sub> atmosphere.

### 3.2 Fourier Transform Infrared Spectroscopy (FT-IR)

Fourier Transform Infrared Spectroscopy (FTIR) measures the different infrared frequencies absorbed by a sample positioned in the path of infrared beam. The main goal of this technique is to determine the chemical functional groups present in the sample. Different functional groups absorb characteristic frequencies of infrared radiation. Thus, it is an important and popular tool for structural elucidation and compound identification. Infrared region is divided into three smaller areas: near IR ( $14000 - 4000 \text{ cm}^{-1}$ ), mid IR ( $4000 - 400 \text{ cm}^{-1}$ ) and far IR ( $200 - 12.5 \text{ cm}^{-1}$ ). The mid infrared region is used to measure the fundamental vibrations associated with rotational – vibrational structure. The major types of molecular vibrations are stretching and bending. The molecules having dipole moment respond to the infrared radiations and hence are infrared active [4,5]. There are three basic components of an FTIR system: radiation source, interferometer, and detector. A simplified layout of FTIR system is shown in Figure 3.2.

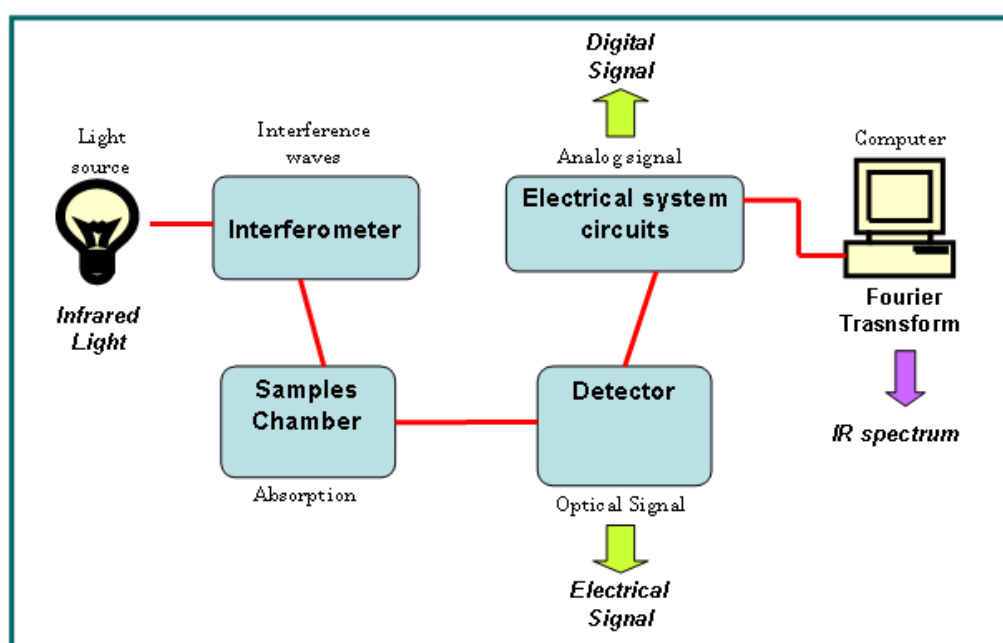


Figure 3.2: Layout of FTIR system.



- **FT-IR Measurements**

FT-IR spectra were obtained on a Bruker EQUINOX 55 FTIR spectrometer. All spectra were acquired at room temperature from 4000 to 550  $\text{cm}^{-1}$  in  $\text{N}_2$  atmosphere. The samples were previously dried at 100°C for several days and stored in vacuum desiccator. The number of scans taken was 128 with spectral resolution of 2  $\text{cm}^{-1}$ .

### 3.3 Nuclear Magnetic Resonance Spectroscopy (NMR)

Nuclear magnetic resonance (NMR) spectroscopy is one of the most effective and useful techniques for characterization of polymers, through by determination of the concentration of protons,  $^1\text{H}$ -NMR, or carbons  $^{13}\text{C}$ -NMR. NMR also provides the means for identifying the intermediate structures formed during the reactions, thus permits more detailed reaction mechanism to be proposed. Only those atoms whose nuclei contain nuclear spin exhibit nuclear magnetic resonance. Atoms or isotopes whose nuclei contain either odd number of protons or odd number of neutrons possess nuclear spin and hence are detectable by NMR [6,7]. The operation of NMR spectrometer is illustrated schematically in figure 3.3.

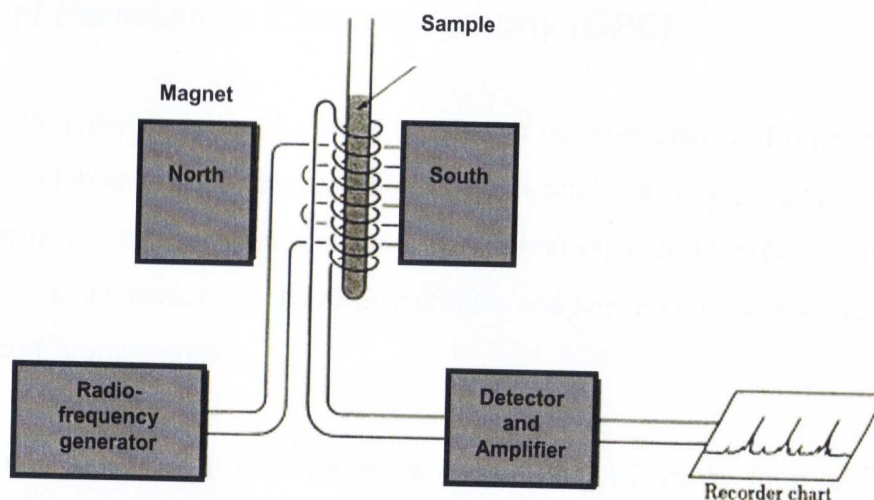


**Figure 3.3:** Schematic diagram of NMR spectrometer.

In the absence of external magnetic field, nuclear spins of magnetic nuclei are randomly oriented. With the application of magnetic field, they align either parallel or anti parallel to the applied field. The parallel orientation is slightly lower in energy than the anti parallel one. If electromagnetic radiation of the proper frequency is irradiated on these oriented nuclei, absorption of energy takes place and the lower energy state spin-flips to the higher energy state. When this spin-flip occurs, the nucleus is said to be in resonance with the applied radiation and hence the name nuclear magnetic resonance. A sensitive detector monitors the absorption of the radio frequency energy and displays it in the form of electronic signal. NMR spectra are plotted as absorption versus chemical shift,  $\delta$ . Chemical shift is the frequency of absorption for a nucleus of interest relative to the frequency of absorption of a molecular standard. By understanding different chemical environments, the chemical shift can be used to obtain some structural information about the molecule in a sample. The conversion of the raw data to this information is called *assigning* the spectrum. For example, for the  $^1\text{H}$ -NMR spectrum for ethanol ( $\text{CH}_3\text{CH}_2\text{OH}$ ), one would expect three specific signals at three specific chemical shifts: one for the  $\text{CH}_3$  group, one for the  $\text{CH}_2$  group and one for the  $\text{OH}$  group. A typical  $\text{CH}_3$  group has a shift around 1 ppm, a  $\text{CH}_2$  attached to an  $\text{OH}$  has a shift of around 4 ppm and an  $\text{OH}$  has a shift around 2–3 ppm depending on the solvent used. Depending on the local chemical environment, different protons in a molecule resonate at slightly different frequencies. Since both this frequency shift and the fundamental resonant frequency are directly proportional to the strength of the magnetic field, the shift is converted into a *field-independent* dimensionless value known as the chemical shift. The molecular standard for both  $^1\text{H}$  and  $^{13}\text{C}$ -NMR spectroscopy is tetramethylsilane

(TMS) because of its highly shielded protons and it acts as the zero point on NMR spectra. Chemical shift is expressed in parts per million (ppm) and is given by the following relation

$$\text{Chemical shift } (\delta) = (\nu_{\text{samples}} - \nu_{\text{TMS}}) / \nu_0$$

where  $\nu_0$  represents the operating frequency of the spectrometer. For  $^1\text{H}$ -NMR the chemical shift lies typically in the range 0 – 10 ppm and  $^{13}\text{C}$ -NMR between 0 – 250 ppm [6,7].

- **NMR Measurements**

Both  $^1\text{H}$ - and  $^{13}\text{C}$ -NMR (300 MHz and 75 MHz, respectively) were performed at 25°C in deuterated acetone (acetone- $d_6$ ) (Aldrich) and deuterated chloroform ( $\text{CDCl}_3$ ) (Aldrich) using a Bruker AV-300 spectrometer. Solvent signals were used as internal chemical shift references (acetone- $d_6$ :  $\delta = 2.05$  ppm [ $^1\text{H}$ -NMR] and  $\delta = 30.5$  ppm [ $^{13}\text{C}$ -NMR];  $\text{CDCl}_3$ :  $\delta = 7.26$  ppm [ $^1\text{H}$ -NMR] and  $\delta = 77.45$  ppm [ $^{13}\text{C}$ -NMR]). The content of PEG was determined using the peak integral ratio of PEG ( $\delta = 3.6$  ppm) to the combined phenyl signal group  $7.1 \text{ ppm} > \delta > 6.5 \text{ ppm}$ .

### 3.4 Gel Permeation Chromatography (GPC)

A synthetic polymer material always consists of polymer chains of different degrees of polymerization and molar masses. The gel permeation chromatography (GPC) operates on the principle that polymer molecules in solution separate according to their size and not chemical interaction or chemical retention and hence GPC is also referred as size exclusion chromatography. The column in GPC is filled with gel or glass. The gel is in the form of fine spherical beads usually 100  $\mu\text{m}$  in diameter and

made of cross-linked styrene-divinyl benzene copolymer. The gel contains large amount of micropores of uniform size. Separation in GPC takes places by a size exclusion and by a dispersion process which is controlled by molecular diffusion. When GPC column is filled with suitable solvent, the solvent occupies not only free volume between beads (void volume) but also the volume of the pores (pore volume) inside the gel beads. The solvent phase occupying the void volume acts as the mobile phase, while that occupying the pore volume acts as stationary phase. When polymer solution is injected into the column, the mobile phase around gel beads now contains polymer molecules whereas the stationary phase does not contain any. Due to this difference in polymer concentration between the mobile and stationary phases, the polymer molecules start diffusing into the stationary phase so as to equalize concentration. Although all polymer molecules try to enter the pore volume, the pore size restricts the entry and allows molecules up to certain hydrodynamic size only to enter the pores. Molecules of large sizes are excluded from entering the pores and are washed down the column first. Hence separation of polymer molecules goes on and small or low molecular weight molecules are washed out at the end. GPC measurements yields a purely empirical relationship between the molar mass  $M$  and the elution volume  $V_e$ . The elution volume  $V_e$  of a polymer may be described by the following equation.

$$V_e = V_o + (K_d \times V_i) \quad (3.1)$$

where  $V_o$  is the volume between the gel particles (void volume)  $V_i$  is the overall sum of all pore volumes (pore volume) and  $K_d$  is regarded as partition coefficient between mobile and stationary phase [8]. These can easily be understood by the given figure 3.4 .

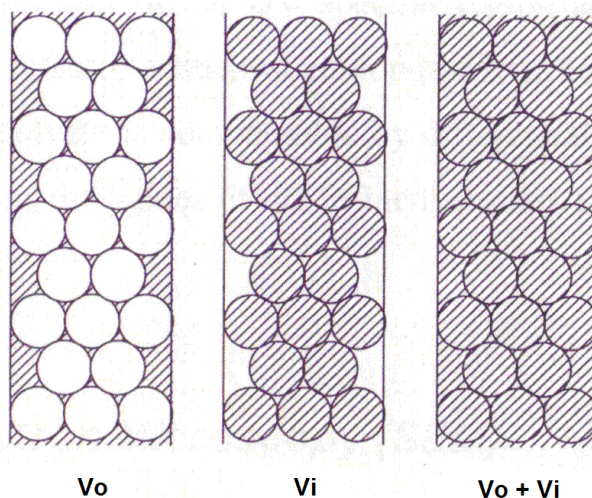


**Figure 3.4:** The two different volumes available in the GPC column [8].

Divinyl benzene cross-linked polystyrene gels, porous glasses or silica gels are used as column packing materials for separation of synthetic polymers by GPC. The range of permeation of a gel lies between the upper exclusion limit and the limit of total permeation, which are shown in the figure 3.5.

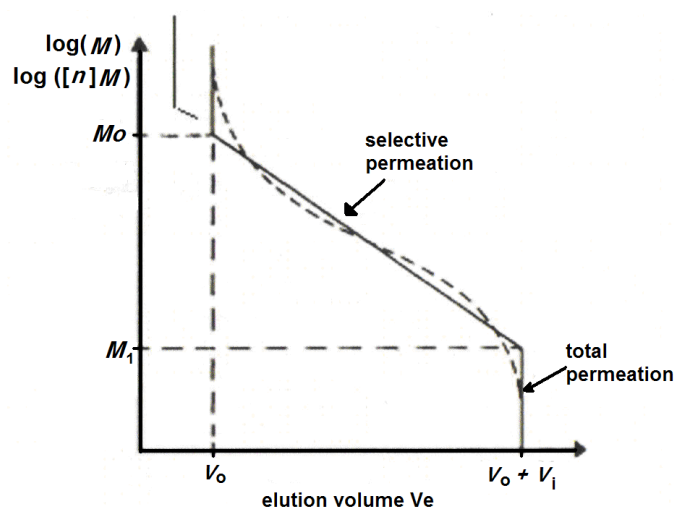


**Figure 3.5:** Idealized dependency of the molecular weight and elution volume  $V_e$  [9]

The most commonly used detectors for GPC are the UV photometer and differential refractometer. Also light scattering photometers and viscometers are growing in

importance. An UV detector is very sensitive and very selective detector. Only those molecules which show absorption in the UV region are used detected and only those solvents which do not show absorption in the UV spectral region are used. With differential refractometer the overall refractive index of elution (solvent + sample) is determined [9]. The refractive index of pure solvent is compensated by differential procedure to obtain exact values of samples. Thus the values of the refractive index for the pure sample will be obtained. Normally the GPC is calibrated by a standart solution like styrene in the same solvent used for determination of elugrams in each sample.

When characterizing apolymer, it is important to consider the polydispersity index (PDI) as well the molecular weight because this value represent a measure of the distribution of molecular mass in a given polymer sample, also we can evaluate the optimization of synthesis and quality control procedures for the preparation of the polymer. Each polymer has a distribution of molar masses and the PDI represents the broadness of the distribution. The PDI is calculated as the weight average molecular weight ( $M_w$ ) divided by the nummber average molecular weight ( $M_n$ ).

$$PDI = \frac{M_w}{M_n} \quad (3.2)$$

The *weight average molecular weight* ( $M_w$ ) is average of the molecular weight of all the poblation of molecules polymer and it is way of describing the molecular weight of a polymer. The *nummber average molecular weight* ( $M_n$ ) is average of the molecular weight of the individual macromelecules and it is considering a way of determining the molecular weight of a polymer [9]. GPC allows the determination of PDI as well as  $M_w$  and  $M_n$ .

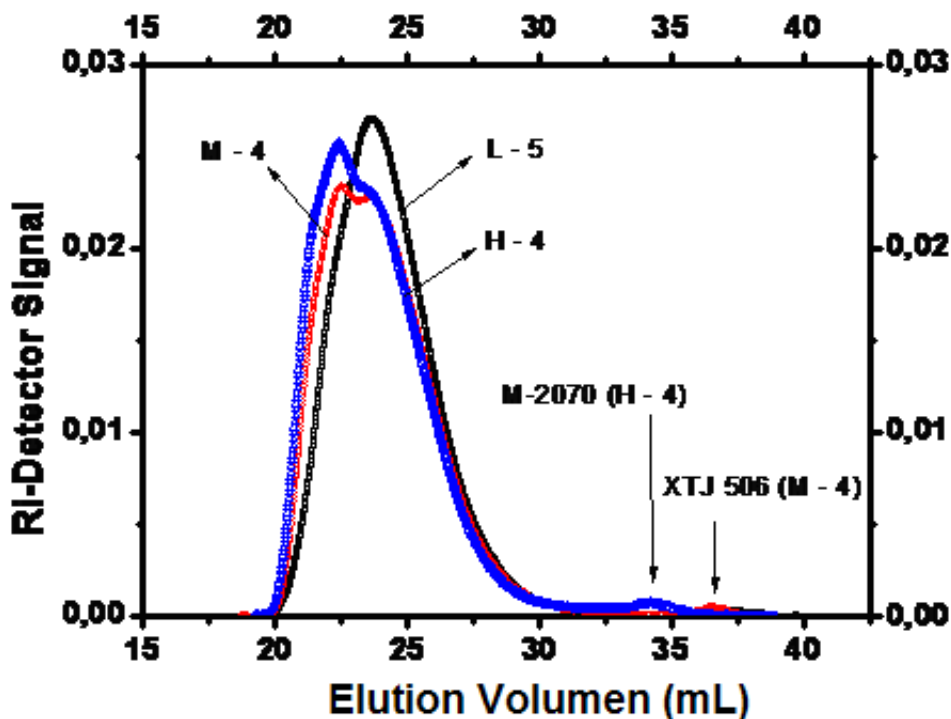


Figure 3.6: A typical elugrams of the some graft-copolymers prepared in this thesis

- **Gel Permeation Chromatography Measurements**

GPC measurements were performed at room temperature in THF using 5 $\mu$  PSS SDV gel columns ( $10^2$ ,  $10^3$ ,  $10^4$ ,  $10^5\text{\AA}$ , 8-300 mm each, PSS GmbH, Mainz, Germany) at a flow rate of 1.0 ml/min (VWR-Hitachi 2130 pump). A Waters 2410 refractive index detector ( $\lambda = 930$  nm) was used for concentration detection. Samples were injected employing a Waters 717 autosampler (injection volume 20  $\mu$ L). To compensate for flow-rate fluctuations, 20ppm 2,6-di-*tert*-butyl-hydroxytoluene (BHT) was added as internal standard to each sample. Raw data were processed using the PSS WinGPC Unity software package. Elugrams are flow-rate corrected; polystyrene calibration was used to calculate the molar mass distribution.

### 3.5 Scanning Electron Microscopy (SEM)

Scanning electron microscopy (SEM) is a type of electron microscope that magnified images the samples surfaces by scanning it with a high-energy beam of electrons in a raster scan pattern. The electrons interact with the atoms, molecules and in general with chemical environmental that make up the samples producing signals that contain information about the sample's surface topography, morphology, composition and other properties such as electrical conductivity. In this work the SEM is applied to examine the polymers morphology, chemical analysis and thickness of layers involves in the membrane using a cross-section image. This image can show different layers and location of the dense material "graft-copolymer" and the PAN support, however is possible to visualize a primary dimension of any possible interface. This interface in the membrane is where the materials can coincide, for instance, the graft-copolymer and the PAN. In order to have accurate permeability calculation, the SEM helps to determinate specifically each layer in the membrane and to determinate the thickness applicable during the membrane performance. Another important aspect is to analyze the SEM cross-section image to discuss a possible explanation of this interface between the graft-copolymer and the PAN.

The specimen is attached to the fast-setting adhesive to a platform and a conductive coating (e.g gold or aluminium) is applied onto the surface of the specimen. A monoenergetic and narrow beam of electrones is the requirement of SEM for best resolution. The electron beam is accelerated by keeping the filament at large negative potential and keeping the anode and the specimen at earth potencial. The beam of electron passes through a hole in the anode and is focused onto the



specimen using an electromanegnetic lens or system of the lenses [10]. As the electron beam impinges the specimen, following interactions take place:

- Some electrons are back-scattered because of electrostatic attraction between negatively charged incident primary beam and positively charged nucleus within the specimen.
- Some electrons within the specimen are knocked out by the primary electrons and are regarded as the secondary electrons.
- After knocked out electrons (secondary electrons) have been removed from the inner shell, an electron from less tightly bound state fall into the less tightly bound state with the emission of a photon which is detectable in the x-ray range of the electromagnetic spectrum.

Various detectors are arranged in specimen chamber for the measurement of the several signals which are characteristic for the region of the specimen under bombardment. The detectors which are reported in the literature include secondary electron detectors, back-scattered electron detectors, energy dispersive detectors and wavelength dispersive detectors. The signal detected by any of the detectors changes continuously with changing the characteristics of the surface probed by the electrom beam. The amplified sinal is used to control the brightness of the spot on a cathode ray tube. The cathode ray scan is controlled by the same scan genarator which controls the SEM beam position thus spatial correspondence between the specimen and cathode ray image is maintained [10,11], figure 3.7 exhibits a layout of the instrumentation of SEM.

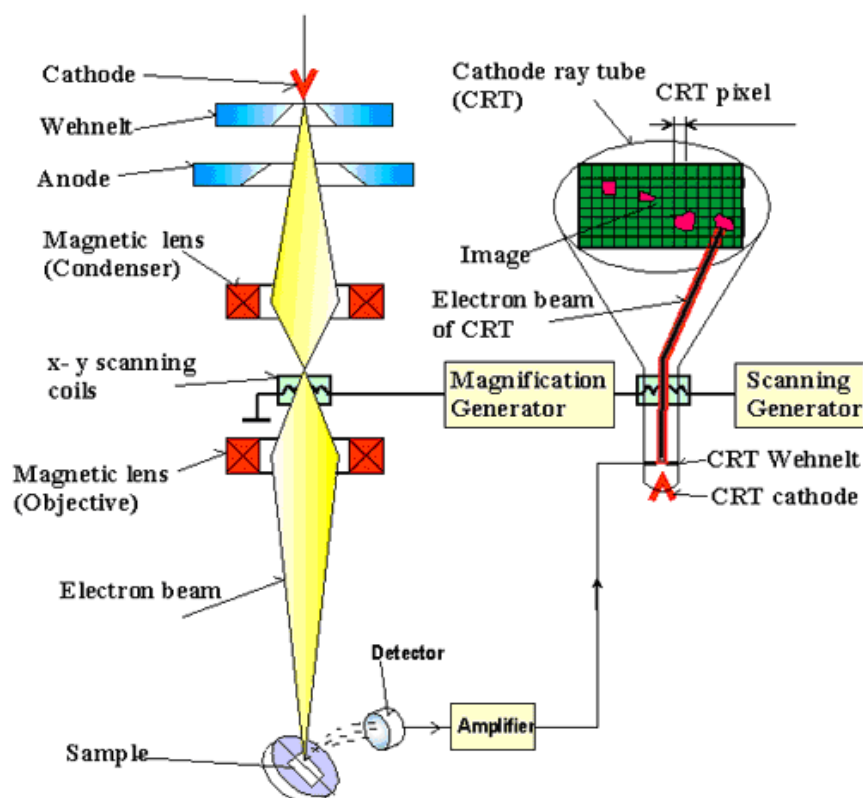


**Figure 3.7:** Layout of the instrumentation of SEM [11].

- **Electron Microscopy Images**

Scanning electron microscopy (SEM) images were obtained using a LEO Gemini 1550 VP (Fa. Zeiss) field emission gun microscope operated at 30kV with high vacuum, with an In-Lens secondary electron detector, 3kV, 20 $\mu$ m aperture. Samples were obtained (cross-section) using the breaking technique under liquid nitrogen after a cooling time of about 30 seconds and a conductive Au/Pd coating of 2,5 nm thickness was sputtered onto the samples prior measurement.

### 3.6 Elementary Analysis (EA)

Elemental Analysis is an experiment that determines the amount (typically a weight percent) of an element in a compound. Just as there are many different elements,

there are many different experiments for determining elemental compositions. The most common type of elemental analysis is for carbon, hydrogen, and nitrogen (CHN analysis). The elemental analysis of a compounds is particularly useful in determining the empirical formula of the compound. The most common form of elemental analysis, CHN analysis, is accomplished by combustion analysis. In this technique, a sample is burned in an excess of oxygen, and various traps collect the combustion products — carbon dioxide, water, and nitric oxide [12,13]. The weights of these combustion products can be used to calculate the composition of the unknown sample.

- **Elementary Analysis Measurement**

A CHNS Analysis by Flash EA 1112 Series Analyzer from ThermoFinnigan – CE Instruments was used. The configuration operates according to the dynamic flash combustion of the sample. The sample is weighed in tin capsule and introduced into the combustion reactor via MAS 200 auto-sampler together with a proper amount of oxygen. After combustion, the gases produced, N<sub>2</sub>, CO<sub>2</sub>, H<sub>2</sub>O and SO<sub>2</sub> are carried by a helium flow to a layer filled with copper, then swept through a GC column that provides their separation and finally are detected by a thermal conductivity detector. Total run time is less than 12 minutes. A complete CHNS report is automatically generated by the Eager 300 data handling software package and displayed at the end of the analytical routine.

**Analytical conditions**

T Combustion Reactor: 900°C

T Oven GC column: 65°C

Helium: Carrier Flow: 130ml/min

Reference Flow: 100ml/min

Oxygen Flow: 250ml/min

Oxygen Injection End: 7 sec

Sample Delay Time: 12 sec

Run Time: 720 sec

Standard and Sample Weight: 2-3 mg

For this analysis the compound BBOT [2,5-Bis (5-ter-butyl-benzoxazol-2-yl) thiophene] was used as calibration standard whose composition is 6.51 %N, 72.53 %C, 6.09% H and 7.44 % S, and K factor as a method of calibration. Figure 3.8 shows a scheme of the principle of the elemental analysis [13].

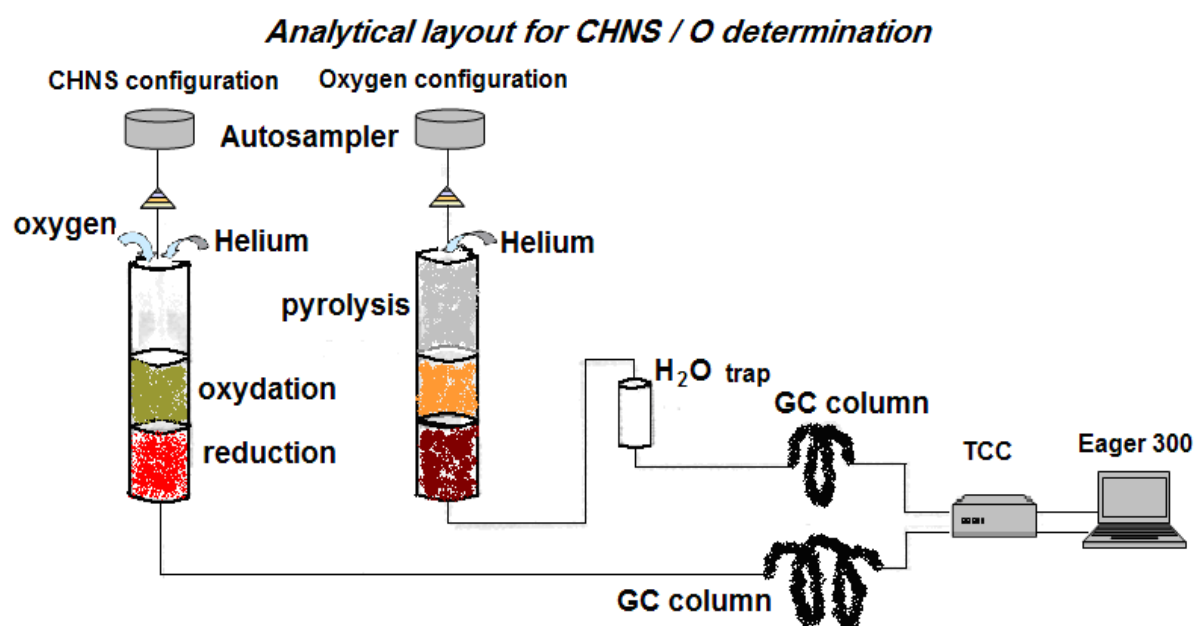


**Figure 3.8:** Basic scheme of Elementary Analysis [13], thanks to Carla Rodriguez, Analysis Laboratory - REQUIMTE- Universidade Nova de Lisboa.

### 3.7 References

- [1] David I. Bower, *An Introduction to Polymer Physics*, Cambridge University Press, Published in USA, New York, 1<sup>st</sup> Edition 2002, Reprint 2004, pp 27-30
- [2] Ferdinand Rodriguez, Claude Cohen, Christopher Ober, Lynden A. Archer *Principles of Polymer Systems* 5<sup>th</sup>, Edition, Taylor & Francis, New York – London, 1996, pp 700-701
- [3] Jen Ed. Chiu, *Polymer Characterization by Thermal Methods of Analysis*, Marcel Dekker, INC New York, USA, 1974
- [4] David I. Bower, *An Introduction to Polymer Physics*, Cambridge University Press, Published in USA, New York, 1<sup>st</sup> Edition 2002, Reprint 2004, pp 42-44
- [5] Ferdinand Rodriguez, Claude Cohen, Christopher Ober, Lynden A. Archer *Principles of Polymer Systems*, 5<sup>th</sup> Edition, Taylor & Francis, New York – London, 1996, pp 696-699
- [6] David I. Bower, *An Introduction to Polymer Physics*, Cambridge University Press, Published in USA, New York, 1<sup>st</sup> Edition 2002, Reprint 2004, pp 44-46
- [7] Ferdinand Rodriguez, Claude Cohen, Christopher Ober, Lynden A. Archer *Principles of Polymer Systems*, 5<sup>th</sup> Edition, Taylor & Francis, New York – London, 1996, pp 703 – 706
- [8] Ferdinand Rodriguez, Claude Cohen, Christopher Ober, Lynden A. Archer *Principles of Polymer Systems*, 5<sup>th</sup> Edition, Taylor & Francis, New York – London, 1996, pp. 209, 220-226
- [9] Paul C. Hiemenz, *Polymer Chemistry -The Basic Concepts* - Marcel Dekker, INC. New York 1984, pp 642-644.

- [10] Joseph Goldstein, Dale Newbury, David Joy, Charles Lyman, Patrich Echlin, Erick Lifshin, Linda Sawyer, and Joseph Michael, *Scanning Electron Microscopy and X-ray Microanalysis*, 3th. Edition, Springer Science Inc., New York, USA 2003, chapter 12, pp 565-576.
- [11] R.E. Lee *Scanning Electron microscopy and X-ray microanalysis*, Prentice Hall, New York, USA, 1993, pp.93-95
- [12] Christopher M. Barshick, Douglas C. Duckworth, David H. Smith, *Inorganic Mass Spectroscopy-Fundamentals and Application*, Marcel Dekker Inc., New York, USA, pp 329 – 372
- [13] Rezl V., *Mikrochimica Acta*, 2 (1982) 107.

---

**Chapter IV      Grafting of Poly (styrene - co - maleic anhydride)  
via Maleic Anhydride with Poly(ether amines)**

---

Different strategies towards the construction of more efficient membranes have been suggested by Powel [1] and Ulbrich [2], in which are using polymers such as polyacetylenes, polyaniline, poly(arylene ether)s, polycarbonates, polyimides, polysulfones, etc. For instance, polyether/amide block copolymers [PE-b-PA] have extremely high polar/nonpolar (e.g., H<sub>2</sub>S/CH<sub>4</sub>, CO<sub>2</sub>/H<sub>2</sub>, or CO<sub>2</sub>/N<sub>2</sub>) gas selectivity [3], making them potentially interesting membrane material for the removal of CO<sub>2</sub> from synthesis gas, natural gas, and flue gas. These phase separated, segmented block copolymers consist of linear chains of relatively rigid polyamide segments interspersed with flexible polyether segments. One of these strategies is to graft copolymers containing hydrophilic side chains, which have been used in many industrial applications. For example, application of graft or comb-like copolymers in industry of new materials has grown dramatically in the past decade [4,5]. Academically, many papers on the subject of graft copolymers containing poly(ethylene glycol) (PEG) and poly(ethylene glycol) monomethyl ethers (mPEG) segments as a side chain to apply as membrane for gas separation were published [6,7]. Typically, these types of graft copolymers can be synthesized by polymerization of mPEG macromonomers [8], direct anionic polymerization of ethylene oxide onto main chain polymers [9] or alkaline trans-esterification to graft mPEG onto different acrylate and methacrylate copolymers [10]. At the same time, as a representative alternating copolymer, poly(styrene-co-maleic anhydride) (SMA) has been in focus to study the behavior of copolymers [11]. Compared with general thermoplastics, SMA has a higher thermal stability and exhibits a good miscibility

with styrenic polymers [12,13], providing a wide range of application in industrial use. Recently, industrial interests have arisen in the field of surface treatment or modification of styrenic polymers as well. Some groups are focused in: hybrid materials [14], nano-materials [15] and the fuel cell applications [16]. However, there are few applications for SMA in the membranes field [16-18] in particular in gas separation and especially in combination with  $\alpha$ -polyetheramines (Jeffamine-monoamines) [19,20]. The objectives of this chapter are to describe the preparation of a novel graft-copolymer via amidation based on poly(styrene-co-maleic anhydride) using Jeffamine®-monoamines grafts. Details on the synthesis as well as the characterization by  $^1\text{H}$  and  $^{13}\text{C}$ -NMR spectroscopy, gel permeation chromatography (GPC), and thermal analyses (DSC, TGA) will be given.

## 4.1 Experimental Part

### 4.1.1 Materials

Commercial poly (styrene-co-maleic anhydride) (7 % weight in maleic anhydride; Aldrich) with a weight-average molar mass of 220.000 g/mol was used as received. Methyl ethyl ketone (MEK) was used as received and dried over molecular sieves. Monofunctional  $\alpha$ -amino- $\omega$ -methoxy polyether was either purchased from Aldrich (XTJ 505;  $M = 600$ ) or kindly supplied from Huntsman Company (XTJ 506;  $M = 1000$  and M-2070;  $M = 2000$ , also commercially available under the trade name Jeffamine® Monoamine). Its chemical structure is sketched in Figure 4.1 and the properties are outlined in the fig. 2.7, page 22.



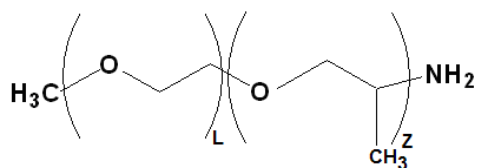


**Figure 4.1:** Structure of  $\alpha$ -amino- $\omega$ -methoxy polyether (Jeffamine<sup>®</sup>).

### 4.1.3 Preparation of Graft-Copolymers

The graft-copolymers were prepared by amidation reaction [21] of poly(styrene-co-maleic anhydride) (SMA, content of maleic anhydride units 7 wt.%) with the corresponding poly (ether amines) (Figure 4.2). In the preparative procedures, it is crucial to dry the SMA at 120°C under reduced pressure for 12 h. SMA was dissolved in MEK under stirring for 6 h. A solution of jeffamine in MEK was added drop wise within 1 h and the reaction mixture was heated under continuous stirring up to 50 °C for 24 hours. On completion of the reaction, 80% of the MEK was removed from the crude product under reduced pressure to recover the graft-copolymer. It was precipitated in a large excess of a non-solvent (*iso* - propanol, ethanol or H<sub>2</sub>O), recovered by filtration and washed with more non-solvent. Finally, the product was dried at room temperature *in vacuo* for 48 h.

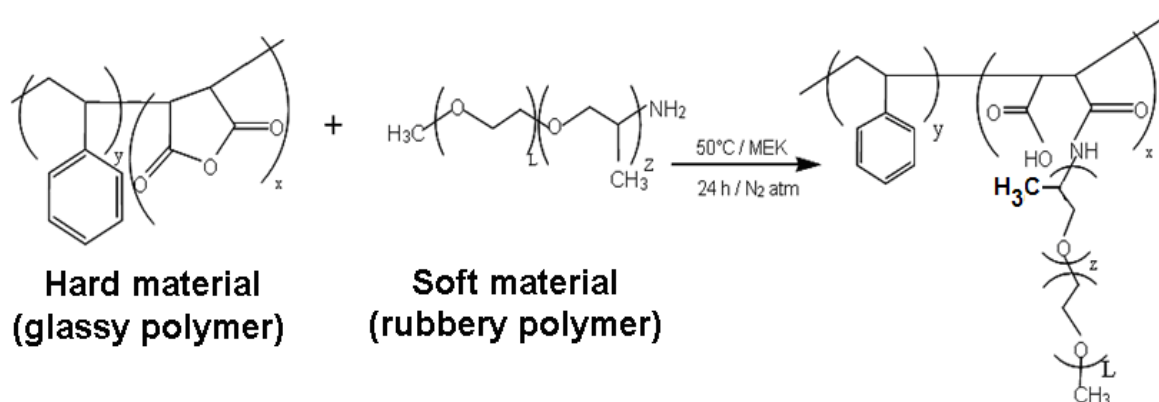


**Figure 4.2:** Scheme and strategy of the amidation reaction

The conditions to obtain graft-copolymers in dependence of the type of jeffamine, the molar ratio of maleic anhydride (MA) to poly(ethylene glycol (PEG), and the type of non-solvent used are summarized in Table 4.1.

**Table 4.1:** Experimental data of the reaction.

Graft - Copolymer	Jeffamine used	Non solvent	Molar Ratio MA : PEG	Yield (%)
L - 1	XTJ 505	<i>i</i> -prop	1 : 1	67
L - 2		Et-OH/H <sub>2</sub> O	1 : 0.5	87
L - 3		Et-OH	1 : 0.5	91
L - 4		Et-OH	1 : 1	83
L - 5		H <sub>2</sub> O	1 : 0.5	93
M - 1	XTJ 506	H <sub>2</sub> O	1 : 1	74
M - 2		H <sub>2</sub> O	1 : 0.5	67
M - 3		Et-OH	1 : 0.5	86
M - 4		Et-OH/ <i>i</i> -prop	1 : 0.5	77
H - 1	M-2070	<i>i</i> -prop	1 : 1	40
H - 2		Et-OH/H <sub>2</sub> O	1 : 0.5	83
H - 3		Et-OH	1 : 0.5	41
H - 4		Et-OH / <i>i</i> -prop	1 : 0.5	68

**Note:** When using a binary solvent the ratio was 3 : 1 vol. / vol.

## 4.2 Results and Discussion

### 4.2.1 <sup>1</sup>H-NMR and <sup>13</sup>C-NMR Analysis

The <sup>1</sup>H-NMR spectra of the graft-copolymer (H-1) in acetone-*d*<sub>6</sub> and the chemical shifts of the characteristic protons in H-1 are depicted in Figure 4.3.

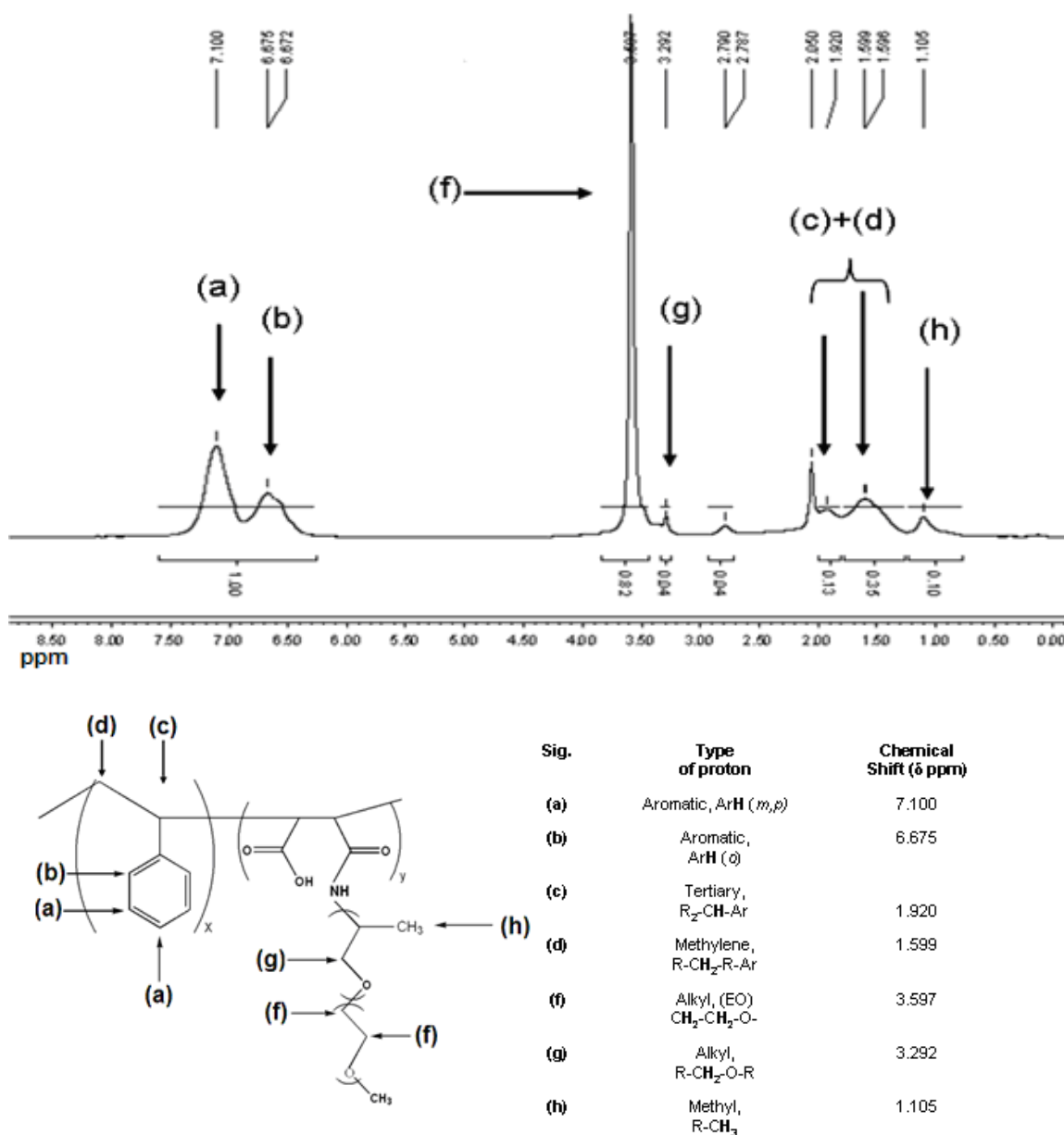


**Figure 4.3:**  $^1\text{H-NMR}$  spectrum of the polymer H-1 in acetone- $d_6$ , structure and assignment of the spectrum [22,23].

The characteristic resonance signals for the five aromatic ring protons of styrene are observed from  $\delta = 7.1$  ppm to  $\delta = 6.5$  ppm (a) and (b), respectively. The  $-\text{CH}-$  signal of maleic anhydride, expected at chemical shifts of 2.6 – 2.5 ppm was not detected; probably due to the low concentration of MA (7 wt. %) in the SMA copolymer. The

styrene signals, aromatic and aliphatic show a single broad resonance peak, which is characteristic for the polymer backbone. The alkyl proton signal (f), typical for poly(ethylene oxide) unit, can be identified at  $\delta = 3.59$  ppm and a resonance peak of low intensity appears at  $\delta = 3.29$  ppm (g) which is typical for the alkyl proton signals R -CH<sub>2</sub>-O-R of poly(propylene oxide). Finally, the characteristic peaks for the methyl proton signal (h) appears at  $\delta = 1.10$  ppm.

Figure 4.4 shows the <sup>13</sup>C-NMR spectrum of H-1 in CDCl<sub>3</sub>, the chemical structure and the assignments. The spectrum exhibits a distinct single signal (q) at ~171.0 ppm, typical of the carbonyl carbon resonance indicating the presence of maleic anhydride functionality in the copolymer. Note, that this peak is normally difficult to detect due to presence of dipolar broadening [24]. The benzylic carbon signal (m) can be identified at 145.20 ppm. The spectra also exhibit signals (Z<sub>1</sub>, Z<sub>2</sub>) of the aromatic region at 127.95 and 125.66 ppm respectively. The alkyl carbons (CH<sub>2</sub>-CH<sub>2</sub>-O-) can be seen at 70.57 ppm. The broad signals (x) and (y) at 43 and 40 ppm respectively, stem from the polystyrene main chain. Finally, when comparing the <sup>13</sup>C-spectra of the different graft copolymers variations in the signal intensities of (w), (r) and (p) at 38.05, 35.22 and 21.52 ppm can be found. As the resonance signals are assigned to the PEG units, their presence and variation may serve as an indirect evidence of the structure proposed in figures 4.3 and 4.4.

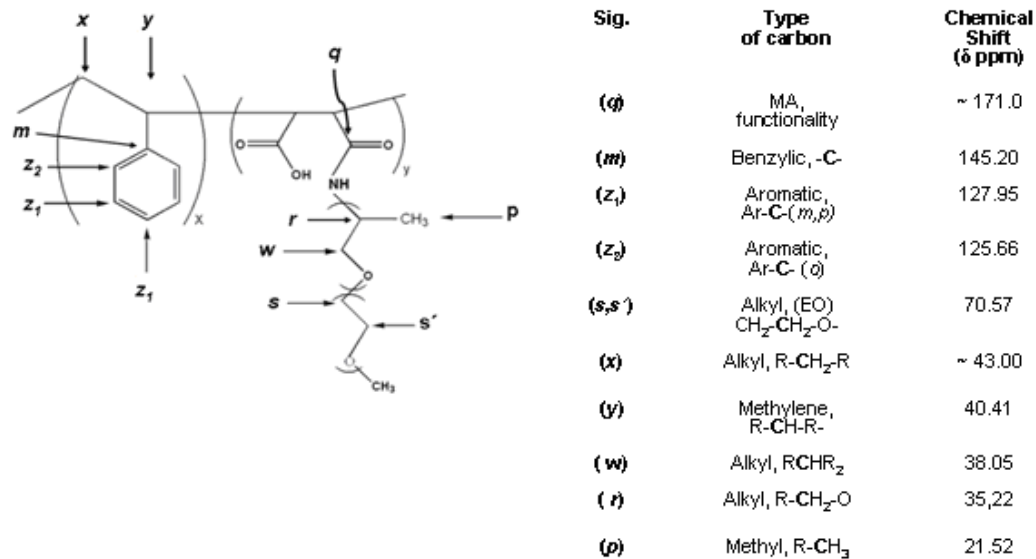
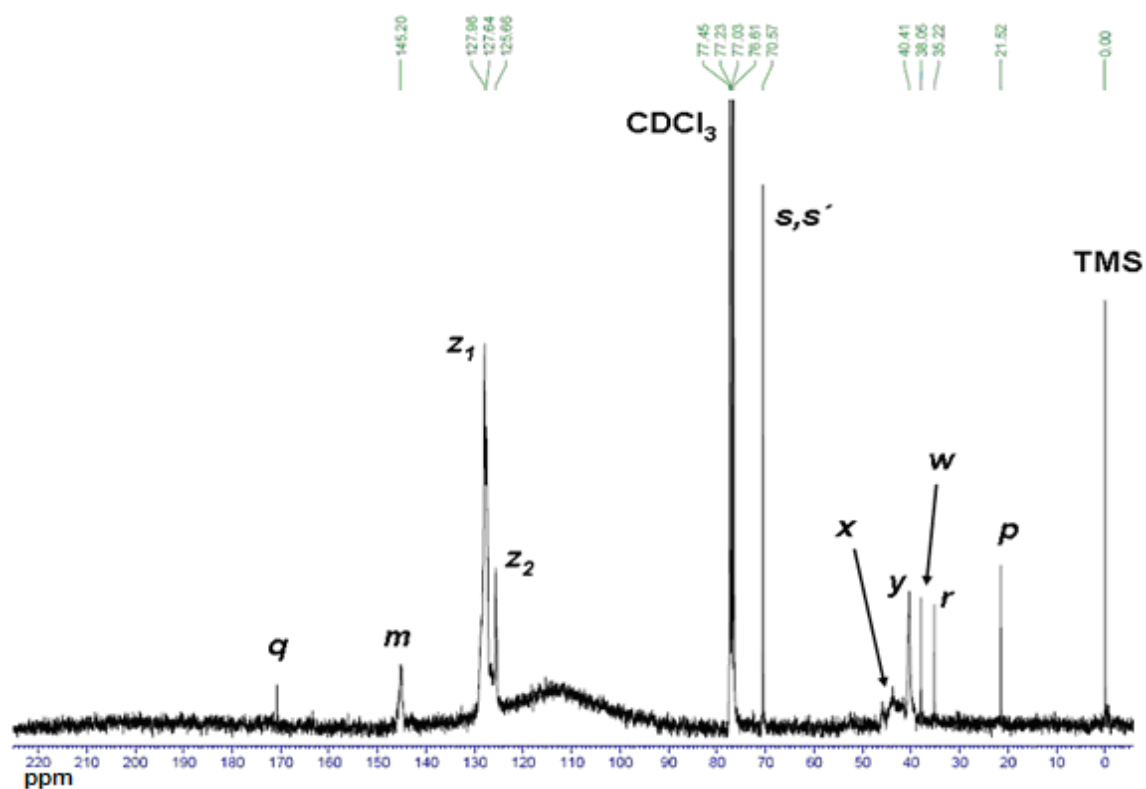


**Figure 4.4:**  $^{13}\text{C}$ -NMR spectrum of the polymer H-1 in  $\text{CDCl}_3$ , structure and assignments [22-24].

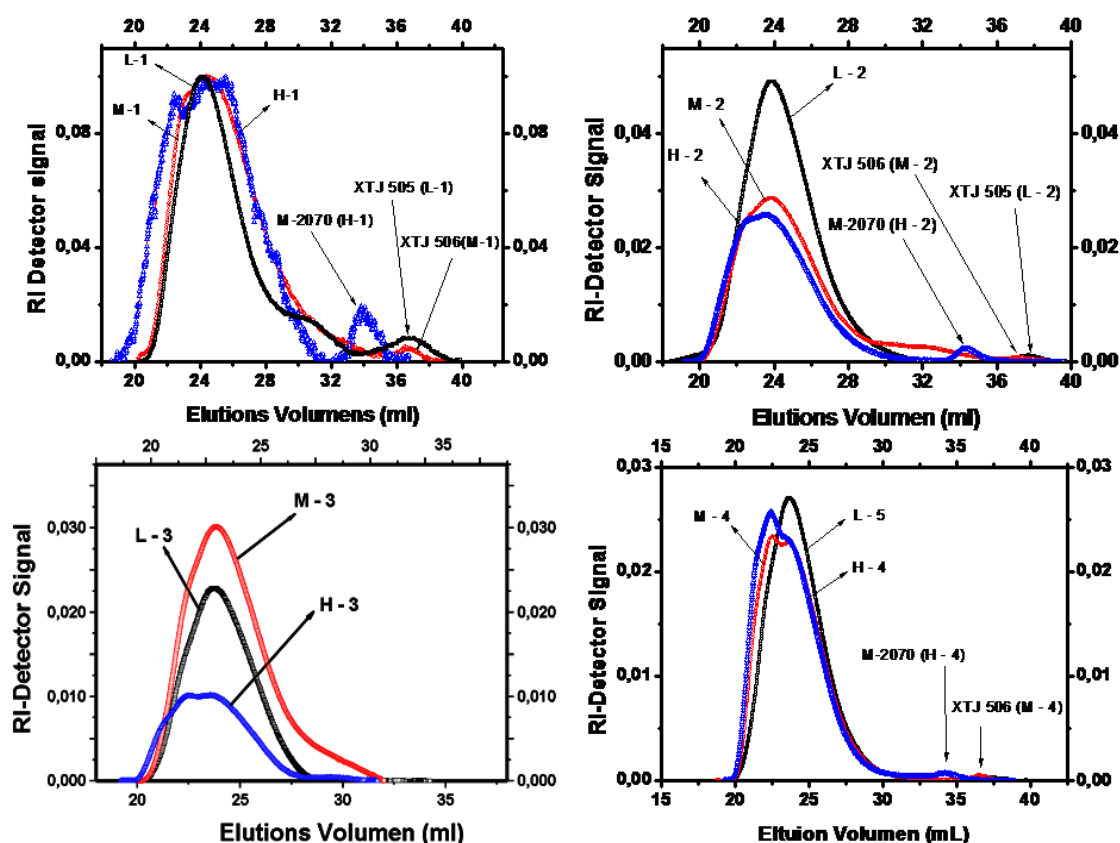
Table 4.2, highlights the final composition (PEG, PS and PPG) in each graft-copolymer calculated from  $^1\text{H-NMR}$  spectra using the normalized signal intensity of the polystyrene's phenyl ring ( $6.5 < \delta/\text{ppm} < 7.5$ ; 5 protons) and the signals of the poly (ethylene glycol) ( $\delta/\text{ppm} = 3.5$ ; 4 protons). Note, that the content of PPG can directly be calculated from the PEG content as the ratio of the two repeating units is predetermined by the type of Jeffamine used (cf. Table 4.1)

**Table 4.2:** Weight percentages of PEG, PS and PPG in the graft-copolymer as determined by  $^1\text{H-NMR}$

<b>Graft-copolymer</b>	<b>PS (wt %)</b>	<b>PEG (wt %)</b>	<b>PPG (wt %)</b>
L – 1	59.1	3.2	37.7
L – 2	48.9	4.0	47.1
L – 3	48.9	4.0	47.1
L – 4	22.6	6.0	71.4
L – 5	49.7	4.0	46.5
M – 1	73.8	21.7	4.5
M – 2	77.9	18.3	3.8
M – 3	75.7	20.0	4.3
M – 4	73.0	22.0	4.7
H – 1	70.5	20.7	8.8
H – 2	66.7	23.5	9.8
H – 3	65.5	24.2	10.3
H – 4	63.2	26.0	11.0

## 4.2.2 Gel Permeation Chromatography

Figure 4.5 shows the elugrams of the purified graft-copolymer of the L-, M- and H- series and the corresponding residual jeffamine (RJ). The signal of residual jeffamine in the graft-copolymer appears at elution volumes ( $V_e$ ) ranging from 34 to 39 mL.



graft	L-1	L-2	L-3	L-4	L-5	M-1	M-2	M-3	M-4	H-1	H-2	H-3	H-4
RJ (%)	5.2	0.7	0.0	0.0	0.3	1.4	1.0	0.0	0.5	4.1	2.6	0.0	1.1

**Figure 4.5:** Elugrams of the graft-copolymer (graft) and content of residual jeffamine (RJ)

The residual Jeffamine content is clearly visible in elugrams (a) and (b), and less obvious in (c) and (d). As its intensity is small in comparison to the signal of the reaction products ( $20 < V_e < 32$  mL) it can be concluded that most of residual jeffamine was successfully removed. The peak areas of the graft-copolymer and of the residual jeffamine were integrated as the area ratio of jeffamine over the area of the entire GPC trace should roughly be proportional to residual jeffamine (RJ) content in the graft-copolymer (RJ). The RJ in the graft-copolymers is below 6 %. Figure 4.6 outlines a scheme to remove the residual jeffamine. The case of *solvent in* or *good solvent* (e.g ethanol) is used to identify a solvent which tends to increase coil dimensions, hence polymer-solvent interactions are thermodynamically favorable and help to remove the residual jeffamine from the graft-copolymer. In the case *solvent out* or *poor solvent* (e.g iso-propanol and water) the solvent tends to decrease the coil dimension; so the chance to remove the RJ from the centrum of the coil is reduced [25]. Both procedures were employed to remove the Jeffamine. The first procedure (*solvent in*, ethanol) was used in most of the purifications of the graft-copolymers. Water could be regarded as an intermediate solvent because on the one hand it is able to remove polar polymers like Jeffamine but on the other it should behave as a bad solvent due to the high amount of poly(styrene) in the graft-copolymer. Hence, in terms of Figure 4.6 water should be regarded as a poor solvent.



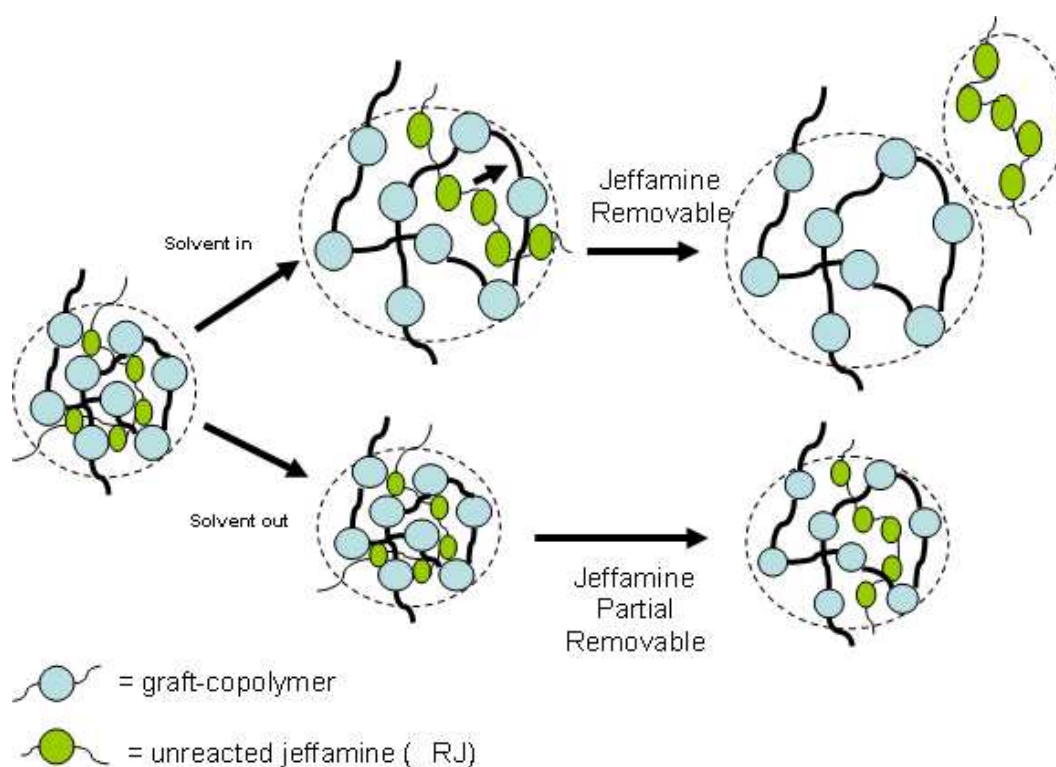


**Figure 4.6:** Scheme to remove the residual jeffamine (RJ), e.g. solvent in (ethanol) and solvent out (*iso*-propanol).

Table 4.3 presents the number average molar mass ( $M_n$ ) and polydispersity index ( $M_w / M_n = D$ ) of the graft-copolymers (L-, M- and H-series) and the SMA(7). The graft-copolymers exhibit expectedly a higher  $M_n$  in comparison to the parent SMA (7), on account of the grafting of Jeffamine. As grafting is a statistical process it is likely that two different graft copolymers possess strong variations in their number of grafts – leading to an increase of the polydispersity index (D) compared to the parent SMA(7).

**Table 4.3:** Apparent number average molar mass ( $M_n$ ) and polydispersity (D), the degree of grafting (DG) and number of chain ( $N_c$ ), as determined by GPC for the graft copolymers and SMA(7)

<b>Graft-copolymer</b>	<b><math>M_n</math> (g/mol)<math>\times 10^5</math></b>	<b>D</b>	<b><math>N_c</math></b>	<b>DG (%)</b>
L – 1 <sup>a</sup>	0.83	3.09	26	2.1
L – 2 <sup>b</sup>	1.30	2.50	85	5.6
L – 3 <sup>b</sup>	2.0	1.85	201	13
L – 4 <sup>b</sup>	1.70	2.76	151	10
L – 5 <sup>c</sup>	1.60	2.32	33	1.2
M – 1 <sup>a</sup>	0.75	3.35	8	0.6
M – 2 <sup>b</sup>	1.50	2.53	71	4.7
M – 3 <sup>b</sup>	1.20	2.78	41	2.7
M – 4 <sup>c</sup>	1.70	2.72	30	1.1
H – 1 <sup>a</sup>	1.20	3.69	26	2.1
H – 2 <sup>b</sup>	1.60	2.91	40	2.7
H – 3 <sup>b</sup>	2.20	2.6	70	4.7
H – 4 <sup>c</sup>	2.10	2.66	35	1.3
<b>SMA (7)<sup>a</sup></b>	0.67	2.89		
<b>SMA (7)<sup>b</sup></b>	0.79	2.56		
<b>SMA (7)<sup>c</sup></b>	1.40	1.89		

<sup>a, b, c</sup> For each group of graft-copolymers samples the SMA was analyzed by GPC leading to variations in the molar mass distribution

Table 4.3 exhibits besides the number of chain ( $N_c$ ) the degree of grafting ( $DG$ ).

These quantities were defined as

$$N_c = \frac{Mn_{\text{grafted}} - Mn_{SMA}}{Mn_{\text{jeffamine}}} \quad (1)$$

and

$$DG = \frac{N_c}{2N_{MA}} \cdot 100\% = \frac{N_c}{2 \frac{M_{SMA}}{x_S M_S + x_{MA} M_{MA}}} \cdot 100\% \quad (2)$$

where  $M_S$  and  $M_{MA}$  represent the molar mass of the respective repeat unit and  $x_S$  and  $x_{MA}$  represent the fraction of styrene (S) and maleic anhydride (MA).  $N_c$  and  $N_{MA}$  represent the number of chains and the number of maleic anhydride units respectively.

Obviously, the DG is high for the L-series and lower for both the M- and the H-series. As indicated in fig. 2.7, page 22, and table 4.2 the series differ both in the jeffamines' molar mass and their PEG content. The jeffamine XTJ 505 used for the L-series exhibits the lowest molar mass as well as the lowest PEG content, whereas in the H-series the jeffamine has the highest molar mass and the highest PEG content. Considering the amidation reaction this result may be expected, because jeffamine with a shorter chain should have a higher reactivity, due to a less pronounced steric hindrance. Nevertheless, the difference between the M- and H-series is not very strong; possibly the effect of the chain size on the steric hindrance levels off.

### 4.3.3 Thermal Properties of the Graft-Copolymers

#### 4.3.3.1 Differential Scanning Calorimetric (DSC)

Table 4.4 presents the glass transition temperatures ( $T_g$ ) and the heat capacity ( $\Delta c_p$ ) of the graft-copolymers both values were taken directly from the DSC thermogram. Furthermore, it features the relative difference of the graft copolymer's glass transition temperature ( $\Delta T_g$ ) compared to the glass transition temperature of the parent poly(styrene-co-maleic anhydride) (SMA(7)) in dependency of the samples' PEG content. Besides the  $T_{g_{SMA(7)}}$  is fixed at 120,6°C as typical experimental value obtained from the DSC heating thermograms.

Following results may be extracted from Table 4.5: (i) The glass transition temperature of the graft-copolymers can be found between the glass transition of the parent poly(styrene-co-maleic anhydride) (121.6°C) and the Jeffamines (-82, -66, and -51°C). Except for sample L-5 the L-series exhibits higher glass transition temperatures compared to the other graft-copolymers of the M- or H-series. (ii) the M-series shows intermediate glass transition temperatures between 50 and 60°C and (iii) the H-series exhibits the lowest glass transition temperature around 20°C. The exception of the general trend is sample H-1 with a low PEG content of 20.7% for which glass transition temperature is closer to M-series. In most cases the decrease of the graft-copolymers' glass transition temperature ( $\Delta T_g$ ) with respect to the original poly(styrene-co-maleic anhydride) shows a strong influence of the jeffamine type.

**Table 4.4:** Glass transition temperatures,  $T_g$ , heat capacity  $\Delta c_p$  and the relative difference of the graft copolymers' glass transition temperature with respect to the parent poly(styrene-co-maleic anhydride) in dependency of the PEG content.

Graft – Copolymer	$T_g$ (°C)	$\Delta C_p$ (J/g*K)	$\Delta T_g^*$ (%) <sup>b</sup>	PEG (wt %)
SMA	121.6	0.339	-	
L - 1	88.0	0.262	-27.6	3.2
L - 2	76.7	0.218	-37.0	4.0
L - 3	79.8	0.228	-34.4	4.0
L - 4	71.5	0,122	-41.2	6.0
L - 5	29.3	0.040	-76.0	4.0
M - 1	56.1	0.124	-54.0	21.7
M - 2	68.0	0.151	-44.0	18.3
M - 3	60.2	0.141	-50.5	20.0
M - 4	48.2	0,064	-60.4	22.0
H - 1	50.9	0.278	-58.1	20.7
H - 2	21.7	0.040	-82.2	23.5
H - 3	22.4	0.074	-81.6	24.2
H - 4	25.4	0.091	-79.1	26.0
XTJ - 505	-81.6	-----	-----	10.0
XTJ - 506	-66.5	-----	-----	86.4
M - 2070	-51.3	-----	-----	75.6

$\Delta T_g$  was calculated as:  $(\Delta T_g \%) = [(T_{g \text{ graft-copolymer}} - T_{g \text{ SMA}(7)}) / T_{g \text{ SMA}(7)}] \times 100\%$ , for  $\Delta T_g$  calculation,  $T_{g \text{ SMA}}$  (121,6°C) is a constant value, \* = negative values means a decrease of the  $T_g$  with respect of the  $T_g$  of the parent poly(styrene-co-maleic anhydride),  $\Delta c_p$  = for each sample were taken directly from DSC plot .

Generally, the effect is strongest for H-series ( $\Delta T_g \sim 80\%$ ), less pronounced for the M-series (60 %) and the least obvious for the L-series. However, there is a group of samples not following this tendency, e. g. L-5 ( $\Delta T_g \sim 76\%$ ), it is possible that the  $T_g$  is affected by reaction solvent (MEK) remaining after the precipitation process of the sample, hence the results show a unusual trend, the low decrease in case of H-1 ( $\Delta T_g \sim 58\%$ ) may be explained as H-1 possesses a similar PEG content as M-4; hence the variation of the glass transition temperature ( $\Delta T_g$ ) can also be assumed to be in the same range.

It is important to remember that the content of jeffamine in the graft-copolymer is limited by several factors, (i) the synthetic procedure and (ii) the content of the maleic anhydride (7 wt %).

Neat PEG is a semi-crystalline polymer. Nevertheless, no melting transitions [26] due to a semi-crystalline behaviour of the polyethylene glycol (PEG) units in the graft-copolymer structure could be detected. Probably the PEG content (spanning from 10 to 26 %, see table 4.5) is still too low to allow a crystallisation. Hence, we can consider the graft-copolymers as amorphous materials.

Table 4.5 also presents an overview of the polymers' heat capacity change at constant pressure,  $\Delta C_p$  ( $\Delta C_p$ ), during the glass transition temperature ( $T_g$ ). In general terms and without taking sample H-1 into account it follows the trend  $\Delta C_p$  (H-series) <  $\Delta C_p$  (M-series) <  $\Delta C_p$  (L-series) <  $\Delta C_p$  (SMA). This may be caused by the increase of the molar mass of the graft-copolymer due to the grafting of the jeffamine (soft material) onto the main chain poly(styrene-co-maleic anhydride) (hard material). The variation of  $\Delta C_p$  observed can be considered as an indicator of structural changes. The samples of the H-series show a higher  $\Delta C_p$  in comparison the  $\Delta C_p$

of poly(styrene-co-maleic anhydride) due to their higher PEG content (around 25) and their higher Jeffamine molar mass (2000 g/mol). The introduction of the PEG block makes the graft-copolymer softer in comparison the SMA and consequently affects the glass transition temperature and the  $\Delta c_p$ . The M- and L-series follow the same trend, the  $\Delta c_p$  of the grafted copolymers is lower compared to that of poly(styrene-co-maleic anhydride) and the  $\Delta c_p$  decreases with increasing PEG content.

Figure 4.7 shows DSC heating thermograms of the graft-copolymers. A typical immiscible blend exhibits two glass transitions; the results of DSC show the existence of only one transition, clearly indicating the formation of the desired graft-copolymers. Figure 4.7 also demonstrates that the glass transition of the graft copolymers spans over a broader temperature range than the one of the poly(styrene-co-maleic anhydride), which could also be explained in terms of a higher heterogeneity. As the glass transition temperatures of the graft-copolymers are lower than the one of the poly(styrene-co-maleic anhydride) it can be assumed that the graft-copolymers have a higher mobility and elasticity due to the presence of the poly(ethylene glycol) soft segments. If these conformational changes can take place, space must be available for molecular segments to move. Hence, a comparable amount of free space per unit volume (fractional free volume,  $V_f$ ) can be realised for graft-copolymer at lower temperatures (20 – 80 °C) in comparison to the poly(styrene-co-maleic anhydride) with a glass transition at 122°C [26].

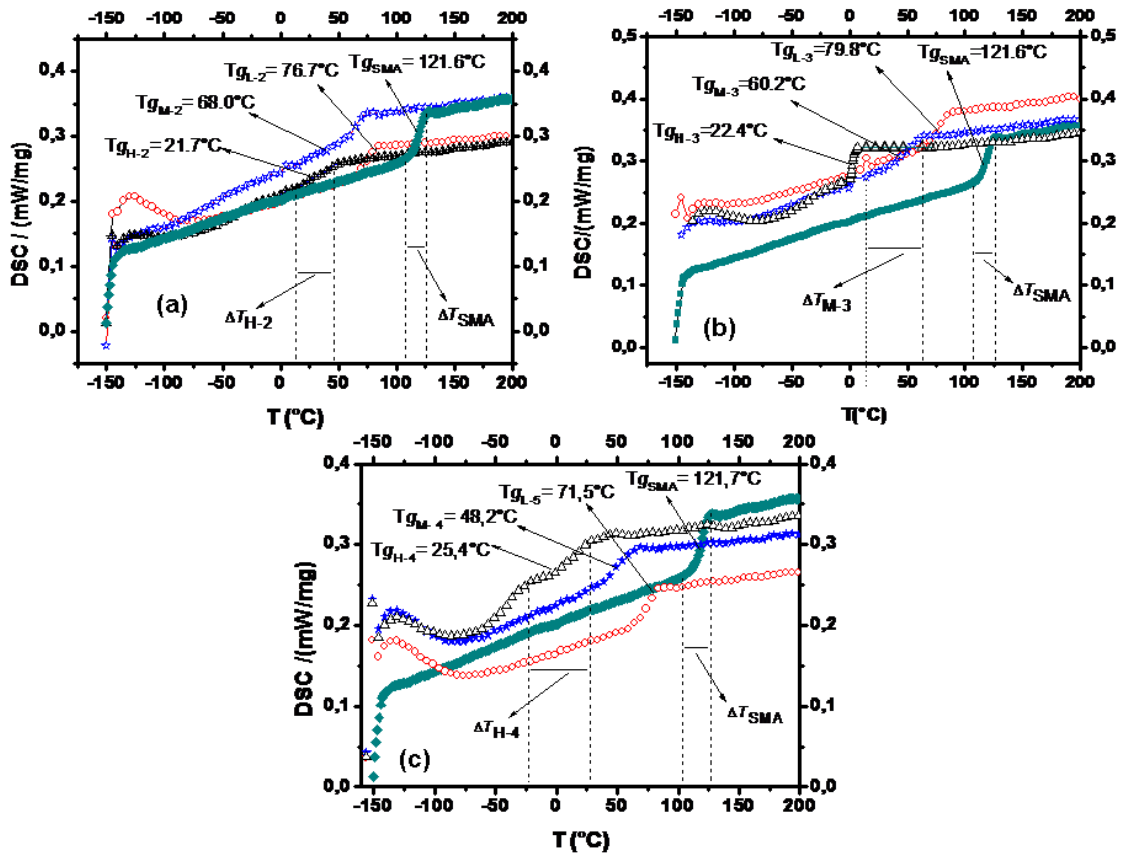


**Figure 4.7:** DSC heating thermograms of: (a) L-2, M-2 and H-2, (b) L-3, M-3 and H-3 and (c) L-5, M-4 and H-4.  $\Delta T = T_{\text{final}} - T_{\text{initial}}$  of the glass transition process

In a temperature range of 25 – 100 °C, i. e. the usual temperature of operation for most industrial processes, the graft-copolymers possess a higher free volume compared to SMA, making the graft-copolymer a potential material for gas separation. Furthermore, when the temperature in a membranes process exceeds the glass transition temperature of the membrane material the permeability is governed by solubility phenomena. Consequently, these graft-copolymers are potentially interesting materials for gas separation processes, because they possess a high free volume in combination with a material (PEG) which is well known to solubilise carbon dioxide [7].



#### 4.3.3.2 Variation of Glass Transition Temperature with the [PEG].

Figure 4.8 highlights the variation of the glass transition temperature ( $T_g$ ) with the poly(ethylene glycol) content in the graft-copolymer. For an increasing PEG content the  $T_g$  of the graft copolymers decreases in a continuous manner.

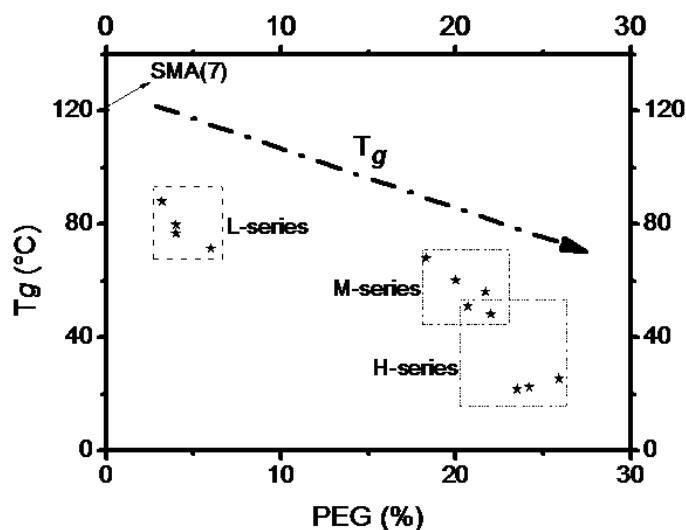


**Figure 4.8:** Dependency of the graft copolymers'  $T_g$  on the PEG content

The difference in the glass transition temperature behavior can be divided in two sectors: a first one containing the L-series which exhibits higher glass transition temperatures and a second sector containing the H- and M-series which show only slight differences to each other. The L-series with a low content of PEG resembles a polymer with characteristics of a more glassy state, whereas the M- and H-series are more similar to rubbery state materials as indicated by their low glass transition temperatures. These lower  $T_g$  values behavior in case of the H- and M-series indicate a high mobility and flexibility of the polymer chains in comparison to the L-series samples due to their higher PEG content. Also it could be a proof that the graft-copolymer's H- and M-series could be affected by weak intermolecular forces in comparison to the L-series and SMA. The results in the section 4.2 (GPC) which

showed the content of residual Jeffamine (RJ) in overall average the samples is about 1.5% and also that DSC heating thermograms of graft-copolymer's (fig. 4.7) exhibited only one T<sub>g</sub>, so these graft-copolymer's are not blends neither miscible mixtures, hence, the usual mixing rules cannot be applied, see Fox equation (3).

$$\frac{1}{T_g} = \frac{x_1}{T_{g,1}} + \frac{1-x_1}{T_{g,2}} \quad (3)$$

T<sub>g</sub> pertains to the blend, T<sub>g,i</sub> to pure component *i*, and *x<sub>i</sub>* is the mass (weight) fraction of component *i*. Clearly *x<sub>2</sub>* = 1 - *x<sub>1</sub>*. Equation (3) is symmetric with respect to the components and allows prediction from properties of pure components only.

#### 4.3.3.3 Thermal Stability of the Graft-Copolymers (TGA)

Table 4.5 exhibits the results of the thermo gravimetric analysis. Three weight loss stages can be identified for the graft-copolymers: First a weight loss stage ranging from 75 to 120°C which can be attributed to the release of moisture absorbed (graft-copolymer is a hygroscopy material) on the PEG unit during preparation samples previous to TGA- measurement. The second stage occurs in between 150 and 300°C caused by the decomposition of the jeffamine chain attached to the maleic anhydride group. The last loss stage from 360 to 500°C is caused by the final decomposition of the polymer. In comparison to SMA the graft copolymers show a lower temperature, at which a 10% mass loss has been detected (*T<sub>d10</sub>*). Probably the poly(styrene-co-maleic anhydride)'s high polystyrene content causes the higher thermal stability. Some samples e. g. L-2, L-3, M-1 and M-2 show an initial decomposition temperature (TID) around 380°C similar to SMA. A second group features the polymers L-1, M-3, M.4, H-2, and H-3 with a TID at 370°C and finally a

group with a decomposition temperature at 360°C can be identified. Most of graft-copolymers exhibit a residual mass at the initial decomposition temperature (Res.<sub>TID</sub>) between 70 to 50 wt% whereas the poly(styrene-co-maleic anhydride) shows a residual mass at this temperature as high as 90 wt-%. Hence, the thermal stability of the graft-copolymers is worsened by the presence of the jeffamine, however the effect can be regarded as acceptable in comparison with SMA and therefore these polymers can also be applied in high temperature applications.

**Table 4.5:** Results of the thermo gravimetric analysis of the graft-copolymers

<b>Samples</b>	<b>T<sub>d10</sub> (°C)</b>	<b>TID (°C)</b>	<b>Res.<sub>TID</sub> (%)</b>	<b>PEG* (%) (wt/wt)</b>
SMA(7)	375	382	88	0.0
L - 1	340	368	67	3.2
L - 2	358	380	57	4.0
L - 3	357	380	55	4.0
L - 5	356	355	59	4.0
M - 1	357	383	66	21.7
M - 2	360	380	55	18.3
M - 3	359	374	58	20.0
M - 4	356	370	62	22.0
H - 1	363	365	88	20.7
H - 2	361	372	52	23.5
H - 3	359	370	63	24.2
H - 4	310	360	61	26.0

T<sub>d10</sub> = temperature where a 10% mass loss has been detected, TID = first degradation temperature, Res.<sub>TID</sub> = Residual mass determined at the first degradation temperature.

### 4.3 Conclusions

√ Characterization results obtained by  $^1\text{H-NMR}$ ,  $^{13}\text{C-NMR}$ , GPC, DSC, and TGA highlight the successful synthesis of a graft-copolymer using poly(styrene-co-maleic anhydride) and poly(ether amines) (Jeffamine) with PEG contents from 5 to 26 wt-%.

√ Employing a molar ratio (1:0.5) in the synthesis and ethanol as a non-solvent proved optimal conditions to reach yields in average of ~80% and maximum residual jeffamine contents of 5 wt-% and in average less than 1 wt-%.

√ The graft copolymers exhibit only one thermal glass transition indicating that the final product could be an amorphous material. The results also indicate that the content of PEG bonded to the matrix poly(styrene-co-maleic anhydride) can be varied over a wide range leading to a decrease of the glass transition temperature. The incorporation of jeffamine leads to materials with lower thermal stability.

√ Polymers with a lower content of PEG tend to be more in a glassy state, whereas the graft copolymers containing higher amount of PEG are better described as a rubber-type material with an increased fractional free volume (FFV).

#### 4.4 References

- [1] Powell C. E., Qiao G. G., *Journal Membrane Science* 279 (2006) 1.
- [2] Ulbricht M., *Polymer* 47 (2006) 2217.
- [3] Bondar, V.; Freeman, B.;Pinnau, I. *Process American Chemical Society Division of Polymeric Materials: Science and Engineering* 77 (1997) 311.
- [4] W. J. Koros, R. Mahajan, *Journal Membrane Science* 175 (2000) 181.
- [5] A. F. Ismail, L.I.B. David, *Journal Membrane Science* 193 (2001)1.
- [6] Hirayama Y., Tanihara N., Kusuki Y., Kase Y., Haraya K., Okamoto K-i. *Journal of Membrane Science*, 163 (1999) 373.
- [7] Bondar V. I., Freeman B. D., Pinnau I. *Journal Polymer Science, Part B: Polymer Physics*, 38 (2000) 2051.
- [8] Gramain P. and Frere, Y. *Polymer Communication*, 27 (1986) 16.
- [9] Derand H. and Wesslen, B. *Journal Polymer Science, Part A: Polymer Chemistry*, 33 (1995) 571.
- [10] Wesslen B. and Wesslen, K. B. *Journal Polymer Science, Part A: Polymer Chemistry*, 27 (1989) 3915.
- [11] Young, L. J. in *Polymer Handbook*, 2<sup>nd</sup> ed.; Brandrup, J., Immergut, E. H. Eds.; Wiley-Interscience: New York, 1975.
- [12] Shiomi T., Karasz, F. E., McKnight W. J., *Macromolecules*, 19 (1986) 2274.
- [13] Aoki Y., *Macromolecules*, 21 (1988) 1270.
- [14] Zhou W., Dong H. J., Qiu K. Y. Wei Y. *Journal Polymer Science Part A: Polymer Chemistry*, 36 (1998) 1607.
- [15] Bhattacharyya A. R., Bose S., Kulkarni A. R., Pötschke P. Häußler L. Fischer D., Jehnichen D., *Journal of Applied Polymer Science*, 106 (2007) 345.

- [16] Saxena A., Tripathi, B. P. and Shahi V. K., *Journal Physical Chemistry B.*, 111 (2007) 12454.
- [17] Walsby N., Paronen M., Juhanoja J., Sundholm F., *Journal of Applied Polymer Science*, 81 (2001) 1572.
- [18] Yang J. Ch., Jablonsky M., Mays J. W., *Journal of Polymer*, 43 (2002) 5125.
- [19] Wei K-L., Wu J-Y., Chen Y-M., Hsu Y-C., Lin J-J., *Journal Applied Polymer Science*, 103 (2007) 716.
- [20] Wang Z. Pinnavaia T. J., *Journal Material Chemistry*, 13 (2003) 2127.
- [21] Hazer B, Synthesis and characterization of block copolymers, in Handbook of Polymer Science and Technology, Vol. 1, ed. by Cherermisinoff, Marcel Dekker, New York, 1989, pp. 133 – 176.
- [22] Pham Q. T., Pétiard R., Waton H., and Llauro-Darricades M-F., Proton and Carbon NMR Spectra of Polymers; CRC Press, Inc., Boca Raton, U.S.A., 1991, pp. 113-311.
- [23] Brandolini A. J., Hills D.D., NMR Spectra of Polymers and Polymers Additives; Marcel Dekker Inc. New York, USA, 2000, pp. 143 – 360.
- [24] Rengarajan R., Parameswaran, VR., Lee S., Vicic M., Rinaldi P., *Polymer* 31 (1990) 1703.
- [25] Paul C. Hiemenz, Polymer Chemistry, The Basic Concepts, Marcel Dekker, Inc. New-York – USA, 1984, pp. 59-60.
- [26] Paul C. Hiemenz, Polymer Chemistry, The Basic Concepts, Marcel Dekker, Inc. New-York – USA, 1984, pp. 200 – 203.

---

**Chapter V Grafting of Poly(styrene) and Poly(styrene-co-maleic anhydride) via Sulfonation**

---

Due to numerous applications in industrial processes gas separation membranes have been in a constant interest [1-3] and several reviews about this theme have been published [4-6]. The strategy to improve the performance of the membrane preparing a polymeric membrane based on the introduction of the PEG moiety using a sulfonic group can be also a good option. In this direction, the application of graft-copolymers containing some type of sulfonic groups as membranes for gas separation is a promising approach [7-9]. In the past different synthesis routes of PEG segments have been reported [10-12]. At the same time polystyrene functionalization has also been studied to find new applications and to tailor the final materials properties [13]. For example, the preparation of new linear sulfonated [14,15] polystyrene showing different substitution degrees and the effects on charge density has been examined [16]. Also the use the poly(styrene-co-maleic anhydride) or poly(styrene) have been reported for several applications [17-19], but very few papers on gas separation membranes and especially in combination with polyetheramine (Jeffamine) [20-21] have been published. This chapter shows a new alternative to prepare a novel graft-copolymer based on poly(styrene) or poly(styrene-co-maleic anhydride), respectively, and Jeffamine attached via sulfonation and its characterization by spectroscopy as well as thermal analysis.

## 5.1. Experimental Part

### 5.1.1 Materials

The starting polymer was poly(styrene) (PS) ( $M_w = 270\,000\text{ g mol}^{-1}$ ,  $M_w / M_n = 1.05$ ). The commercially available poly(styrene-co-maleic anhydride) (7 % weight in maleic anhydride,  $M_w = 220\,000\text{ g mol}^{-1}$ ; Aldrich) was used as received. Jeffamine® and the monofunctional  $\alpha$ -amino- $\omega$ -methoxy polyether were either purchased from Aldrich (XTJ 505;  $M = 600$ ) or kindly supplied from Huntsman Company (XTJ 506;  $M = 600$  and M-2070;  $M = 2000$ , structures and the properties are summarised in Fig. 4.1 and tab. 4.1. 2-Butanone (MEK) (99+% Sigma-Aldrich), sulfuric acid (96%, Merck), acetic anhydride (98.5%, Merck), dichloromethane (99.8%, Merck), 1,2-dichloroethane (99 % Fluka), methanol (99.8% Fluka) and 2-propanol (99.8%, Merck) were used as received.

### 5.1.2 Graft-Copolymer Synthesis

#### 5.1.2.1 Homogeneous Sulfonation of Polystyrene.

Polystyrene and SMA(7) were sulfonated with analogous methods either in  $\text{CH}_2\text{Cl}_2$  at 40°C or in  $\text{ClCH}_2\text{CH}_2\text{Cl}$  at 50°C with acetyl sulfate as described by Martins *et al.* [22] and Smitha *et al.* [23], respectively. Both procedures are similar to the one patented by Makowski *et al.* [24] to obtain sulfonated polystyrene. The main steps for the homogeneous sulfonation are:

- *Polymer Sulfonation*

*Acetyl sulfate solution preparation.* This solution was prepared by mixing dichloromethane or 1,2-dichloroethane and acetic anhydride under an inert



atmosphere ( $N_2$ ). The solution was cooled to 0 °C and 95 – 97% sulfuric acid was carefully added. This reaction mixture (figure 5.1A) was stirred at room temperature until a homogeneous and clear solution was obtained. During the preparation, an excess of acetic anhydride was used to scavenge traces of water. The acetyl sulfate was freshly prepared prior to each sulfonation reaction.

*Sulfonation Reaction.* Different amounts of PS or SMA (7%) were dissolved in  $CH_2Cl_2$  or 1,2-  $CH_2CH_2Cl_2$  in a three-neck-round-bottomed flask (250 mL) equipped with mechanical stirring, thermometer and dropping funnel. The mixture was heated to 40-50°C to ensure total solubilization of the components and purged with  $N_2$  (30 min). A freshly prepared acetyl sulfate solution was added drop wise using a dropping funnel. The reaction mixture (figure 5.1B) was maintained at 40-50°C under stirring for 1-2 h. The solution became pale yellow after adding the sulfonating agent. The reaction was stopped by adding an excess of methanol or 2-propanol for 30 min and cooling to room temperature. Figure 5.1 shows the reaction scheme.

*SMA- or PS-SO<sub>3</sub>H Isolation.* The method of isolating of PS-SO<sub>3</sub>H depended on the sulfonation degree. The PS-SO<sub>3</sub>H was precipitated by dropping the crude reaction products into a large volume of chilled water, followed by washing copiously with water to eliminate and hydrolyze the acetyl sulfate. The product was filtered and dried under vacuum up to a constant weight. The PS-SO<sub>3</sub>H samples were stored in desiccators containing silica gel, due to their hygroscopic nature.

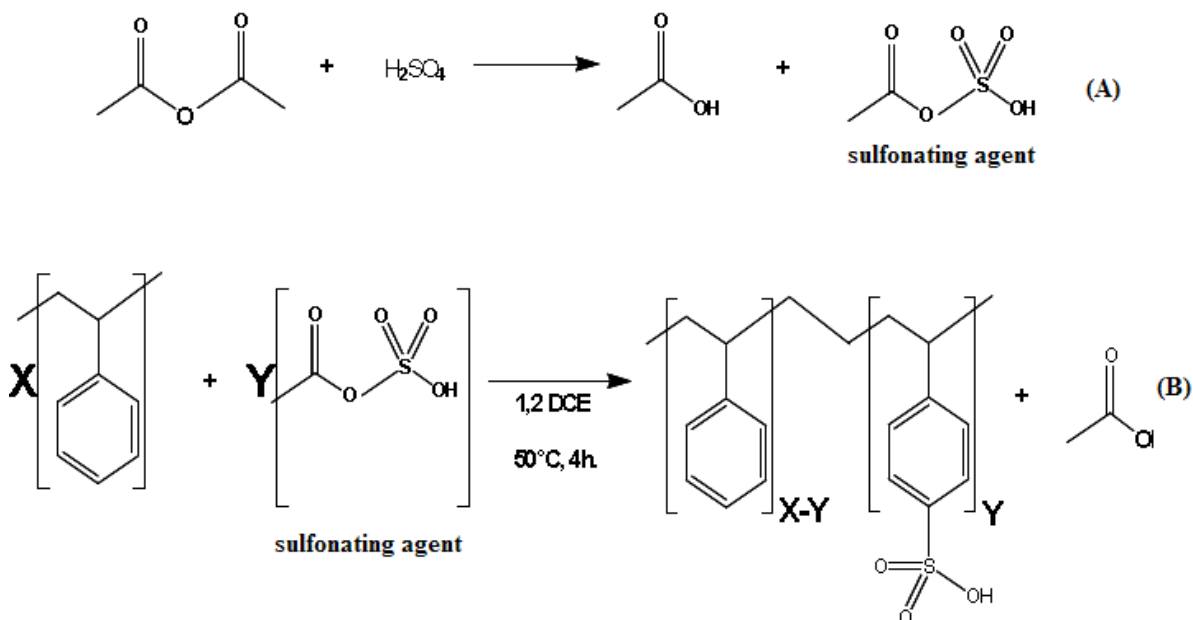


**Figure 5.1:** Reaction scheme of homogeneous sulfonation: (A) acetylsulfate generation (sulfonating agent) and (B) sulfonation of PS.

#### 5.1.2.2 Amidation of the Sulfonated Polymer

The PS-SO<sub>3</sub>H or SMA-SO<sub>3</sub>H was dried in vacuum at 90°C overnight. Thereafter, the sulfonated compound was dissolved in DMF and vigorously stirred at 60°C for 2 hours. Then, the Jeffamine was added dropwise. After 3 days of reaction, the solvent was partially removed under reduced pressure, the product was precipitated in iso-propanol and finally the sulfonated polymer was dried in vacuum at 25°C for three days, see figure 5.2.

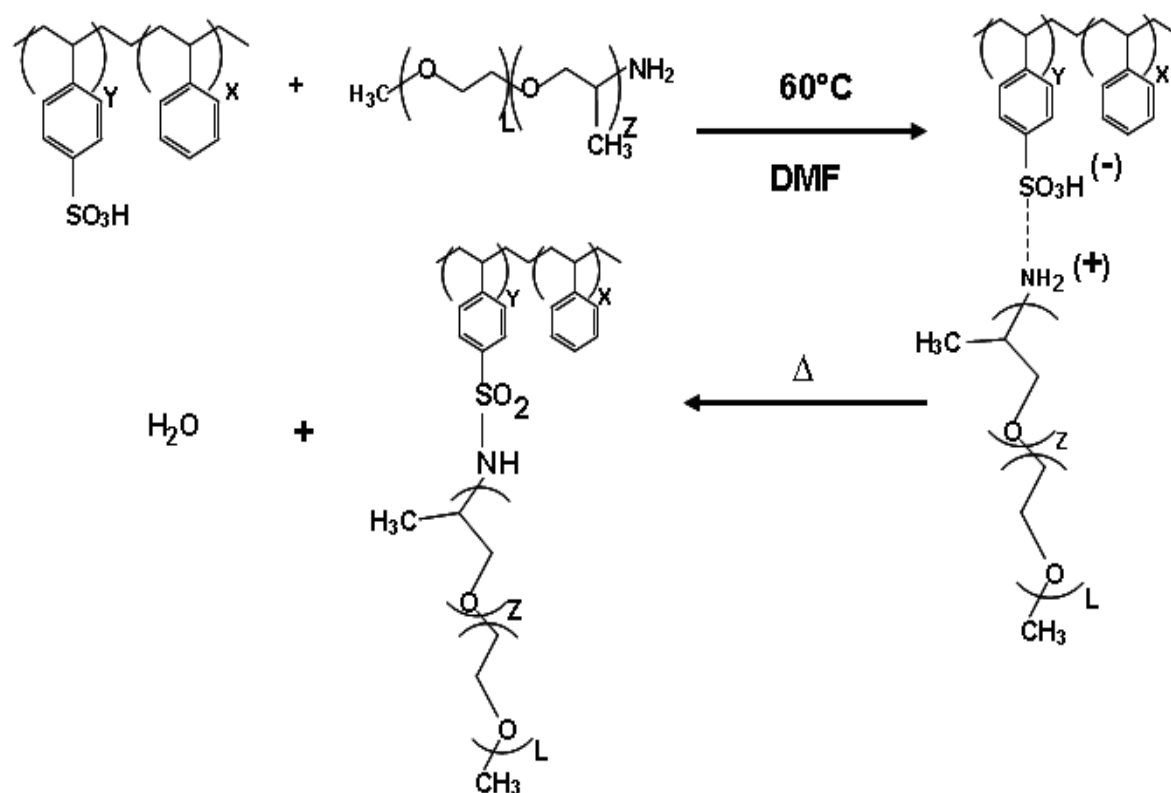


**Figure 5.2:** Grafting reaction of the sulfonated polystyrene with  $\alpha$ -amino- $\omega$ -methoxy polyether.

The table 5.1 exhibits the experimental conditions for the sulfonation process. In the case of the amidation reaction the sulfonated compounds with a higher degree of sulfonation were used, i. e. PS-SO<sub>3</sub>H(24), and SMA-SO<sub>3</sub>H(23) respectively.

**Table 5.1:** Experimental data of the sulfonation of SMA and PS.

Samples	$n_{PS}$ (mol) $\times 10^{-2}$	$V_{S.Ag.}$ (mL)	$n_{Ag.S.}$ (mol) $\times 10^{-2}$	Mol Ratio PS : S. Ag.
SMA-SO <sub>3</sub> H(9)	4.7	6	0.6	8 / 1
SMA-SO <sub>3</sub> H(13)	4.7	8	0.83	6 / 1
SMA-SO <sub>3</sub> H(15)	4.7	10	1.0	5 / 1
SMA-SO <sub>3</sub> H(20)	4.7	14	1.5	3 / 1
SMA-SO <sub>3</sub> H(23)	4.7	12	1.3	3.6 / 1
SMA-SO <sub>3</sub> H(35)	4.7	25	2.6	2 / 1
PS-SO <sub>3</sub> H(9)	3.9	20	0.06	70 / 1
PS-SO <sub>3</sub> H(12)	3.2	20	0.15	21 / 1
PS-SO <sub>3</sub> H(14)	5,0	4	0.41	12/1
PS-SO <sub>3</sub> H(15)	5,2	6	0.62	8.4 / 1
PS-SO <sub>3</sub> H(21)	4,6	8	0.83	6 / 1
PS-SO <sub>3</sub> H(22)	5,2	12	1.3	4 / 1
PS-SO <sub>3</sub> H(24)	5,0	14	1.5	3 / 1

SMA (7) (Mw) = 220000 g mol<sup>-1</sup>, PS (Mw) = 270000 g mol<sup>-1</sup> Mw: weight averages values obtained from GPC. S. Ag. = Sulfonating Agent;  $n_{PS}$  = number of mol of poly(styrene) repeating units.

## 5.2 Results and Discussion

### 5.2.1 Characterization. Evaluation of the Sulfonation

#### 5.2.1.1 Sulfonation Degree by Elemental Analysis

Table 5.2 shows the experimental data obtained from the elemental analysis: Carbon (C), hydrogen (H), oxygen (O) and sulphur (S). From these values the

**Table 5.2:** Elemental Analysis (EA) of the sulfonated polymers

Samples	C (wt. %)	H (wt. %)	O (wt. %)	S (wt. %)	DS (%)
<i>SMA</i>	88.81	7.65	3.54	0.00	
<b>SMA-SO<sub>3</sub>H(9)</b>	80.32	7.09	11.58	1.01	9
<b>SMA-SO<sub>3</sub>H(13)</b>	77.77	7.06	13.69	1.48	13
<b>SMA-SO<sub>3</sub>H(15)</b>	73.86	6.83	17.64	1.67	15
<b>SMA-SO<sub>3</sub>H(20)</b>	76.38	6.85	14.56	2.21	20
<b>SMA-SO<sub>3</sub>H(23)</b>	75.64	6.79	15.02	2.55	23
<i>PS</i>	92.79	8.20	0.00	0.00	
<b>PS-SO<sub>3</sub>H(9)</b>	83.82	7.71	6.95	1.52	9
<b>PS-SO<sub>3</sub>H(12)</b>	84.51	7.75	5.76	1.98	12
<b>PS-SO<sub>3</sub>H(14)</b>	75.34	7.01	15.26	2.39	14
<b>PS-SO<sub>3</sub>H(15)</b>	76.83	7.08	13.60	2.49	15
<b>PS-SO<sub>3</sub>H(24)</b>	80.31	7.56	8.03	4.10	24

Maximum content of sulfur according to theory (S) (100% sulfonation):

SMA-SO<sub>3</sub>H = 11.3 wt.% and PS-SO<sub>3</sub>H = 17.2 wt.%. See Appendix III

degree of sulfonation is calculated. In order to judge the success of sulfonation we define of the degree of sulfonation (DS) as follows, for example, see equation (1):

$$DS = \left[ \frac{\text{Content } S(\%)_{EA}}{\text{Content } S(\%)_{Theory}} \right] \times 100\% \quad (1)$$

The calculation is explained in detail in appendix III. The resulting degree of sulfonation obtained is given in table 5.2; in all the discussion of this thesis the degree of sulfonation will be indicated in brackets.

#### 5.2.1.2 Gel Permeation Chromatography Analysis

Table 5.3 shows the apparent number average molar masses ( $M_n$ ) and the polydispersity index (D) of the sulfonated polymer and also the variation of the  $M_n$  ( $\Delta M_n$ ) and polydispersity ( $\Delta D$ ) with respect to the parent poly(styrene-co-maleic anhydride) and poly(styrene), respectively. The results exhibit that the sulfonation process in SMA and PS increased the molar masses ( $\Delta M_n$ ) and also the polydispersity index ( $\Delta D$ ). They also imply that the increase depends on the degree of sulfonation of each sample. For instant, in the case of  $\Delta D$  the idea is to verify if the sulfonation reaction affect the polydispersity index before the subsequent amidation. However, if solely the increase of molar masses due to the existence of the newly created  $\text{SO}_3\text{H}$  groups is taken into account, the resulting averages should be lower. This behaviour in the variation of molar mass could be explained due to that the sulfonated poly(styrene)s can exhibit different conformations due to the ion-ion interactions between the sulfonate groups. These interactions can be regarded even as electrostatic repulsion at the molecular level (i.e. on short length scales), which

results in different swelling or dissolution of the polar and non-polar components of the polymer, which can be called polyelectrolyte effect. This is also relatable with some ionomers like Nafion® (sulfonated fluorinated polymer), which exhibits ionic cluster even in diluted solutions [25,26].

**Table 5.3:** Gel permeation chromatography results

Sample	DS (%)	$Mn$ (g / mol) $\times 10^5$	D	$\Delta Mn$ (%)
<i>SMA</i>		1.3	2.7	
<b>SMA-SO<sub>3</sub>H(9)</b>	9	1.6	2.7	23
<b>SMA-SO<sub>3</sub>H(13)</b>	13	2.2	3.1	69
<b>SMA-SO<sub>3</sub>H(15)</b>	15	2.1	3.2	62
<b>SMA-SO<sub>3</sub>H(20)</b>	20	2.4	3.2	85
<b>SMA-SO<sub>3</sub>H(23)</b>	23	2.5	3.1	92
<i>PS</i>		2.7	1.03	
<b>PS-SO<sub>3</sub>H(9)</b>	9	2.8	1.03	3.7
<b>PS-SO<sub>3</sub>H(12)</b>	12	2.9	1.04	7.4
<b>PS-SO<sub>3</sub>H(14)</b>	14	3.0	1.2	11
<b>PS-SO<sub>3</sub>H(15)</b>	15	3.1	1.2	14.8
<b>PS-SO<sub>3</sub>H(21)</b>	21	3.3	1.3	18
<b>PS-SO<sub>3</sub>H(22)</b>	22	3.5	1.7	30
<b>PS-SO<sub>3</sub>H(24)</b>	24	2.4	1.1	-11

$\Delta Mn$ = Difference between  $Mn$  (PS or SMA(7)) sulfonated and non-sulfonated.

$$\Delta Mn = \left[ \frac{(Mn_{\text{Polymer-sulf}} - Mn_{\text{Polymer non-sulf}})}{Mn_{\text{Polymer non-sulf}}} \right] \times 100\%$$

### 5.2.1.3 Thermal Analysis: DSC and TGA

- *Differential Scanning Calorimetric (DSC)*

Differential Scanning Calorimetric (DSC) measurements were carried out using the conditions already reported in section 3.1.1, page 60.

Figure 5.3 shows the DSC thermograms for SMS-SO<sub>3</sub>H and PS-SO<sub>3</sub>H samples. In both graphics we can see that an increase of the degree of sulfonation leads to higher glass transition temperatures. For instance in the case of polystyrene, the final PS-SO<sub>3</sub>H(24) reaches the glass transition at approximately 140°C, corresponding to a +34 °C shift compared to the parent polystyrene ( $T_g = 106^\circ\text{C}$ ). In the case of SMA, the final SMA-SO<sub>3</sub>H (23) reaches a  $T_g$  of 146°C, i.e. an increase of 26°C compared to the parent SMA ( $T_g = 120^\circ\text{C}$ ). This behavior could be understood by the fact that the sulfonic groups have ion-ion and ion-dipole interactions with sulfonic group of other chains. The interaction leads to an increase in intermolecular bond energy resulting in elevated glass transition temperatures ( $T_g$ ) of the final sulfonated compounds. To elucidate this phenomenon the variation of heat capacity ( $\Delta c_p$ ) was evaluated.



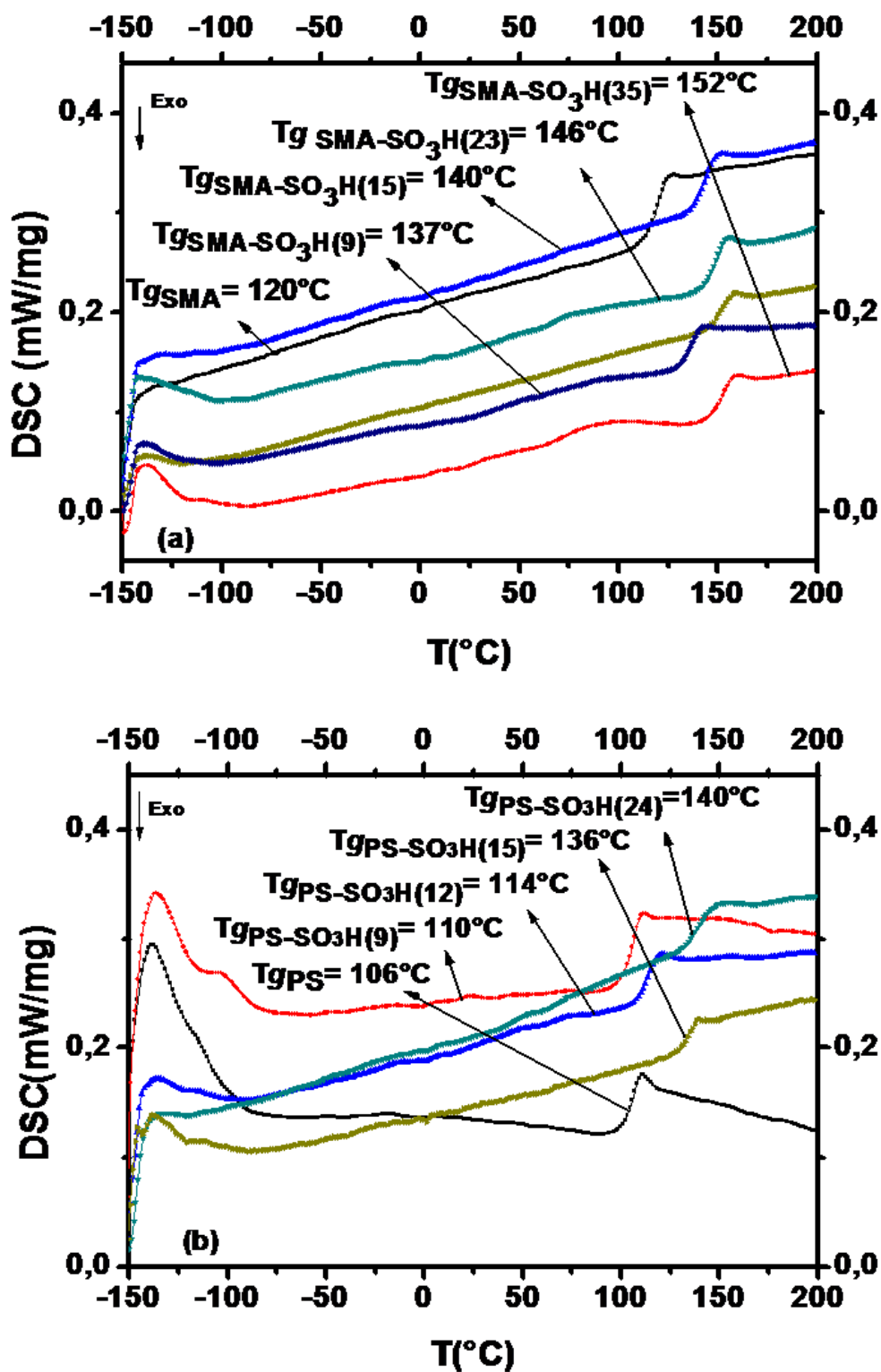


Figure 5.3: DSC for (a) SMA-SO<sub>3</sub>H and (b) PS-SO<sub>3</sub>H samples.

Table 5.4 shows that a decrease of  $\Delta c_p$  is observed during glass transition. This can be considered as an indicator of an increased structural rigidity of the materials as a function of the amount of sulfonic groups [23].

**Table 5.4:** DSC results in SMA-SO<sub>3</sub>H and PS-SO<sub>3</sub>H.

Samples	T <sub>g</sub> (°C)	ΔT <sub>g</sub> (%)	Δc <sub>p</sub> (J/g*K)
<b>SMA (7)</b>	<b>121.6</b>		<b>0.401</b>
<b>SMA-SO<sub>3</sub>H(9)</b>	137.4	13	0.385
<b>SMA-SO<sub>3</sub>H(15)</b>	140.0	15.3	0.308
<b>SMA-SO<sub>3</sub>H(23)</b>	146.2	20.2	0.267
<b>SMA-SO<sub>3</sub>H(35)</b>	152.4	25.3	0.207
<b>PS</b>	<b>106.1</b>	—	<b>0.298</b>
<b>PS-SO<sub>3</sub>H(9)</b>	110.0	3.7	0.272
<b>PS-SO<sub>3</sub>H(12)</b>	114.1	7.5	0.256
<b>PS-SO<sub>3</sub>H(15)</b>	136.2	28.4	0.260
<b>PS-SO<sub>3</sub>H(24)</b>	139.8	31.8	0.173

T<sub>g</sub> = glass temperature, Δc<sub>p</sub> = Delta-Cp ΔT<sub>g</sub> = Variation of T<sub>g</sub> with the sulfonation with respect of SMA  $\Delta T_g = [(T_{g_{SMA-SO_3H(x)}}) - T_{g_{SMA}}] / T_{g_{SMA}} \times 100 \%$

- *Thermogravimetric Analysis (TGA)*

Thermogravimetric analysis (TGA) experiments were carried out using the equipment reported chapter 3.1.2 The samples about (8 – 10 mg) were heated from 25 – 1000°C under nitrogen atmosphere at 10°C/min. Figure 5.4 shows the

thermograms of the copolymer SMA-SO<sub>3</sub>H (a) and PS-SO<sub>3</sub>H (b). Generally, all curves appear similar in shape. Three weight loss stages can be clearly identified for the sulfonated polymers. These occur at 50 – 125°C (1<sup>th</sup>), 150 – 310°C (2<sup>nd</sup>) and 350 – 500°C (3<sup>rd</sup>). The weight loss in the 50 – 150°C range can be attributed to the release of moisture that is adsorbed as a result of the samples' hygroscopic nature. The weight loss occurring in the 200 – 320°C range is due to the breakdown of the sulfonated group attached to the styrene rings. This assignment agrees with data published by Smitha *et al.* [23] for sulfonated polystyrene. The last loss stage at 350 – 500°C is the final decomposition of the polymer. Expectedly, the polymers with higher sulfonation degree exhibit poorer thermal stability due to the weight loss associated with the elimination of the sulfonic groups.

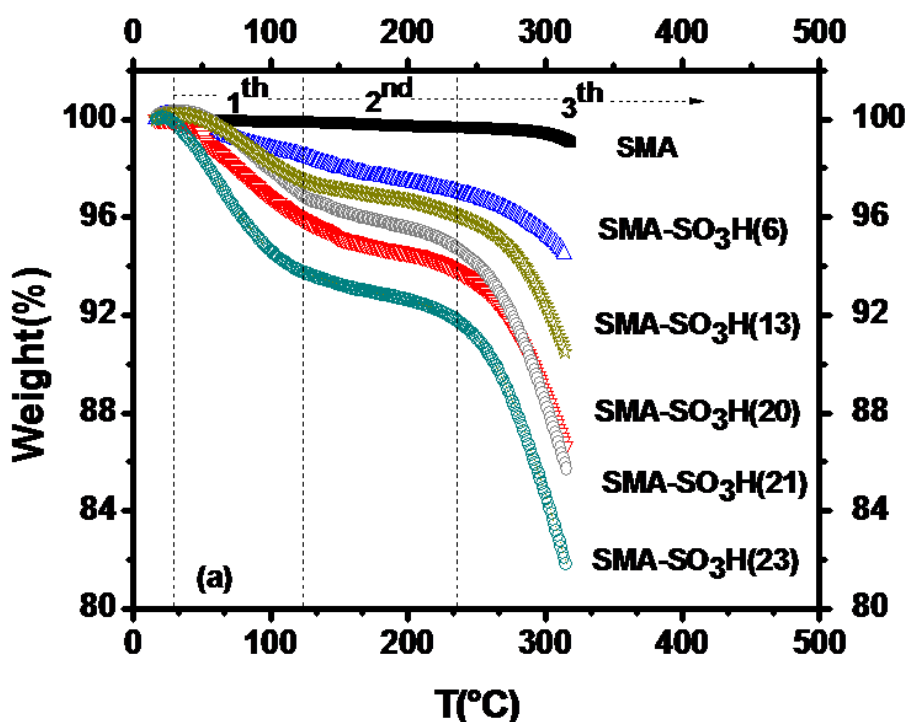
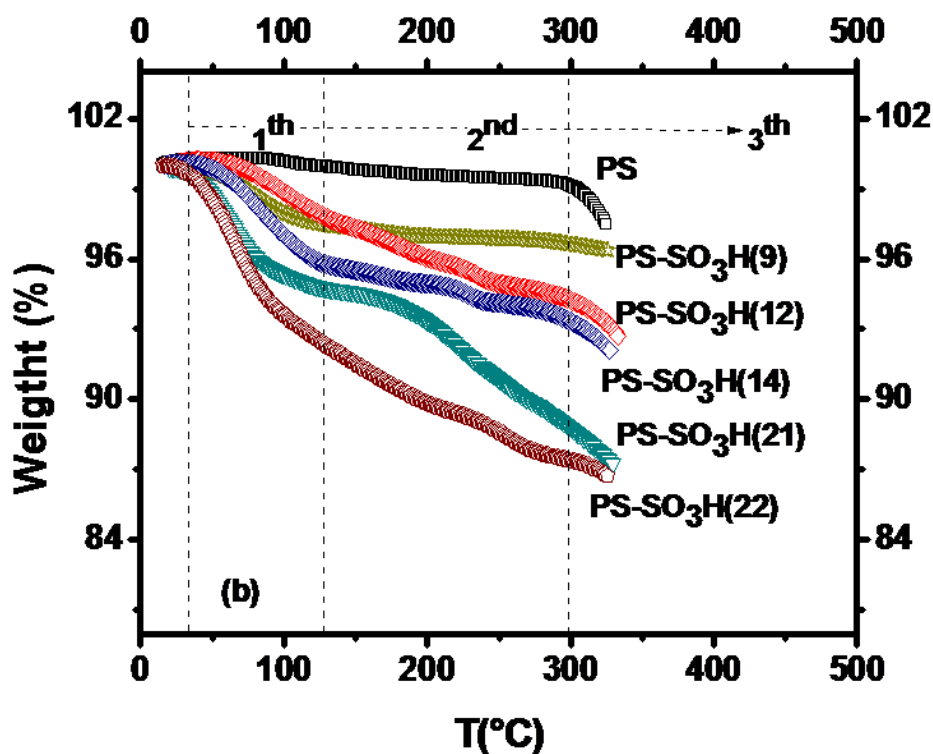


Figure 5.4: TGA of (a) SMA(7%) and (b) PS after sulfonation between 25–320°C.



**Figure 5.4** TGA of (a) SMA(7%) and (b) PS after sulfonation between 25–320°C (continued).

#### 5.2.1.4 FT-IR Spectroscopy

Infrared spectra were recorded on spectrometer already report in the chapter 3.2. Figure 5.5, shows the FTIR spectra of SMA-SO<sub>3</sub>H (a). The bands in the region 2980 – 2920 cm<sup>-1</sup> at medium intensity represent aromatic C-H stretching vibrations. The strong and sharp absorption bands around 1860 cm<sup>-1</sup> ( $\nu_{\text{sym}}\text{C}=\text{O}$ ), and 1780 cm<sup>-1</sup> ( $\nu_{\text{sym}}\text{C}=\text{O}$ ) are due to the asymmetric and symmetric stretching vibrations typical of an anhydride carbonyl group assigned to maleic anhydride (MA). The C = C stretching vibration in the region 1495 – 1440 cm<sup>-1</sup> is representative of the phenyl ring of “styrene”. The band around 1210 and 1030 cm<sup>-1</sup> is due to the asymmetric and

symmetric S=O stretching vibration of the sulfonic acid group [24]. Figure 5.5(b), the FT-IR spectra of assignment without aromatic stretching vibrations and the carbonyl group assigned to the maleic anhydride.

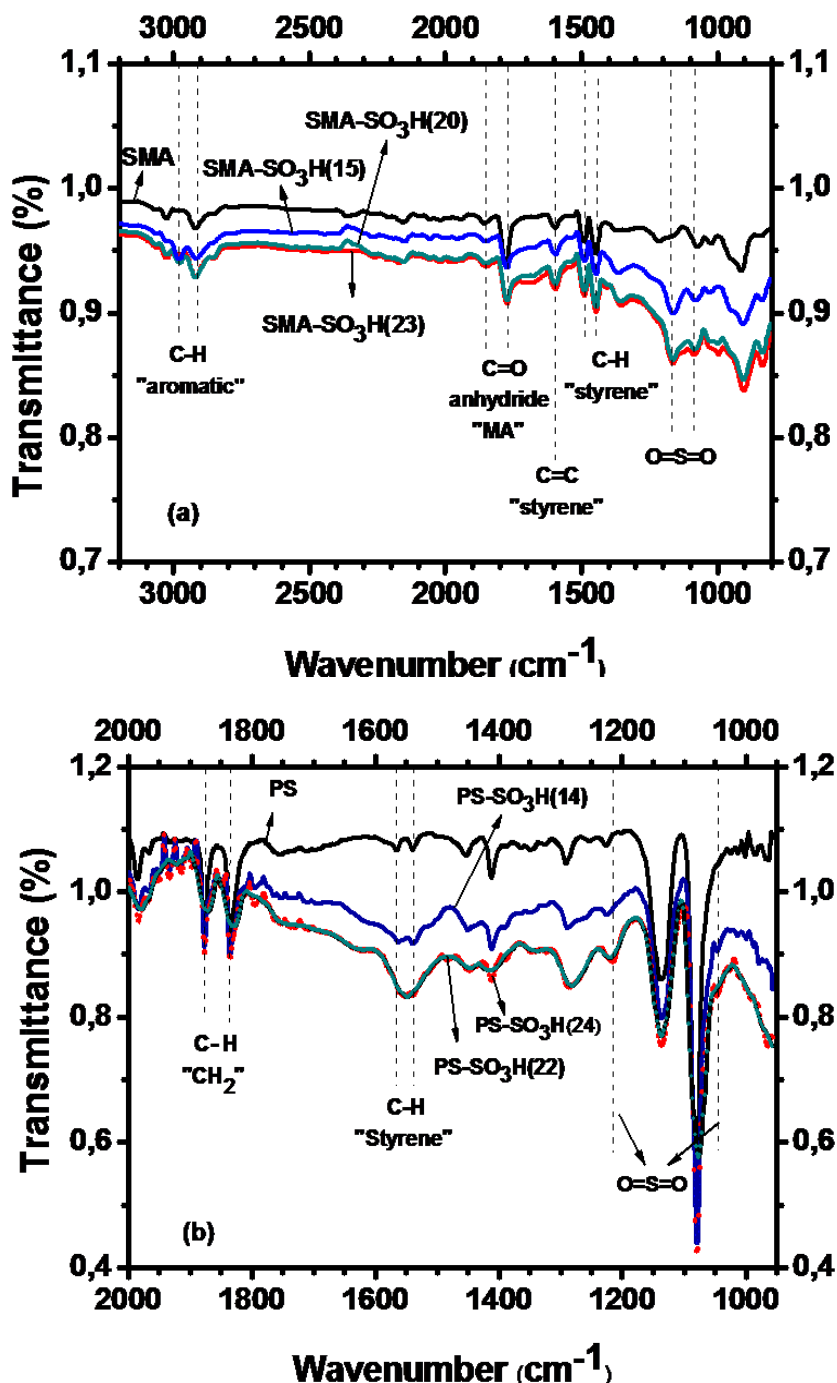


Figure 5.5: Infrared spectra of (a) SMA (7%) after sulfonation and (b) PS after sulfonation

As FTIR spectroscopy indicates the existence of strong maleic anhydride signals and sulfonic groups these results are proving the reaction between SMA and sulfonation agent has taken place at the aromatic ring.

## 5.2.2 Characterization of Graft-Copolymers: SMA-SO<sub>3</sub>H-jeffamine and PS-SO<sub>3</sub>H-jeffamine

### 5.2.2.1 Analysis by <sup>1</sup>H-NMR

<sup>1</sup>H-NMR spectra were collected for the graft-copolymers in CDCl<sub>3</sub> at 25°C. Figure 5.6 exhibits the spectrum of the sample GPSS-2 (PS-SO<sub>3</sub>H(24)-Jeffamine).

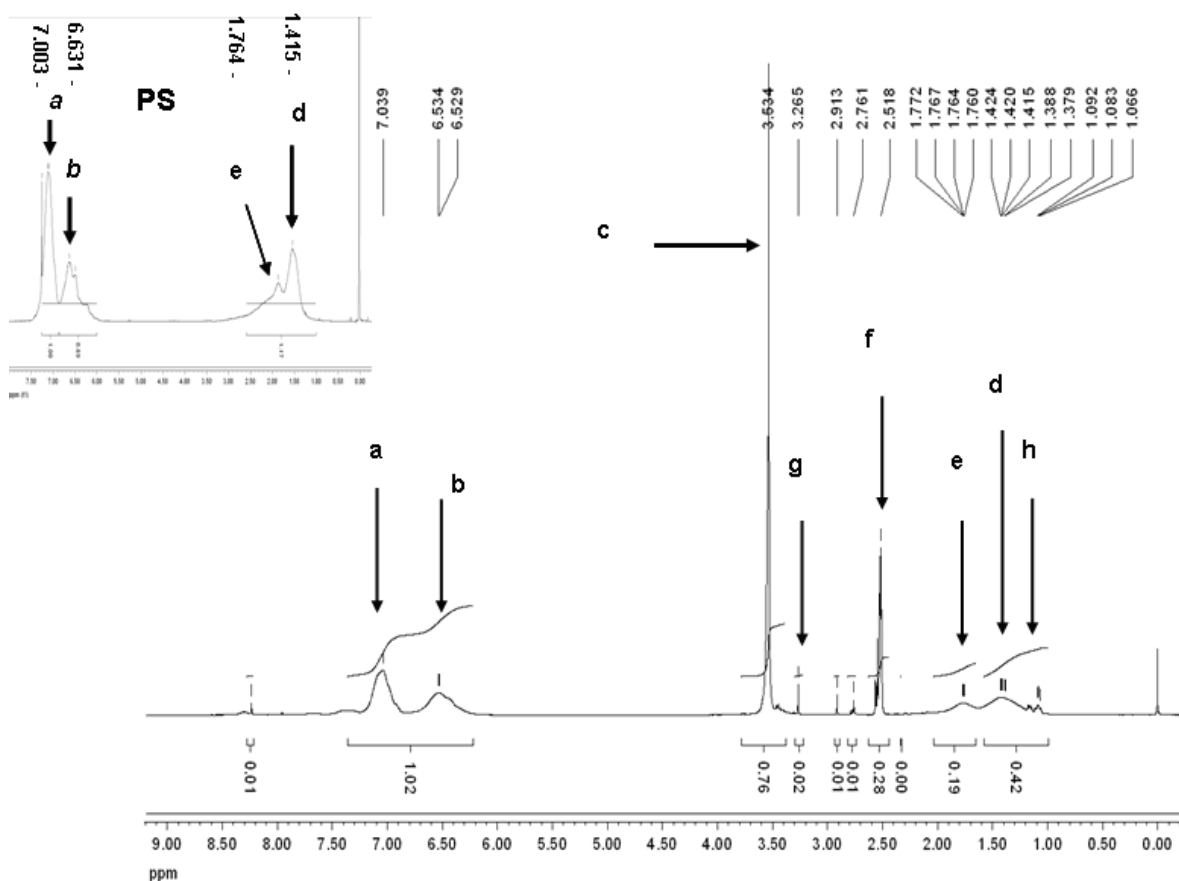


**Figure 5.6:** <sup>1</sup>H-NMR spectrum in CDCl<sub>3</sub> of PS-SO<sub>3</sub>H grafted with Jeffamine (XTJ 506).

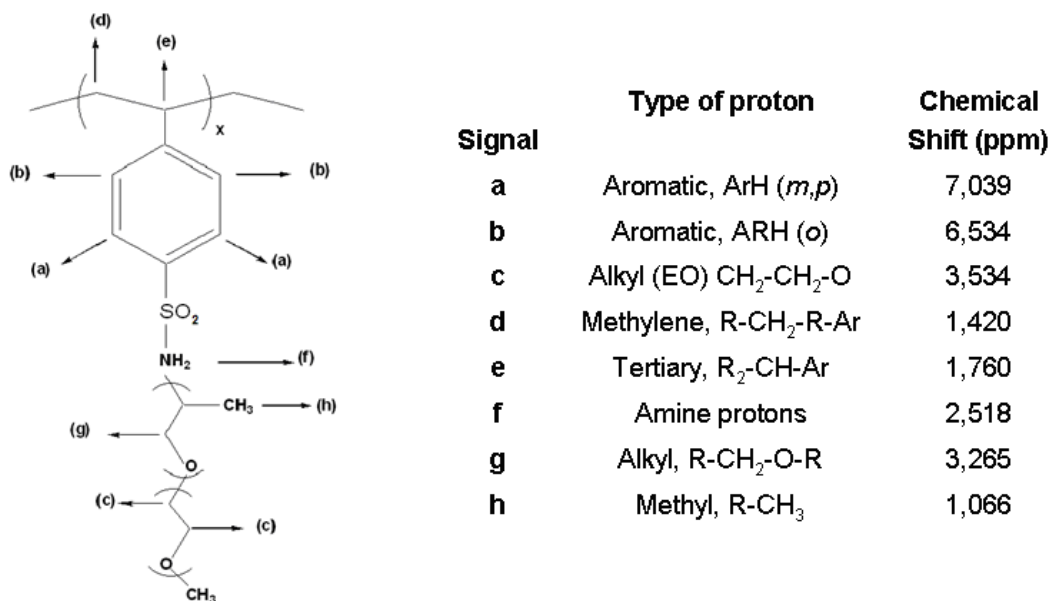


**Figure 5.6:** <sup>1</sup>H-NMR spectrum in CDCl<sub>3</sub> of the graft-copolymer PS-SO<sub>3</sub>H grafted with Jeffamine (XTJ 506) and structural assignment (continued)

The <sup>1</sup>H-NMR peaks of the sulfonated samples are very broad compared to the <sup>1</sup>H-NMR of PS which could be regarded as first indication of the sulfonation of the aromatic ring.

The modification from one peak (-*b* in the spectra) with a shoulder (insert, unmodified PS) to another well-resolved peak (below, graft-copolymer) and the considerable drop in the intensity of the peak at  $\delta = 6.63$  ppm, which is attributed to the meta/para protons of polystyrene indicates the conversion into the sulfonated PS at the para position. Another indication could be the low-field shift of the meta protons from 7.00 to 7.10 ppm due to the presence of the adjacent electron withdrawing sulfonic acid group [13,16], however, the resolution of the spectra is low to confirm the sulfonic group directly. The <sup>1</sup>H-NMR spectrum show a resonance peak around 3.5 – 3.6 ppm corresponding to the poly(ethylene glycol) units [27]. Using this

signal in combination with the one of the aromatic group at 6.2 – 7.3 ppm allows the calculation of the composition of the graft copolymers (Figure 5.6, table 5.5). The chemical shifts (f) at 2.52 ppm indicate the proton adjacent to the amino group. The  $^1\text{H-NMR}$  spectra of the graft-copolymer GSMA-2 (SMA-SO<sub>3</sub>H(23)- jeffamine “XTJ 506”) in CDCl<sub>3</sub> and the chemical shifts are depicted in Figure 5.7. As indicated in Figure 5.6, the characteristic broad peak for the aromatic ring protons of styrene also appears in Figure 5.7. This may indicate that the sulfonation of the aromatic ring has been successful. Here the peak at  $\delta = 6.68$  ppm (*meta/para* protons of the polystyrene) is also absent which confirms the conversion to the sulfonated compound at the *para* position. Furthermore, an analogous low-field shift of the *meta* protons at 7.07 ppm due to the sulfonate group can be observed [13,16]. The alkyl proton signal (c), typical for poly(ethylene oxide) unit [27], can be identified at  $\delta = 3.60$  ppm and a peak of low intensity appears at  $\delta = 3.37$  ppm (g) which is typical for the alkyl proton signal R –CH<sub>2</sub>–O–R of poly(propylene oxide). The characteristic peaks for methyl proton signal (h) appear at  $\delta = 1.05$  ppm, approximately. The chemical shifts (f) at approximately 2.59 ppm indicate the proton adjacent to amino group. The –CH– signal of maleic anhydride (MA), which is expected at chemical shifts of 3.0 – 3.7 ppm was not detected, probably due to the low concentration of MA (7 wt. %) in the SMA copolymer [28]. Table 5.5 shows a compilation of the compositions of the graft-copolymer discussed in this chapter. In all the samples PS is the majority component with contents from 56 until 94 wt. %. GSMA-3 and GSMA-2 show a higher PEG content with 35 and 25 wt.%, respectively.



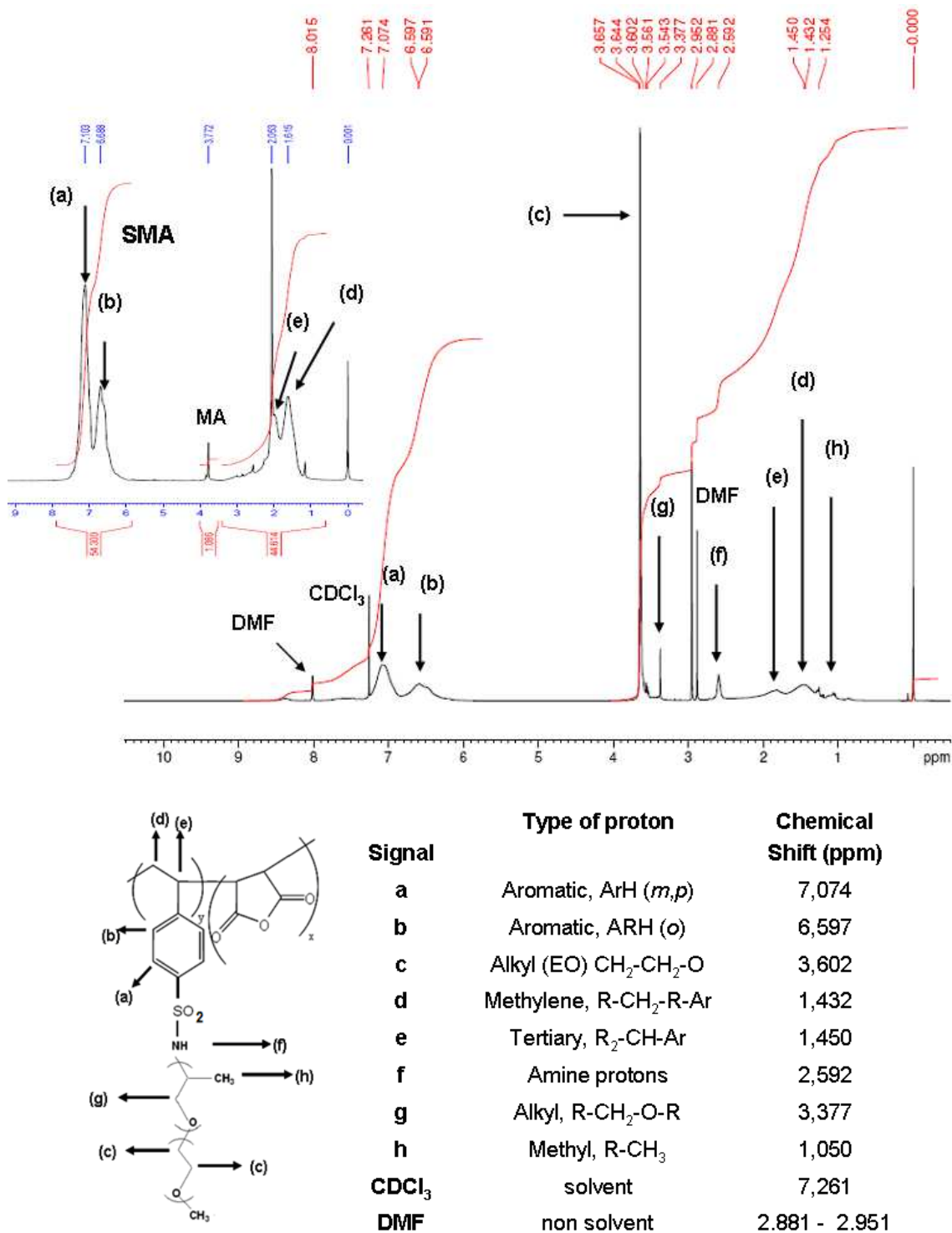


**Figure 5.7:** <sup>1</sup>H-NMR spectra in CDCl<sub>3</sub> of graft-copolymer of SMA-SO<sub>3</sub>H with Jeffamine XTJ 506 and, identification of the structure.

**Table 5.5:** Content of PEG, PS and PPG in the graft-copolymers

Sample	Graft-copolymer	PEG (wt. %)	PS (wt. %)	PPG (wt. %)
<i>PS-SO<sub>3</sub>H(23) +</i>				
<b>GPSS-1</b>	XTJ 505	3.0	62.2	34.8
<b>GPSS-2</b>	XTJ 506	17.4	79.0	3.6
<b>GPSS-3</b>	M-2070	14.5	79.3	6.2
<i>SMA-SO<sub>3</sub>H(24) +</i>				
<b>GSMAS-1</b>	XTJ 505	0.5	94.0	5.5
<b>GSMAS-2</b>	XTJ 506	35.8	56.7	7.5
<b>GSMAS-3</b>	M-2070	25.8	63.2	11.0

#### 5.2.2.2 FT-IR Spectroscopy

Figure 5.8, shows the FTIR spectra of SMA-SO<sub>3</sub>H(35)-jeffamine (a) and PS-SO<sub>3</sub>H(23)-jeffamine (b). Both spectra exhibit two absorption bands for poly(ethylene glycol); the absorption band at 1100 cm<sup>-1</sup> is due to stretching vibration of the C-O-C and other absorption at 1290 – 1350 cm<sup>-1</sup> is caused by the stretching vibration of CH<sub>2</sub>. The absorption band in (a) at 1790 cm<sup>-1</sup> is the stretching vibration of the carbonyl groups coming from the anhydride which remains after sulfonation (SMA-SO<sub>3</sub>H(35)); hence it may be concluded that sulfonation reaction has taken place at the aromatic ring of poly(styrene-co-maleic anhydride).

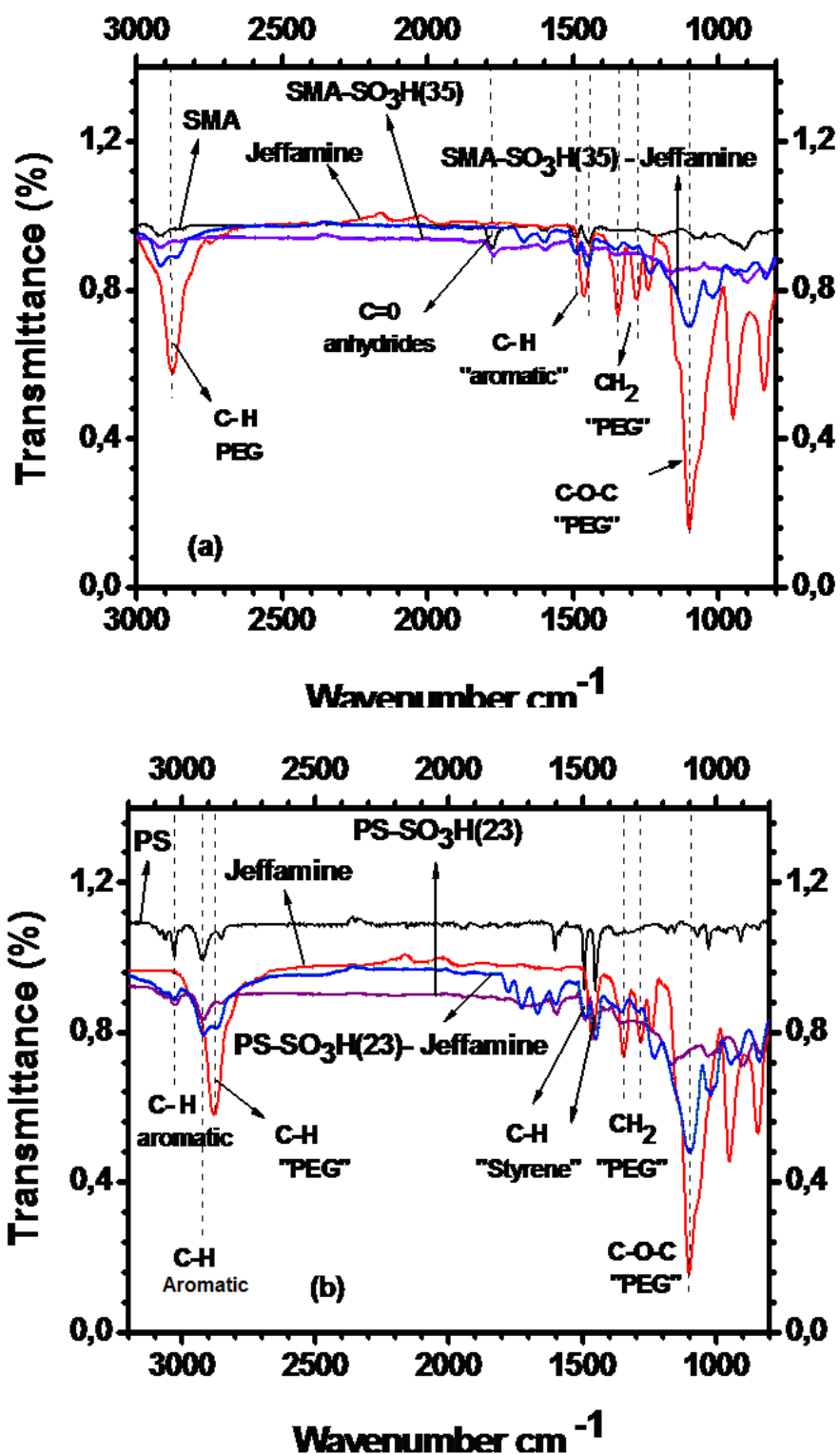


Figure 5.8: FTIR spectra: (a) SMA-SO<sub>3</sub>H(35)-Jeffamine and (b) PS-SO<sub>3</sub>H(23)-Jeffamine

In spectra, (a) and (b), the absorption band at  $2890\text{cm}^{-1}$  stemming from the stretching vibrations of the C–H of the PEG can clearly be seen. This indicates that a graft copolymer has been formed by sulfonation with the Jeffamine chains emerging as branches.

### 5.2.2.3 Gel Permeation Chromatography

Table 5.6 shows the molar mass averages of the graft-copolymers as obtained by GPC. Sample GPSS-3 exhibits an increase of 42% in the apparent molar mass average, in case of GPSS-2 the increase is ~13%, and for GPSS-1 only 4%.

**Table 5.6:** Molar masses (Mn) and polydispersity (D) grafted copolymers

Sample	PEG (wt. %)	Mn <sub>Sulf</sub> (g/mol)x10 <sup>5</sup>	Mn <sub>GFT-Sulf</sub> (g /mol)x10 <sup>5</sup>	D	ΔMn <sup>b</sup> (%)
PS-SO <sub>3</sub> H		2.4		1.1	
GPSS-1	3.0	—	2.5	1.1	4.0
GPSS-2	17.4	—	2.7	1.1	12.5
GPSS-3	14.5	—	3.4	1.4	41.6
SMA-SO <sub>3</sub> H		2.5		2.0	
GSMAS-1	0.5	—	2.5	2.2	0.0
GSMAS-2	35.8	—	2.7	2.5	8.0
GSMAS-3	25.8	—	2.8	2.6	12.0

Mn = number average molar mass using calibration with PS;

$$\Delta Mn = \left[ \frac{(Mn_{GFT-Sulf} - Mn_{PS-SO_3H})}{Mn_{PS-SO_3H}} \right] \times 100\%$$

In the case of the GSMAS types, polymers the variation of the molar mass average is: the GSMAS-3 (12%) > GSMAS-2 (8%) > GSMAS-1 (0 %). However,  $\Delta M_n$  values for GPSS-1 and GSMA-1 are lower, it can be due to the short-chain branch (SCB) effect, which a chain that comprises constitutional units, joined to each other through one single atom on only one of the units and hence shows lower number average molar mass ( $M_n$ ) in comparison to other samples, the effects of short chain branching on properties of polymer have been described [29,30]. The results show a strong relation between PEG content and the variation of the molar mass average, because with increasing the poly(ethylene glycol) content, the molar mass increases as well. The results demonstrate that synthesis of graft-copolymer via sulfonated poly(ether amide) was successful.

#### 5.2.2.4 Thermal Analysis: DSC and TGA

- *Differential Scanning Calorimetric (DSC)*

Figure 5.9 shows the DSC of the GSMAs and GPSSs samples. The results indicate that an increase of the PEG content in the samples (e.g GSMAS-3 and GSMAS-2 (~29%) and GSMAS-1 (1.5%)) leads to a decrease of the glass transition temperature; an analogous behavior is observed for the GPSS samples. Even though the sulfonate group gives a strong tendency to increase the  $T_g$  (fig. 5.9), the thermal behavior of these graft-copolymers changes with the poly(ethylene glycol) content, reflecting the softening effect of poly(ethylene glycol) attached to the rigid sulfonated PS backbone. Hence, the DSC results corroborate the findings of the GPC that the synthesis of graft-copolymer by reaction of a sulfonated backbone with

a poly(ether amide) was successful and indicate that the content of the poly(ethylene glycol) plays a crucial role in the thermal behavior of the graft-copolymer.

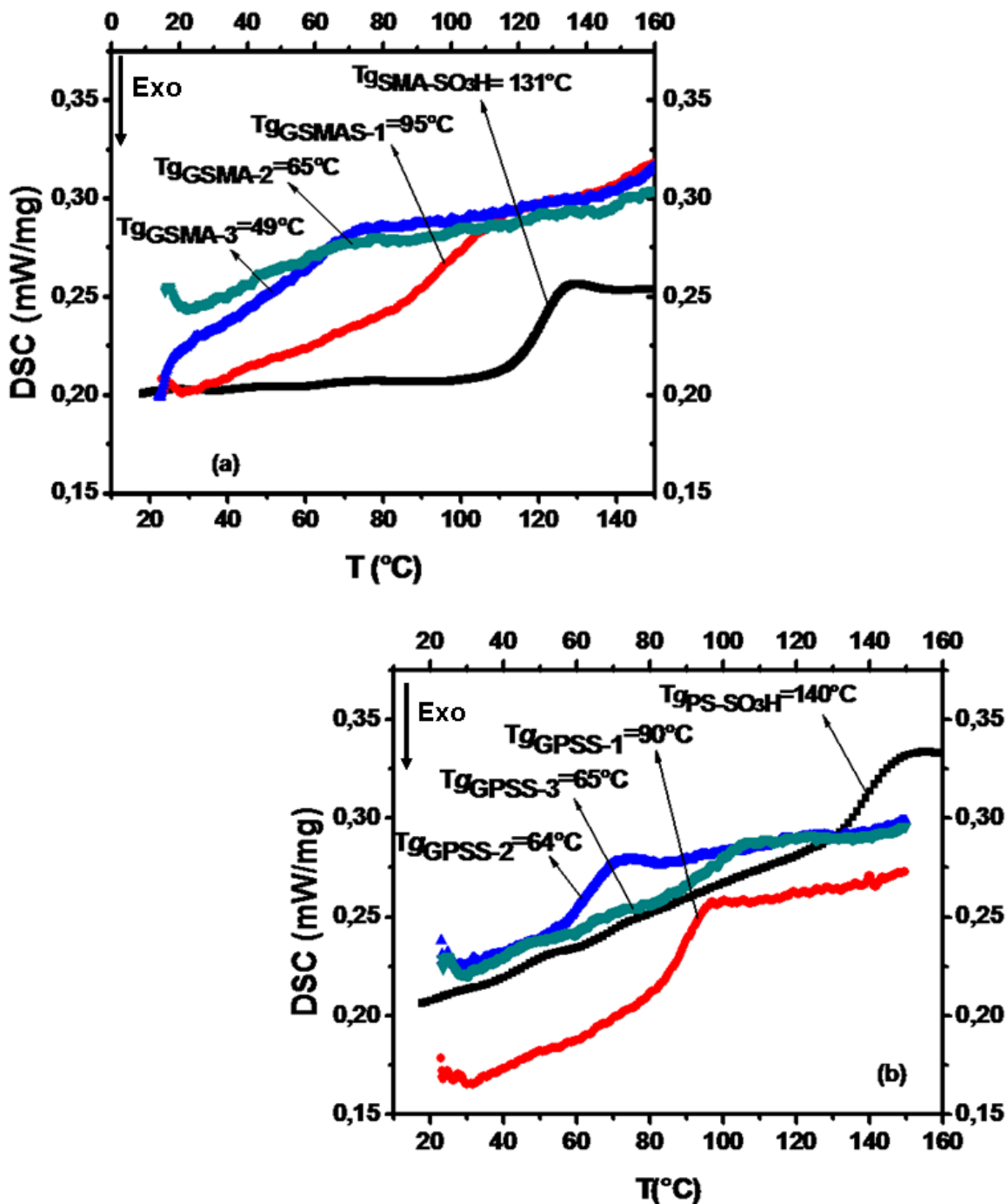


**Figure 5.9:** DSC thermograms (second run) for (a) GSMAS and (b) GPSS series.

The DSC thermograms with original data are reported in Appendix IV.

- Thermogravimetric Analysis (TGA).

The thermal stability of the copolymer (a) GSMAS and (b) GPSSs samples was investigated by TGA and is presented in Figure 5.10.

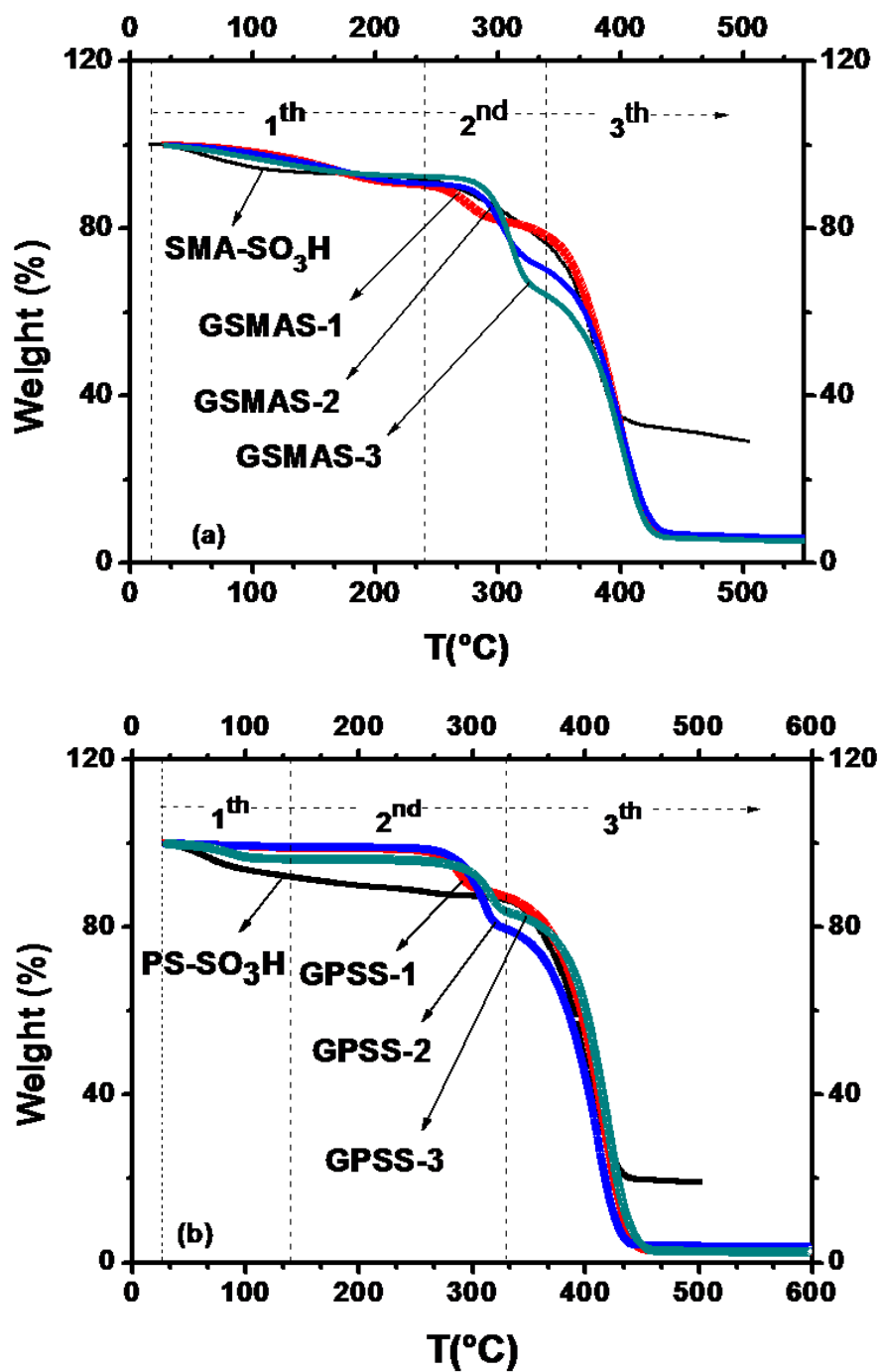
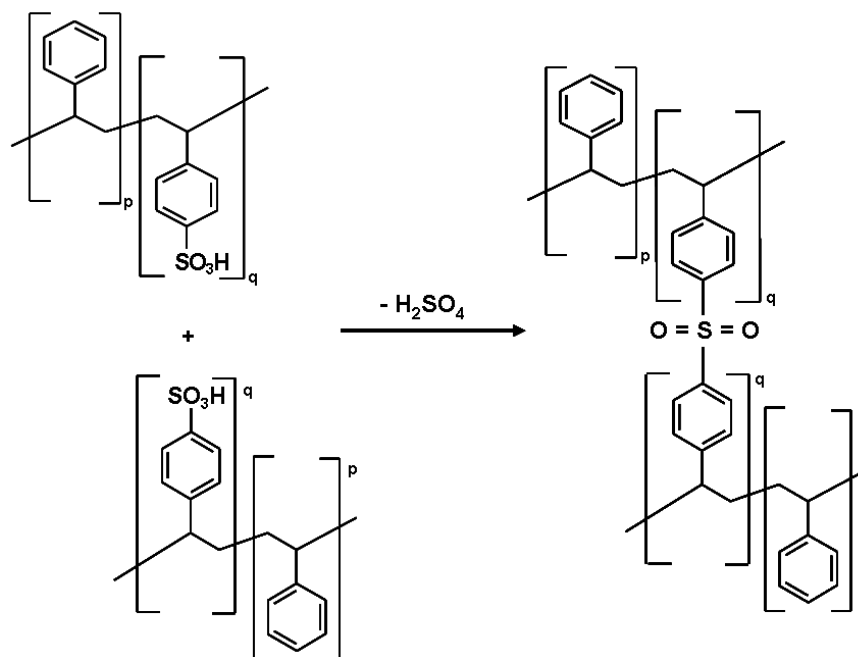


Figure 5.10: TGA Analysis of (a) GSMAS and (b) GPSS copolymers.

Figure 5.10 (a) exhibits a typical three-step degradation pattern. The first weight loss up to ca. 220°C is ascribed to the loss of water, adsorbed by the highly hygroscopic –SO<sub>3</sub>H group; in all the samples the mass change is almost constant (9 – 7%) analogous to the original sulfonated sample SMA-SO<sub>3</sub>H(23). The second step in the range of 240 – 340°C is attributed to the cleavage of sulfonic acid groups. The mass change in the second decomposition temperature was different in each sample, for instance, GSMA-3 (28%) > GSMA-2 (19%) > GSMA-1 (9.2 %). This behavior can be correlated to the PEG-content in the graft-copolymer since it follows the same trend, as shown in table 5.6. The third stage weight loss 350 – 460°C (3<sup>th</sup>) is assigned to the decomposition of the polymer main chain. In figure 5.10 (b), the first weight loss stage is reached at 120°C and can be attributed to the release of atmospheric moisture which occurs only in the GPSS-3, as a result of the hygroscopic nature, (mass change ~4%). These results could indicate that in the samples GPSS-1, GPSS-2 the amidation reaction has been performed in higher yield which could also result in a lower content of free sulfonated groups. If the behavior of the GPSS and GSMAS samples at the step is compared, it is reasonable to assume that in the case of the GPSS samples most of the -SO<sub>3</sub>H group have reacted with the respective jeffamine. In the second step the weight loss occurs between 240 – 330°C due to the breakdown of the sulfonated group attached to the styrene rings. In this range the weight loss order found is GPSS-2 (20%) > GPSS-3 (13%) > GPSS-1 (11%) and as was mentioned above, the third stage weight loss 350 – 460°C (3<sup>th</sup>) is assigned to the decomposition of the polymer main chain, again a relation with the PEG content, can be seen table 5.6.5. Figure 5.10 also shows that at 500°C the PS-SO<sub>3</sub>H and SMA-SO<sub>3</sub>H samples do not completely decompose still 20 or 30% weight remains as



residue. A possible explanation is that the sulfonate groups of the polymer crosslink inter- or intramolecularly. The most probable crosslinking reaction mechanism is shown in figure 5.11; see reference [22].



**Figure 5.11:** Crosslinking reaction of PS- $\text{SO}_3\text{H}(x)$  [22]

### 5.3 Conclusions

√ Graft-copolymers of the series GSMA and GPSS were synthesized by sulfonation of poly(styrene) and poly(styrene-co-maleic anhydride) with acetyl sulphate solution and subsequent amidation reaction using the poly(ether amine) “jeffamine®”.

√ The successful synthesis was proved by the characterization of the graft-copolymer by elemental analysis (EA), GPC, FT-IR, thermal analysis (DSC and TGA), and <sup>1</sup>H-NMR.

√ Polymers of PEG contents until 35 %-wt. with a maximum sulfonation degree of 24%-wt were obtained. An increase of the PEG content in the graft-copolymer leads to a decrease of the glass transition temperature in comparison to the sulphonated polystyrene, even though the sulphonate group as such caused an increase of the glass transition temperature due to the ionic interactions.

√ The graft-copolymer of the series GSMA and GPSS showed an increase in the molar masses ( $\Delta M_n$ ) of 42%-wt and an interesting thermal resistance with maximum operating temperatures of around 220°C.

#### 5.4 References

- [1] Baker R. W., Future directions of membrane gas separation technology, *Industrial Engineering Chemistry Research* 41 (2002) 1393.
- [2] Maclean, D. L.; Bollinger, W. A.; King, D. E.; Narayan, R. S. Gas separation Using Composite Hollow Fiber Membranes. Li. N. N., Calo, J. M., Eds.; CRC Press: Boca Raton, U.S.A., 1986.
- [3] Henis, J. M. S. Commercial and Practical Aspects of Gas Separation Membranes. In *Polymeric Gas Separation Membranes*; Paul, D. R. Yampol'skii, Y. P. Eds.; CRP Press: Boca Raton, U.S.A., 1994.
- [4] Koros W. J., *Macromolecular Symposia*, 188 (2002) 13.
- [5]. Mier G., *Angewandte Chemie International Edition*, 37 (1998) 2960.
- [6] Stern S. A., *Journal Membrane Science*, 94 (1994) 1.
- [7] Ozcayir Yurdaguld F., Goetz Gertrud, Bikson Benjamin, Praxair Technology, Inc., US-patent- 5618334, April 8, 1997.
- [8] Hamad F., Matsuura T., *Journal of Membranes Science*, 253 (2005)183.
- [9] Yoshihawa M., Niimi A., Guiver M.D., Robertson G.P., *Sen'i Gakkaishi Journal Society Fiber Science Japan*, 56 (2000) 272.
- [10] Gramain P. and Frere, Y. *Polymer Communication*, 27 (1986) 16.
- [11] Derand H. and Wesslen, B. *Journal of Polymer Science Part A: Polymer Chemistry*, 33 (1995) 571.
- [12] Wesslen B. and Wesslen, K. B. *Journal Polymer Science, Part A: Polymer Chemistry*, 27 (1989) 3915.
- [13] Fernyhough C.M., Young R. N., Ryan A. J., Hutchings L. R., *Polymer*, 47 (2006) 3455.

- [14] Vink H., *Macromolecular Chemistry and Physics*, 182 (1981) 279.
- [15] Kucera F., Jancar J., *Journal Polymer Engineering Science*, 38 (1998) 783.
- [16] Baigl D., Seery T., Williams C., *Macromolecules*, 35 (2002) 2318.
- [17] Saxena A., Tripathi, B. P. and Shahi V. K., *Journal Physical Chemistry B.*, 111 (2007) 12454.
- [18] Walsby N., Paronen M., Juhanoja J., Sundholm F., *Journal of Applied Polymer Science*, 81 (2001) 1572.
- [19] Yang J. Ch., Jablonsky M., Mays J., *Polymer*, 43 (2002) 5125.
- [20] Wei K-L., Wu J-Y., Chen Y-M., Hsu Y-C., Lin J-J., *Journal applied Polymer Science*, 103 (2007) 716.
- [21] Wang Z. Pinnavaia T. J., *Journal of Materials Chemistry*, 13 (2003) 2127.
- [22] Martins C. R, Ruggeri G., De Paoli M-A., *Journal of the Brazilian Chemical Society*, 4 (2003) 797.
- [23] Smitha B., Sridhar S., Khan A. A., *Journal of Membrane Science*, 225 (2003) 63.
- [24] Makowski, H. S., Lundberg, R.D.; Singhal, G. H.; *US pat.* 3.870.841.
- [25] Gebel G., *Polymer* 41 (2000) 5829.
- [26] Baigl D., Seery T., Williams C.E., *Macromolecules* 35 (2002) 2318.
- [27] Jankova K. and Kops J., *Journal Applied Polymer Science*, 54 (1994) 1027.
- [28] Park Eun-Soo, Kim Mal-Nam, Lee Ik-Mo, Lee H. S. Yoon J-S, *Journal of Polymer Science: Part A: Polymer Chemistry*, 38 (2000) 2239.
- [29] Mortimer G.A., *Journal of Applied Polymer Science*, 15 (1971) 1231.
- [30] Hammed T., Hussein I. A., *Macromolecular Materials and Engineering*, 289 (2004) 198.

---

**Chapter VI Membrane Properties of Series-ML,-MM, -MH and Series-GSMA and -GPSS**

---

In the study of CO<sub>2</sub>-selective membranes, commonly known as “reverse selective membranes, due to the fact that larger CO<sub>2</sub> molecules permeate preferentially across the membranes, the gas solubility plays an important role. The performance of these membranes is governed by different factors such as condensability, kinetic diameter and chemical affinity of the gas (such as molecule polarization) along with the chemical composition of the membrane polymer. For instance, in the case of the CO<sub>2</sub>-N<sub>2</sub> gas pair the chemical affinity between the gas and the polymer is the main factor that influences solubility and solubility-selectivity. Notably, some CO<sub>2</sub>-selective membranes are mainly based on rubbery polymers that interact with CO<sub>2</sub> molecules. For examples, copolymers based on poly(ethylene oxide) have been identified as promising membrane materials for CO<sub>2</sub> separation. In this regard, PEO (polar ether segment) is a very attractive polymer due to the strong affinity of CO<sub>2</sub> towards the oxygen of the oxyethylene segments which increase the solubility of CO<sub>2</sub> in the membrane. In case of the CO<sub>2</sub>-CH<sub>4</sub> pair, the permeability in rubbery polymers could be affected by the CO<sub>2</sub> solubility, due to the higher CO<sub>2</sub> affinity (higher polarity) in comparison to CH<sub>4</sub> (apolar hydrocarbon). On the other hand, for glassy polymers, the selectivity is determined by the diffusion or “molecular sieving” effect. CO<sub>2</sub> selectivity polymeric membranes can be designed to amplify the solubility-selectivity ( $S_{CO_2}/S_{N_2}$ ) while minimizing the diffusivity selectivity ( $D_{H_2}/D_{CO_2}$ ) [1]. This chapter presents a new alternative to prepare novel membranes based on graft-copolymer introduced in chapters IV and V, respectively, and a study of their membranes properties. Figure 6.1 shows the principle idea of this work to improve the

permeability of CO<sub>2</sub> with respect to other gases, using a glassy polymer like polystyrene as main chain and rubbery polymer like PEG-segments as grafts, an explanation about this idea is exhibit in section 2.11.2, page 45.

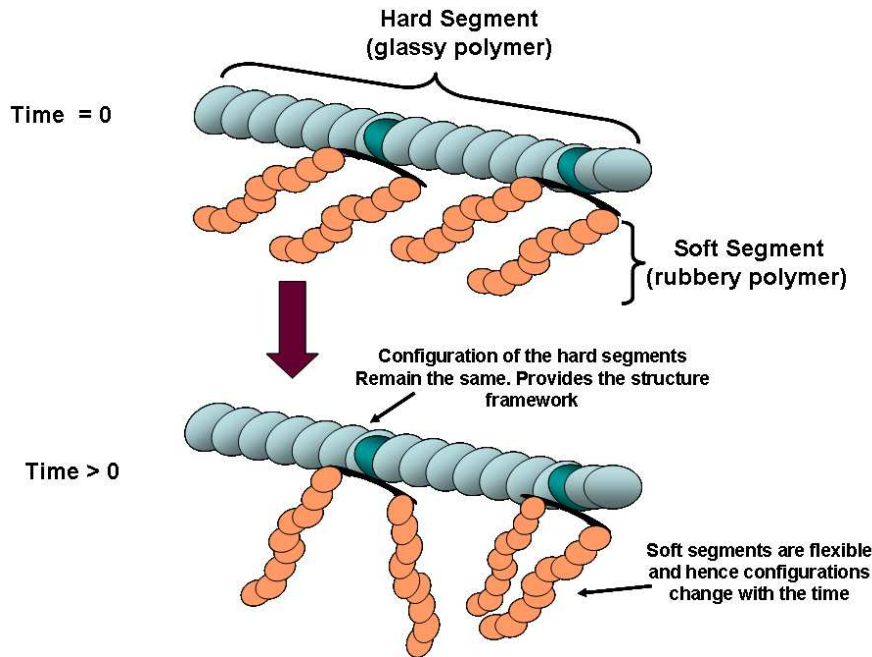


**Figure 6.1:** Principle idea of a copolymer suitable for CO<sub>2</sub> separation, graft-copolymer.

## 6.1 Experimental Part

### 6.1.1 Preparation of the Membrane

The composite membranes were prepared by casting of a 2.5 wt % graft copolymer solution (grafting of styrene-co-maleic anhydride by polyetheramides "series -ML, -MM, -MH" or grafting of styrene-co-maleic anhydride and polystyrene via sulfonated by polyetheramide "series-GSMA or -GPSS") in methyl ethyl ketone after 24 h of stirring on porous supports of polyacrylonitrile (PAN-HV3/T) [2] (cf. table 6.1). After 24 h the membranes were coated with 2% polydimethylsiloxane PDMS (a commercial silicone rubber copolymer supplied by Wacker-Chemie GmbH) solution

in *i*-octane. As the thin PDMS layer had a high flux and an adequate selectivity for many gases it was exclusively used with the purpose of closing the defects in the membrane. In figures 6.2 – 6.3 the flow schemes and stages of the membrane preparation procedure are shown.

**Table 6.1:** Properties of different types of PAN support [2].

Type	$J_w$ , ( $l/m^2 \times h^3 bar$ )	$d_{50}$ , (nm)	Cut-off <sub>100%</sub> , Dalton
HV1/T	6150	37.7	$15.7 \times 10^6$
HV2/T	688	11.6	$2.0 \times 10^5$
HV3/T	330	6.7	$9.5 \times 10^4$

$J_w$ , water permeability;  $d_{50}$ , average of pore diameter.

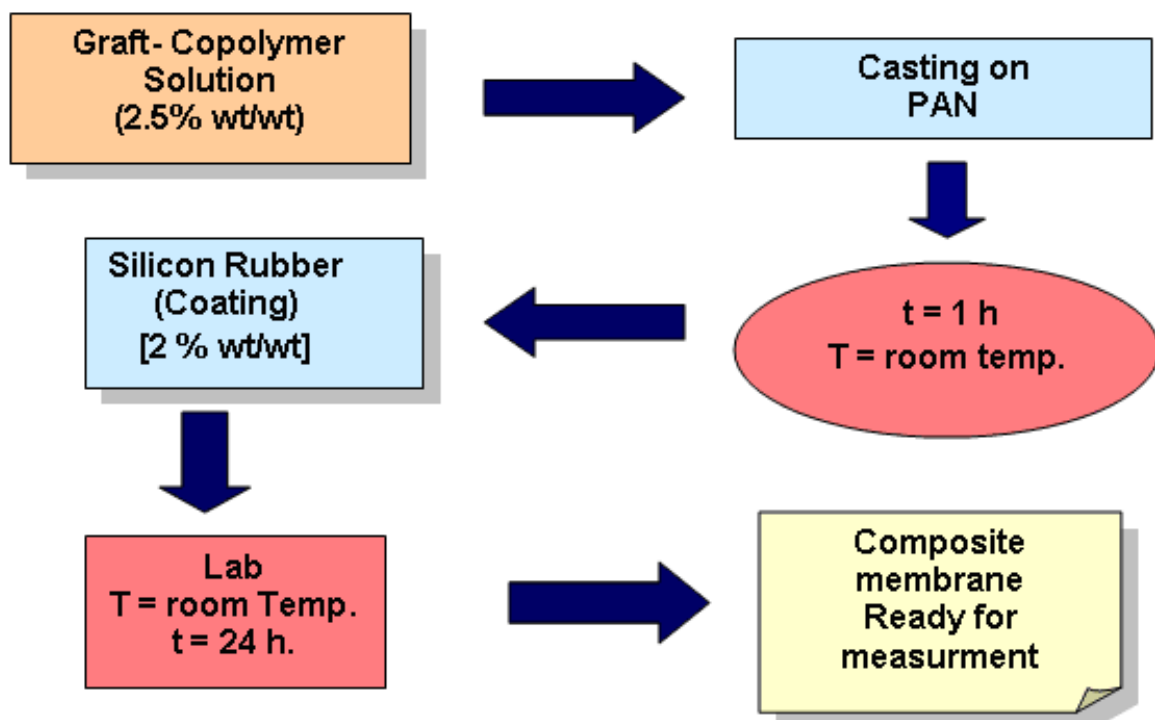


**Figure 6.2:** Flow - scheme of composite membrane preparation



**Figure 6.3:** Dip-coating equipment, coating stage.

### 6.1.2 Single Gas Measurements and Determination of Permeability

The permeation cell is a stainless steel filter holder from Millipore corporation (diameter of 65 mm in the disc filter) with an area of 37 cm<sup>2</sup>. Membrane samples were partially masked using impermeable aluminum tape on the upstream and downstream faces. The o-ring in the permeation cell was in direct contact with the aluminum tape so that the soft rubbery membrane would not be damaged by the o-ring. After aluminum tape masking, the surface area of the sample available for gas transport was 34.20 cm<sup>2</sup>, see figure 6.4.

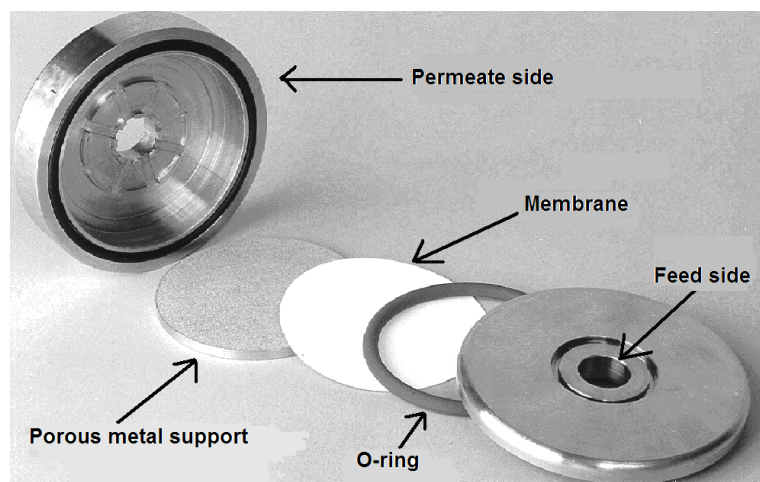


**Figure 6.4** Assembly of a membrane test cell



Permeability coefficients of  $N_2$ ,  $H_2$ ,  $CO_2$ ,  $CH_4$ , and  $CO_2$  were determined at  $35^\circ C$  and 1 bar of feed pressure. A GKSS-made pressure increase test unit [3], see figure 6.5, was utilized to measure the single gas flows through the composite membranes. The basic principle is a simple pressure increase measurement which is independent of the type of gas used (cf. figure 6.6). During the measurement an additional calibrated volume is connected to the permeate side and with the resulting small pressure changes on the permeate side are being recorded measured with a pressure transducer. The permeance of a membrane with an unknown thickness of the selective layer is called flux ( $J$ ) and can be calculated by equation 6.1. The whole measurement is automatically controlled by a computer including the filling, refilling and evacuation process. Permeability measurements can be made using a set-up, a schematic drawing of such a gas permeability test apparatus is given in figure 6.5. In short a measurement procedure can be outlined as follows: First, the membrane test cell (4) containing a composite membrane of unknown thickness is evacuated for 2 hours using the vacuum pump (6). Then the cell is pressurized from feed pressure volume (3) using the gas selection (1), for example,  $H_2$ ,  $N_2$ , or  $CO_2$  until 1000 mbar are reached. From now on, the cell with membrane is ready for measurements and all is set-up with computer programs using an automatic registration of the data and controlling steps. The extent of gas permeation through the membrane is determined by means of a measurement of the permeate volume through a detector of pressure. Finally, when the pressure applied  $p_F$  and the permeate pressure  $p_p(t)$  exhibit a similar values the measurements is finished, see (cf. Figure 6.6). The dependence of permeability on temperature and swelling can be determined in one step. The unit of permeability is defined by volume ( $V/m_N^3$  STP) per time unit ( $t/h$ ) which penetrates a

defined membrane area ( $A/m^2$ ) driven by a pressure difference ( $\Delta p/\text{bar}$ ). The permeance values of a membrane with an unknown thickness of the selective layer are called fluxes ( $J/ m^3/m^2\text{hbar}$ ), which can be calculated using the following equation:

$$J = \frac{V \times 22.4}{R \times T \times A \times t} \ln \left[ \frac{(p_f - p_0)}{(p_f - p_p(t))} \right] \quad (6.1)$$

where  $V$  is the permeate volume in  $m^3$ ,  $R$  the gas constant,  $T$  the temperature,  $A$  the membrane area, and  $t$  the time of measurement. The quantity  $p_0$  represents the initial permeate pressure, whereas  $p_f$  is the pressure applied, and  $p_p(t)$  the variation of the permeate pressure with time. The single gas selectivity ( $\alpha$ ) between two components A and B (cf. 2.6), can also be expressed, by the following equation:

$$\alpha_{AB} = \frac{J_A}{J_B} \quad (6.2)$$

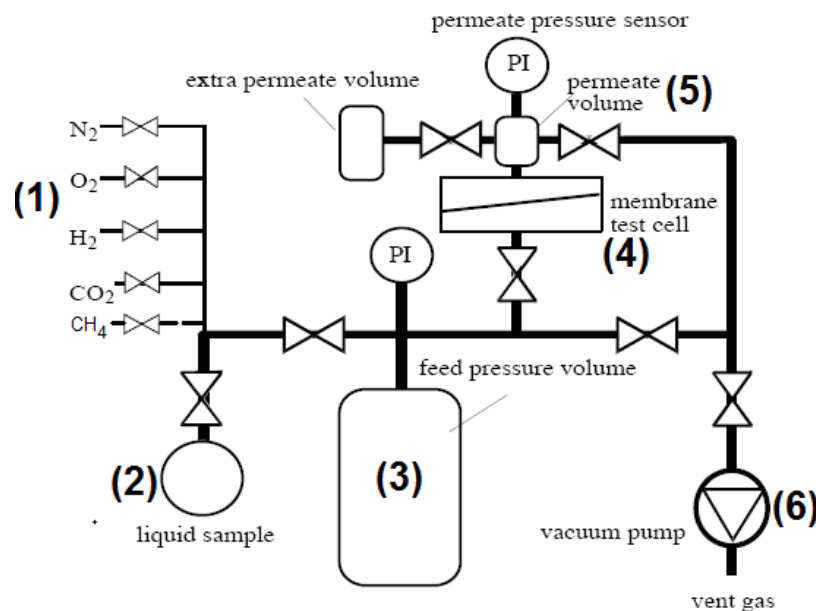


**Figure 6.5:** Pressure increase test unit (a): (1) gas inlet, (2) chamber for liquid samples, (3) feed pressure volume, (4) membrane test cell, (5) permeate volume, (6) vacuum pump, and (PTPI) pressure sensor.

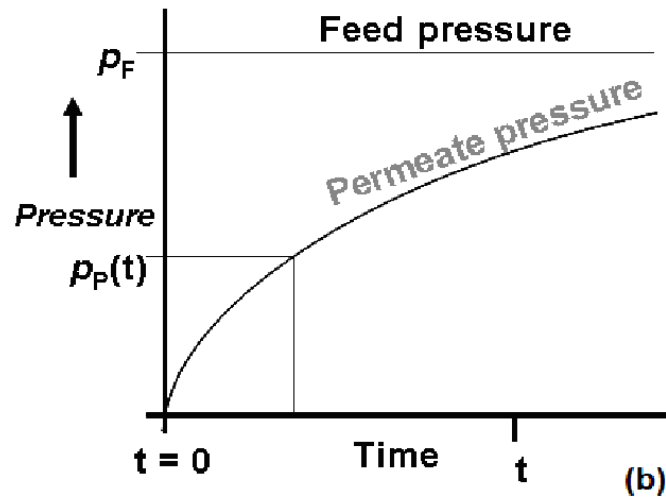


**Figure 6.6:** Principle time run of a pressure increase measurement.

A picture of equipment is show in figure 6.7.

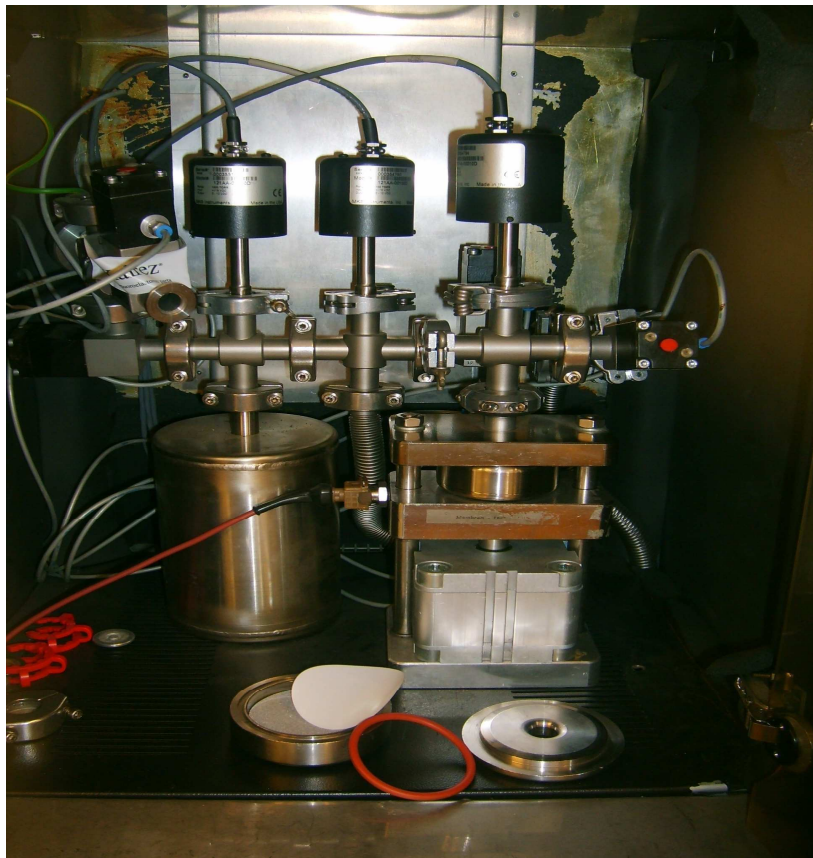


**Figure 6.7:** A picture of the pressure increase test unit .

In this work the permeability ( $P$ ), is calculated as the product of the flux ( $J$ ) and the thickness ( $l$ ) of the respective membrane, taken from the SEM micrographs, (equation 6.3).

$$P_A = J_A \times l \quad (6.3)$$

The single gas selectivity between two gases A and B, ( $\alpha_{P_A/P_B}$ ) is expressed by equation 2.6, page 30.

### 6.3 Results and Discussion

#### 6.2.1 Characterization and Analysis of the Membranes Series-L, -M, -H by SEM

##### 6.2.1.1 Membranes Based on Series-L Graft-Copolymer, -ML

Figures 6.8 – 6.12 depict the SEM micrographs of the membranes based on L-1, L-2, L-3, L-4 and L-5 graft copolymers. In most of these cross-section images a three layer structure is observed; on the bottom a PAN layer [2], in the middle a layer where the graft-copolymer is mixed with the PAN support (thickness “long”) and finally on the top a layer (thickness “short”) consisting solely of the graft-copolymer, see figure 6.8(a). The two thicknesses are reported in table 6.2., page 143.

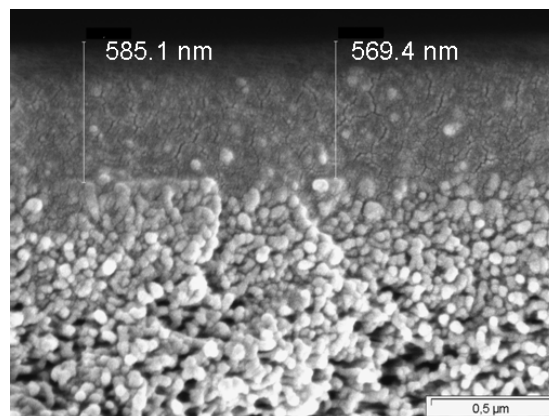


**Figure 6.8:** SEM images (cross-section) of the membranes based on L-1

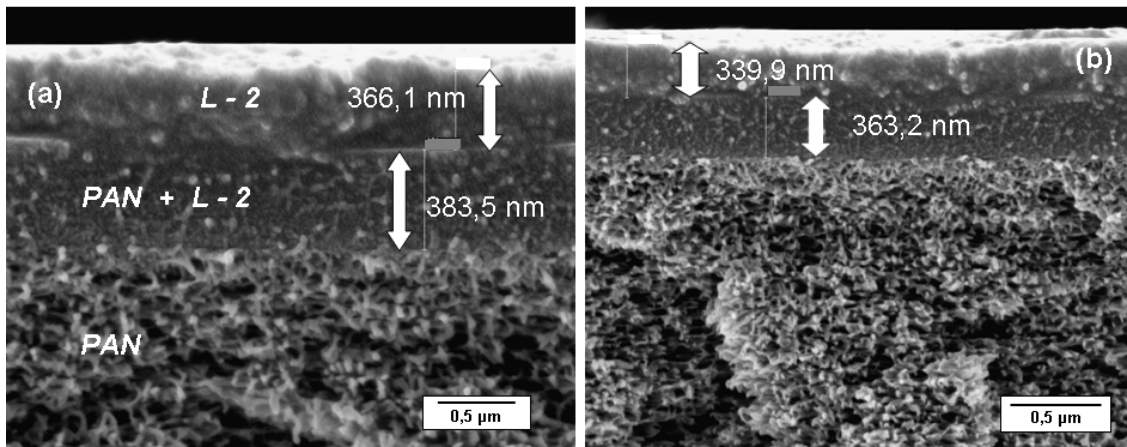


Figure 6.9: SEM images (cross-section) of the membranes based on L-2

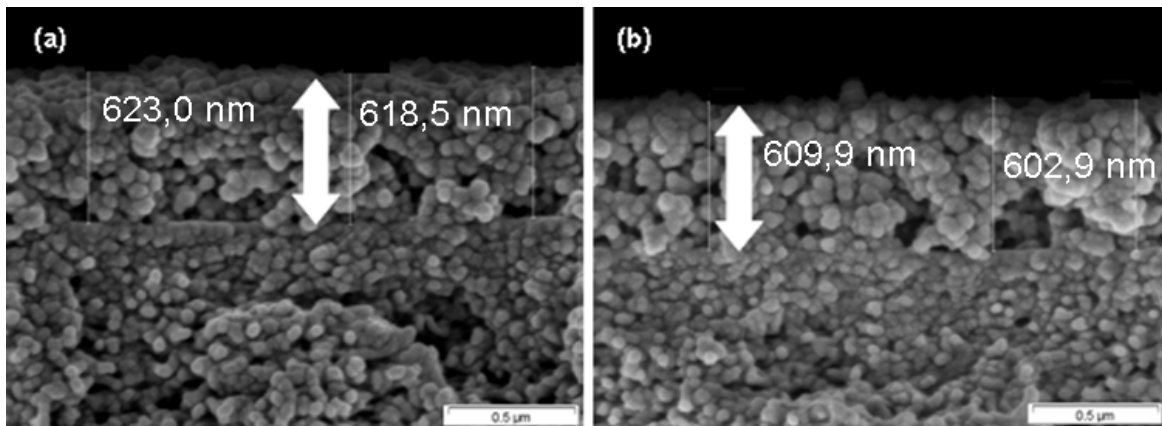


Figure 6.10: SEM images (cross-section) of the membranes based on L-3

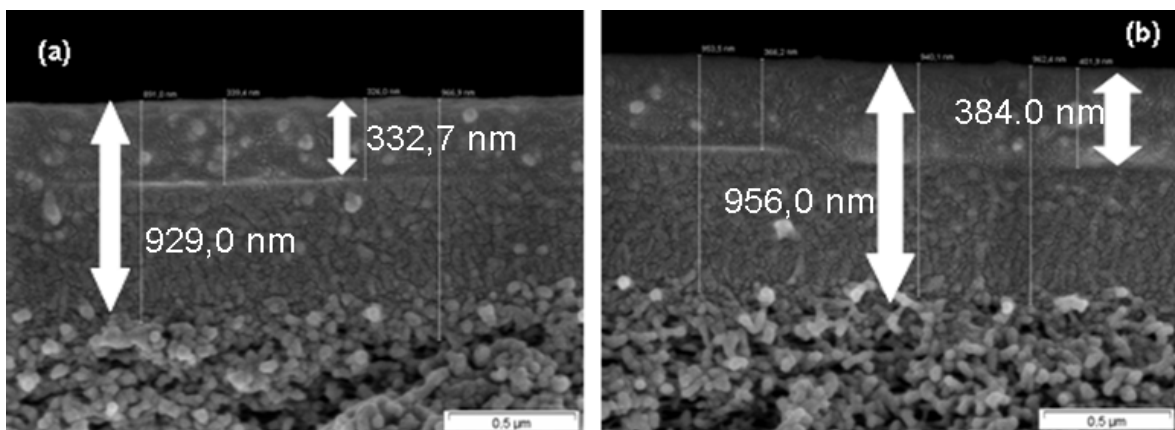
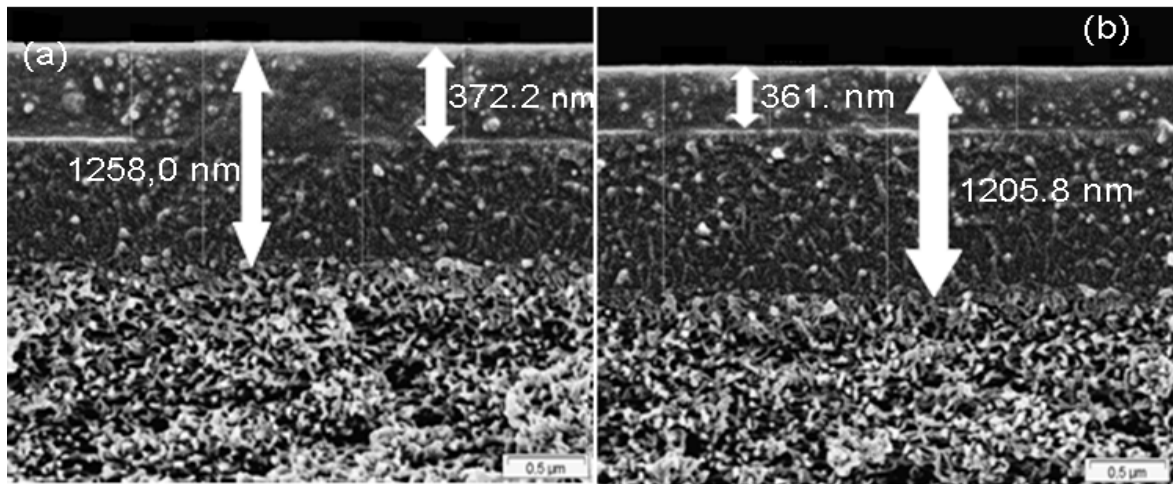


Figure 6.11: SEM images (cross-section) of the membranes based on L-4



**Figure 6.12:** SEM images (cross-section) of the membranes based on L-5

The micrographs show that graft-copolymer film is dense without any pores. This indicates that the performance (permeability and selectivity) is determined by the intrinsic properties of the material, e.g. gas solubility in the rubbery segment of the polymer. From a theoretical point of view [4], the extent of interaction between a polymer and a (penetrant) gas is generally very small in comparison with the interaction of a polymer with liquids and consequently the solubility of the gas in the polymer is low. The permeation strongly depends on the solubility of the dissolved gas in the rubbery segment, whereas the diffusion coefficient of the gas transport can be considered constant. Consequently, the permeability of a gas in membranes basically depends on the solubility of the gas in the membrane material.

#### 6.2.1.2 Membranes Based on Series-M Graft-Copolymer, -MM

Figures 6.13 – 6.16 present the micrographs of M-type polymer based membranes. Obviously, the top-layer consists of the graft-copolymer (short scale), in the middle a

mixture of graft-copolymer and PAN (long scale) and in the bottom is made up of PAN. The thicknesses of the membranes are given in table 6.2.

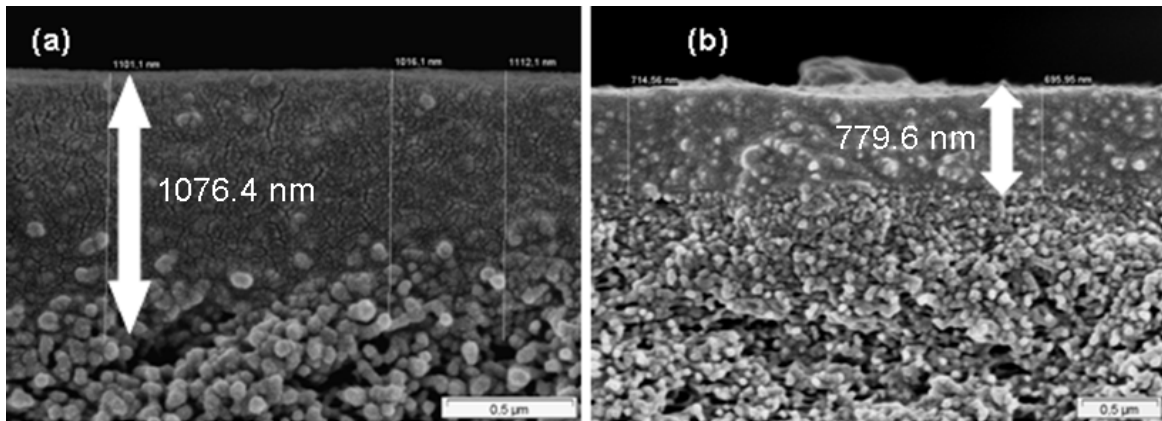


**Figure 6.13:** SEM images (cross-section) of the membranes based on M-1

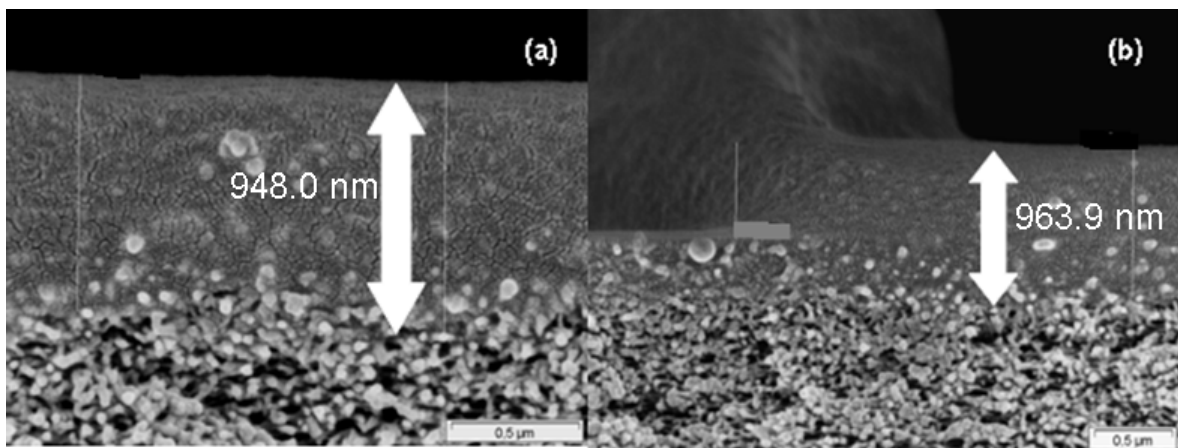


**Figure 6.14:** SEM images (cross-section) of the membranes based on M-2

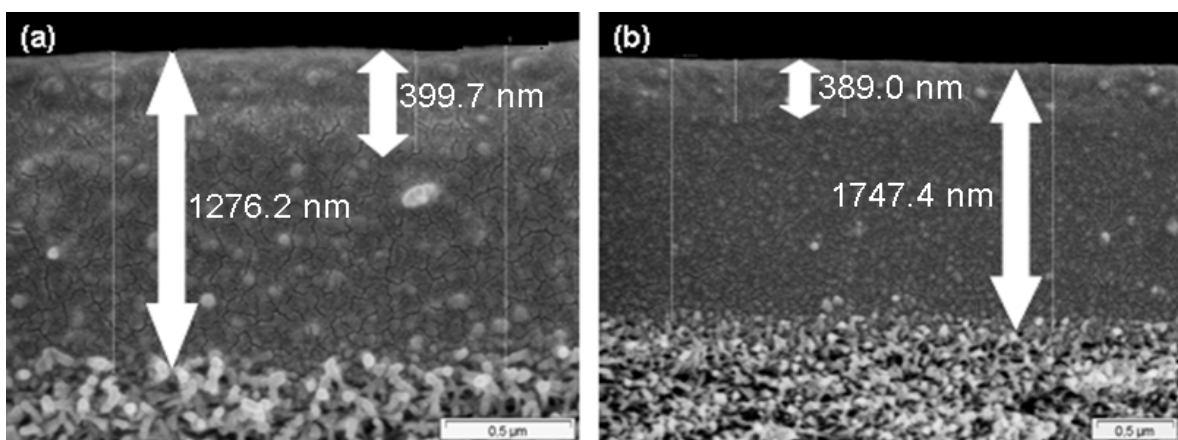


**Figure 6.15:** SEM images (cross-section) of the membranes based on M-3

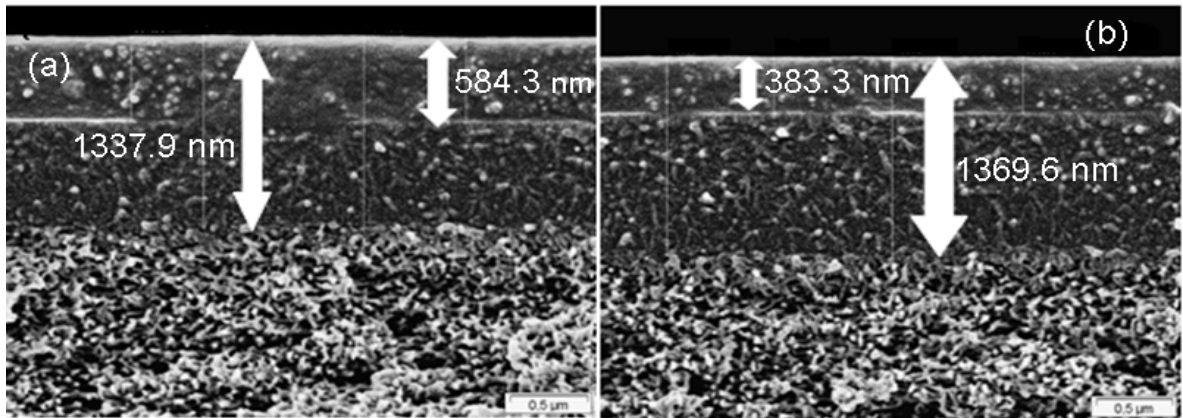


**Figure 6.16:** SEM images (cross-section) of the membranes based on M-4

### 6.2.1.3 Membranes Based on Series-H Graft-Copolymer, -MH

Finally, the figures 6.17 – 6.20 show the micrographs (cross-section) of the membranes based on copolymers H-1, H-2, H-3 and H-4.

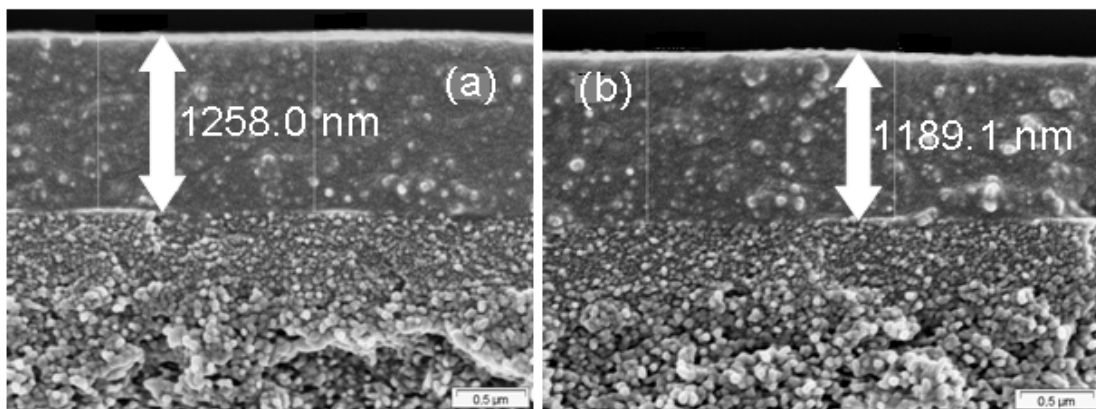


**Figure 6.17:** SEM images (cross-section) of the membranes based on H-1

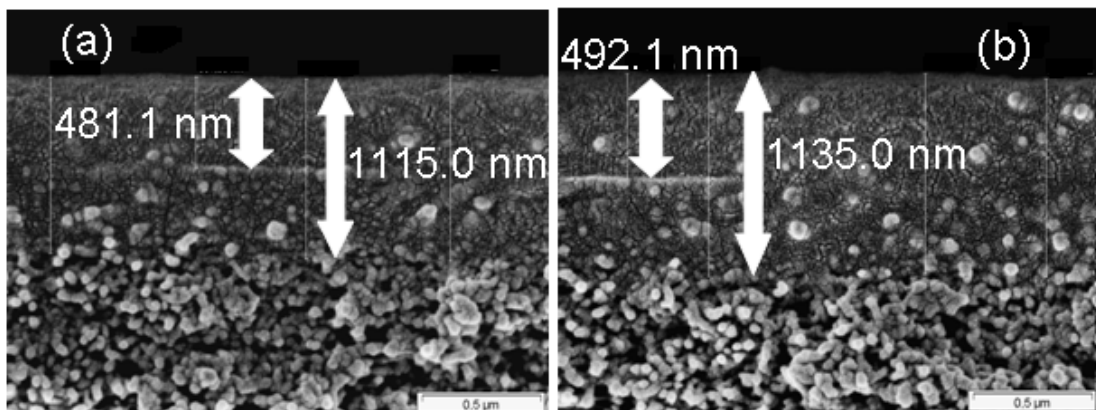


**Figure 6.18:** SEM images (cross-section) of the membranes based on H-2.



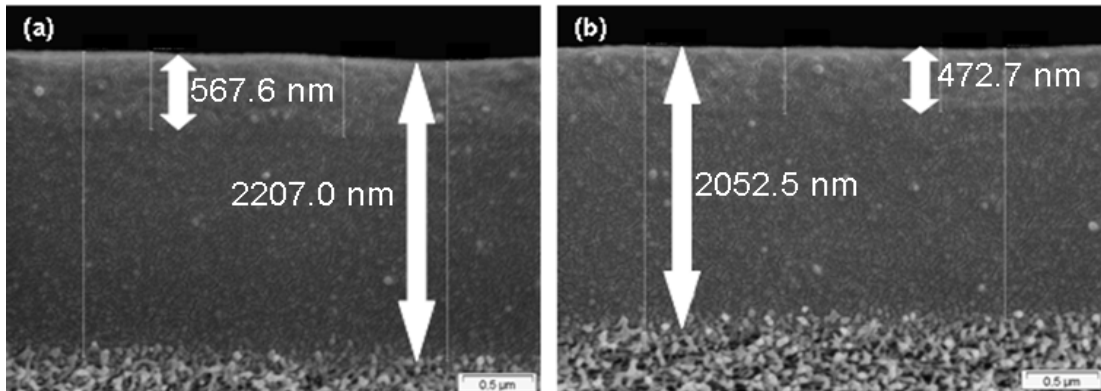


**Figure 6.19:** SEM images (cross-section) of the membranes based on H-3

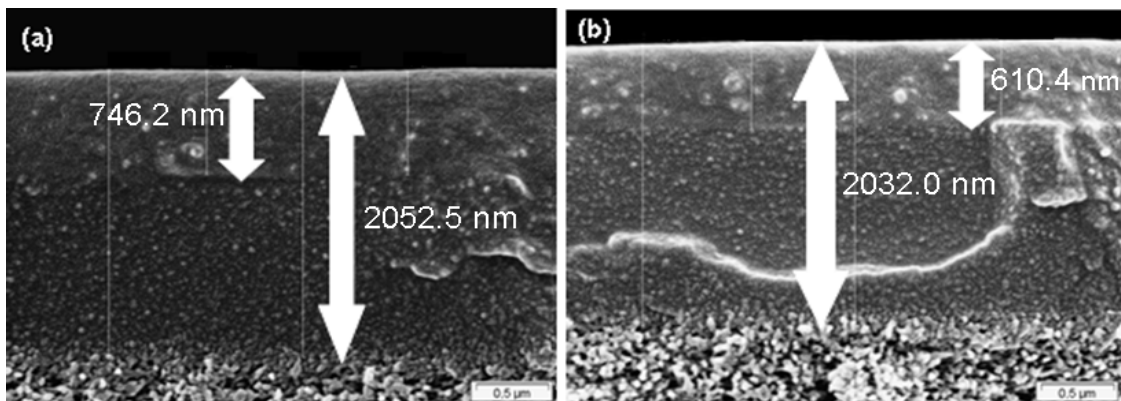


**Figure 6.20:** SEM images (cross-section) of the membranes based on H-4

In analogy to the L-type based membranes three different zones can be identified in the cross-section images, which can be explained by an interaction of the graft-copolymer and the PAN. Figure 6.21, shows a tentative scheme of this interaction. The polyacrylonitrile's nitrile group is less nucleophilic than a primary amine. However, this group may be able to interact with the graft-copolymers by a hydrogen bridge or nucleophilic attack on carboxyl group of the grafted copolymer.

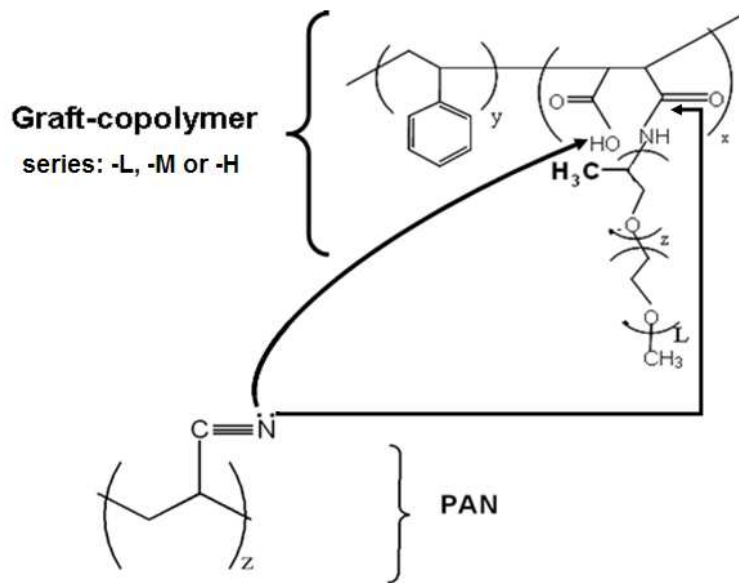


**Figure 6.21:** Tentative scheme of interaction between the PAN support layer and graft-copolymers of L-, M- and H-type

Using the micrographs the thickness of the membrane can be determined (cf. Table 6.2). Using the thickness the single gas permeability of the membrane can be calculated (cf. Table 6.4.). To calculate the permeability the “long” thickness will be considered because a part of the polymer is mixed with the PAN support and that will also influence the permeability of the gases. As it was mentioned on page 138, the top-layer (short scale) consists of a pure membrane dense material, hence only a graft-copolymer layer, then in the middle layer a mixture of graft-copolymer and PAN (long scale) can be found, due to the graft-copolymer “membrane material” wet the support, this wetting process could be more or less extensive according to the interaction between the graft-copolymer and support, see figure 6.21. Finally, in the bottom is the pure PAN. The influence of this middle layer (dense), a mixture of graft-copolymer and PAN, in the permeation of CO<sub>2</sub> is high due to a part of or all the graft-copolymer is inside of the pore support allowing a high contact surface

between CO<sub>2</sub> and graft-copolymer (rubbery segment). Such contact surface is represented by the long scale thickness ( $l$ ), see table 6.2, and it is used in the calculation of the permeability, see equation 6.3, page 136.

**Table 6.2:** Thickness of the membranes based on series-ML, -MM and -MH

Membranes	Thickness “short” (nm)	Thickness “long” (nm)
ML - 1	...	577
ML - 2	353	726
ML - 3	620	...
ML - 4	358	943
ML - 5	367	1232
MM - 1	...	928
MM - 2	...	956
MM - 3	394	1512
MM - 4	484	1354
MH - 1	....	1224
MH - 2	487	1125
MH - 3	520	2130
MH - 4	678	2042

### 6.2.2 Characterization and Analysis of the Membranes Series-GSMA and -GPSS by SEM.

Figures 6.22 – 6.27 show the cross-section micrographs of the GSMAS-1 - GSMAS-3, i.e. the GPSS-1 - GPSS-3 based membranes. In the micrographs three different zones can be observed: PAN at the bottom, in middle a mixed phase of PAN and the graft-copolymer (thickness “long”) and the pure graft-copolymer film at the top (thickness “short”).

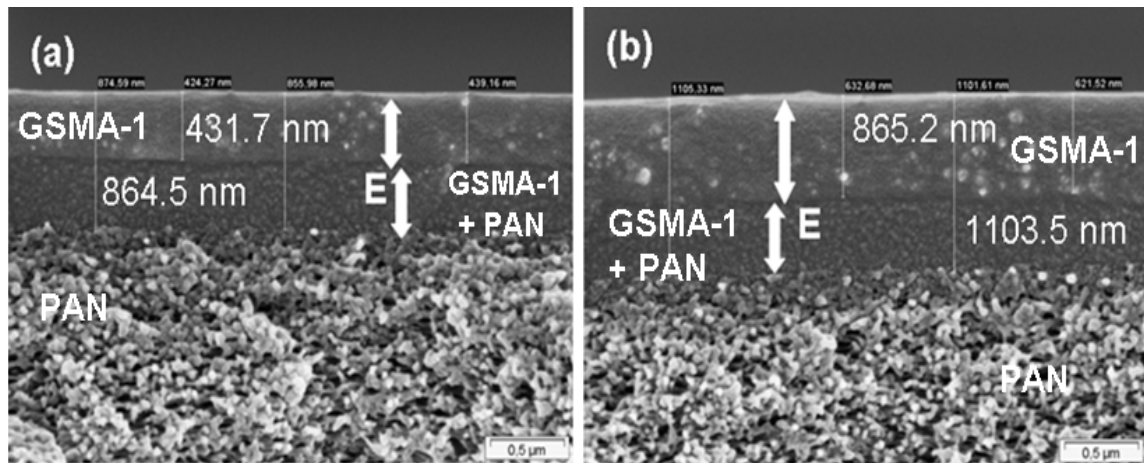


Figure 6.22: SEM images (cross-section) of the membranes based on GSMAS-1(E)

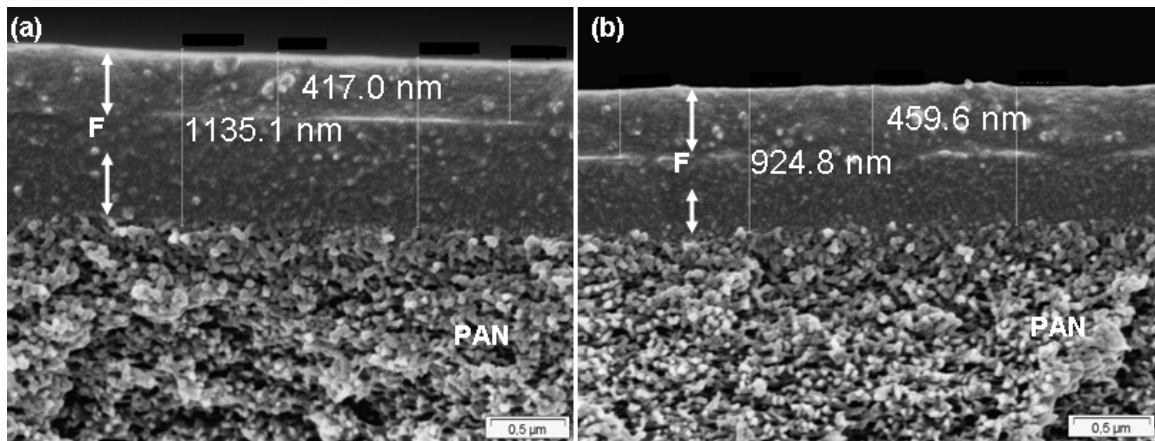


Figure 6.23: SEM images (cross-section) of the membranes based on GSMAS-2(F)

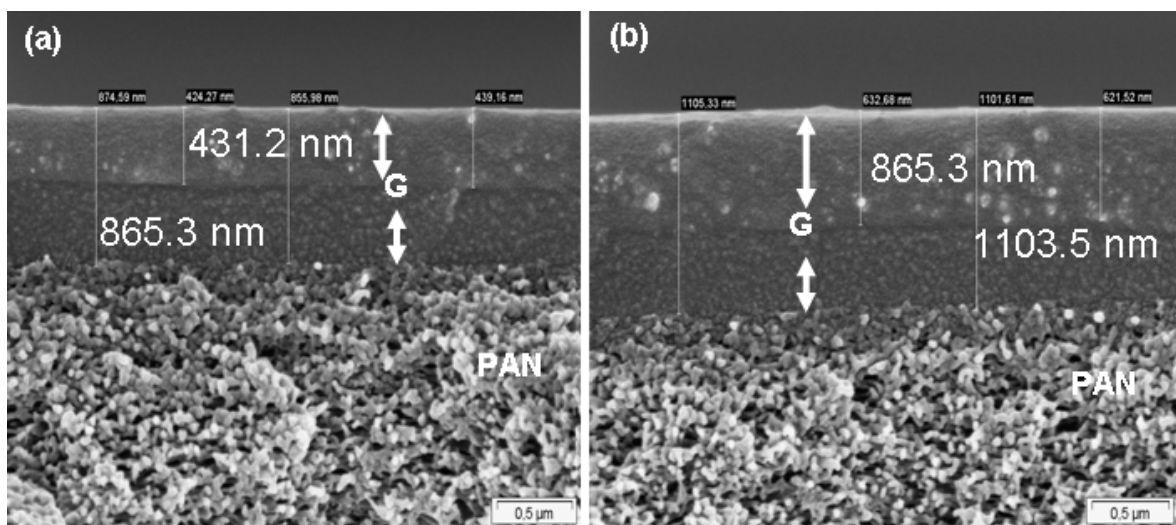


Figure 6.24: SEM images (cross-section) of the membranes based on GSMAS-3(G)

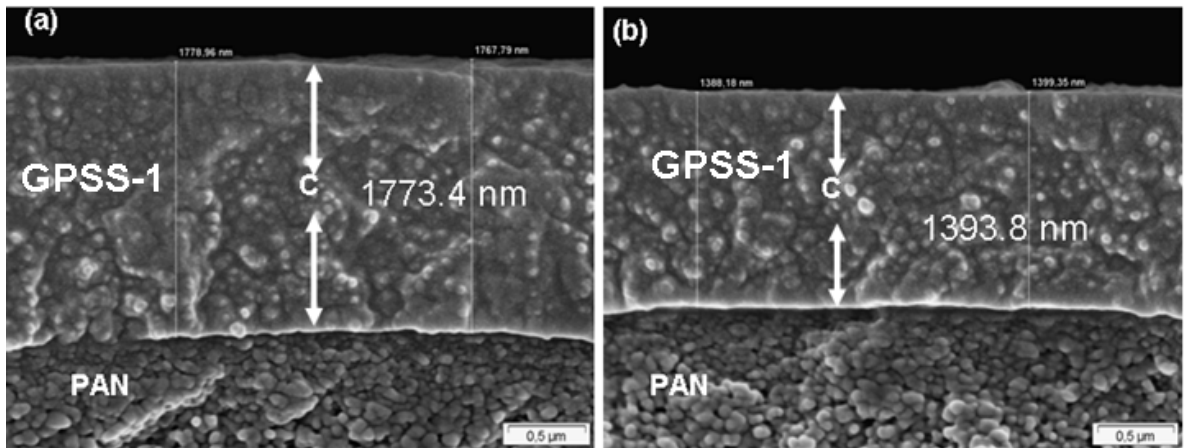


Figure 6.25: SEM images (cross-section) of the membranes based on GPSS-1 (C)

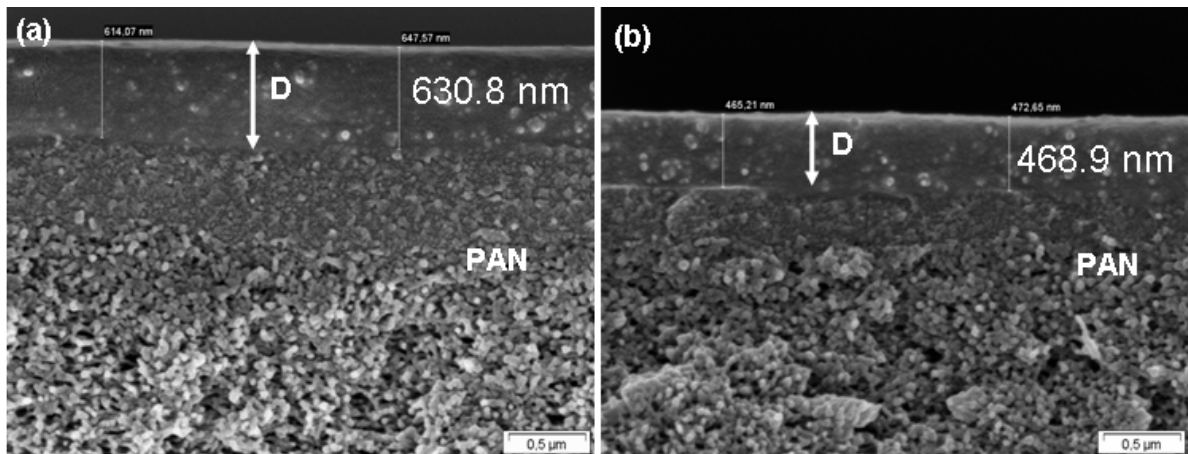


Figure 6.26: SEM images (cross-section) of the membranes based on GPSS-2 (D)

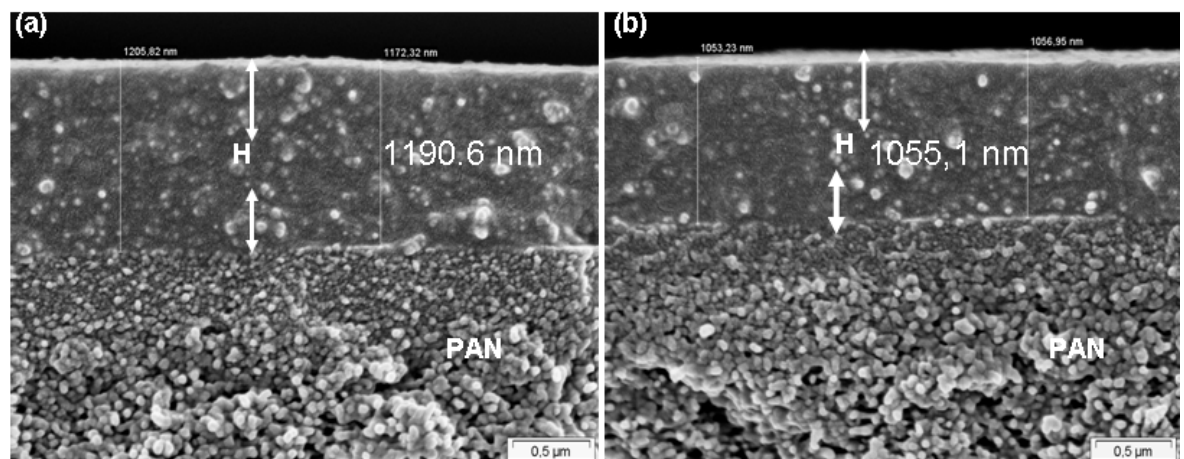
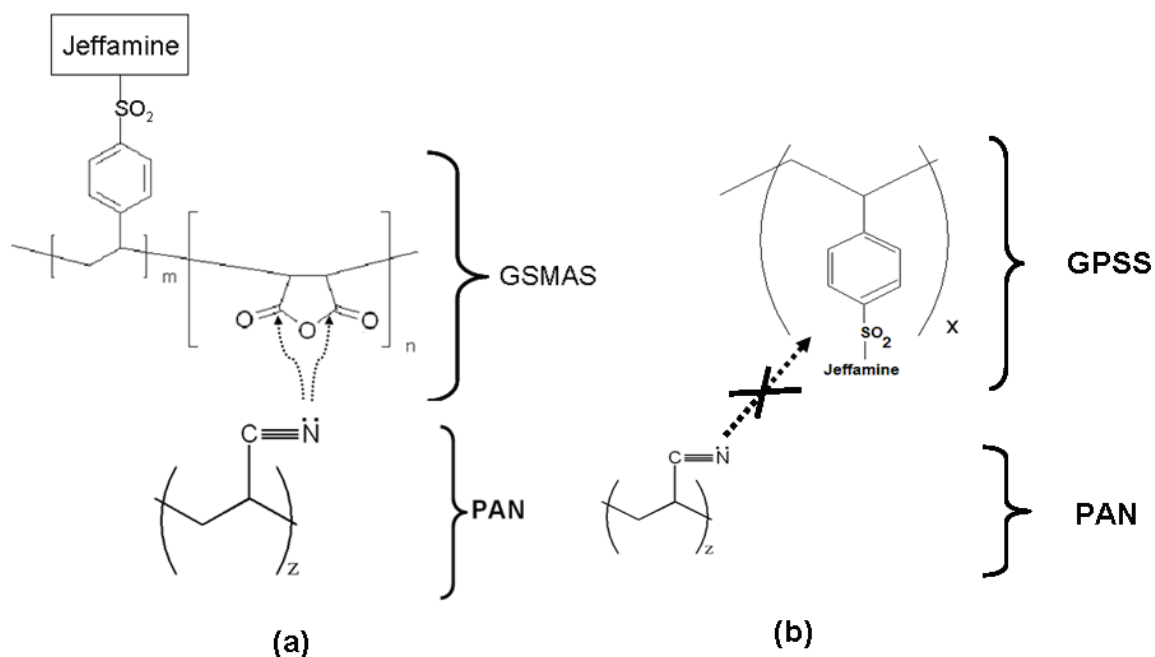


Figure 6.27: SEM images (cross-section) of the membranes based on GPSS-3 (H)



**Figure 6.28:** Possible dipole-dipole interactions between PAN: (a) GSMAS and (b) GPSS.

The differences of the micrographs of the series-GSMAS and the series-GPSS may be explained by different extents of interaction between the membrane material and the PAN support. As indicated in figure 6.28(a) the polyacrylonitrile's nitrile group is able to interact with the anhydride group or after hydrolysis the carboxyl groups, which generates the "mixed zone" between the top (GSMAS-1) and bottom (PAN) layer, see figure 6.22. In GPSS however, figure 6.28(b), on interaction of the PAN (nitrile group) with the polystyrene main chain is unlikely, hence most of the series-GPSS does not exhibit this mixed zone", see figure 6.25. Again, the thicknesses of the membranes can be determined from Fig. 6.22 to 6.27 and with the thickness the permeability of single gases as  $CO_2$ ,  $CH_4$  can be calculated (cf. Table 6.4). Average values obtained of the "short" thickness are approximately 500 nm whereas the "long" thickness ranges from 1000 to 1500 nm. In the case of the series-GPSS

(Figure 6.25 – 6.27), only one zone can be detected, as explained above, this could indicate that the interaction between the support and the graft-copolymer depends of the type of the grafted-copolymers. The different degrees of interaction may lead to different morphologies of the membranes, for instance, a pattern with three zones (series-GSMA) or with two zones (series-GPSS) and the different patterns may also affect the penetration of the gases across the membrane.

**Table 6.3:** Thickness of the membrane based on (series-GSMAS and series-GPSS)

Membranes	Thickness “short” (nm)	Thickness “long” (nm)
GSMAS - 1	649	984
GSMAS - 2	438	1030
GSMAS - 3	530	984
GPSS - 1	-----	1584
GPSS - 2	-----	550
GPSS - 3	-----	1123

### 6.2.3 Membranes Properties of Series-ML, Series-MM and Series-MH.

Table 6.4 shows the results of permeabilities of CO<sub>2</sub> ( $P_{CO_2}$ ) and of CH<sub>4</sub> ( $P_{CH_4}$ ), the selectivities of CO<sub>2</sub> with respect to N<sub>2</sub> ( $\alpha(CO_2/N_2)$ ) and to CH<sub>4</sub> ( $\alpha(CO_2/CH_4)$ ) for the parent polymers (SMA “hard block copolymer”) and the corresponding graft-copolymers (series-ML, -MM and -MH). The permeability was determined using the theory presented in section 6.1.2, pages 134-135.

**Table 6.4:** Flow, permeability of CO<sub>2</sub> and CH<sub>4</sub> at 35°C and 1 atm for the ML-, MM- and MH-type membranes

MEM	$J$ ( $m^3/m^2 h bar$ )	$P_{CO_2}$ (Barrer)	$\alpha$ (CO <sub>2</sub> /N <sub>2</sub> )	$P_{CH_4}$ (Barrer)	$\alpha$ (CO <sub>2</sub> /CH <sub>4</sub> )	PEG (%)
SMA(7)	0.02	5	6	0.5	10.0	0.0
ML-1	0.50	107	25	7	15.3	3.2
ML-2	0.50	134	14	27	5.0	4.0
ML-3	1.72	395	9	246	1.6	4.0
ML-4	0.04	14	29	1	14.0	6.0
ML-5	0.30	137	20	50	2.8	4.0
MM-1	0.2	70	38	0.2	350	21.7
MM-2	0.13	46	30	0.7	65.7	18.3
MM-3	0.03	17	5	5.7	3.0	20.0
MM-4	0.45	226	24	19	12.0	22.0
MH-1	0.26	121	6	6.0	20.2	20.7
MH-2	0.42	175	34	10	17.5	23.5
MH-3	0.24	189	42	10	19.0	24.2
MH-4	0.38	287	35	18	16.0	26.0

### 6.2.3.1 Analysis of the Permeability of CO<sub>2</sub> and the CO<sub>2</sub>/N<sub>2</sub> Selectivity

Figure 6.29 presents the effect of the polyethylene glycol content (PEG) of the graft-copolymer (in each membrane) on the CO<sub>2</sub> permeability. In general terms, the trend of the results exhibits that all the membranes have a higher permeability in comparison to SMA(7) basically due to the increase of the PEG content and the heterogeneity of the graft-copolymer. ML-3 shows a high permeability of 395 Barrer



in spite of the low PEG content. However, the ML-series exhibit lower values around 140 – 100 Barrer with one sample (ML-4) possessing a permeabilities as low as 14 Barrer. The MM-series represents second group with higher PEG contents but lower CO<sub>2</sub> permeabilities (70 – 17 Barrer). Sample MM-4 is the exception from the rule as its permeability of 226 Barrer is unusually high. Finally, the MH-series show an increase of the CO<sub>2</sub> permeability in comparison to the other samples; the values are in an interval of 120 – 290 Barrer approximately. It is reasonable to assume that the PEG content in the graft-copolymer affects the performance of the membranes as it helps to increase the permeability of CO<sub>2</sub>. Finally, inspire of the results showing for series-MM we observe that there is a trend respect of the  $PCO_2$  and PEG content, membrane with high PEG content exhibit high  $PCO_2$ . The results shows that there is a transition behavior in the membranes between series-ML and series-MH and which is exhibit by the series-MM results and could be also observe by the selectivity (CO<sub>2</sub>/N<sub>2</sub>), see figure 6.30. The order of this trend is: series-MH > series-ML > SMA(7) and with series-MM as transition state.

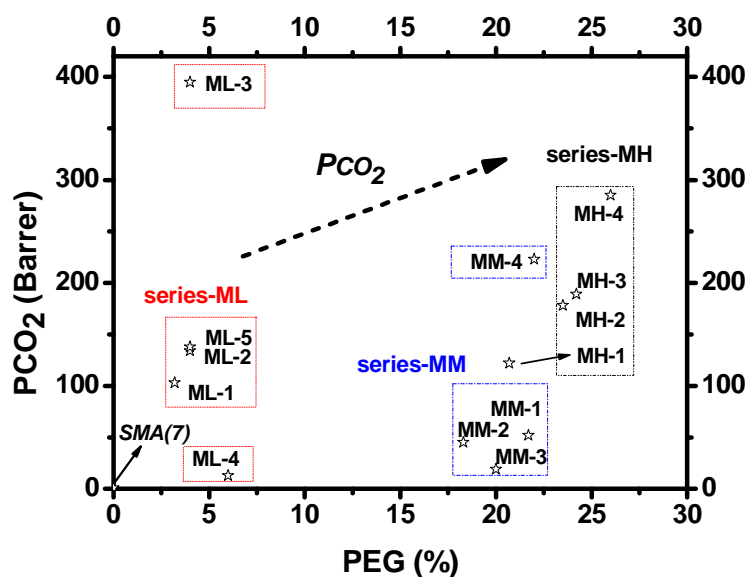


**Figure 6.29:** Variation of the CO<sub>2</sub> permeability in dependency of the PEG content

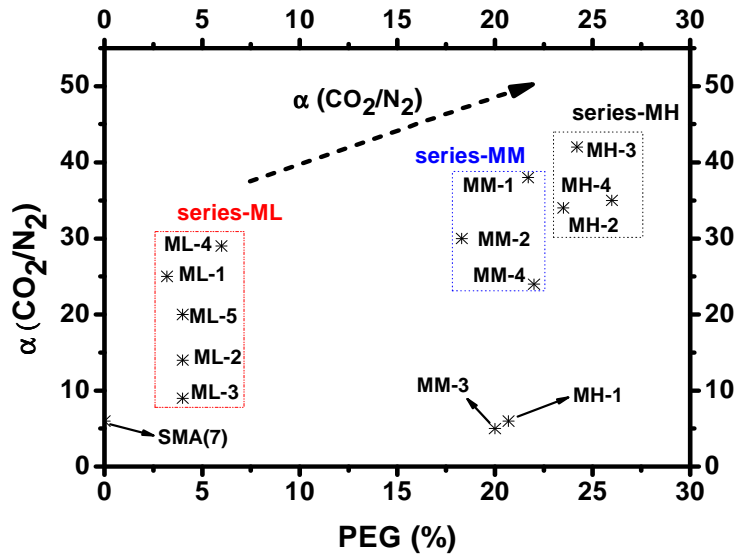


**Figure 6.30:** Variation of  $\alpha$  CO<sub>2</sub> / N<sub>2</sub> in dependency of the PEG content.

Figure 6.30 highlights the dependency of the CO<sub>2</sub>/N<sub>2</sub> selectivity on the PEG content in the graft-copolymers. The results indicate that in the ML-, MM-, and MH- series the selectivity increases with PEG content in comparison to SMA(7). In general terms, the CO<sub>2</sub>/N<sub>2</sub> selectivity increases in the order MH > MM > ML > SMA(7). The same behavior can be observed in figure 6.30. The increase of the CO<sub>2</sub>/N<sub>2</sub> selectivity and  $P_{CO_2}$  with increasing of the PEG content is probably due to the introduction of a polar group into the polymer, resulting in a higher CO<sub>2</sub> solubility in comparison to N<sub>2</sub>. The series-MM is follows a different trend, here the inverse the relation between permeability and selectivity (permselectivity) is found, that is to say a high selectivity (CO<sub>2</sub>/N<sub>2</sub>) is usually accompanied with a low permeability [5], (cf. figure 6.29 und 6.30). Mostly likely the series-MM follow mostly a size selective sieving mechanism (thus diffusion controlled), in which the CO<sub>2</sub> diffusivity is larger than the N<sub>2</sub> diffusivity [5]. The preferential permeation of CO<sub>2</sub> relative to N<sub>2</sub> observed for most of the graft-copolymer membranes may be explained by a solution-diffusion

mechanism. Based on this model which describes the gas transport through dense polymeric membranes the gas permeability ( $P$ ) across the membrane is a product of solubility ( $S$ ) and diffusivity ( $D$ ).

$$P = S \times D \quad (6.4)$$

In our case, the gas pair ( $\alpha(\text{CO}_2/\text{N}_2)$ ) permselectivity comprises the solubility ( $S_{\text{CO}_2}/S_{\text{N}_2}$ ) and diffusivity ( $D_{\text{CO}_2}/D_{\text{N}_2}$ ) selectivities, which should both be high to result in an optimal separation factor. To obtain an effective separation of the  $\text{CO}_2$  from the  $\text{N}_2$  it is therefore important to have a high solubility of the  $\text{CO}_2$  in the membrane material, these requirements can be fulfilled by the introduction of polar PEG segment and a membrane structure, which having a  $\text{CO}_2$  diffusivity higher than the  $\text{N}_2$  diffusivity.

$$\alpha(\text{CO}_2/\text{N}_2) = (P_{\text{CO}_2}/P_{\text{N}_2}) = \left( \frac{S_{\text{CO}_2}}{S_{\text{N}_2}} \right) \times \left( \frac{D_{\text{CO}_2}}{D_{\text{N}_2}} \right) \quad (6.5)$$

The gas solubility of polymeric membranes depends on the condensability of the penetrate gases, the nature of interaction between the polymer and penetrates, and the chain packing density in glassy polymers [6]. The solubility of  $\text{CO}_2$  is higher than that of  $\text{N}_2$  due to the significant difference in the condensability of the gases ( $T_{\text{condensability, CO}_2} = 304 \text{ K (31}^\circ\text{C)}$  and  $T_{\text{c, N}_2} = 125,2\text{K (-148}^\circ\text{C)}$ ). At the same time, the graft-copolymers consisting of flexible poly(ethylene glycol) (PEG) segment are very attractive for the polar  $\text{CO}_2$  molecules as it has a strong affinity to the polar PEG segment [4]. On the other hand, since the gas diffusivity mainly depends on the kinetic diameter ( $d_{\text{KT}}$ ) of the penetrants, the diffusivity of  $\text{CO}_2$  is expected to be larger than  $\text{N}_2$  ( $d_{\text{KT, CO}_2} = 3.3 \text{ \AA}$ ,  $d_{\text{KT, N}_2} = 3.64 \text{ \AA}$ ) [7], hence the separation of a common gas

pair (e.g. CO<sub>2</sub>/N<sub>2</sub>) is accomplished by a size selective sieving mechanism (diffusion) in which CO<sub>2</sub> must diffuse faster than N<sub>2</sub>.

Figure 6.31 presents the effect of glass transition temperature (*T<sub>g</sub>*) of the graft-copolymer used in each membranes on the CO<sub>2</sub> permeability at 35°C. For a decreasing *T<sub>g</sub>* an increase in the CO<sub>2</sub> permeability can be found. The relative increase in the MH-series is large than that for the MM-series and less than that observed for the ML -series. An analogous effect is found in figure 6.33 where the permselectivity ( $\alpha(\text{CO}_2/\text{N}_2)$ ) is plotted as a function of the glass transition temperature. In both cases the order of CO<sub>2</sub> permeability and permselectivity  $\alpha(\text{CO}_2/\text{N}_2)$  is the same: series-MH > series-ML >> SMA(7). The series-MM is inconsistent with the other series (-MH and -ML), as mentioned above, the series-MH follows rather the diffusion mechanism. However, an increase the CO<sub>2</sub> diffusion into the materials should be visible caused by the increase of the fractional free volume (FFV), but the permeability of CO<sub>2</sub> does not change, maybe because, first, the decrease of *T<sub>g</sub>* is not increase the CO<sub>2</sub> diffusion due to packing effect into membrane, that is to say the material is packing without order in the membrane avoiding the diffusion the gas. Second, because the contribution from the polar group to increase solubility of CO<sub>2</sub> is blocked by this disorder into the material. Hence, the interaction between PEG-segment and the CO<sub>2</sub> is blocked by this unordered structure. Therefore the change in the disposition and mobility of the PEG-segment during the increase of the PEG content in the graft-copolymer could affect the membranes performance. A varying gas permeability values depends strongly on the detailed morphology, such as the domain shape and spatial

arrangement, which could be influenced by the hard segment composition (PS) and the lengths of the PEO and hard segment blocks [7].

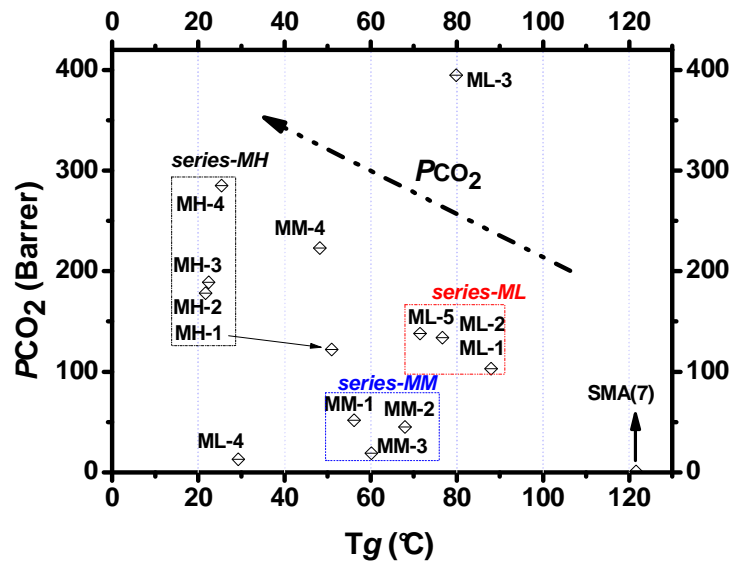


**Figure 6.31:** Variation of the CO<sub>2</sub>-permeability with the glass transition temperature for the graft copolymer based membranes

The higher PEG content increases the number of soft segment in the graft-copolymer resulting in decrease of the glass transition temperatures (as shown in figures 6.31 and 6.32) and an increase in the fractional free volume. This, in turn, is responsible for the observed increases in CO<sub>2</sub> permeability and the corresponding trends in the CO<sub>2</sub>/N<sub>2</sub> selectivity [8,9].

For a detailed explanation the relation between the free volume (FFV) and the glass transition temperature will be used. For a graft-copolymer with rubbery PEG segments, the FFV can be estimated by [7]:

$$\text{FFV} = \text{FFV}(T_g) + \alpha_r(T - T_g)$$

**Figure 6.32:** Schematic of the fractional free volume model characterizing the effect of copolymer composition, temperature, and CO<sub>2</sub> fugacity of the feed gas.

In Figure 6.32,  $\text{FFV}(T_g)$  is the apparent fractional free volume at  $T_g$ , and  $\alpha_r$  is the expansion coefficient of the fractional free volume in the rubbery phase ( $T > T_g$ ). The equation summarizes and shows the correlation between the FFV of polymer-penetrant gases and the three factors of interest (i.e., copolymer composition, temperature, CO<sub>2</sub> fugacity effect) that exert significant influence on gas permeation: The FFV increases linearly with the temperature ( $T - T_g$ ), the copolymer composition influences  $T_g$ , and the CO<sub>2</sub> fugacity affects the  $T_g$  of polymer mixture. From this analysis, it is evident that a decrease in the glass transition temperature leads to an increase of the free volume which finally results in higher CO<sub>2</sub> permeabilities and permselectivities. For example see figure 6.33,  $\alpha(\text{CO}_2/\text{N}_2)$ , series-MM and -ML, could be explain because the  $T_g$  the material is above to the room temperature, hence the permeability process is affected mostly by higher diffusion of CO<sub>2</sub> in comparison of N<sub>2</sub>; because in the material the FFV increases in comparison to SMA and PS polymers. Consequently selectivity is determined by the diffusion or “molecular sieving” effect due to the kinetic diametric of CO<sub>2</sub> and N<sub>2</sub> ( $d_{\text{KT}, \text{CO}_2} = 3.3 \text{ \AA}$ ,  $d_{\text{KT}, \text{N}_2} = 3.64 \text{ \AA}$ ).

For a material having  $T_g$  below of the room temperature, series-MH, the permeability is more controlled by the solubility process, because the PEG content increase so the solubility of the  $\text{CO}_2$  is higher than series-MM and -ML. Therefore, the selectivity of  $\text{CO}_2 / \text{N}_2$  increases. In these conditions, the diffusion increases, due to the very high FFV value. However, the “molecular sieving” effect is not so dominant, since all the gases diffuse very fast through the membrane

In this study the permselectivity is dominated by the solubility of  $\text{CO}_2$  in the membrane over the  $\text{N}_2$  diffusion process “molecular sieving” hence across of this temperature range the final trend is that the permselectivity increase.

The incorporation of Jeffamine leads, in general, to a decrease in  $T_g$ . The material can be regarded as a rubbery polymer, for which the selectivity is determined mostly by the differences in solubility. In fact,  $\text{CO}_2$  is more soluble in PEO than  $\text{N}_2$ . Therefore, the experimental results somehow are in line with the theory proposed by the solubility-diffusion model.

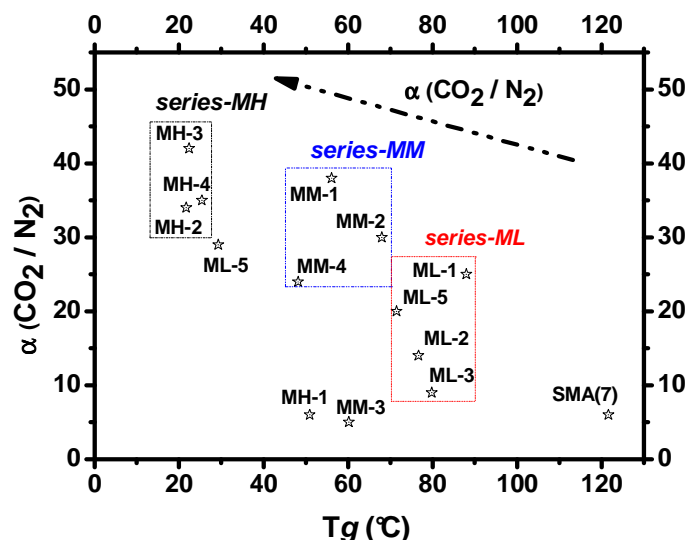


**Figure 6.33:** Variation of selectivity ( $\text{CO}_2 / \text{N}_2$ ) with the glass transition temperature for the graft copolymer, series-MH, -MM and -ML, based membranes

### 6.2.3.2 Analysis of the CH<sub>4</sub> Permeability and CO<sub>2</sub>/CH<sub>4</sub> Selectivity

The dependency of the CH<sub>4</sub> permeability on the PEG content is presented in the figure 6.34. In general term, the CH<sub>4</sub> permeability is not affected by the increase of the PEG content. However, ML-5 shows a high value (~50 Barrer) but this may not be representative for all series-ML. Obviously, the CH<sub>4</sub> permeability is not depending on the solubility of CH<sub>4</sub> in PEG material, due to the low methane condensation temperature ( $T_c$ , CH<sub>4</sub> = 191 K). Also the penetration of CH<sub>4</sub> by diffusion is only valid for the glassy polystyrene segment. In the polar segment (PEG) CH<sub>4</sub> is insoluble, hence the solubility-diffusion mechanism may not be applied to explain the CH<sub>4</sub> permeability. The theory of gas sorption and diffusion in glassy polymers could be a more appropriate approach to explain such a behavior. Several models have been established to explain the sorption of gas molecules in polymeric membranes but the use of a model based on the dual-mode sorption theory has been more prevalent [10]. The dual-mode sorption model (presented on page 45) suggests the presence of Henry and Langmuir sorption sites in glass polymers [11-14]. Hence, in case of CH<sub>4</sub> the permeability depends on the diffusion of the gas into the membrane. CH<sub>4</sub> is not soluble in the PEG segment but can be sorbed into the dense polystyrene matrix (glassy segment) and then diffuse through it.



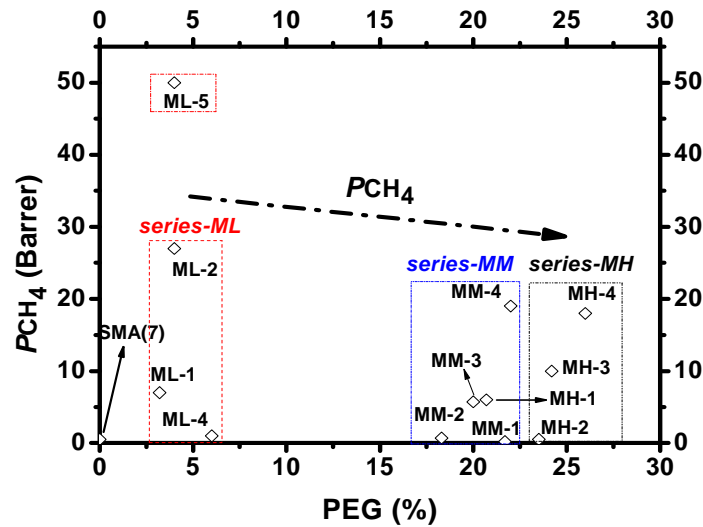


**Figure 6.34:** Variation of the  $CH_4$  permeability in dependency of the PEG content for the graft copolymer based

Figure 6.35 presents the effect of the PEG content on the  $CO_2/CH_4$  selectivity ( $\alpha(CO_2/CH_4)$ ). In general terms the selectivity values are in between 10 – 20, the MH-samples show the highest selectivity values (18-20), the selectivity of the ML- and MM-type samples is more or less the same. The  $CO_2/CH_4$  selectivity shows an increase from series-MM to the series-MH when the PEG content reaches 22 % which may indicate that PEG contents of more than 22% are needed to obtain an effect on the  $CH_4$  selectivity. As expected the PEG content (polar segment) has an influence on the  $CO_2/CH_4$  selectivity, as it already mentioned for the case  $CO_2 - N_2$  pair (fig. 6.30). As shown in figure 6.29 (permeability of  $CO_2$  vs PEG content) the  $CO_2$  solubility is dependent on the condensability, the interactions of the polymer with the gas, and the chain packing density in glassy polymers [15]. The solubility of  $CO_2$  is higher than that of  $CH_4$  due to the difference in the condensability of the gases ( $T_{c, CO_2} = 304$  K and  $T_{c, CH_4} = 191$  K). Due to the contribution of the glassy polymer segment (PS), the gas diffusivity mainly depends on the kinetic diameter

( $d_{KT}$ ) of the gases, diffusivity of  $\text{CO}_2$  exceeds that of  $\text{CH}_4$  ( $d_{KT, \text{CO}_2} = 3.3\text{\AA}$  and  $d_{KT, \text{CH}_4} = 3.8\text{\AA}$ ) [7]. This explains the preferential permeation of  $\text{CO}_2$  relative to  $\text{CH}_4$  for graft-copolymer membranes as shown in figure 6.35.

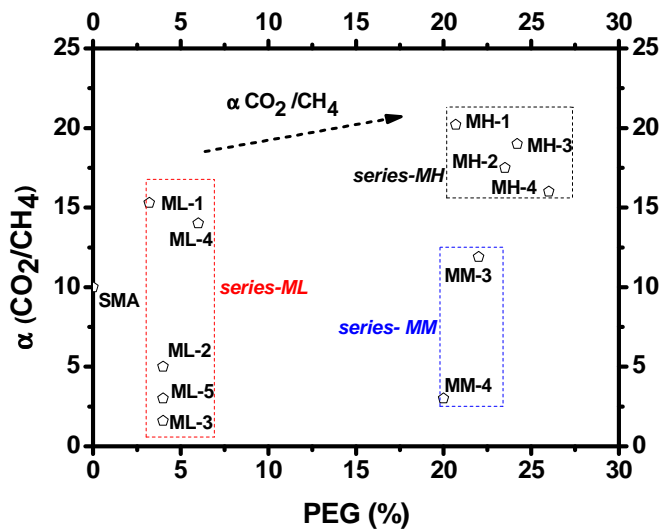


**Figure 6.35:**  $\text{CO}_2 / \text{CH}_4$  selectivity of in dependency of the PEG content for the graft copolymer based membranes

### 6.2.3.3 Comparison of Membranes Performances between Series-ML, -MM and -MH, Polyimides and others Polymers reported

The recent developments in membranes and the attention over the last two decades make the polyimides an interesting polymer to be used as comparative references. Figure 6.36 shows some types of polyimides, reported in table 6.5, and other polymers. In spite of the polyimide structure is not complete comparable to the graft-copolymers of this work, see figure 6.36, it should be emphasized that polyimides are a group of polymer membranes that have been very well studied due to their very interesting performance [4]. Finally, the polyimides general structure is rather similar to the graft-copolymers discussed in this work, figure 6.36 (A, C) due to the

presence of carbonyl and amino groups may be regarded as an “amide moiety” like the one adjacent to the PEG group.

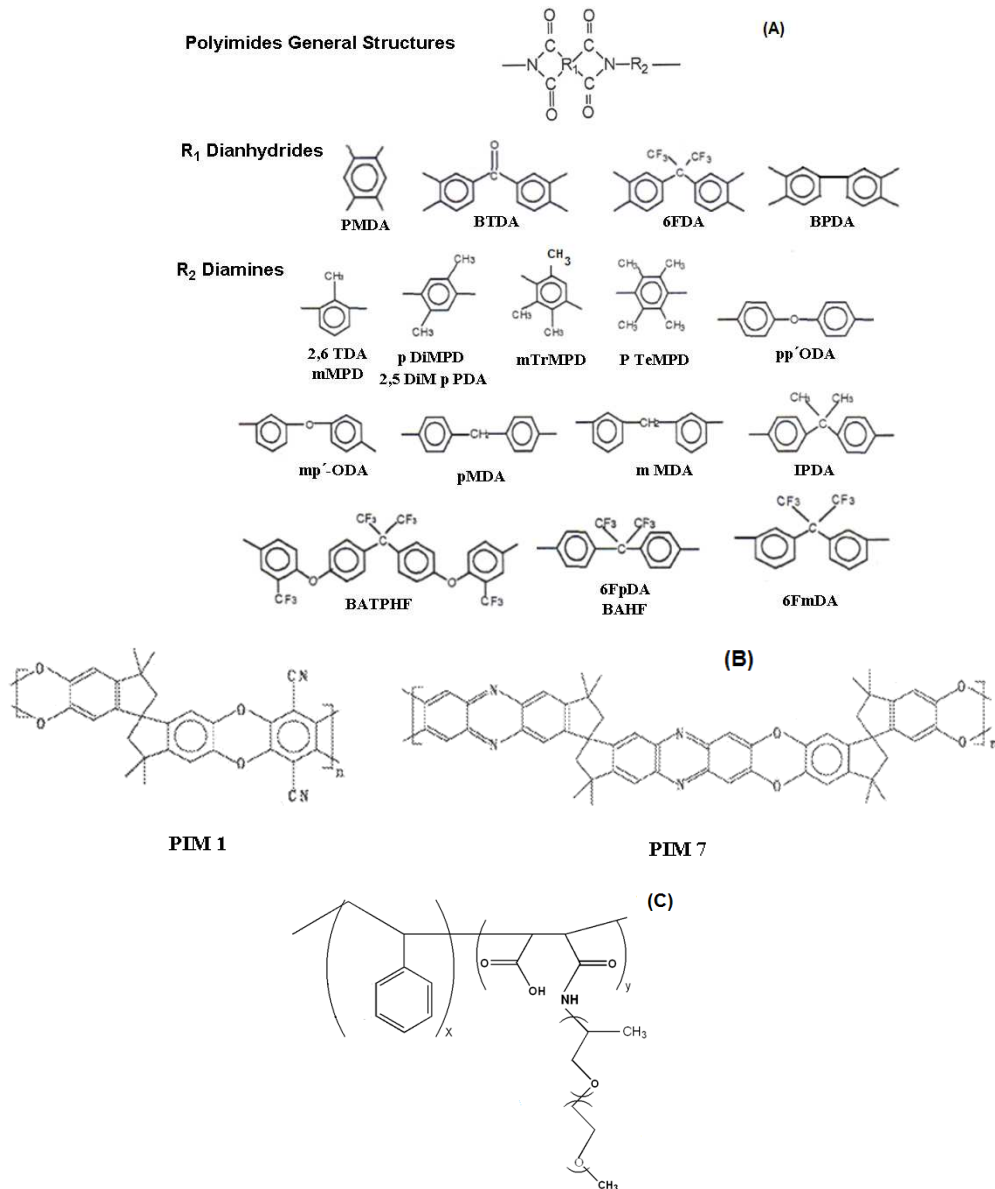


**Figure 6.36:** Structures types of: (A) polyimides (B) PIM polymers (C) graft-copolymer

Table 6.5 contains the permeability values of CO<sub>2</sub> ( $PCO_2$ ), N<sub>2</sub> ( $PN_2$ ), CH<sub>4</sub> ( $PCH_4$ ) and fractional free volume (FFV) of the polyimides reported in literature and the results of the graft-copolymer membranes prepared in this work (MH-, MM- and ML-series).

**Table 6.5:** Permeability of gases for polymers from literature and graft-copolymers (series-ML, -MM and -MH) prepared in this work.

<b>MEMBRANES</b>	$P_{CO_2}$ (Barrer)	$P_{N_2}$ (Barrer)	$P_{CH_4}$ (Barrer)	<b>FFV</b>	<b>Reference.</b>
<i>SMA(7)</i>	1.0		0.5	----	----
<b>MH-4</b>	285.0	8.140	18.0	----	----
<b>MH-3</b>	189.0	4.50	10.0	----	----
<b>MH-2</b>	178.0	5.23	10.0	----	----
<b>MH-1</b>	122.0	20.3	6.0	----	----
<b>MM-4</b>	223.0	9.30	19.0	----	----
<b>ML-5</b>	138.0	6.90	50.0	----	----
<b>PMDA-ODA</b>	3.550	0.1450	0.0937	0.129	[7,16]
<b>PMDA-MDA</b>	4.000	0.2000	0.0930	0.117	[16,18]
<b>PMDA-IPDA</b>	27.000	1.500	0.900	0.137	[16-18]
<b>PMDA-BAPHF</b>	17.600	0.9430	0.6380	0.165	[7,17]
<b>PMDA-BATPHF</b>	24.600	1.500	0.9370	0.182	[7,17]
<b>6FDA-MDA</b>	19.000	0.8100	0.4200	0.160	[16-18]
<b>6FDA-IPDA</b>	30.000	1.3400	0.7000	0.168	[16-18,21]
<b>6FDA-6FpDA</b>	64.000	3.4000	1.6000	0.272	[17,21,22]
<b>6FDA-TeMPD</b>	455.800	35.600	28.400	0.182	[19,23,24]
<b>6FDA-mTrMPD</b>	431.000	31.600	26.000	0.182	[19]
<b>6FDA-pDiMPD</b>	42.7000	2.6700	1.0700	0.175	[19]
<b>[6FDA-BAHF</b>	51.200	3.1100	1.3400	0.182	[7,17]
<b>6FDA-DDBT</b>	91.000	5.1400	2.5100	0.169	[17,20]
<b>6FDA-2,6TDA</b>	40.100	2.2400	0.8770	0.176	[19,26]
<b>6FDA-2,5DiMpPDA</b>	42.700	2.6700	1.0700	0.175	[19,26]
<b>6FDA-DATPA</b>	23.000	1.2400	0.6800	---	[25,26]

Table 6.5: (continued)

<b>BPDA-mTrMPD</b>	137.00	8.4200	8.0800	0.155	[19]
<b>BPDA-BAPHF</b>	4.960	0.2450	0.1450	0.158	[7,17]
<b>BPDA-BATPHF</b>	9.150	0.5630	0.2790	0.177	[7,17]
<b>BTDA-mTrMPD</b>	27.70	1.3900	0.7800	0.157	[7,17]
<b>BTDA-mTrMPD</b>	30.90	1.5500	1.2500	0.131	[19]
<b>BTDA-BAPHF</b>	4.370	0.1950	0.1050	0.163	[17]
<b>BTDA-BATPHF</b>	6.940	0.3700	0.1890	0.170	[17]
<b>BTDA-BAHF</b>	10.10	0.4500	0.2260	0.153	[7,26]
<b>BTDA-DATPA</b>	3.30	0.1440	0.093	---	[25,26]
<b>6F-BisPhenol-A-</b>					[17]
<b>(PC)</b>	111.0	7.700	4.700	0.216	[27]
<b>PIM1</b>	2300.0	92.0	125.0	---	[5]
<b>PIM7</b>	1100	42.0	62.0	---	[5]

$P$  = permeability, FFV = fractional free volume.

Also, membranes made up of polymers of intrinsic microporosity (PIM) (PIM1 and PIM7) are included, which are useful in gas separation applications [28-30].

From table 6.5, the following results can be drawn:

(a) As expected the CO<sub>2</sub>-permeability is highest for PIM1 and PIM7 ranging from 2300 to 1100 Barrer; it is intermediate for 6FDA-TeMPA and 6FDA-mTrMPD with values of 455.8 – 431 Barrer whereas the MH-4, MM-4, MH-3, MH-2, ML-5 and MH-1 based membranes follow with values ranging in between 285 – 122 Barrer. Even lower permabilities are reported for a series of polyimides. Similar trends can be

observed for in the  $N_2$  permeability and are less obvious in case of the  $CH_4$  permeability. In samples MH, MM and ML the fractional free volume (FFV) was not determined but for most of the polymers listed in table 6.5, a closer examination of the FFV reveals that the polyimides having a higher of FVV are closer to the upper bound line, according to the following values: PI derived from 6FDA dianhydrides have FFV between 0.15 and 0.27, those derived from BPDA and BTDA dianhydrides are between 0.12 and 0.17 and finally, those derived from PMDA are between 0.11 and 0.19 (Fig. 35 - 36). One can assume that the FFV for the MH's, MM-4 and ML-5 might exceed that of polyimide membranes. In order to confirm this hypothesis one could measure the FFV using positron annihilation life-time spectroscopy.

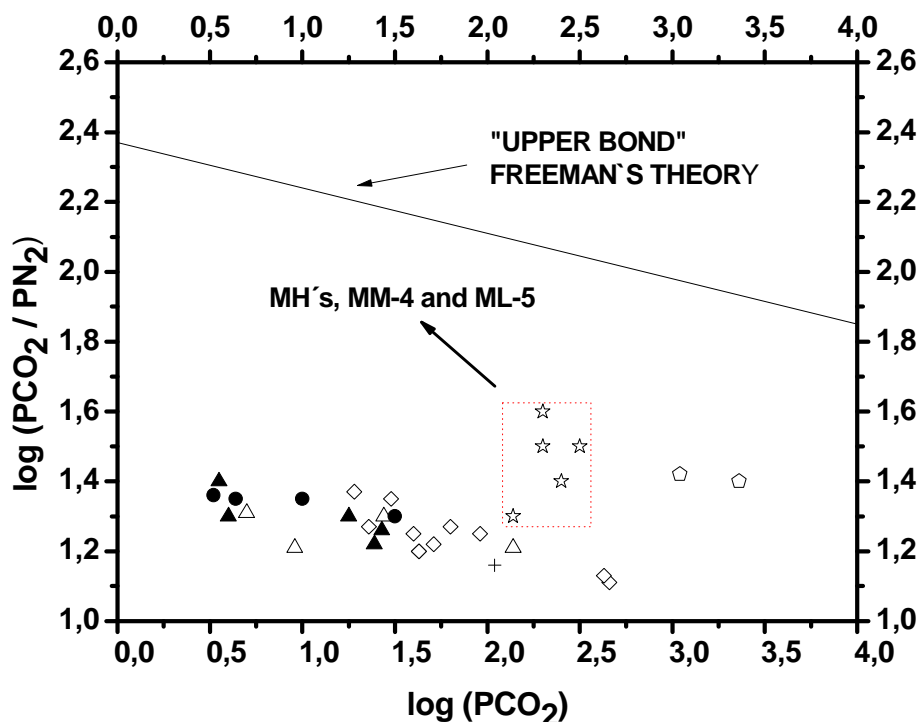


**Figure 6.37:** Experimental permeability of gases into polyimides and other polymers, Relationship between log selectivity ( $CO_2/N_2$ ) and log permeability ( $CO_2$ ) and the theoretical upper bound limit defined by Freeman's theory. (\*) MH's, (▲)PMDA, (◊)6FDA, (△)BPDA, (●)BTDA, (+) PC and (△) PIM1 und PIM7.

Besides the values from Table 6.5, Figure 6.37 also presents the upper bound curve for carbon dioxide – nitrogen gas pair and the relation between log selectivity ( $\text{CO}_2/\text{N}_2$ ) on the log permeability of  $\text{CO}_2$ . Figure 6.37 demonstrates that the samples MH-4, MH-3, MH-2, MM-4 and ML-5, exhibit a selectivity ( $\alpha$ ) for the separation of  $\text{CO}_2 / \text{N}_2$  of ranging in between 42- 20 which in combination with a high permeability of  $\text{CO}_2$  places these materials closer to the upper bound line according to Freeman's theory, in comparison with the other membranes reported in this graph. It must be noticed that no upper bound correlation was found in Robeson's analysis (1994) of  $\text{CO}_2\text{-N}_2$  separation by polymeric membranes [31], thus the position of the upper bound for this gas mixture was not reported. It is also important to mention that, due to the logarithmic nature of the plot, the values for MH, MM, and ML based membranes are significantly different and higher in comparison with the rest of polyimides. This points out that this materials are very interesting and may present competitive polymer membranes in comparison to polyimides and other polymers with a prospective industrial application (PIM1 and PIM7) [28]. Figure 6.37 also indicates that graft-copolymer membranes of MH-4, MH-3, MH-2, MM-4 and ML-5 are particularly interesting for the removal of  $\text{CO}_2$  in the air purification application or the purification of  $\text{N}_2$  in industrial processes like the dehydrogenation process (HDN) in the refinement of oil.

Similarly, Figure 6.38 presents the relationship between the  $\text{CO}_2 / \text{CH}_4$  selectivity and the  $\text{CO}_2$  permeability in a double logarithmic manner with the position of the corresponding upper bound lines according to Robeson's and Freeman's theory. The plot presents the best results for the  $\text{CO}_2/\text{CH}_4$  separation by polyimides based membranes. Note, that PIM1 and PIM7 are located close to both upper bound lines;

the rest of polyimides and also the graft-copolymers are can be found far away from both upper bound lines. The graft-copolymers (series MH, MM, and ML) shown in figure 6.38 are basically located in middle of the polyimides. The graft-copolymers selectivities are close to unity ( $\log(\alpha_{\text{CO}_2/\text{CH}_4}) \sim 1.15 - 1.3$ ); the corresponding selectivity values range from 15 to 20. However, these results indicated that the graft-copolymer prepared in this work possess a  $\text{CO}_2/\text{CH}_4$ -selectivity comparable to other polyimides reported in the literature (cf. table 6.5).

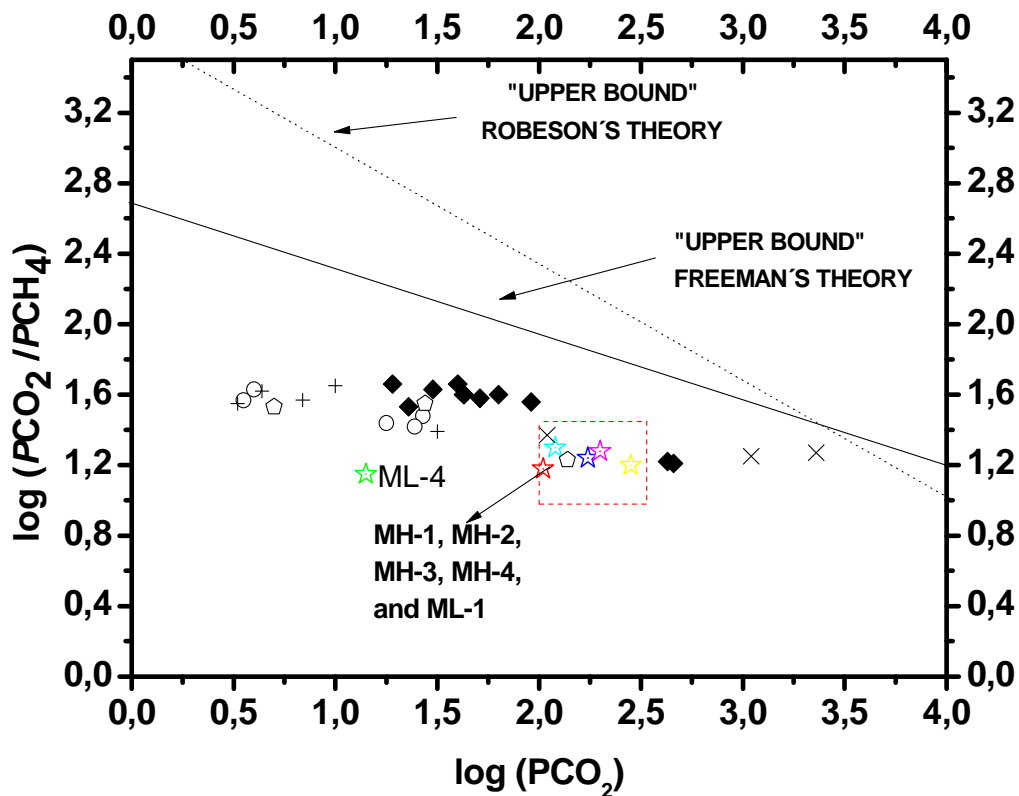


**Figure 6.38:** Double logarithmic plot of the dependency of the  $\text{CO}_2/\text{CH}_4$  selectivity in dependency of the  $\text{CO}_2$ -permeability. The theoretical upper bound limits are calculated according to Freeman's and Robeson's theory, respectively. MH's (\*), PMDA ( $\circ$ ), 6FDA ( $\blacklozenge$ ), BPDA ( $\triangle$ ), BTDA (+), PC - PIM1 und PIM7 ( $\times$ )



For both gas pairs, CO<sub>2</sub>/N<sub>2</sub> and CO<sub>2</sub>/CH<sub>4</sub> it is difficult to make predictions based on dense solution-diffusion membranes model, because of the permeants differences in solubility and mobility in the membrane materials. However, the permeation of gases through these polymers is often understood in terms of a solution-diffusion model for which the permeability coefficient is expressed by means of Eq. (6.4). First, using the lightest gases as H<sub>2</sub>, N<sub>2</sub>, O<sub>2</sub>, CO<sub>2</sub> and CH<sub>4</sub> and using their gas kinetic diameter, see table 6.6, as a good approximation of the penetrant size, diffusion phenomena can be analyzed. Due to CO<sub>2</sub> and N<sub>2</sub> have very similar sizes, see table 6.6, ( $\Delta d_{KT} = 0.34\text{\AA}$ ) as well as the pair CO<sub>2</sub>/CH<sub>4</sub> ( $\Delta d_{KT} = 0.50\text{\AA}$ ), their solubilities should depend significantly upon the specific interactions between the polymer and the penetrant. This effect will further be enhanced by the “molecular sieving” effect of glassy polymers which becomes more and more significant with an increasing size difference of the penetrant molecules.

**Table 6.6:** Transport properties and molecular parameters of penetrant gases

Gas Molecular data [ref.]	H <sub>2</sub>	CO <sub>2</sub>	O <sub>2</sub>	N <sub>2</sub>	CH <sub>4</sub>
Kinetic diameter, $d_{KT}$ (Å) [30,31]	2.89	3.3	3.46	3.64	3.8
Collision diameter, $D_{\text{van Krevelen}}$ [31-33] (Å)	2.83	3.94	3.47	3.8	3.76
Critical temperature, $T_c$ (K) [34]	33	304	154.2	126	190.5
$\Delta d_{KT}$ (Å)	CO <sub>2</sub> /CH <sub>4</sub> = 0.50		CO <sub>2</sub> /N <sub>2</sub> = 0.34		

### 6.2.5 Membranes Properties of Series-GSMA and -GPSS.

Table 6.7 lists the thickness of the membranes, cf. section 6.2.2, results of the flow measurement and the calculated permeability for the CO<sub>2</sub> and CH<sub>4</sub> gas pair. Apparently there is no relation between the thickness and the flow. GSMA-1, GPSS-1 and maybe GPSS-2 exhibit higher flow performances for CO<sub>2</sub> and CH<sub>4</sub> than the rest of the series. This could be caused by defects (pinholes), however, PDMS was used to fix defects into the membranes, and it seems rather unlikely, especially as this behavior was reproducible. Tables 6.7 and 6.8, exhibit a clear trend: GSMA-1 and GPSS-1 present higher CO<sub>2</sub> flow but lower CO<sub>2</sub>/N<sub>2</sub> selectivities whereas the rest of the membranes (GSMA-2, -3 and GPSS-2, -3) behave in an opposite direction.

**Table 6.7:** Flows, Permeability of CO<sub>2</sub> and CH<sub>4</sub> for.

Membranes	Thickness (nm)	Flow <sub>CO2</sub> (m <sup>3</sup> /m <sup>2</sup> hbar)	Flow <sub>CH4</sub> (m <sup>3</sup> /m <sup>2</sup> hbar)
<b>GSMAS-1 (E)</b>	984	1.0038	0.5252
<b>GSMAS-2 (F)</b>	1030	0.0172	0.0010
<b>GSMAS-3 (G)</b>	984	0.0179	0.0011
<b>GPSS-1 (C)</b>	1584	1.207	0.4987
<b>GPSS-2 (D)</b>	549	0.2210	0.1180
<b>GPSS-3 (H)</b>	1123	0.0300	0.0020

Table 6.8 highlights the permeation properties of CO<sub>2</sub> and N<sub>2</sub> and selectivity ( $\alpha$ ) of (CO<sub>2</sub>/N<sub>2</sub>) and (CO<sub>2</sub>/CH<sub>4</sub>) pairs at 35°C. All these membranes are more permeable to CO<sub>2</sub> than to N<sub>2</sub>; as it already was discussed in section 6.2.3 this is in accordance with the solubility-diffusion model. The results show that the graft-copolymers of

series-GSMA and-GPSS are taking advantage of the higher solubility of CO<sub>2</sub> in the rubbery (PEG segment). Also being rubbery materials, they have a weak ability to sieve penetrant molecules based on size (diffusion). However the differences ( $d_{KT}(N_2) 3.64\text{Å} > d_{KT}(CO_2) 3.3\text{Å}$ ) are too small to be relevant, hence, the final selectivity will be governed by the selectivity ratio  $S_{CO_2}/S_{N_2}$  and, as a result, these rubbery polymers have CO<sub>2</sub>/N<sub>2</sub> selectivities greater than unity. Note that in fact, all CO<sub>2</sub>/N<sub>2</sub> selectivities exceed unity by a factor of five and in some cases the selectivity is even higher: GSMA-3 (29), GSMA-2, (25) and GPSS-3 (23). The reason of that effect may be caused by the presence of PEG which is known to have high CO<sub>2</sub> permeability coefficients. As the graft-copolymers prepared in this work, are composed of a hard segment (polystyrene) enhancing the film formation and mechanical properties and of more soft PEG segments it can be considered as more or less a rubbery polymer substance.

**Table 6.8:** CO<sub>2</sub> and CH<sub>4</sub> permeabilities as well as CO<sub>2</sub>/N<sub>2</sub> and CO<sub>2</sub>/CH<sub>4</sub> selectivities for membranes based on the GSMAS and GPSS polymers

Membranes	$P_{CO_2}$ Barrer	$\alpha$ (CO <sub>2</sub> /N <sub>2</sub> )	$P_{CH_4}$ (Barrer)	$\alpha$ (CO <sub>2</sub> /CH <sub>4</sub> )	PEG (wt. %)	T <sub>g</sub> (°C)
<b>GSMAS - 1</b>	366	4.9	307.4	1.2	0.5	95
<b>GSMAS - 2</b>	6.60	25.0	0.40	16.5	38.7	65
<b>GSMAS - 3</b>	6.50	29.1	0.40	16.3	29.0	49
<b>GPSS - 1</b>	704	7.70	292	2.4	4.5	90
<b>GPSS - 2</b>	45.0	23.5	24.0	1.9	18.0	65
<b>GPSS - 3</b>	92	22.7	49.0	1.9	15.4	64

## 6.2.5.1 Membranes Properties in Dependency of the PEG Content

Figure 6.39 and 3.40 shows the effect of the PEG content on the CO<sub>2</sub> permeability and the CO<sub>2</sub>/N<sub>2</sub> selectivity respectively at 35°C for the GPSS and GSMA series. Figure 6.39, shows that the permeability of CO<sub>2</sub>,  $P_{CO_2}$ , decreases with increasing PEG content for both series. The GPSS-series exhibit a steep decrease from 700 to 45 Barrer with a relative low PEG content of maximum 18%. In contrary in the GSMA-series the  $P_{CO_2}$  decreases not so abruptly, it ranges from 366 until 7 Barrer at approximately 30 % PEG content. The differences could be explained by the higher PEG content (soft segment) in the GSMA-series compared to the GPSS-series for which the  $P_{CO_2}$  decrease is not so emphasized.

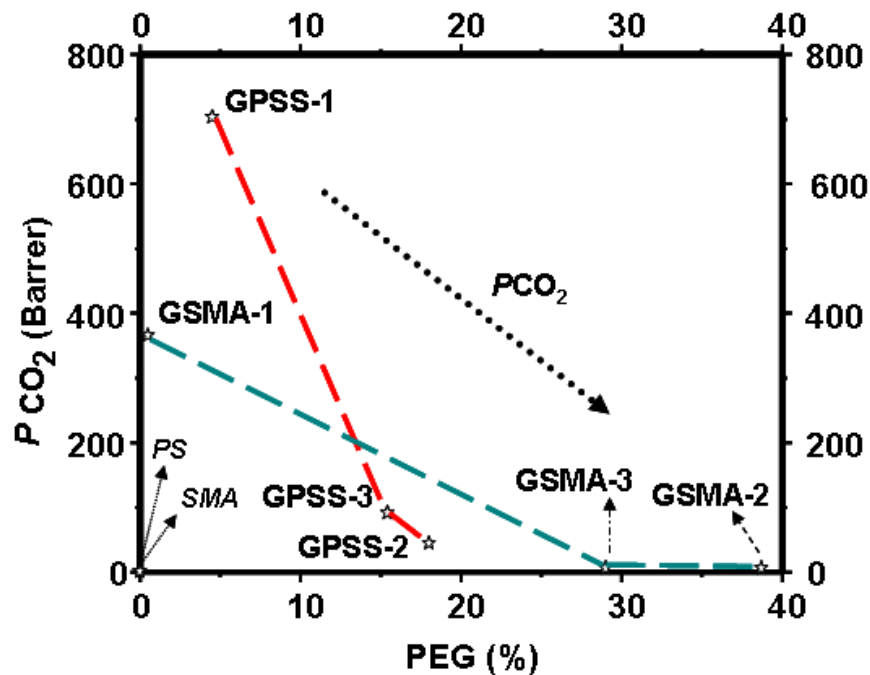


**Figure 6.39:** Effect of PEG content on CO<sub>2</sub> permeability at 35°C for membranes based on GPSS and GSMAS series

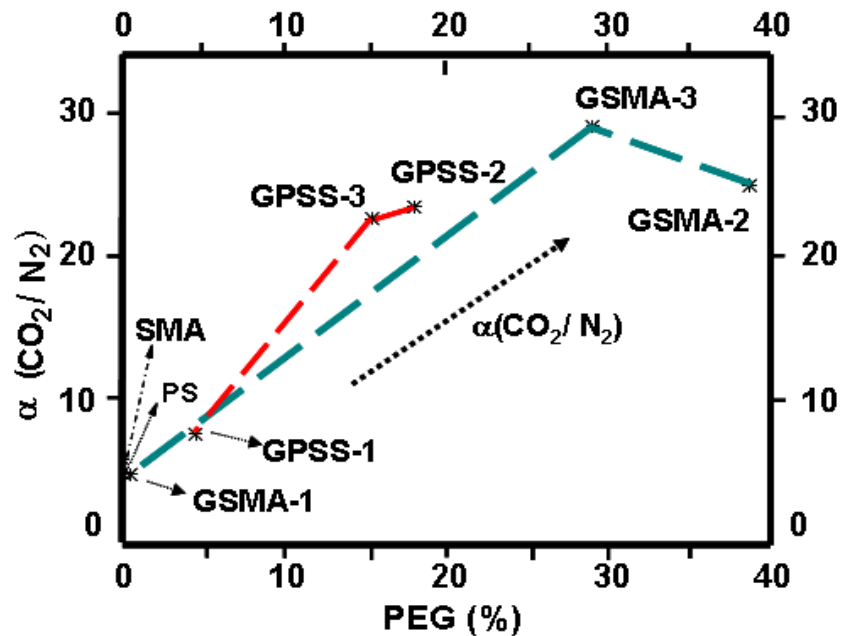


**Figure 6.40:** Effect of PEG content on the  $\text{CO}_2/\text{N}_2$  selectivity at  $35^\circ\text{C}$  for membranes based on GPSS and GSMAS series

The  $\text{CO}_2/\text{N}_2$  selectivity increases with the PEG content up to 30 and 23, respectively, (cf. Figure 6.40), however, the GSMAS-series exhibits higher selectivities because exhibits two types of functional groups to link the Jeffamine. The sulphonic and the maleic anhydride group can both serve that purpose it is possible to realize a higher amount of PEG in the final graft copolymer. There are different contents of PEG in each membrane, hence the membranes properties should also be evaluated in dependency of the different thermal glass transition temperatures ( $T_g$ ).

#### 6.2.5.2 Membranes Properties in Dependency of the $T_g$ .

Figure 6.41 and 6.42 present the effect of  $T_g$  on the  $\text{CO}_2$  permeability and  $\text{CO}_2/\text{N}_2$  selectivity respectively at  $35^\circ\text{C}$  for the GPSS and GSMAS series. Evidently,

polystyrene (PS) and styrene-co-maleic anhydride (SMA) show higher glass transition temperatures ( $T_{g_{PS}} = 106^{\circ}\text{C}$  and  $T_{g_{SMA}} = 121^{\circ}\text{C}$ ), in comparison to the series-GSMA and -GPSS. The graphs also show that in the membranes series GSMA and GPSS the  $\text{CO}_2$  permeability and the  $\text{CO}_2/\text{N}_2$  selectivity are higher in comparison to PS and SMA which demonstrates an improvement in the performance with respect of the original polymer. Besides the significant increase relative to the parent PS and SMA, the  $\text{CO}_2$  permeability decreases when the glass transition temperature becomes lower.

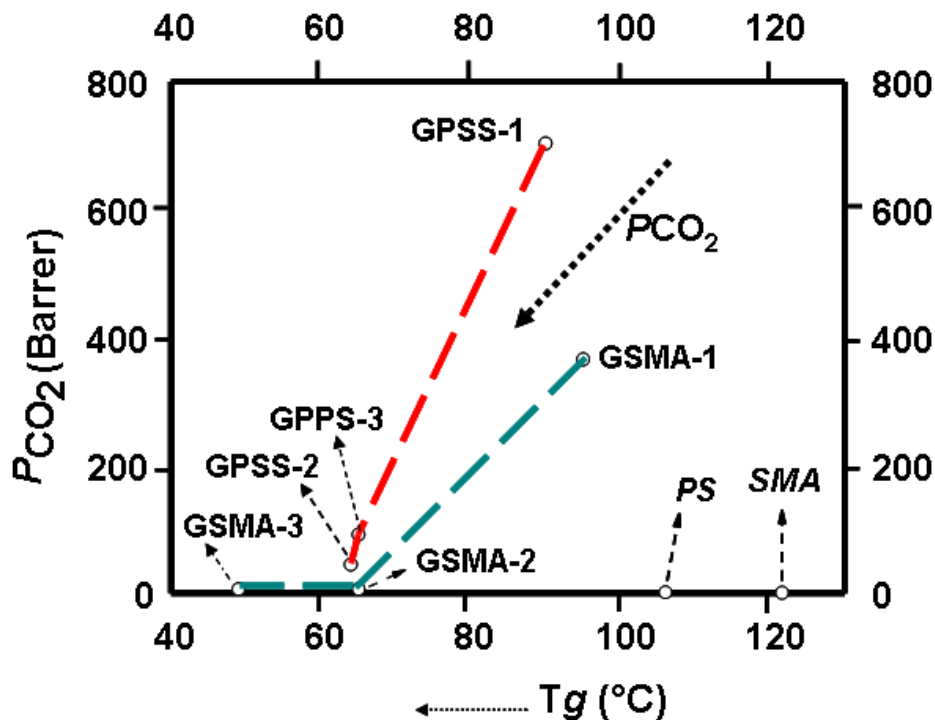


**Figure 6.41:** Effect of the glass transition temperature ( $T_g$ ) on the  $\text{CO}_2$  permeability at  $35^{\circ}\text{C}$  for the GPSS and GSMAS series

This behavior seems contradictory as the solubility of  $\text{CO}_2$  in the membranes increases due to the higher PEG content. However, the permeability also depends on the diffusion of  $\text{CO}_2$  into the membrane.

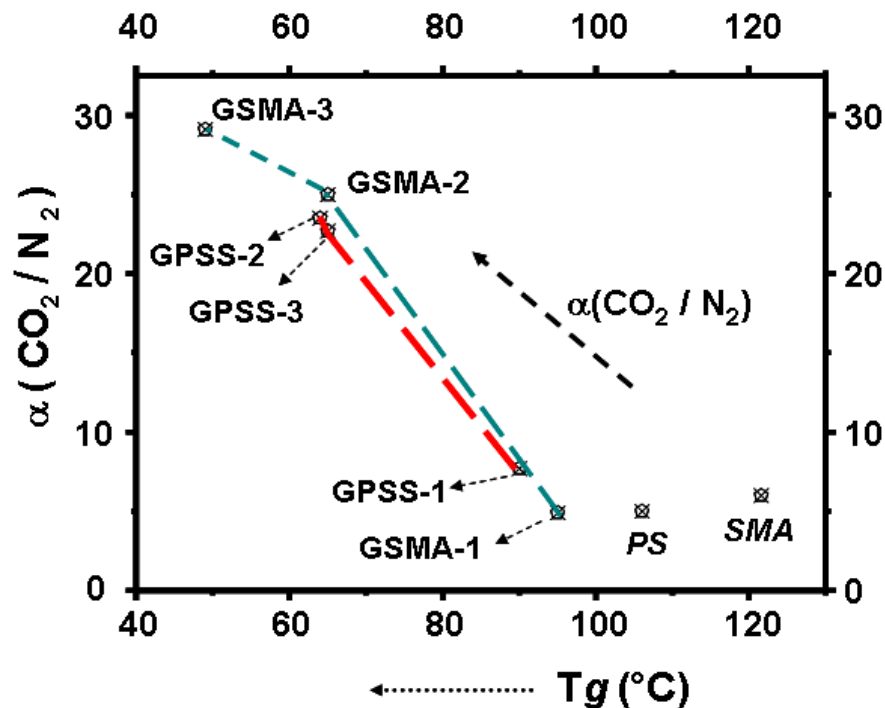


**Figure 6.42:** Effect of the glass transition temperature ( $T_g$ ) on the  $\text{CO}_2/\text{N}_2$  selectivity at  $35^\circ\text{C}$  for the GPSS and GSMA series

As the membranes series (GSMA and GPSS) are non-porous materials, the permeability is obviously limited by this effect. Nevertheless, from figure 6.42 it can be anticipated that the decrease of the permeability is stronger for  $\text{N}_2$  compared to  $\text{CO}_2$ , hence in total the  $\text{CO}_2/\text{N}_2$  selectivity is increasing in a very interesting way. Sulfonated polystyrenes exhibit a very complex situation, characterized by the clustering of the sulfonic groups [35]. It may be possible that the interactions/reactions between Jeffamine and these groups cause a change in the arrangement of the starting sulfonated polymers. Therefore, the performance of the membrane has been affected not only by the changes in the glass transition, but also due to changes in the morphology. This hypothesis can be confirmed by further investigations using small angle X-ray scattering. T

### 6.3 Conclusions.

#### Membranes series-ML, -MM and -MH: Characterization and Performance.

- √ Three series of composites membranes (ML, MM and MH) with different PEG content were prepared by casting techniques using graft-copolymers synthesized in chapter IV and characterized by permeability and selective separation of CO<sub>2</sub> from N<sub>2</sub> and CH<sub>4</sub>.
- √ In all the membranes three zones were identified, the support layer of "PAN", in the middle a PAN-graft-copolymer mixture and on top of the membrane a layer of the graft-copolymer.
- √ The overall CO<sub>2</sub>/N<sub>2</sub> and CO<sub>2</sub>/CH<sub>4</sub> selectivity increases compared to poly(styrene-co-maleic anhydride) when the poly(ethylene glycol) (PEG) content in the membranes increases.
- √ When the PEG content increases the CH<sub>4</sub> permeability decreases, because in the case of methane the permeability is governed by the diffusion of and not by the solubility.
- √ The membranes made from SMA and Jeffamine (M-2070), with a PEG content of 20 – 26, exhibit a CO<sub>2</sub> permability of 120 – 280 Barrer and a CO<sub>2</sub>/N<sub>2</sub> selectivity of 34 – 42 at 35°C and 1 atm of feed p ressure, which can be regared as competitive to membranes based on polyimides reported in the literature.
- √ The membrane permeabilities can be explained by a higher solubility of CO<sub>2</sub> in the PEG -rubber segment in comparison to N<sub>2</sub>. An import contribution of a CO<sub>2</sub> or a N<sub>2</sub> diffusion processes into the membrane is not observed.



- √ Due to the PEG incorporated into the membranes the glass transition ( $T_g$ ) decreases and in consequence  $\text{CO}_2$  permeability and the  $\text{CO}_2/\text{N}_2$  selectivity are enhanced.

**Membranes series-GSMA and GPSS, characterization and performance.**

- √ Two series of composite membranes (GSMA and GPSS) based on graft-copolymer containing PEG were prepared by casting on PAN. The single gas permeability and the  $\text{CO}_2/\text{N}_2$  and  $\text{CO}_2/\text{CH}_4$  selectivities were determined.
- √ For both series an increase of the polymers' PEG content resulted in a decrease of the  $\text{CO}_2$  permeability, whereas the overall  $\text{CO}_2/\text{N}_2$  selectivity increases. The results confirm that for high selectivities lower permeabilities are observed. However we think the phenomenon may be explained by the solubility-diffusion model.
- √ The increase of the PEG content leads a decrease of the  $\text{CO}_2$  permeability and an increase of the  $\text{CO}_2/\text{N}_2$  selectivity as expected by theory.
- √ In both series-GSMA and –GPSS a decrease of the glass transition temperature ( $T_g$ ) leads to lower  $\text{CO}_2$  permeabilities and to higher the  $\text{CO}_2/\text{N}_2$  selectivities.
- √ The increase of the  $\text{CO}_2/\text{N}_2$  selectivity seems mainly be governed by the solubility of  $\text{CO}_2$  in the “PEG” rubber segment whereas the diffusion coefficients are more governed by the molecular size of the gases.

**6.4 References**

- [1] Shao Lu, Low Ting B., Chung T-Sh., Greenberg A. R., *Journal of Membrane Science*, 327(2009) 18.
- [2] Scharnagl, N., Buschatz H., *Desalination*, 139 (2001) 191.
- [3] Car A., Stropnik Ch., Yave W., Peinemann K-V., *Separation and Purification Technology*, 62 (2008) 110.
- [4] Cecopieri-Gomez ML, Palacios-Alquisira J., Dominguez J. *Journal of Membrane Science*, 293 (2007) 53.
- [5] Robeson L.M. *Current Opinion in Solid State and Materials Science*, 4 (1999) 549.
- [6] Bhide B., Voskericyan A., Stern S., *Journal of Membrane Science*, 140 (1998) 27.
- [7] Lin H., Freeman B., *Journal Molecular Structure*, 739 (2005) 57.
- [8] Budd P., Msayib K., Tattershall C., Ghanem B., Reynolds N., Mckeown, Fritsch D., *Journal of Membranes Science*, 251 (2005) 263.
- [9] Tanaka K., Kita H., Okano M., Okamoto K., *Polymer* 33 (1992) 585.
- [10] Xiao Y., Low B. T., Hosseini S. S., Chung T. S. Paul D. R. *Progress in Polymer Science*, 34 (2009) 6 , 561-580.
- [11] Sanders E.S., *Journal of Membrane Science* 37 (1988) 63.
- [12] Koro WJ, Paul DR, Rocha AA., *Journal of Polymer Science Polymer Physic Edition* 14(1976) 687.
- [13] Paul D.R., Koros W.J., *Journal Polymer of Science Polymer Physics Edition*, 14(1976) 675.
- [14] Wang R, Cao C, Chung T, *Journal of Membrane Science* 198(2002) 259.

- [15] Okamoto K., Umeo N., Okamoto S., Tanaka K. and Kita H., *Chemical Letters*, (1993) 225.
- [16] Koros W. J., Fleming G., Jordan S., Kim T., Hoehn H., *Progress in Polymer Science*, 13 (1988) 339.
- [17] Park J.Y., Paul D., *Journal of Membranes Science*, 125 (1997) 23.
- [18] Kim T., Koros W. J., Husk G. O'Brien, *Journal of Membranes Science*, 37 (1988) 45.
- [19] Park J.Y., Paul D., *Journal of Membranes Science*, 125 (1997) 23.
- [20] Kim T., Koros W. J., Husk G. R., O'Brien K. C., *Journal of Membranes Science*, 37 (1988) 45.
- [21] Tanaka K., Okano M., Toshino H., Kita H., Okamoto K., *Journal of Polymer Science, Part B: Polymer Physics*, 30 (1992) 90.
- [22] Tanaka K., Osada Y., Kita H., Okamoto K., *Journal of Polymer Science, Part B: Polymer Physics*, 33 (1995) 907.
- [23] Staudt-Bickel C., Koros W. J., Paul D. R., *Journal of Membranes Science*, 170 (2000) 205.
- [24] Costello L.M., Koros W. J., *Journal of Polymer Science, Part B: Polymer Physics* 33 (1995) 135.
- [25] Lin W., Chung T., *Journal of Membranes Science*, 186 (2001) 183.
- [26] Tanaka K., Taguchi A., Hao J., Kita H., Okamoto K., *Journal of Membrane Science*, 121 (1996) 197-207.
- [27] Okamoto K., Tanaka K., Kita H., Ishida M., Kakimoto M., Imai Y., *Polymer Journal*, 24 (1992) 451 – 457.

- [28] Langsam M., Polyimides from gas separation, Ghosh M.K., Mittal K.L., Eds., Marcel Dekker, New York, USA, 1996, Chapter 22, pp. 697-741.
- [29] Hellmus M., Koros W. J. Husk G., Paul D., *Journal of Membranes Science*, 46 (1989) 93.
- [30] Ohaya H., Kudryavtsev V., Semenova S., Polyimide Membranes. Applications, Fabrications and Properties, Gordon and Breach Publishers, Amsterdam, The Netherlands, 1996, chapter 6, pp. 243-260.
- [31] Robenson L.M., Burgoyne W.F., Langsam M., Savoca A.C., Tien C.F., *High Performance Polymers for Membrane Separation*, 35 (1994) 4970.
- [32] Breck D. W., Zeolita, Molecular Sieves, John Wiley and Sons, New York, U.S.A., 1974, Chapter 8, p. 636.
- [33] Babari T.A., Koros W. J., Paul D. R., *Journal Polymer Science, Part B: Polymer Physics*, 26 (1988) 709.
- [34] Welty J. R., Wicks C.E., Wilson R.E., Fundamentals of Momentum, Heat and Mass Transfer, Wiley and Sons, New York, U.S.A., 1986, pp. 764 – 765.
- [35] Baigl D., Seery T., Williams C.E., *Macromolecules* 35 (2002) 2318.

---

**Chapter VII      Summary**

---

**7.1 Summary**

The present work highlights the synthesis, characterization and membrane properties of new graft copolymers obtained either by direct amidation of poly(styrene-co-maleic anhydride) or by sulphonation of polystyrene and subsequent amidation with different poly(ether amide)s “jeffamines®” as grafts. These materials were tested as membranes for CO<sub>2</sub> and CH<sub>4</sub> separation.

***Direct amidation of poly(styrene-co-maleic anhydride)***

Characterization results obtained by <sup>1</sup>H-NMR, <sup>13</sup>C-NMR, GPC, DSC, and TGA demonstrated the successful synthesis of graft copolymers with PEG contents from 5 to 26 wt.% (series-ML,-MM and -MH) using poly(styrene-co-maleic anhydride) and Jeffamine. Employing an educt molar ratio of 1:0.5 and ethanol as non-solvent proved to be optimal conditions resulting in average yields of ~80% and maximum residual jeffamine contents of less than 5 wt.%. The graft copolymers' thermal analyses indicated the final products to be amorphous materials with glass transition temperatures decreasing for an increasing content of PEG bonded to the matrix poly(styrene-co-maleic anhydride). Polymers with a lower content of PEG tended to be in a more glassy state, whereas the macromolecules (graft-copolymer) containing higher amounts of PEG were better described as a rubber-type materials.

***Sulphonation of polystyrene and subsequent amidation***

A second group of graft copolymers (series GSMA and GPSS) were synthesized by sulfonation of poly(styrene) and poly(styrene-co-maleic anhydride), respectively, and

subsequent amidation with Jeffamine. The successful synthesis was proven by elemental analysis (EA),  $^1\text{H-NMR}$ , GPC, FT-IR, and thermal analyses (DSC and TGA). Polymers of PEG contents up to 35 wt.% with a degree of sulfonation up to 24 wt.% were obtained. An increase of the PEG content in the graft-copolymer lead to a decrease of the glass transition temperature in comparison to the sulphonated polystyrene. Finally, the graft-copolymer of the series GSMA and GPSS showed an increase in the molar mass averages compared to the educt polymers ( $\Delta M_n$ ) of 42 wt.% and an interesting thermal resistance with maximum operating temperatures of around 220°C.

#### ***Membranes series-ML, -MM and -MH (direct amidation)***

Three series of composites membranes (series-ML, MM and MH) with different PEG contents were prepared by casting and their  $\text{CO}_2$ ,  $\text{N}_2$ , and  $\text{CH}_4$  permeabilities as well as their  $\text{CO}_2/\text{N}_2$  and  $\text{CO}_2/\text{CH}_4$  selectivities were determined. All membranes exhibited three zones (as showed by SEM), the support layer of PAN, the middle layer of a PAN-graft-copolymer mixture, and the top layer consisting of the graft-copolymer. Generally, the overall  $\text{CO}_2/\text{N}_2$  and  $\text{CO}_2/\text{CH}_4$  selectivity increased with higher poly(ethylene glycol) contents. The membranes made from SMA and Jeffamine (M-2070) (series-MH) with PEG contents of 20 – 26 wt.% exhibited a  $\text{CO}_2$  permeability of 120 - 280 Barrer and a  $\text{CO}_2/\text{N}_2$  selectivity of 34 – 42 at 35°C and 1 atm of feed pressure, which can be regarded as competitive to membranes reported in literature and to the theoretical upper bound limit defined by Freeman's theory. The high selectivity of the  $\text{CO}_2/\text{N}_2$  pair was explained by the high solubility of  $\text{CO}_2$  in the PEG. Due to the incorporation of PEG the glass transition temperature decreased, the  $\text{CO}_2$

permeability increased stronger than the N<sub>2</sub> permability, and in consequence the CO<sub>2</sub>/N<sub>2</sub> selectivity was enhanced. In case of the CO<sub>2</sub>/CH<sub>4</sub> pair the selectivity was further influenced by a decrease of the CH<sub>4</sub> permeability. Hence, it may be presumed that the transport of CH<sub>4</sub> through the membrane is controlled rather by diffusion rather than by solution.

#### *Permeability of CO<sub>2</sub> and CO<sub>2</sub>/N<sub>2</sub> selectivity*

The high CO<sub>2</sub> permeability can be explained by two concurrent contributions, the solubility and the diffusivity. The solubility of CO<sub>2</sub> is higher than that of N<sub>2</sub> due to the significant differences in the condensability of both gases. At the same time, the graft copolymers consisting of flexible and polar poly(ethylene glycol) (PEG) segments are very attractive for the polar CO<sub>2</sub> molecules. On the other hand, the gas diffusivity mainly depends on the kinetic diameter ( $d_{kT}$ ) of the penetrants. The diffusivity of CO<sub>2</sub> is therefore expected to be larger than N<sub>2</sub>, hence, the separation of the CO<sub>2</sub>/N<sub>2</sub> gas pair is also accomplished by a size selective sieving mechanism (diffusion) and CO<sub>2</sub> permeates faster in comparison N<sub>2</sub>.

#### ***Membranes series GSMA and GPSS (via sulphonated PS)***

Two series of composite membranes (GSMA and GPSS) based on graft copolymers containing PEG were prepared by casting on PAN support and single gas permeabilities as well as the CO<sub>2</sub>/N<sub>2</sub> and CO<sub>2</sub>/CH<sub>4</sub> selectivities were determined. For both series an increase of the polymers' PEG content resulted in lower glass transition temperatures leading to a decrease of the CO<sub>2</sub> permeability and an increase of the overall CO<sub>2</sub>/N<sub>2</sub> selectivity. The results confirmed that for lower

permeabilities higher selectivities were observed, however, the phenomenon is probably explained by the solubility-diffusion model. As the diffusion coefficients were governed by the molecular size of the gases the increase of the CO<sub>2</sub>/N<sub>2</sub> selectivity should be caused by the increased solubility of CO<sub>2</sub> in the PEG rubber segment.

#### *Permeability of CO<sub>2</sub> and CO<sub>2</sub>/CH<sub>4</sub> (Membranes GSMA and GPSS)*

Generally, the membranes of this series possess lower CO<sub>2</sub> permeabilities compared to the other series despite their comparable PEG content. According to the solution-diffusion model this observation should be due to changes in the solubility of CO<sub>2</sub>, probably caused by the presence of the sulfonic groups in the polymer. Hence, the CO<sub>2</sub>/CH<sub>4</sub> selectivity is mainly driven by the size differences of CO<sub>2</sub> and CH<sub>4</sub> and in consequence lower than the one obtained for the other membrane series.

## **7.2 Zusammenfassung**

Die vorliegende Arbeit beschreibt die Synthese, Charakterisierung und die Bestimmung der Membraneigenschaften neuer Kammcopolymere, welche zum Einen durch direkte Amidierung von Poly(styrol-co-maleinsäureanhydrid) und zum Anderen durch Sulfonierung von Polystyrol und anschließende Amidierung mit jeweils unterschiedlichen Polyetheramiden (Jeffamin) hergestellt wurden. Das Verhalten der Kammcopolymere als Membranen zur Gastrennung wurde für die Gase N<sub>2</sub>, CO<sub>2</sub> und CH<sub>4</sub> untersucht.

#### ***Direkte Amidierung von Poly(styrol-co-maleinsäureanhydrid)***

<sup>1</sup>H NMR, <sup>13</sup>C NMR, GPC, DSC und TGA haben gezeigt, dass die Synthese von



Kammcopolymeren durch die Reaktion von Poly(styrol-co-maleinsäureanhydrid) mit Jeffamin (Serie ML, MH und MM) erfolgreich ausgeführt werden konnte. Die Bedingungen der Synthese wurden optimiert – bei einem Edukt- Verhältnis von 1:0.5 und der Verwendung von Ethanol als Fällungsmittel konnten im Durchschnitt Ausbeuten von 80 % bei einem maximalen 5%igen Restgehalt an nicht umgesetzten Jeffamin erreicht werden. Thermische Analysen zeigen, dass die Kammcopolymeren amorph sind, wobei ein Anstieg des Jeffamin-Anteils in einem Rückgang der Glasübergangstemperatur resultiert. Polymeren mit geringem PEG-Gehalt zeigen ein glasartiges Verhalten, während ein höherer PEG-Gehalt zu kautschukähnlichen Eigenschaften führt.

### ***Sulfonierung von Polystyrol und anschließende Amidierung***

Eine zweite Gruppe an Kammcopolymeren (Serie GSMA and GPSS) konnten durch Sulfonierung von Polystyrol bzw. Poly(styrol-co-maleinsäureanhydrid) und anschließende Amidierung mit den entsprechenden Jeffaminen synthetisiert werden. Die Anlagerung des Jeffamins wurde durch Elementaranalyse (EA), <sup>1</sup>H-NMR, GPC, FT-IR, und thermischer Analyse (DSC and TGA) nachgewiesen. In den Polymeren konnten Jeffamin Anteile bis zu 35% bei einem Sulfonierungsgrad von bis zu 24 gew% realisiert werden. Eine Erhöhung des PEG-Gehalts führte zu einer Senkung der Glasübergangstemperatur im Vergleich zum sulfonierten Polymer. Die Kammcopolymeren dieser Serie zeigten einen Anstieg der Molekulargewichtsmittelwerte im Vergleich zu den Edukten ( $\Delta M_n = 42\%$ ). Die per TGA ermittelte Zersetzungstemperatur von 220°C lässt diese Materialklasse für Hochtemperaturanwendungen als geeignet erscheinen.

**Membranen -ML, -MM and -MH (direkte Amidierung)**

Drei unterschiedliche Serien an Membranen wurden durch Casting der Kammcopolymer auf einen PAN-Träger hergestellt und sowohl die CO<sub>2</sub>-, CH<sub>4</sub>- und N<sub>2</sub>- Permeabilität als auch die CO<sub>2</sub>/CH<sub>4</sub> und CO<sub>2</sub>/N<sub>2</sub> Selektivität der entsprechenden Komposit-Membranen bestimmt. Rasterelektronmikroskopische Aufnahmen zeigen, dass die Membran aus drei verschiedenen Zonen besteht: der PAN-Träger, eine gemischte Zwischenschicht aus PAN und dem Copolymeren und schließlich auf der Zwischenschicht ein dünner Film aus reinem Kammcopolymer. Allgemein führt ein höherer Anteil an Polyethylenglycol zu höheren CO<sub>2</sub>/N<sub>2</sub> und CO<sub>2</sub>/CH<sub>4</sub> Selektivitäten. Membrane der Serie MH (hergestellt mit Jeffame M-2070) mit PEG-Anteilen bis zu 26 Gewichtsprozent besitzen eine CO<sub>2</sub>-Permeabilität von 120- bis 280 Barrer und eine CO<sub>2</sub>/N<sub>2</sub> Selektivität von 34 bis 42 bei 35 °C und einem Feed-Druck von 1 atm – durchaus vergleichbar zum gegenwärtigen Stand der Technik und der theoretischen "Upper-bound"-Grenze nach Freemans Theorie. Die hohe CO<sub>2</sub>/N<sub>2</sub> Selektivität kann durch die hohe Löslichkeit des Kohlendioxids im PEG erklärt werden. Eine Erhöhung des PEG-Anteils führt zu niedrigeren Glassübergangstemperaturen und zu einem vergleichsweise stärkeren Anstieg der CO<sub>2</sub>-Permeabilität gegenüber der N<sub>2</sub>-Permeabilität; letztlich resultiert hieraus der Anstieg der CO<sub>2</sub>/N<sub>2</sub> Selektivität. Im Falle der CO<sub>2</sub>/CH<sub>4</sub> Trennung wird die Selektivität weiterhin durch einen Rückgang der CH<sub>4</sub> Permeabilität beeinflusst. Es kann daher gemutmaßt werden, dass der Transport des Methans durch die Membran eher durch Diffusion als durch Löslichkeit kontrolliert wird.

*CO<sub>2</sub> Permeabilität und CO<sub>2</sub>/N<sub>2</sub>-Selektivität*

Die hohe CO<sub>2</sub> Permeabilität kann durch das Zusammenspiel von Diffusion und Löslichkeit gedeutet werden. Die Löslichkeit des CO<sub>2</sub> übersteigt die des N<sub>2</sub> aufgrund der stark unterschiedlichen Kondensierbarkeit beider Gase. Da die Kammpolymere flexible und gleichzeitig polare PEG-Segmente enthalten, sind sie für das polare CO<sub>2</sub> sehr attraktiv. Andererseits wird die Diffusion der Gase im Wesentlichen durch deren kinetischen Durchmesser bestimmt. Die Diffusivität des CO<sub>2</sub> sollte daher bedeutend größer als die von N<sub>2</sub> sein; somit erfolgt die Trennung eines CO<sub>2</sub> /N<sub>2</sub> Gemischs weiterhin durch einen Größenausschluss, bei dem CO<sub>2</sub> schneller als N<sub>2</sub> durch die Membran permiiert.

**Membranen GSMA and GPSS (Sulfonierung von Polystyrol)**

Zwei unterschiedliche Kompositmembranen aus Kammcopolymeren der Serie GSMA und GPSS wurden durch Casting auf einen PAN-Träger hergestellt und sowohl deren N<sub>2</sub>-, CO<sub>2</sub>- und CH<sub>4</sub>-Permeabilitäten als auch die CO<sub>2</sub>/N<sub>2</sub>- und CO<sub>2</sub>/CH<sub>4</sub>-Selektivitäten bestimmt. In beiden Serien führt ein höherer PEG-Anteil zu einer Senkung der Glasübergangstemperaturen und einem Rückgang der CO<sub>2</sub> Permeabilität bei gleichzeitiger Zunahme der CO<sub>2</sub>/N<sub>2</sub>-Selektivität. Die Ergebnisse belegen, dass für kleinere Permeabilitäten höhere Selektivitäten gefunden werden; ein Verhalten, dass nach dem Löslichkeits-Diffusions Modell gedeutet werden kann. Da die Diffusionskoeffizienten durch die Größe der Gase beeinflusst werden, kann der Anstieg der CO<sub>2</sub>/N<sub>2</sub>-Selektivität weiterhin durch die erhöhte Löslichkeit des CO<sub>2</sub> im gummiartigen PEG-Segment erklärt werden.

*CO<sub>2</sub> Permeabilität und CO<sub>2</sub>/ CH<sub>4</sub>-Selektivität*

Im Allgemeinen weisen die Membranen dieser Serie gegenüber dem erstgenannten Typ geringere CO<sub>2</sub> Permeabilitäten auf - trotz ihres vergleichbaren PEG-Gehalts. Gemäß dem Löslichkeits-Diffusions Modell lässt dieser Unterschied eine geänderte CO<sub>2</sub> Löslichkeit vermuten, die wahrscheinlich in der Gegenwart der Sulfonsäuregruppen begründet liegt. Somit kann die wesentliche Triebkraft der CO<sub>2</sub>/ CH<sub>4</sub> Selektivität auf die Unterschiede im kinetischen Durchmesser beider Gase zurückgeführt werden; der zusätzliche Einfluss der Löslichkeit fehlt hier und resultiert in geringeren Selektivitäten.

---

**Chapter VIII      Appendix**


---

**I.      Reaction Yield Calculation**

The calculation of the theoretical yield of the reaction, see figure 4.2 chapter IV, is based on the amount of the limiting reagent (MA or Jeffamine, see table 4.2) which determines the moles of product

$$n_i = \frac{m_i}{M_i} \quad (8.1)$$

$n_i$  represent the number of moles,  $m_i$  the mass of SMA or Jeffamine (reactants) used in each reaction and  $M_i$  molar mass of reactants. Using the eq. (8.1) and the composition (i.e. the amount of styrene and maleic anhydride) in the SMA 7 %,  $n_{MA}$ ,  $n_{SMA}$  and the  $n_{\text{jeffamine}}$  can be calculated. The reaction, fig. 4.2, show that 1 mol of MA react with 2 moles of Jeffamine, hence, it's known the moles of the limiting reagent (Maleic anhydride) so its calculated the moles of product and finally the theoretical mass of product,  $w_{\text{theo}}$ . After graft-copolymer preparation the experimental mass of products is determinate,  $w_{\text{exp}}$ . The yield of the reaction is defined as

$$Yield = \left( \frac{w_{\text{exp}}}{w_{\text{theo}}} \right) \times 100\% \quad (8.2)$$

**II.      Calculation of PS, PEG and PPG content**

The calculation starts from the weight ratio of the poly(styrene-co-maleic anhydride) copolymer. As they are given as wt/wt, they have to be converted into a number fraction,  $x$ . It is defined for the  $i$ -th component as

$$x_i = \frac{n_i}{\sum_i n_i} \quad (8.3)$$

The corresponding weight fraction  $w_i$  is defined as

$$w_i = \frac{m_i}{\sum_i m_i} \quad \text{with } m_i = M_i n_i \quad (8.4)$$

Using the molar mass,  $M_i$  a SMA 7 % of 100g is composed of  $m_{MA} = 7$  g maleic anhydride and  $m_S = 93$  g of styrene. Using eqs. (8.3) and (8.4) find  $x_{MA} = 0.074$  and  $x_S = 92.6$ . The corresponding values for the content of propylene oxide (PO) and ethylene glycol (EG) repeating units in the Jeffamine is calculated analogous. The number fraction  $x_i$  is calculated from the (normalized) signal intensity of the  $^1\text{H-NMR}$  spectra. If  $I$  is the integral value of a resonance signal originating from  $r$  protons, we can calculate the number fraction of the  $i$ -th component,  $x_i^{\text{NMR}}$  as

$$x_i^{\text{NMR}} = \frac{I_i/r_i}{\sum_i I_i/r_i} \quad (8.5)$$

The reaction product is a Jeffamine grafted on a SMA in which it's evaluate the resonance signals of the phenyl ring (S;  $6.5 < \delta/\text{ppm} < 7.5$ ;  $r_S = 5$ ) and the signals of the ethylene glycol (EG;  $\delta/\text{ppm} = 3.5$ ;  $r_{EG} = 4$ ). Strictly speaking, the grafted product is a quaterpolymer, composed of four different repeating units, however first we use the relation between the ethylene glycol and phenyl ring. Hence, eq. (8.5) reads for the number fraction of polystyrene in the graft-copolymer,  $x_S^G$ ,

$$x_S^G = \frac{I_S/r_S}{I_S/r_S + I_{EG}/r_{EG}} \quad (8.6)$$

Unfortunately,  $I_{PO}$  cannot be determined from the spectra. However, the amount of PO is directly proportional to the amount of EG, later it is use another relation to find it. Also it's know that 1 mol SMA (7%) contains 0.926 mole of styrene, therefore the styrene molar fraction ( $X_s^{SMA}$ ) can be calculated.

Inserting the styrene molar fraction in to (8.6) leads to the number fraction of styrene in the graft copolymer

$$x_S^G = \frac{\frac{I_s}{r_s} (x_s^{SMA})}{\frac{I_s}{r_s} (x_s^{SMA}) + \frac{I_{EG}}{r_{EG}}} \quad (8.7)$$

and accordingly

$$x_{EG}^G = \frac{\frac{I_{EG}}{r_{EG}}}{\frac{I_s}{r_s} (x_s^{SMA}) + \frac{I_{EG}}{r_{EG}}} \quad (8.8)$$

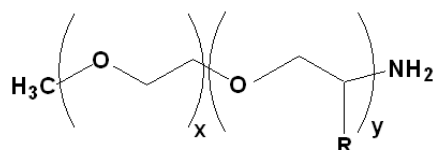
The weight fractions in the graft copolymer can directly be derived from eqs. (8.7) –

(8.8) and the molar masses of the repeating units,  $M_i$

$$w_S^G = \left[ \frac{x_S^G \times M_s}{x_S^G \times M_s + x_{EG}^G \times M_{EG}} \right] \times 100\% \quad (8.9)$$

$$w_{EG}^G = \left[ \frac{x_{EG}^G \times M_{EG}}{x_S^G \times M_s + x_{EG}^G \times M_{EG}} \right] \times 100\% \quad (8.10)$$

As is know, the Jeffamine composition used is report below,



R = H for (EO), or CH<sub>3</sub> for (PO)

Polyetheramines	M (g/mol)	PEO / PPO Mol ratio	PEG (%)
XTJ 505	600	1/9	10
XTJ 506	1000	19/3	86
M-2070	2000	31/10	76

Therefore, and in an analogous manner using the number fraction of ethylene glycol (EG) in the Jeffamine the number fraction of propylene glycol (PO) in the graft-copolymer can be determined and the overall graft-copolymer final composition can be calculated.

An example of the calculation,

*Samples M – 3*, this the graft-copolymer was prepared using Jeffamine XTJ 506, i.e. a molar ratio of EG/PO (19:3),

Using eq. 8.4 the weight of EG and PO in the Jeffamine is calculated:

$$\text{EG} (w_{EG}^{Jeff}) \quad \text{and} \quad \text{PO} (w_{PO}^{Jeff}),$$

Due to the fact that it is know previously the content of EG in the ( $w_{EG}^G$ ) in this cases (21,0 wt.%), it's can be determine the content of PO, as follow



$$w_{PO}^G = \frac{w_{EG}^G \times w_{PO}^{Jeff}}{w_{EG}^{Jeff}} \quad (8.11)$$

Hence, in analogous form all the weights of the graft-copolymer segments can be calculated:

Styrene ( $w_S^G$ )    Ethylene glycol ( $w_{EG}^G$ )    and    Propylene glycol ( $w_{PO}^G$ )

Now we need to recalculate using the equation 8.11 and finally we have the overall graft-copolymer final composition

$$w_i = \frac{m_i}{\sum_i m_i} \quad (8.12)$$

### III. Elemental Analysis: Carbon, Hydrogen, Oxygen and Sulphur

#### Composition by Mass

First, the composition of the sulfonated poly(styrene-*c*-maleic anhydride) is expressed in terms of the weight percentage of each element in the compound.

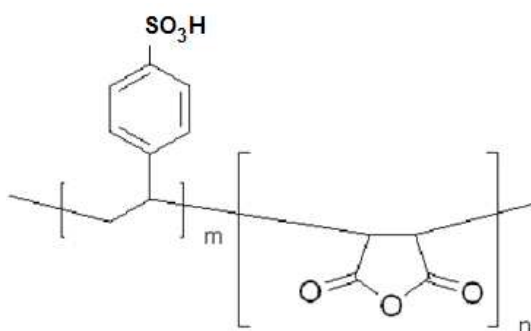


**Figure 8.1:** Idealized structure of sulfonated poly(styrene-*c*-maleic anhydride).

For example, the idealized structure of figure 8.1 has the formula  $C_{12}H_{12}O_6S$ . One mol of the compound has a mass of 284.06 g ( $M_i$ ). The elemental formula indicates that one mole of sulfonated poly(styrene-*c*-maleic anhydride) contains 12 moles of carbon (C), 12 moles of hydrogen (H), 6 moles of oxygen and 1 mole of sulphur (S). Thus the theoretical composition of the compounds for each element by mass is defined as

$$EA_{theo} = \left[ \frac{n_i \times m_i}{M_i} \right] \times 100\% \quad (8.13)$$

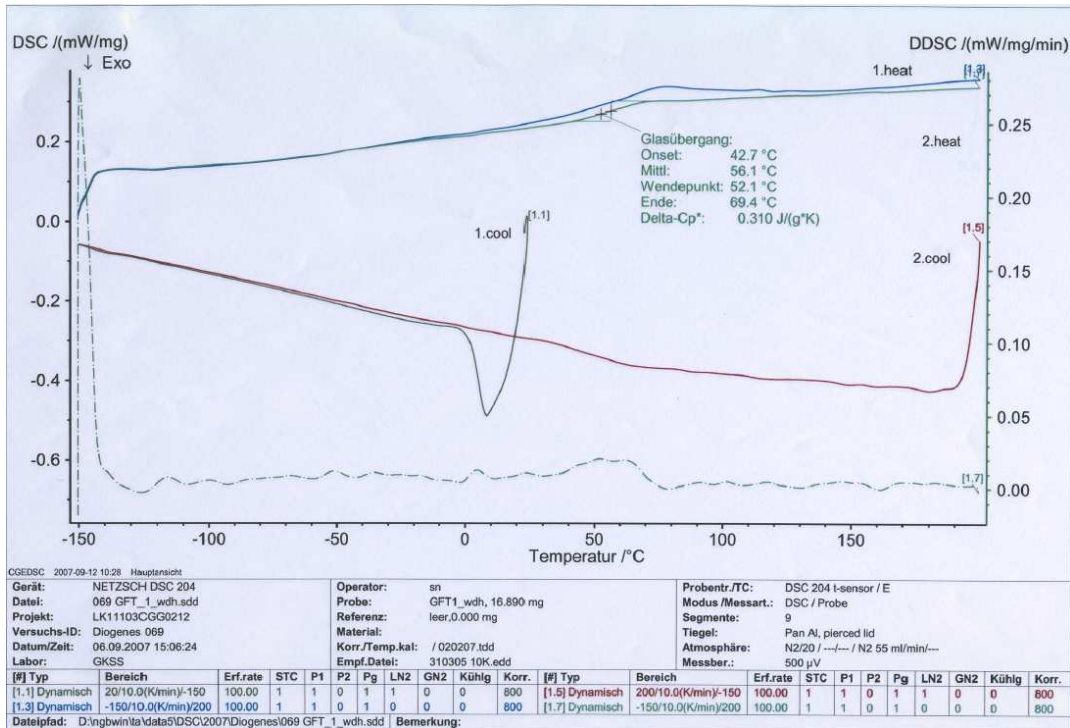
Where  $EA_{theo}$  is the theoretical content of element in the compound,  $n_i$  is the number of mole of the respective elements in the elemental formula,  $m_i$  is the molar mass of the element and  $M_i$  is the molar mass of the compound. In this calculation it is assumed that only one sulphonic group is substituted at the phenyl ring and that a degree of sulfonation of 100% is reached.

The experimental elemental analysis gives the experimental sulphur content  $EA_{exp}(S)$  in each sample. Finally, the degree of sulfonation (DS) is calculated as

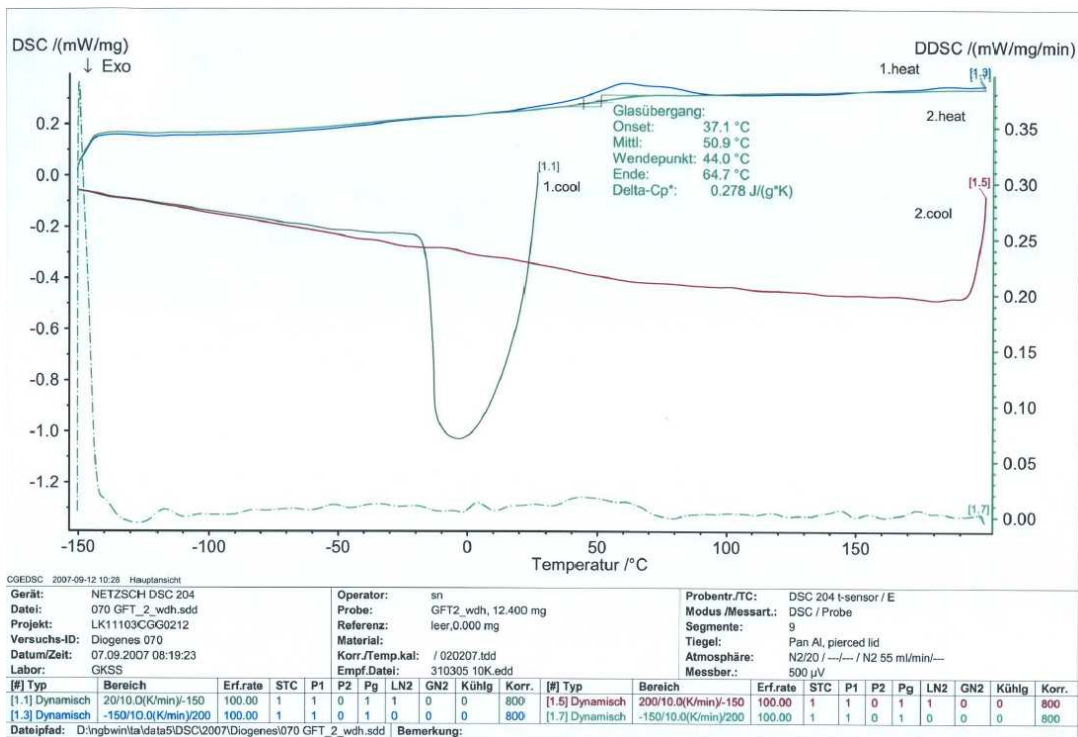
$$DS = \left( \frac{EA_{exp}(s)}{EA_{theo}(S)} \right) \times 100\% \quad (8.14)$$

IV. Examples of DSC thermograms with original data.

- DSC Thermograms of graft-copolymer M-1



- DSC Thermograms of graft-copolymer H-1





# Diógenes Rojas

Born **22.04.1970** in Caracas – Venezuela (Venezuelan)

## Education

**Dr. rer. nat.**

Christian - Albrechts - Universität zu Kiel (CAU), Germany  
Technische Fakultät, Materials Science

**Master in Chemistry**

Simón Bolívar University (USB), Chemistry Department. Caracas  
- Venezuela

**Bachelor degree in Chemistry**

Simón Bolívar University (USB), Chemistry Department. Caracas  
- Venezuela

**T.S.U in Chemistry**

University Institute of Technology, “Dr. Federico Rivero Palacio”  
Chemistry Department, Caracas - Venezuela

## Workshops and Scientific Meetings (Only during PhD)

**New Materials for Membranes, Marie Curie Workshop**  
European Commission, GKSS - Geesthacht, Germany  
*“Grafting of Poly(styrene-co-Maleic Anhydride) with poly(ether amine) as new possibility to increase the selectivity in gas separation” (Poster presentation)*

**EMS Summer School on Membranes “SMART MATERIALS”**, Institute of Macromolecular Chemistry, Prague - Czech Republic. *“Grafting of Poly(styrene-co-Maleic Anhydride with PEG for membrane preparation”*. (Poster presentation)

**Polymer/Metal Nanocomposite 2<sup>nd</sup> International-Workshop**. GKSS Research Centre, Geesthacht - Germany

**Bayreuth Polymer Symposium, BPS '05**  
Universität Bayreuth. Germany

## Scientific Publication

*Journal of Polymer Science Part A: Polymer Chemistry*

**Poly (styrene-co-maleic anhydride) grafted with poly(ether amines): synthesis, characterization and gas separation performance. (In Preparation)**